

**ADVERTIMENT.** La consulta d'aquesta tesi queda condicionada a l'acceptació de les següents condicions d'ús: La difusió d'aquesta tesi per mitjà del servei TDX ([www.tesisenxarxa.net](http://www.tesisenxarxa.net)) ha estat autoritzada pels titulars dels drets de propietat intel·lectual únicament per a usos privats emmarcats en activitats d'investigació i docència. No s'autoritza la seva reproducció amb finalitats de lucre ni la seva difusió i posada a disposició des d'un lloc aliè al servei TDX. No s'autoritza la presentació del seu contingut en una finestra o marc aliè a TDX (framing). Aquesta reserva de drets afecta tant al resum de presentació de la tesi com als seus continguts. En la utilització o cita de parts de la tesi és obligat indicar el nom de la persona autora.

**ADVERTENCIA.** La consulta de esta tesis queda condicionada a la aceptación de las siguientes condiciones de uso: La difusión de esta tesis por medio del servicio TDR ([www.tesisenred.net](http://www.tesisenred.net)) ha sido autorizada por los titulares de los derechos de propiedad intelectual únicamente para usos privados enmarcados en actividades de investigación y docencia. No se autoriza su reproducción con finalidades de lucro ni su difusión y puesta a disposición desde un sitio ajeno al servicio TDR. No se autoriza la presentación de su contenido en una ventana o marco ajeno a TDR (framing). Esta reserva de derechos afecta tanto al resumen de presentación de la tesis como a sus contenidos. En la utilización o cita de partes de la tesis es obligado indicar el nombre de la persona autora.

**WARNING.** On having consulted this thesis you're accepting the following use conditions: Spreading this thesis by the TDX ([www.tesisenxarxa.net](http://www.tesisenxarxa.net)) service has been authorized by the titular of the intellectual property rights only for private uses placed in investigation and teaching activities. Reproduction with lucrative aims is not authorized neither its spreading and availability from a site foreign to the TDX service. Introducing its content in a window or frame foreign to the TDX service is not authorized (framing). This rights affect to the presentation summary of the thesis as well as to its contents. In the using or citation of parts of the thesis it's obliged to indicate the name of the author

# Web crippling and local buckling response of stainless steel sections

Doctoral thesis by:  
Marina Bock

Supervised by:  
Esther Real

Barcelona, November 2014



Universitat Politècnica de Catalunya  
Departament d'Enginyeria de la Construcció

# DOCTORAL THESIS



## ABSTRACT

The usage of stainless steel in construction is continuously expanding and therefore, so is the need to provide practitioners and researchers suitable structural design guidance. As part of a larger Research Found for Coal and Steel (RFCS) project of the European Comission under the acronym SAFSS (Structural Applications of Ferritic Stainless Steels) and a National Project of the Ministerio de Ecomía y Competitividad entitled “Estudio del comportamiento de estructuras de acero inoxidable ferrítico”, both of which addressed the use of ferritic stainless steels in structural applications, this thesis examines the response of stainless steel members when subjected to transverse and normal forces triggering the instability phenomena called web crippling and local buckling, respectively. Stainless steel members often comprise slender elements which are susceptible to local instabilities such as web crippling and local buckling. Currently, the part of Eurocode dealing with stainless steel, EN 1993-1-4 (2006) misses design provisions for web crippling and the applicability of some of its aspects is yet to be fully verified especially for application to ferritic stainless steel.

The first part of the thesis laid in the development of design equations for the treatment of web crippling in stainless steel sections which are currently designed following specifications given in EN 1993-1-3 (2006) for cold-formed carbon steel. Through the use of comprehensive finite element models supported by experiments, two design approaches were derived and statistically verified covering austenitic and ferritic stainless steels: an empiric equation, in line with the current provisions for web crippling design given in EN 1993-1-3 (2006); and an alternative semi-empiric design method based on strength curves  $\chi(\bar{\lambda})$  which enables a better understanding of the phenomenon and showed to significantly improve web crippling predictions.

For the second part of the thesis, the applicability of the local buckling design provisions given in EN 1993-1-4 (2006) to ferritic stainless steel was examined giving focus to the slenderness limits and the effective width equations used for the design of slender sections. Building on numerical models carefully validated against existing tests and later complemented with an experimental investigation, the results showed that current EN 1993-1-4 (2006) can safely be applied to ferritic stainless steel, though the code is rather conservative in comparison with other methods. The scope of alternative design approaches for application to ferritic stainless steel was also assessed and design recommendations were given. Finally, a modification of the effective width equation incorporating element interaction effects was proposed. This resulting equation offers improved cross-section capacity predictions and enables to amend the effective width method to the same level of alternative design approaches but promoting the use of the concepts currently considered in Eurocode.



## ACKNOWLEDGEMENTS

I would like to express my sincere gratitude to my supervisor Esther Real for her patience and belief in me and her invaluable advice throughout my doctoral studies in the Department of Construction Engineering at Universitat Politècnica de Catalunya (UPC). I do appreciate the chance I was given to join this research team which has been indispensable to my growth as a researcher and as a person.

I would like to acknowledge the financial support from the PhD studentship provided by UPC and the Secretaria d'Universitats i de Recerca del Departament d'Economia i Coneixement de la Generalitat de Catalunya i del Fons Social Europeu.

I am also thankful to the members of staff in the Department, in particular to Professor Enrique Mirambell and Dr. Rolando Chacón for their valuable advice and opinion, and my colleague Itsaso Arrayago for her help and for making our room an ideal working environment.

Very special thanks are due to Leroy Gardner, Professor at Imperial College London, who let me contribute with his intrepid team during my stay there. I am extremely grateful to him for his patience, kindness, generous guidance and the welcomes I got during my visits after my stay in London. The thanks are also extended to Jonathan Gosaye Fida Kaba, Dr Andrew Liew, Dr Andrew Foster, May Su, Dr Huanxin Yuan and Ou Zhao for making my research time there a very nice and memorable experience.

It was a pleasure for me to work in collaboration with Asko Talja and Petr Hradil from VTT Technical Research Centre of Finland to whom I would also like to express my sincere gratitude for their expert advice and contribution in this research.

The support of the technicians of the Laboratori de Tecnologia d'Estructures Luís Agulló at the Department of Construction Engineering, which was essential to undertake the experimental part of this thesis, is also acknowledged.

The list of people I would like to thank for accompanying me alongside this trip is numberless and includes all the friends I met before and during my undergraduate and postgraduate studies. A person I believe he deserves to be mentioned is Marios for his continuous encouragement and affection which helped me to have all the endurance and patience I needed.

Last, yet above all, I would like to express my deepest thankfulness to my parents and my brother for their continuous support and unconditional love without which, my achievements at all levels would have never been possible. I would like to dedicate to them the completion of my thesis with all my love.



---

**CONTENTS**

<b>ABSTRACT .....</b>	<b>3</b>
<b>ACKNOWLEDGEMENTS .....</b>	<b>5</b>
<b>CONTENTS .....</b>	<b>7</b>
<b>NOTATION .....</b>	<b>13</b>
<b>CHAPTER 1 – Introduction.....</b>	<b>21</b>
1.1 Background.....	21
1.2 Applications of stainless steel in construction.....	23
1.3 Behaviour of cold-formed stainless steel sections.....	24
1.3.1 Material modelling of stainless steel.....	24
1.3.2 Cold-formed products .....	26
1.3.3 Web crippling .....	28
1.3.3 Local buckling .....	29
1.4 Aims and objectives of the thesis .....	30
1.5 Thesis Outline .....	31
<b>CHAPTER 2 – Study of web crippling in cold-formed ferritic stainless steel sections.....</b>	<b>35</b>
Abstract.....	35
Highlights.....	35
Keywords .....	35
2.1 Introduction.....	36
2.1.1 Background.....	36
2.1.2 Literature review.....	37
2.1.3 EN 1993-1-3 (2006).....	38
2.2 Numerical model.....	39
2.2.1 Numerical test arrangement .....	39
2.2.2 Modelling parameters .....	40
2.2.3 Finite element model validation .....	42
2.3 Sensitivity study.....	44
2.3.1 Introduction.....	44
2.3.2 Results and comparison with EN 1993-1-3 (2006) .....	45
2.3.3 Material influence .....	49
2.3.4 Internal radius influence .....	49



## CONTENTS

---

2.3.5 Bearing length influence .....	50
2.3.6 New proposal .....	51
2.4 Parametric study .....	51
2.4.1 Introduction.....	51
2.4.2 Coefficients adjustment .....	52
2.4.3 Comparison between numerical and analytical predictions .....	53
2.5 New proposal validation with experimental results.....	55
2.6 Conclusions.....	57
Acknowledgments .....	58
Appendix 2.A.....	59
2.A.1 IOF models for SHS and RHS .....	60
2.A.2 IOF models for hat sections .....	61
2.A.3 EOF models for SHS and RHS .....	63
2.A.4 EOF models for hat sections .....	65
<b>CHAPTER 3 – Statistical evaluation of a new resistance model for cold-formed stainless steel cross-sections subjected to web crippling .....</b>	<b>67</b>
Abstract.....	67
Keywords .....	67
3.1 Introduction.....	68
3.2 Existing design guidance .....	69
3.2.1 European design rule EN 1993-1-3 (2006).....	69
3.2.2 SEI/ASCE 8-02 American standard .....	71
3.3 Summary of the proposed web crippling resistance function for stainless steel cross-sections .....	71
3.4. Statistical analysis.....	74
3.4.1 Annex D of EN 1990 .....	74
3.4.2 Adaptation of the procedure to a numerical database.....	75
3.5 Numerical analyses .....	76
3.5.1 Available numerical database .....	76
3.5.2 Parametric study .....	76
3.6. Results of the statistical evaluation.....	78
3.6.1 General.....	78
3.6.2 Estimation of $V_{FEM}$ .....	78
3.6.3 Resulting partial safety factors .....	79

3.6.4 Recalibration of the proposed resistance function .....	83
3.7 Validation of the revised design equation with experimental results .....	84
3.8 Conclusions.....	86
Acknowledgments .....	87
Appendix 3.A.....	87
<b>CHAPTER 4 – Strength curves for web crippling design of cold-formed stainless steel hat sections.....</b>	<b>93</b>
Abstract.....	93
Highlights.....	93
Keywords .....	93
4.1 Introduction.....	94
4.2 Current design equations .....	100
4.2.1 EN 1993-1-3 .....	100
4.2.2 ASCE standard SEI/ASCE 8-02 .....	101
4.3 Numerical modelling .....	102
4.3.1 Modelled tests .....	102
4.3.2 Mesh and material.....	103
4.3.3 Boundary conditions and loading .....	104
4.3.4 Verification of the numerical model.....	104
4.3.5 Cross-section geometries and load configurations for the parametric study ...	106
4.4 Strength curves controlled by slenderness-based functions.....	107
4.4.1 Basis of the method.....	107
4.4.2 Data required for the design method.....	108
4.4.3 Results from the analyses.....	108
4.5 Proposed strength curves and predictive models .....	110
4.5.1 Predictive model for $R_{w,cr}$ .....	110
4.5.2 Predictive model for $R_{w,pl}$ .....	112
4.5.3 Proposed strength curves and statistical validation .....	114
4.5.4 Comparison with numerical data and design models .....	117
4.6. Validation of the design approach with test data .....	118
4.7 Conclusions.....	120
Acknowledgements.....	121
<b>CHAPTER 5 – Material and local buckling response of ferritic stainless steel sections.....</b>	<b>123</b>

## CONTENTS

---

Abstract.....	123
Highlights.....	124
Keywords .....	124
5.1 Introduction.....	125
5.2 Material response.....	126
5.2.1 Material modelling.....	126
5.2.2 Collection of experimental data.....	127
5.2.3 Assessment of the predictive expression for $\epsilon_u$ .....	128
5.3 Numerical modelling of ferritic stainless steel cross-section behaviour .....	129
5.3.1 Introduction.....	129
5.3.2 FE model.....	130
5.3.3 Validation of the FE model.....	131
5.3.4 Parametric studies .....	134
5.4 Analysis of cross-section resistance results .....	135
5.4.1 General.....	135
5.4.2 Class 3 slenderness limit and effective width formulation .....	135
5.4.3 Class 2 and Class 1 slenderness limits.....	139
5.5 The Continuous Strength Method.....	141
5.5.1 General.....	141
5.5.2 CSM base curve .....	142
5.5.3 CSM material model.....	143
5.5.4 CSM resistance functions .....	145
5.5.5 Comparison with design rules.....	145
5.5.6 Reliability analysis.....	147
5.6 Conclusions.....	148
Acknowledgements.....	149
<b>CHAPTER 6 – Experiments on cold-formed ferritic stainless steel slender sections</b> .....	<b>151</b>
Abstract.....	151
Highlights.....	151
Keywords .....	151
6.1 Introduction.....	152
6.2 Experimental investigation .....	153
6.2.1 Introduction.....	153

---

6.2.2 Material tests .....	154
6.2.3 Stub Column tests .....	156
6.2.4 Beam tests .....	159
6.3 Analysis of results and design recommendations .....	165
6.3.1 General .....	165
6.3.2 Assessment of Class 3 slenderness limit and cross-section resistance .....	166
6.3.2.1 Elements in compression .....	166
6.3.2.2 Elements in bending .....	170
6.3.3 Assessment of Class 2 and 1 slenderness limits .....	171
6.3.3.1 Elements in compression .....	171
6.3.3.2 Elements in bending .....	172
6.4 Conclusions .....	173
Acknowledgements .....	174
<b>CHAPTER 7 – Effective width equations accounting for element interaction for cold-formed stainless steel square and rectangular hollow sections .....</b>	<b>175</b>
Abstract .....	175
Highlights .....	175
Keywords .....	175
7.1 Introduction .....	176
7.2 Numerical investigation .....	177
7.2.1 Modelled stub column tests .....	177
7.2.2 Finite element model .....	180
7.2.3 Validation of the numerical model .....	182
7.2.4 Parametric studies .....	184
7.3 Methods for cross-section design and discussion of results .....	185
7.3.1 General .....	185
7.3.2 Available methods for cross-section design .....	186
7.3.2.1 The effective width method .....	186
7.3.2.2 The regression analysis design method .....	187
7.3.2.3 The direct strength method (DSM) .....	188
7.3.2.4 The effective cross-section method .....	189
7.3.3 Assessment of the design methods .....	190
7.3.3.1 Methods based on plate width .....	190
7.3.3.2 Regression analysis method .....	191

## CONTENTS

---

7.3.3.3 Methods based on gross cross-section .....	192
7.3.3.4 Discussion .....	194
7.4 Proposed design approach allowing for the benefits of element interaction .....	194
7.4.1 Development of the Class 3 limit as a function of the aspect ratio .....	195
7.4.2 Incorporation of the aspect ratio $\alpha$ within the reduction factor $\rho$ .....	196
7.4.3 Reliability analysis.....	197
7.4.4 Applicability of the method to the generated models and other stainless steel	197
7.5 Conclusions.....	198
Acknowledgements.....	199
<b>CHAPTER 8 – Conclusions and suggestions for future research.....</b>	<b>201</b>
8.1 Conclusions.....	201
8.2 Suggestions for further research .....	206
<b>REFERENCES .....</b>	<b>209</b>

---

**NOTATION**

## Latin

A	Gross cross-sectional area
$A_c$	Cross-sectional area of the material coupon
$A_{eff}$	Effective cross-sectional area
$A_r$	Area of the corner
B	Overall section breadth
b	Section breadth
b	Mean value of the correction factor
$b_f$	Flange breadth between the midlines of the webs
$C_1$	Coefficient for web crippling design given in SEI/ASCE 8-02
$C_2$	Coefficient for web crippling design given in SEI/ASCE 8-02
$C_3$	Coefficient for web crippling design given in SEI/ASCE 8-02
$C_4$	Coefficient for web crippling design given in SEI/ASCE 8-02
$C_0$	Coefficient for web crippling design given in SEI/ASCE 8-02
CHS	Circular hollow section
CSM	Continuous strength method
COV	Coefficient of variation
CUFSM	Cornwell University finite strip method
c	Section lip or Flat portion of plate width defined in EN 1993-1-4
$c_f$	Flat width of the flange
$c_w$	Flat width of the web
DSM	Direct strength method
E	Young's modulus
EOF	Exterior one-flange
ETF	Exterior two-flange
$E_{0,LVDT}$	Young's modulus measured by the LVDTs
$E_{0,true}$	Young's modulus measured by the strain gauge
$E_{0.2}$	Tangent modulus at the 0.2% proof stress $\sigma_{0.2}$
$E_{sh}$	Strain hardening slope
e	Clear distance between the load and the end support in EOF
FE	Finite element

## NOTATION

---

$F_{Ed}$	Applied local load or support reaction
$F_{u,num}$	Ultimate achieved local load or support reaction in the FE model
$F_{u,test}$	Ultimate applied local load or support reaction in the test
$f_{yb}$	Basic yield strength
GMNIA	Geometrical and material nonlinear imperfection analysis
$g_{rt}(\underline{X}_m)$	Resistance function (of the mean values of the basic variables $\underline{X}_m$ ) used as the design model
H	Overall section height
HSA	High strength austenitic
h	Section height
$h_w$	Web height between the midlines of the flanges
I	Second moment of area
IOF	Interior one-flange
ITF	Interior two-flange
$k_F$	Dimensionless buckling coefficient
$k_{d,n}$	Design fractile factor
$k_n$	Characteristic fractile factor
$k_\infty$	Characteristic fractile factor for a $\infty$ number of tests/numerical results
$k_{d,\infty}$	Design fractile factor for a $\infty$ number of tests/numerical results
$k_\sigma$	Plate buckling coefficient given in EN 1993-1-5
L	Length
$L_s$	Span
LEA	Linear elastic analysis
LVDT	Linear variable differential transformer
$l_{IOF}$	Span of the member subjected to IOF
$l_a$	Effective bearing length
$l_y$	Yield line length
M	Bending moment
$M_{BD,exp}$	Test ultimate moment capacity
$M_{BD,num}$	Numerical ultimate moment capacity
$M_{Ed}$	Applied bending moment
$M_{c,Rd}$	Cross-section design moment capacity
$M_{el}$	Elastic moment capacity

---

$M_{osr}$	Material over-strength
$M_{pl}$	Plastic moment capacity
$M_{pl,ly}$	Plastic hinge per unit length along the yield line
$M_u$	Ultimate moment capacity
$M_{u,FE}$ or $M_{u,num}$	Numerical ultimate moment capacity
$M_{u,test}$	Test ultimate moment capacity
$M_{u,pred}$	Predicted moment capacity
$M_{y,csm,Rk}$	CSM cross-section characteristic bending moment resistance about the y-y axis
$M_{z,csm,Rk}$	CSM cross-section characteristic bending moment resistance about the z-z axis
$m$	Compound Ramberg-Osgood strain hardening exponent – between $\sigma_{0.2}$ and $\sigma_u$ or material parameter for web crippling
$N$	Axial load
$NA$	Neutral Axis
$N_y$	Yield load
$N_u$	Ultimate compressive load
$N_{u,FE}$ or $N_{u,num}$	Numerical ultimate compressive load capacity
$N_{u,test}$	Test ultimate load capacity
$N_{u,pred}$	Predicted compressive load capacity
$N_{csm,Rk}$	CSM predicted cross-section characteristic compression resistance
$n$	Ramberg-Osgood strain hardening exponent or number of tests/numerical simulations
$n_w$	Number of webs within the cross-section
$R$	Cross-section rotation capacity or external corner radius
$RFCS$	Research fund for coal and steel
$R_{Ed}$	Local transverse resistance
$R_{u,num}$	Numerical cross-section rotation capacity
$R_{u,num}$	Web crippling resistance of the cross-section
$R_{u,test}$	Test cross-section rotation capacity
$R_{WC-BD}$	Reduced web crippling design resistance due to interaction with bending
$R_{WC,exp}$	Test web crippling resistance

---



## NOTATION

---

$R_{w,Rd}$	Web crippling design resistance sum of individual webs
$R_{w,Rk}$	Web crippling characteristic resistance
$R_{w,cr}$	Elastic critical buckling resistance for web crippling per web
$R_{w,pl}$	Plastic resistance for web crippling per web
$R_{w,u}$	Web crippling resistance per web
$R_{w,u,ASCE}$	ASCE predicted web crippling resistance
$R_{w,u,EC}$	Eurocode predicted web crippling resistance
$R_{w,u,test}$	Test web crippling resistance
$R_{w,u,num}$	Numerical web crippling resistance
$R_{w,u,\chi-\lambda}$	Approach based on strength curves web crippling resistance
$R_{w,cr,num}$	Numerical critical resistance for web crippling
$R_{w,cr,pred}$	Predictive model for the critical web crippling resistance
$R_{w,pl,num}$	Numerical plastic resistance for web crippling
$R_{w,pl,pred}$	Predictive model for the plastic web crippling resistance
$r_d$	Design value of the resistance
$r_e$	Experimental/numerical values of the resistance
$r_{e,i}$	Experimental/numerical value of the resistance for specimen i
$r_{FEM,i}$	Numerical value of the resistance for specimen i
$r_i$	Internal radius of the corners
$r_k$	Characteristic value of the resistance
$r_m$	Corner radius of the midline cross-section
$r_n$	Nominal value of the resistance
$r_t$	Theoretical values determined from the resistance function
$r_{t,i}$	Theoretical value determined from the resistance function for specimen i
$R^2$	Squared correlation coefficient
RHS	Rectangular hollow section
SAFSS	Structural applications of ferritic stainless steel
s	Estimated value of the standard deviation $\sigma$
$S_\Delta$	Estimated value of $\sigma_\Delta$
$S_{\Delta,FEM}$	Estimated value of $\sigma_{\Delta,FEM}$
$S_s$ or $S_{sL}$	Bearing length
$S_{sa}$ or $S_{sb}$	Length of the support
SHS	Square hollow section

---

---

$t$	Thickness
$u_{av}$	Average of the deflections
$u_i$	Deflection at the point $i$
$u_{ms}$	Deflection at mid-span
$V_{FEM}$	Coefficient of variation of the numerical model
$V_r$	Combined coefficient of variation
$V_{rt}$	Coefficient of variation of the resistance function
$V_{X,i}$	Coefficient of variation of $X_i$
$V_\delta$	Estimator for the coefficient of variation of the error term $\delta$
$w_0$	Local imperfection amplitude
$W_{el}$	Elastic section modulus
$W_{el,y}$	Elastic section modulus about the y-y axis
$W_{el,z}$	Elastic section modulus about the z-z axis
$W_{pl}$	Plastic section modulus
$W_{pl,y}$	Plastic section modulus about the y-y axis
$W_{pl,z}$	Plastic section modulus about the z-z axis
$X_i$	Basic variables of a design model
$\underline{X}_m$	Array of mean values of the basic variables
Greek	
$\alpha$	Web crippling dimensionless coefficient
$\alpha$	Aspect ratio
$\alpha_f$	Flange slenderness parameter
$\alpha_w$	Web slenderness parameter
$\beta$	Web crippling dimensionless coefficient
$\gamma_{M0}$	Partial safety factor for resistance of cross-sections to excessive yielding including local buckling given in EN 1993-1-4 (2006)
$\gamma_{M1}$	Partial safety factor for resistance of members to instability assessed by member checks given in EN 1993-1-4
$\gamma_M^*$	Corrected partial safety factor
$\bar{\Delta}$	Estimated value for $E(\Delta)$
$\bar{\Delta}_{FEM}$	Estimated value for $E(\Delta_{FEM})$
$\Delta_i$	Logarithm of the error for specimen $i$

---

## NOTATION

---

$\Delta_{FEM,i}$	Logarithm of the error for the modelled specimen i
$\delta$	Web crippling dimensionless coefficient
$\delta$	End-shortening
$\delta_{FEM,i}$	Observed error term for numerical specimen i
$\delta_{LVDT}$	LVDT end-shortening
$\delta_i$	Observed error term for test/numerical specimen i
$\delta_{platen}$	End platen deformation
$\delta_u$	End shortening at ultimate load
$\varepsilon$	Strain or EN 1993-1-4 material parameter
$\varepsilon_{0.2}$	Total strain at the 0.2% proof stress $\sigma_{0.2}$
$\varepsilon_{CSM}$	CSM predicted failure strain of cross-section
$\varepsilon_{max}$	Strain at maximum stress point
$\varepsilon_{nom}$	Nominal (engineering) strain
$\varepsilon_{pl,true}$	Logarithmic plastic strain
$\varepsilon_u$	Ultimate strain at ultimate stress $\sigma_u$
$\varepsilon_y$	Material yield strain
$\theta$	Rotation
$\theta_{pl}$	Elastic portion of the moment-rotation diagram measured at mid-span corresponding to the plastic moment
$\theta_u$	Rotation of the moment-rotation diagram measured at mid-span at the point at which the diagram falls below the plastic moment
$\kappa$	Sectional curvature
$\kappa_{pl}$	Elastic portion of the moment-curvature diagram measured at mid-span corresponding to the plastic moment
$\kappa_u$	Curvature of the moment-curvature diagram measured at mid-span at the point at which the diagram falls below the plastic moment
$\bar{\lambda}$	Relative slenderness
$\bar{\lambda}_{CS}$	Non-dimensional slenderness of the cross-section
$\bar{\lambda}_p$	Non-dimensional plate slenderness
$\bar{\lambda}_{p,f}$	Flange non-dimensional plate slenderness
$\bar{\lambda}_{p,w}$	Web non-dimensional plate slenderness
$\nu$	Poisson's ratio

---

$\xi$	Web crippling dimensionless coefficient
$\rho$	Effective-width reduction factor
$\Sigma$	Summation
$\sigma$	Standard deviation
$\sigma$	Stress
$\sigma_{0.2}$	Material 0.2% yield proof stress
$\sigma_{0.2 \text{ nom}}$	Nominal value of $\sigma_{0.2}$
$\sigma_{0.01}$	Material 0.01% proof stress
$\sigma_{0.05}$	Material 0.05% proof stress
$\sigma_{LB}$	Stress at which local buckling occurs
$\sigma_{c,0.2}$	Material 0.2% yield proof stress at the corner region
$\sigma_{cr}$	Elastic buckling (critical) stress of the cross-section plate
$\sigma_{cr,cs}$	Elastic buckling (critical) stress of the gross cross-section
$\sigma_{csm}$	CSM predicted failure stress
$\sigma_{max}$	Stress at maximum stress point
$\sigma_{nom}$	Nominal (engineering) stress
$\sigma_{true}$	True stress
$\sigma_u$	Ultimate tensile stress
$\sigma_{\Delta}$	Variance of the term $\Delta$
$\sigma_{\Delta, FEM}$	Variance of the term $\Delta_{FEM}$
$\phi$	Relative angle between the web and the flange
$\phi_b$	Resistance factor for bending given in SEI/ASCE 8-02
$\phi_w$	Resistance factor for web crippling given in SEI/ASCE 8-02
$\phi(\alpha)$	Function of the aspect ratio $\alpha$
$\chi$	Web crippling reduction factor



### **1.1 Background**

Ever since its origins in the cutlery industry, stainless steels have been continuously expanding their domain of applications due to their favourable characteristics, with corrosion resistance being one of its major strengths. It is more than one hundred years since the discovery and commercialization of stainless steel in 1912 and as part of the centenary celebrations, special edition books and issues have been commissioned telling the history and story of Harry Brearley's fingerprint (Baddoo (2013), Fielder (2013)).

Stainless steel is a family of iron based alloys with a minimum chromium content of 10.5% by mass which forms a passivation layer of chromium oxide ( $\text{Cr}_2\text{O}_3$ ) when exposed to oxygen. This layer, which possesses the ability of self-repairing, protects the underlying metal surface from further reaction with the environment thereby preventing corrosion and oxidation, and reducing the necessity of continuous maintenance. Hence, despite the initial material cost of stainless steels compared with carbon steel, this is often offset when costs are considered on a whole-life basis (Gardner et al. (2007)). The addition of other alloy elements such as nickel, molybdenum, titanium and chromium,

to the iron-chromium primary alloy enhances certain properties to meet the needs for its specific use which nowadays include structural, industrial, automotive and aerospace applications and products. Stainless steels are classified according to their metallurgical structure into five main groups, namely austenitic, ferritic, duplex (austenitic-ferritic), martensitic and precipitation hardening, see Fig. 1.1. Moreover, there are various stainless steel grades featuring different mechanical properties and characteristics within each group and various designation systems such as the German (DIN) and the US (AISI). The designation system given in EN 10088-1 (2005) and used in the part of Eurocode dealing with the structural design of stainless steels, EN 1993-1-4 (2006) is adopted herein, see Table 1.1.

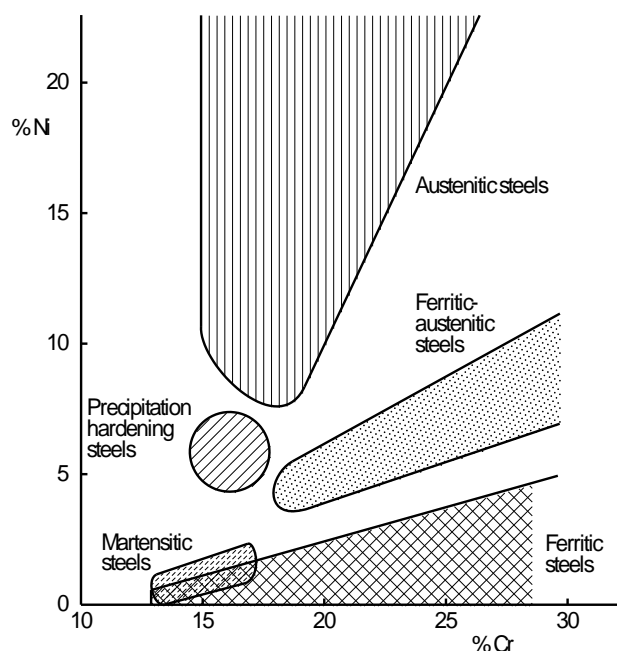


Fig. 1.1 Classification of stainless steels according to nickel and chromium (Euro Inox (2006))

Austenitic and duplex (ferritic-austenitic in Fig. 1.1) steels, which are chromium-nickel based alloys, have been widely used in the construction industry as they provide a good combination of corrosion resistance, forming and fabrication properties, and they have also been the most widely studied and verified for structural applications. However, their initial material cost has been dramatically increasing and fluctuating over the last years owing to the high volatile price of nickel which has led to look for other alternatives. It is therefore when the interest in ferritic steels arose as they are mainly chromium based alloys with no or very low nickel content. Sharing many properties of austenitic and duplex steels such as strength and durability, ferritic steels offer a very competitive solution with low expense and price-stability.

Table 1.1 Grades already in EN 1993-1-4

Type of steel	Designation grade
Ferritic steels	EN 1.4003, EN 1.4016 and EN 1.4512
Basic austenitics	EN 1.4301, EN 1.4306, EN 1.4307, EN 1.4311, EN 1.4318 and EN 1.4541
Moly austenitics	EN 1.4401, EN 1.4404, EN 1.4406, EN 1.4432, EN 1.4435, EN 1.4439, EN 1.4539 and EN 1.4571
Super austenitics	EN 1.4529 and EN 1.4547
Duplex steels	EN 1.4362 and EN 1.4462

Although three typical ferritic grades (EN 1.4003, EN 1.4016 and EN 1.4512) are already included in EN 1993-1-4 (2006), which was derived almost exclusively from work on austenitic and duplex steels, many aspects of the code are yet to be verified for application to those ferritic grades. Moreover, in many cases, ferritic-specific guidance is missing in EN 1993-1-4 (2006) referring to a number of clauses in other parts of Eurocode 3 such as EN 1993-1-2 (2005) for fire design, EN 1993-1-3 (2006) for cold-formed members and sheeting, EN 1993-1-8 (2005) for design of joints, EN 1993-1-9 (2005) for fatigue strength of steel structures and EN 1993-1-10 (2005) for selection of steel for fracture toughness and through-thickness. It is in this context when a Research Found for Coal and Steel (RFCS) project of the European Commission under the acronym SAFSS (Structural Applications of Ferritic Stainless Steels) comprising a large consortium of universities, research centres as well as design offices and steel manufacturers (Cashell and Baddoo (2014)), and a National Project of the Ministerio de Ecomía y Competitividad of Spain entitled “Estudio del comportamiento de estructuras de acero inoxidable ferrítico” began to provide further feedback on the structural response of ferritic stainless steels.

## 1.2 Applications of stainless steel in construction

Traditionally, stainless steel has been employed in landmark structures owing to its appearance. The most iconic examples include the Chrysler Building in New York completed in 1936 with its shinning roof shown in Fig 1.2 (a), the Atomium in Brussels constructed for the 1958 Brussels World’s Fair and the Gateway Arch in St. Louis erected in 1965 as a monument to the westward expansion of the United States. More recent examples of structures are the Walt Disney Concert Hall in Los Angeles clad with stainless steel and the Helix pedestrian bridge in Singapore shown in Fig. 1.2 (b).

Note that all those examples display for viewing all the stainless steel components which is a clear evidence of the importance given to the attractive appeal possessed by this material. A major obstacle for its application as a primary structural element in



conventional construction during last years was the lack of comprehensive guidance on design with stainless steel. Moreover, the numerous grades and types prevent structural engineers to make a straightforward choice; hence, and since material selection is often based on previous experience, they tend to the typical carbon steel solution.



Fig. 1.2 Iconic examples of applications of stainless steel

Stainless steel is a well suited choice to use in construction when durability, long lifespan, easy maintenance and aesthetic appearance are required characteristics. Stainless steel is available in various product forms including plate, sheet, tube, bar, castings, fasteners and fixings, as well as hot-rolled structural sections and cold-formed structural sections among of which this latter are the most commonly used product in structural members. It is also a safe choice for concealed structures difficult to inspect, which can be damaged by moisture if materials with lower corrosion resistance are used.

### 1.3 Behaviour of cold-formed stainless steel sections

As part of the above mentioned larger research projects, this doctoral thesis addresses the local buckling behaviour of stainless steel elements when subjected to transverse forces (web crippling) and normal stresses (local buckling).

#### 1.3.1 Material modelling of stainless steel

The material response of stainless steel displays a rounded stress-strain relationship with considerable strain hardening and ductility. Fig. 1.3 shows a comparison of the stress-strain behaviour for various stainless steel grades and highlights the differences with carbon steel which exhibits a clear elastic region and yield plateau marking its yield stress. In absence of a clear defined yield point, stainless steel yield stress is conventionally defined by a proof stress corresponding to an offset strain value of 0.2%.

Stainless steel material response also depends on the loading type exhibiting asymmetric stress-strain behaviour when loaded in tension and compression. Moreover, the orientation of the material coupon within the sheet from which it was taken, leads to anisotropic stress-strain behaviour with higher strain hardening, hence higher yield stress values, for those coupons extracted transversal to the rolling direction than that taken from the longitudinal direction.

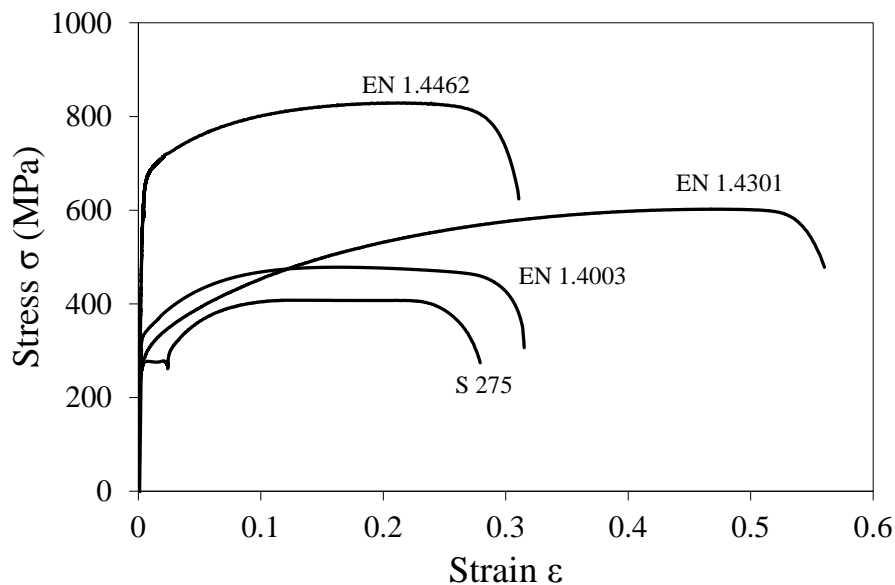


Fig. 1.3 Material behaviour for various steels

Some material models are available in the literature to replicate stainless steel material response. All of them are an evolution of the basic Ramberg-Osgood model (Ramberg and Osgood (1943)), as modified by Hill (1944) and given in Eq. (1.1) where  $\epsilon$  and  $\sigma$  are the engineering strain and stress respectively,  $E$  is the Young's modulus and  $n$  is the strain hardening exponent. This model provided very accurate predictions up to the 0.2% proof stress  $\sigma_{0.2}$  but over-estimations above this stress level. Mirambell and Real (2000) proposed an expression for stresses beyond the  $\sigma_{0.2}$  and up to the ultimate tensile stress  $\sigma_u$  given in Eq. (1.2) which significantly improved predictions and originated the family of the two-stage Ramberg-Osgood models followed by Rasmussen (2003), Gardner and Nethercot (2004a) and Gardner and Ashraf (2006). Three-stage and multi-stage full-range stress-strain models were also proposed by Quach et al. (2008) and Hradil et al. (2013), respectively. In Eq. (1.2),  $\epsilon_{0.2}$  is the total strain at the 0.2% proof stress,  $\epsilon_u$  is the ultimate strain corresponding to the ultimate stress  $\sigma_u$ ,  $E_{0.2}$  is the tangent modulus at the 0.2% proof stress point and  $m$  is the second strain hardening parameter.

Rasmussen's modification of Mirambell and Real model was adopted in EN 1993-1-4 (2006) and it is used in the present study.

$$\varepsilon = \frac{\sigma}{E} + 0.002 \left( \frac{\sigma}{\sigma_{0.2}} \right)^n \quad \text{For } \sigma \leq \sigma_{0.2} \quad (1.1)$$

$$\varepsilon = \frac{\sigma - \sigma_{0.2}}{E_{0.2}} + \left( \varepsilon_u - \varepsilon_{0.2} - \frac{\sigma - \sigma_{0.2}}{E_{0.2}} \right) \left( \frac{\sigma - \sigma_{0.2}}{\sigma_u - \sigma_{0.2}} \right)^m + \varepsilon_{0.2} \quad \text{For } \sigma < \sigma_{0.2} < \sigma_u \quad (1.2)$$

Note that the given equations and actually, the above mentioned material models, express strains as a function of the stresses but in some cases, an explicit formula with stresses as a function of strains is required. Abdella provided an explicit equation for the Mirambell and Real (2000) and Gardner and Ashraf (2006) material model (Abdella (2006, 2007)).

EN 1993-1-4 (2006) gives typical values of E, n,  $\sigma_{0.2}$  and  $\sigma_u$  for various stainless steel grades, as gathered in Table 1.2, that combined with the material model are used to trace the analytical stress-strain relationship. Studies conducted by Arrayago et al. (2014) undertook a revision of the material parameters involved in material modelling.

Table 1.2 Overview of material properties for selected stainless steel grades in EN 1993-1-4 (2006)

Grade	Type	E (GPa)	n	$\sigma_{0.2}$ (MPa)	$\sigma_u$ (MPa)
EN 1.4301	Austenitic	200	6-8	190-230	500-540
EN 1.4401	Austenitic	200	7-9	200-240	500-530
EN 1.4513	Ferritic	220	9-16	210	380
EN 1.4003	Ferritic	220	7-11	260-280	450
EN 1.4016	Ferritic	220	6-14	240-260	400-450
EN 1.4462	Duplex	200	5	450-480	640-660

### 1.3.2 Cold-formed products

The production route of cold-formed products affects the material properties of the sheet material used for cold-forming increasing anisotropy and non-symmetry, and changes the internal stress state of the product owing to the induced plastic deformations. Sheet material is produced through a temper rolling or stretching (cold-working) process and it is often delivered in the annealed condition so that it can be cut and shaped more easily. The sheet material is next coiled for storage and uncoiled to be levelled and processed. A cold-forming technique shapes the final cross-sectional form of the product, of which press-braking and cold-rolling are the most used. Typical examples of

cold-formed sections include square hollow sections (SHS), rectangular hollow sections (RHS), channels, lipped channels, I-sections, circular hollow sections (CHS), hat sections, Z-sections, linear trays and sheeting profiles among others.

This manufacturing process alters the stress state in the longitudinal and transversal direction of the product inducing membrane and bending residual stresses, and cause plastic deformations leading to a strength enhancement of the flat regions and corners of the cross-sections.

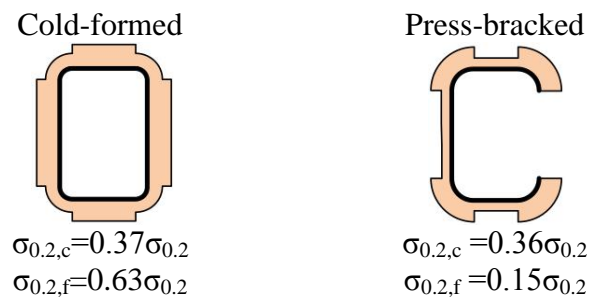


Fig. 1.4 Stress patterns for bending residual stresses. Cruise and Gardner (2008a)

Patterns of residual stresses for austenitic stainless steel sections were proposed by Cruise and Gardner (2009), as shown in Fig. 1.4, while their influence on the structural response was conducted by Jandera et al. (2008). Regarding strength enhancements, notable first studies include those conducted by Coetzee et al. (1990) on press-braked austenitic and ferritic lipped channel sections and Van den Berg and Van der Merwe (1992) where a predictive model for strength enhancement of corner properties was developed. More recent studies worth of mentioning are Ashraf et al. (2005) proposal based on all collated data on stainless steel, the revised models proposed by Cruise and Gardner (2008b) shown in Fig. 1.5, a more theory-based approach developed by Rossi (2008) and the upgrades conducted by Rossi et al. (2013) based on a large test programme.



Fig. 1.5 Stress patterns for strength enhancement in corners. Cruise and Gardner (2008b)

### 1.3.3 Web crippling

Cold-formed sections comprise thin-walled plated elements which are hence susceptible to local buckling when subjected to high stresses. Web crippling is a form of localised buckling that occurs at points of concentrated transverse loads or supports where stresses are excessive. It is often observed, for instance, in secondary structural elements of warehouses such as cladding rails, Fig. 1.6 (a), and in roof decking and trays spanning across multibeam systems, Fig. 1.6 (b). The nature of the cross-section and its geometry defines the failure mode exhibiting typical patterns of web buckling, web crippling and often a combination of both of them. This condition can reduce the load carrying capacity of flexural members as the bearing capacity is governed by the web crippling resistance. Fig. 1.7 shows the load locations and load conditions where this failure mechanism is triggered (Winter and Pian (1946)). Fig. 1.8 shows the typical failure mode observed for a hat section when subjected to internal support reaction applied through one flange (IOF).



Fig. 1.6 (a) Hat sections about to bear roof in a warehouse; (b) Structural roof deck

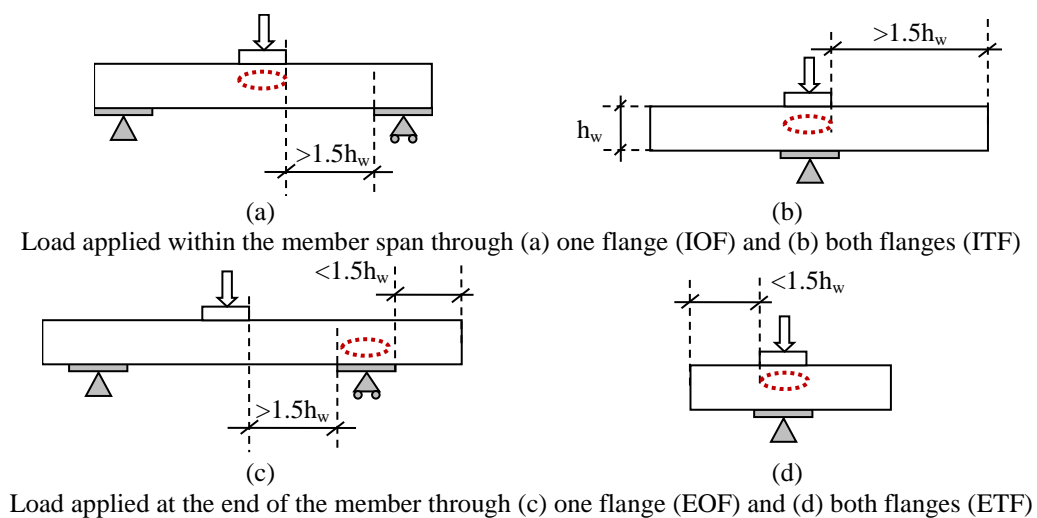


Fig. 1.7 Definition of load cases where web crippling occurs

Traditionally, web crippling has been experimentally investigated since 1950s while the first numerical studies date from the mid 1980s undertaken by Santaputra (1986) and Sharp (1989, 1990) on carbon steel. This slot in time was a consequence of the complex geometrical and physical nonlinearities of the problem which resulted in unfeasible simulations owing to the long required computational time (Sivakumaran (1989), Bakker (1992)). The advancements in computer and numerical modelling softwares overcame this limitation during late 1990s early 2000s when first web crippling parametric studies were conducted (Hofmeyer (2000)). The web crippling structural response has been successfully replicated in various numerical studies including Xiao et al. (2002), Ren et al. (2006), Kaitila (2004), Macdonald and Heiyantuduwa (2012) and Natário et al. (2014) for carbon steel and Zhou and Young (2007b) for stainless steel.

While web crippling behaviour of structural carbon steel members has been widely experimentally investigated, for stainless steel, the available test data is rather limited and confined to certain cross-section geometries and load cases. Consequently, specific guidance for web crippling design of stainless steel members is missing in EN 1993-1-4 (2006) and design provisions for cold-formed carbon steel members and sheeting must be used instead. Those are codified in section 6.1.7 of EN 1993-1-3 (2006) where various empiric equations derived through multi-linear analyses of geometrical parameters for a given cross-section geometry and load case are given. Chapters 2 to 4 address the design of stainless steel members subjected to web crippling where an overview of available research is also provided.

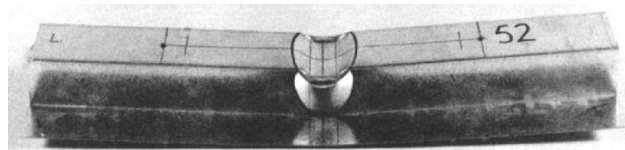


Fig. 1.8 Web crippling failure mode, Bakker and Stark (1994)

### 1.3.3 Local buckling

Thin-walled elements comprising cold-formed sections may buckle prematurely owing to their slenderness nature when subjected to compression, see Fig. 1.6 (a) and (b). This phenomenon is called local buckling and may take place before the attainment of the yield point, or 0.2% proof stress for stainless steel. When local buckling is triggered, the plated elements comprising the cross-section change their shape but the whole cross-section remains in the position, see Fig. 1.6 (c). Once such plated elements achieve the

local buckling stress, they will not necessarily fail and they often will continue to carry increasing loads in excess of that at which local buckling first occurs. Thus, local buckling is allowed in cross-section design as long as the reduction in capacity of the cross-section due to it is considered.

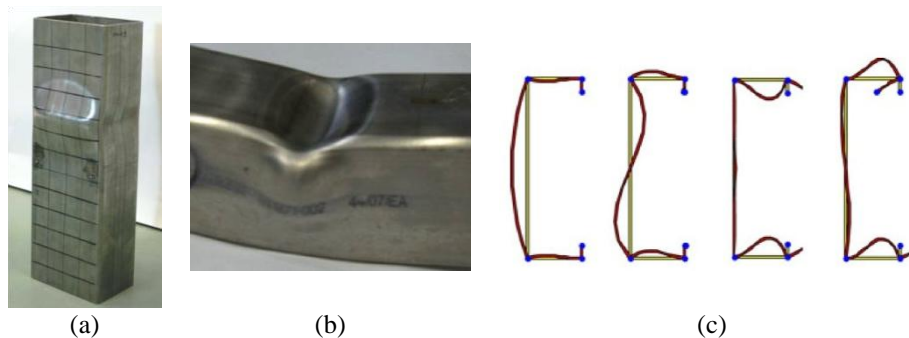


Fig. 1.6 (a) local buckling of compression member, Afshan and Gardner (2013a), (b) local buckling of flexure member, Gardner and Theofanous and Gardner (2010) and (c) Local buckling failure modes, Ádány and Schafer (2008),

The European structural stainless steel design standard, EN 1993-1-4 (2006), accounts for the effects of local buckling through the cross-section classification concept, adapted from EN 1993-1-1 (2006) which deals with carbon steel design, to consider the tendency of the section to locally buckle and uses the effective width method to determine the cross-section resistance. Alternative design approaches have also been developed during recent years in order to increase design efficiency such as the continuous strength method (CSM) proposed by Gardner (2008), the direct strength method (DSM) introduced by Schafer (2008) and adapted for stainless steel by Becque et al. (2008), the regression analysis method developed by Kato (1989) and modified by Theofanous and Gardner (2011) for application to stainless steel and Zhou et al. (2013) approach. However, the current scope of these design methods requires a formal verification and an assessment of their performance for application to ferritic stainless steel as some of them were developed for other materials and/or other stainless steel grades. This is conducted in chapters 5 to 7 where more details regarding numerical modelling and cross-section design are provided and discussed.

### 1.4 Aims and objectives of the thesis

Building on that web crippling provisions are missing in EN 1993-1-4 (2006), one of the aims of this doctoral thesis is to do research on the web crippling of stainless steel members through numerical modelling supported by experimental testing collected

from the literature to develop comprehensive design guidance for application to stainless steel. Within this context, the American design standard SEI/ASCE 8-02 (2002) has also been considered.

The second aim is to assess the applicability the cross-section classification limits and the effective width equations for slender sections given in EN 1993-1-4 (2006) to ferritic stainless steel. Building on existing tests, experimental testing and numerical modelling, appropriate revisions and design recommendations, when required, are given. Moreover, various alternative methods for cross-section design are also considered as they were developed for other stainless steel types or required to extend their scope to ferritic stainless steel.

Hence, the overall objectives are:

- To collect all the data published in research Journals, generated in previous projects, and delivered by the various working groups comprising SAFSS project.
- To carry out experimental tests including the tasks involved in the pre- and post-testing process.
- To develop comprehensive numerical models to extrapolate results and explore those areas that remained unexplored experimentally.
- To compare experimental, numerical and theoretical results to derive relevant conclusions
- To develop comprehensive design guide and recommendations in accordance with the principles given in Eurocode regarding safe design.

### **1.5 Thesis Outline**

This thesis consists of 8 chapters. This first chapter provides a brief overview of stainless steel, highlights the main drawbacks when dealing with its design, particularly for ferritic steels, and establishes the purposes of this investigation. A more focused review on important topics is provided along the main body of the thesis when those have to be discussed in detail.

The main body of the thesis contains the relevant topics examined and has been divided in two parts so that the studied phenomena can be clearly differentiated. Part 1 includes chapters 2 to 4 and investigates the web crippling behaviour of stainless steel members,



while chapters 5 to 7 are focused on the local buckling response of ferritic stainless steel sections. All these chapters are presented in research paper format with their corresponding abstract, highlights when required by the Journal where these chapters were sent, keywords, main sections, conclusions and acknowledgments while the references are given at the end of the document. Details of the outline of the main sections for the chapters follow.

In Chapter 2, the influence of key geometric and material parameters on web crippling response is investigated on the basis of carefully verified FE models. A proposed equation is derived for application to stainless steel keeping the empirical nature of the expression given in EN 1993-1-3 (2006). The proposed equation covers web crippling design of SHS, RHS and hat sections.

Chapter 3 presents a statistical evaluation of the proposed equation in Chapter 2. The numerical database generated in Chapter 2 is expanded in this chapter with additional finite element models. For comparison purposes, the design provisions given in EN 1993-1-3 (2006) and in the American standard SEI/ASCE 8-02 (2002) are also assessed. Some adjustments are set out for the proposed equation.

Chapter 4 contains a more concise and descriptive literature review in a table based format and includes the existing equations for web crippling design. With a refined numerical model successfully matching experimental behavior and performance of parametric studies, this chapter closes the research conducted on web crippling deriving a new semi-empiric method based on strength-curves for stainless steel hat sections.

Chapter 5 begins with an investigation into the material response of ferritic steels giving focus to the model to predict the ultimate strain given in EN 1993-1-4 (2006). Modifications to this model are then made for application to ferritic stainless steels. A numerical investigation is also conducted to study the local buckling response of cold-formed ferritic stainless steel sections. The generated numerical models are used to assess the suitability of the slenderness limits and effective width formulae given in EN 1993-1-4 (2006) and those proposed by Gardner and Theofanous (2008) to ferritic stainless steel. Moreover, the chapter outlines the continuous strength method (CSM) and extends its applicability to cover ferritic stainless steel.

Chapter 6 describes an experimental investigation including material coupon tests, stub column tests and bending test. Tests were undertaken on grade EN 1.4003 ferritic steel square and rectangular hollow sections (SHS and RHS, respectively) sections comprising slender elements and various aspect ratios. The results are used to experimentally verify the conclusions achieved in Chapter 5 and assess the design approach proposed by Zhou et al. (2013) allowing for the element interaction effects that increase the cross-section resistance of RHS.

Complementing the laboratory testing investigation, Chapter 7 follows research developing a comprehensive numerical model to conduct parametric studies and generate further performance data on ferritic stainless steel SHS and RHS. The numerical results are used to assess the applicability of various advanced methods for the design of slender sections to ferritic stainless steel and to propose a modification of the effective width equation revised by Gardner and Theofanous (2008) so that the benefits of element interaction are explicitly considered. With this proposed modification, applicable to all stainless steel families, the effective width method is amended to the same level of those methods already accounting for element interaction.

Finally, a summary of the findings achieved in this thesis are given in Chapter 8 where suggestions for further research are also proposed.



---

**CHAPTER 2 – Study of web crippling in cold-formed ferritic stainless steel sections**

This chapter is currently available in the *Thin-Walled Structures* journal under the reference:

Bock M, Arrayago I, Real E and Mirambell (2013). Study of web crippling in cold-formed ferritic stainless steel sections. *Thin-Walled Structures*, 69, pp.29-44.

<http://dx.doi.org/10.1016/j.tws.2013.03.015>

**Abstract**

Cold-formed stainless steel members are widely used due to their high corrosion resistance and high resistance-to-weight ratio but their susceptibility to buckle implies that instability phenomena such as web crippling, where the web locally buckles due to concentrated transverse forces, must be considered. On the other hand, the emergent ferritic stainless steel has very low nickel content and therefore, they are cheaper and relatively price stable compared to austenitics and duplex. Their promising future has aimed to develop efficient design guidance and as a result, a new unified web crippling resistance expression based on numerical simulations and thereafter validated with experimental results has been proposed.

**Highlights**

- A new formula to predict web crippling resistance for stainless steels sections is proposed.
- The study is based on numerical simulations using finite element program ABAQUS which were previously validated against experimental results.
- The new equation provides more accurate results than current Eurocode formula.
- Other comparisons with different web crippling Eurocode formulae are also presented.

**Keywords**

Web crippling, concentrated forces, ferritic stainless steel, cold-formed sections.

## **2.1 Introduction**

### **2.1.1 Background**

Cold-formed elements are made up from thin sheets and therefore susceptible to buckling phenomena due to their high slenderness. Web crippling is a form of localized buckling that occurs in a cold-formed steel section at points of concentrated loads or supports where stresses are excessive. The theoretical analysis of cold-formed elements subjected to web crippling is very complex because it involves a large number of factors, Yu and LaBoube (2010). For that reason, most of the carried out research have been based on curve-fitting of experimental and numerical results and therefore, current web crippling design specifications are generally conservative and confined to the tested specimens. Some researchers (Rhodes and Nash (1998) and Hofmeyer (2000)) disapproved this adjustment method and developed mechanical models more accurate and descriptive (Bakker (1992) and Hofmeyer (2000)) but their breakthroughs have not been included in design equations since the proposal formulation is quite cumbersome.

On the other hand, stainless steel is a relatively new metallic material that has been often employed for monumental structures due to its aesthetic appeal. Despite their initial material investment, it has been demonstrated that when an efficient design is performed, the whole life cost is favorable to stainless steel, Gardner et al. (2007). According to their crystalline structure there exist five types of stainless steel but only three are applicable to construction: austenitic, duplex and ferritic stainless steel. As ferritic stainless steels do not contain nickel, they are cheaper and relatively price-stable compared to the austenitic and duplex stainless steel whose cost is strongly dependent on the nickel price which is highly volatile and periodically shows dramatic increases. Ferritics also differ from austenitics and duplex in that their stress strain relationship is less rounded and therefore, their behavior has a kind of resemblance to carbon steel. Despite the mechanical and physical properties of ferritic stainless steels make them suitable for a number of structural applications; unfortunately they are not considered in current design specifications due to the lack of research for this stainless steel. Actually, the web crippling European design rules for stainless steel structures, EN 1993-1-4 (2006), are adopted from the specifications for carbon steel cold-formed members, EN 1993-1-3 (2006).

---

This paper presents numerical results from a parametric study and proposes a new equation to predict the ultimate strength of cold-formed stainless steel members subjected to web crippling. The results have also been compared with the European design rules and all available experimental results found in the literature to assess their applicability. The study is focused on square hollow sections (SHS), rectangular hollow sections (RHS) and hat sections undergoing concentrated loads in one flange.

### **2.1.2 Literature review**

A great amount studies involving web crippling strength of carbon steel cross-sections have been conducted since the 1940s. The first research on web crippling was conducted by Winter and Pian at Cornell University (1946), where they labeled the four load cases considered in current design specifications: Interior One-Flange (IOF), Interior Two-Flange (ITF), End One-Flange (EOF) and End-Two-Flange (ETF). Since then, several researchers have carried out comprehensive experimental and numerical studies on different sections, types of loading, and considering interaction with bending in interior load cases including Hetrakul and Yu (1978), Yu (1981), Studnicka (1990), Gerges (1997), Wing (1981), Santaputra (1986), Zhao and Hancock (1995), Hofmeyer et al. (2001), Kaitila (2004) and Hofmeyer (2005).

On the other hand, research on web crippling strength of stainless steel cross-sections is scarce compared to carbon steel ones. The first web crippling study carried out in stainless steel found in the literature was performed by Korvink et al. (1995). They tested lipped channel sections made up with austenitic and ferritic stainless steel in order to assess American Standards. Other experimental research was carried out by Talja and Salmi (1995) and Baddoo et al. (2004) in order to analyze the behavior of different cross sections and to compare experimental and numerical results with European Standards. Later, Zhou and Young (2006a, 2006b, 2007a, 2007b, 2007c, 2008) began a wide experimental investigation on web crippling considering austenitic, high strength austenitic and duplex stainless steel tubular sections. They studied the effect of different load cases as well as interaction with bending and proposed a new design procedure derived through a combination of theoretical and empirical analysis which was validated against European, Australian and American Standards. An exhaustive review regarding cold-formed stainless steel sections subjected to web crippling is gathered in Hradil et al. (2010).

### 2.1.3 EN 1993-1-3 (2006)

According to EN 1993-1-3§6.1.7.1 (2006), there are three procedures to calculate the web crippling resistance, with differences between unstiffened and stiffened webs. The resistance of the former is calculated considering the number of cross-section webs, whereas the latter is estimated multiplying the corresponding value for a similar unstiffened web. Since this study considered hollow and hat sections, which have more than one unstiffened web, the procedure followed was according to EN 1993-1-3§6.1.7.3 (2006) giving Eq. (2.1) to predict web crippling resistance.

$$R_{w,Rd} = n_w \alpha t^2 \sqrt{\sigma_{0.2} E} \left(1 - 0.1 \sqrt{r/t}\right) \left(0.5 + \sqrt{0.02 l_a/t}\right) (2.4 + (\phi/90)^2) / \gamma_{M1} \quad (2.1)$$

This expression depends on geometrical parameters (Fig. 2.1) such as the internal bending radius of the cross-section ( $r$ ), the thickness ( $t$ ), the number of webs ( $n_w$ ) and the relative angle between the web and the flange ( $\phi$ ). Moreover, material mechanical properties are also considered including the Young's modulus ( $E$ ) and the material yield proof strength ( $\sigma_{0.2}$ ), however, material nonlinearities are not taken into account. The values of both  $l_a$ , which is taken as the bearing length ( $s_{sL}$ ) for IOF loading (Fig. 2.7) and 10 mm for EOF loading, and  $\alpha$ , which is a dimensionless coefficient, depend on the load configuration and cross-section type associated with the so-called relevant Categories. EN 1993-1-3 (2006) differentiates between Category 1 and Category 2 when the applied load satisfies some geometrical ratios. In general, Category 1 corresponds to EOF test and Category 2 to IOF test configuration. It is important to point out that EN 1993-1-3 (2006) does not contain explicit rules for rectangular hollow sections, therefore, these sections have been dealt with assuming coefficients for sheeting as Talja and Salmi (1995) suggested.

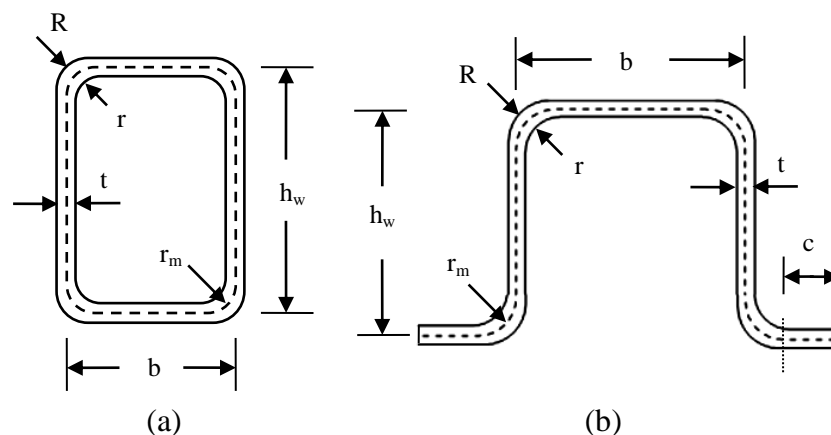


Fig. 2.1 Geometrical nomenclature of (a) hollow and (b) hat sections

Although equations proposed in EN 1993-1-3§6.1.7.2 (2006) to calculate single web sections are not applicable to hollow and hat sections, they will also be assessed herein.

Cold-formed members subjected to interior loading are more vulnerable because of the combined bending and concentrated load. Hence, interaction must be taken into account by means of Eq. (2.2) as specified in EN 1993-1-3§6.1.7.11 (2006). It must be pointed out that assessing interaction in one profile requires results from an IOF test and a bending test. In Eq. (2.2),  $R_{Ed}$  and  $M_{Ed}$  are the IOF action and the produced added bending moment respectively,  $R_{w,Rd}$  is the web crippling resistance and  $M_{c,Rd}$  is the bending resistance that corresponds to the ultimate bending moment in bending test ( $M_{BD,exp}$ ) of the same profile. Substituting the value of the added bending moment in the IOF test as a function of the applied load ( $M_{Ed}=F_{Ed}l_{IOF}/4$ ), the reduced ultimate web crippling resistance is set as Eq. (2.3) where  $l_{IOF}$  is the specimen length in the IOF test.

$$\frac{R_{Ed}}{R_{w,Rd}} + \frac{M_{Ed}}{M_{c,Rd}} \leq 1.25 \quad \frac{R_{Ed}}{R_{w,Rd}} \leq 1 \quad \frac{M_{Ed}}{M_{c,Rd}} \leq 1 \quad (2.2)$$

$$R_{WC-BD} = R_{Ed} = \frac{1.25}{\frac{1}{R_{w,Rd}} + \frac{l_{IOF}}{4M_{c,Rd}}} \leq \min\{R_{Ed}, 4M_{c,Rd}/l_{IOF}\} \quad (2.3)$$

## 2.2 Numerical model

### 2.2.1 Numerical test arrangement

Numerical models have been carried out throughout this study employing ABAQUS (2010) version 6.9 finite element analysis software. A versatile plug-in, which automatically generates and calculates specimens depending on the input data that requires the test configuration, has been developed in collaboration with VTT Technical Research Centre of Finland by Hradil (2010). The implemented web crippling tests in the aforementioned plug-in are the EOF and the IOF. IOF test supports were modeled as rigid faces with boundary conditions in their centre of gravity allowing appropriate displacement and rotation and the load was introduced through two longitudinal lines that impose a vertical displacement (Fig. 2.2). On the other hand, EOF test supports were modeled as two longitudinal lines with a width specified by the user and the load was applied into the specimen through section rigid faces slightly different in both studied sections. These rigid faces were the lips in hat sections and the top flange in SHS and RHS (Fig. 2.3).



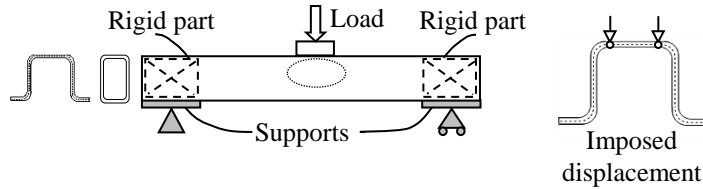


Fig. 2.2 IOF model for hollow and hat sections

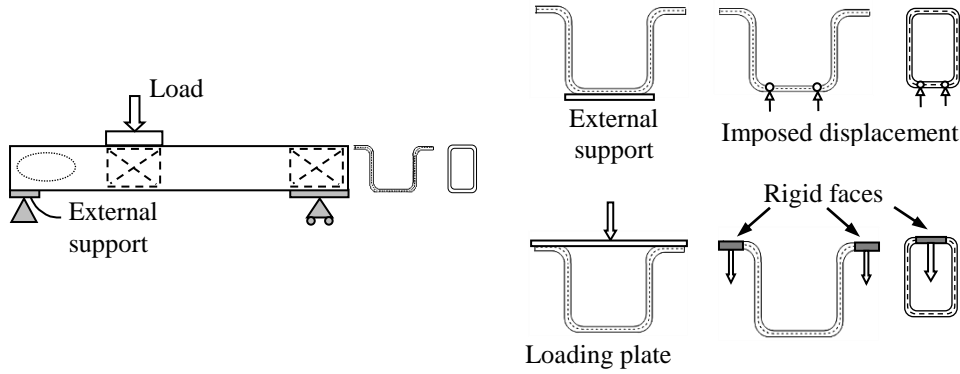


Fig. 2.3 EOF model for hollow and hat sections

In addition, the 4-point bending test has also been modeled to allow for the study of the bending moment interaction in IOF test. The assumed numerical model applies the load at third points of the total length of the member along 50 mm-wide longitudinal lines placed at the lips in hat sections and at the bottom flat part in SHS and RHS. The support is modeled as a rigid face with all degrees of freedom restrained. The length of the specimen remained constant at 1000 mm.

### 2.2.2 Modelling parameters

Cold-formed sections were modeled using S4R elements and convergence studies were conducted to determine an appropriate mesh density to achieve suitable accurate results whilst minimizing computational time. The flat parts were uniformly meshed with a distance between nodes ranging from 5 to 7 mm whereas two or three elements were employed in the rounded corners. The material behaviour is specified in ABAQUS by introducing true stresses and log plastic strain according to Eq. (2.4). The values have been introduced defining a multi-linear stress-strain curve based on a compound two-stage Mirambell and Real (1995) model and modified by Rasmussen (2003) and included in Annex C of EN 1993-1-4 (2006).

$$\begin{aligned}\sigma_{true} &= \sigma_{nom}(1 + \varepsilon_{nom}) \\ \varepsilon_{pl} &= \ln(1 + \varepsilon_{nom}) - \frac{\sigma_{true}}{E}\end{aligned}\tag{2.4}$$

The production route of a cold-formed section produces residual stresses and enhanced corner properties. Both come from the same reason but they have different effects. There exist different studies involving the effect of both residual stresses and enhancement corner properties. A review of all this available data as well as further investigation can be found in Gardner and Cruise (2009) for the former and in Ashraf et al. (2005) for the latter. As a result of these investigations, researchers have proposed different stress patterns for different sections and cold-formed techniques. In this study enhanced strength properties in corners were neglected and the average method proposed in EN 1993-1-3 (2006) was used whereas residual stresses from the sectioning process were not included due to their small effect on the member behaviour as concluded by Gardner and Cruise (2009).

In order to obtain the resistance of cold-formed elements subjected to web crippling, a geometrical and material nonlinear analysis of the imperfect structure (GMNIA) was carried out. Concerning material nonlinearities, ABAQUS allows introducing any stress-strain relationship as mentioned before whereas geometric imperfections have the form of the lowest relevant (i.e. local or global) elastic buckling mode shape, as it is the shape according to which a perfect structure would buckle and eventually fail (Fig. 2.4). To this end an elastic eigenvalue buckling analysis is initially performed to extract the buckling mode shapes which are utilized in subsequent analyses to perturb the idealised geometry. The buckling mode shapes provide only a perturbation pattern and the incorporation of imperfection amplitude into the FE models is required. Since web crippling phenomenon is a local instability, only local imperfections have been considered. As proposed by Theofanous and Gardner (2009) three values of local imperfection amplitude were considered: 1/10 and 1/100 of the cross sectional thickness and the imperfection amplitude obtained from applying Eq. (2.5). This equation was firstly proposed by Dawson and Walker (1972) and adapted for stainless steel in Gardner and Nethercot (2004b). In the equation  $t$  is the plate thickness,  $\sigma_{0.2}$  is the material 0.2% proof stress and  $\sigma_{cr}$  is the elastic buckling stress of the plated elements assuming simply supported conditions. This value was calculated for the different plate elements that make up the section and the least  $w_0$  value was taken.

$$w_0 = 0.023 \left( \frac{\sigma_{0.2}}{\sigma_{cr}} \right) t \quad (2.5)$$

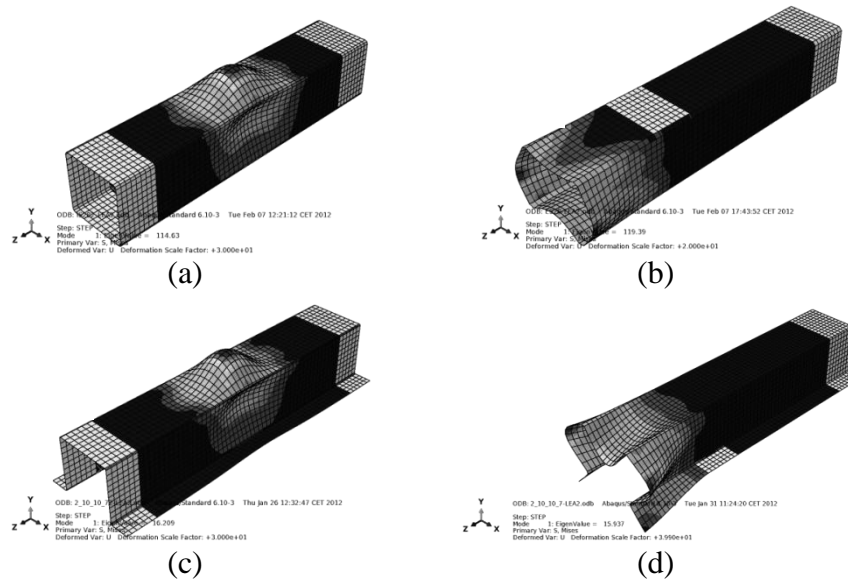


Fig. 2.4 First buckling mode for a SHS subjected to IOF loading (a), SHS to EOF loading (b), hat to IOF loading (c) and hat to EOF loading (d)

Once the linear elastic eigenvalue buckle analysis (LEA) is completed and the imperfection amplitude defined, the deformed shape obtained is introduced as the new geometry member and the GMNIA starts. Since the modified Riks method enables tracing of the structural response beyond the ultimate load as well as taking into account material nonlinearities, it has been used to predict the resistance of each specimen. The two different analysis steps are implemented in the aforementioned plug-in which displays results in real time.

### 2.2.3 Finite element model validation

In order to verify the finite element model, a total of 13 cold-formed stainless steel square and rectangular hollow sections and hat sections subjected to web crippling were analyzed. The calibration was based on experimental results from Gardner et al. (2006) and Talja and Hradil (2011). In the first study three different austenitic cold-formed hollow sections (SHS 100×100×3, RHS 120×80×3 and RHS 140×60×3) were subjected to IOF. In the second one, four ferritic cold-formed hat sections (TH\_10, TH\_15, TH\_20, and TH\_30) as well as one square hollow section (SHS) were subjected to IOF and EOF loading. Experimental and numerical results are summarized in Table 2.1. Both abridgements  $R_{WC,exp}$  and  $M_{BD,exp}$  correspond to experimental results. The former is the ultimate resistant load measured in the web crippling test and the latter is the ultimate bending resistance in the 4-point bending test. Finally, numerical results,  $R_{u,num}$ , are presented by considering three different amplitudes of the initial

imperfection. Fig. 2.5 displays a comparison between the deformed shape from some experimental tests and numerical models. The main conclusions of that FE model assessment are:

- The model is not sensitive to the three initial imperfections studied and therefore, any of them might be used.
- The model is reliable reproducing both ferritic and austenitic stainless steel.
- In general, numerical results present a good agreement with experimental results in any section and test setup.
- Numerical results from hollow sections subjected to EOF are slightly greater than experimental results.
- The numerical deformed shapes resemble the experimental test (Fig. 2.5).

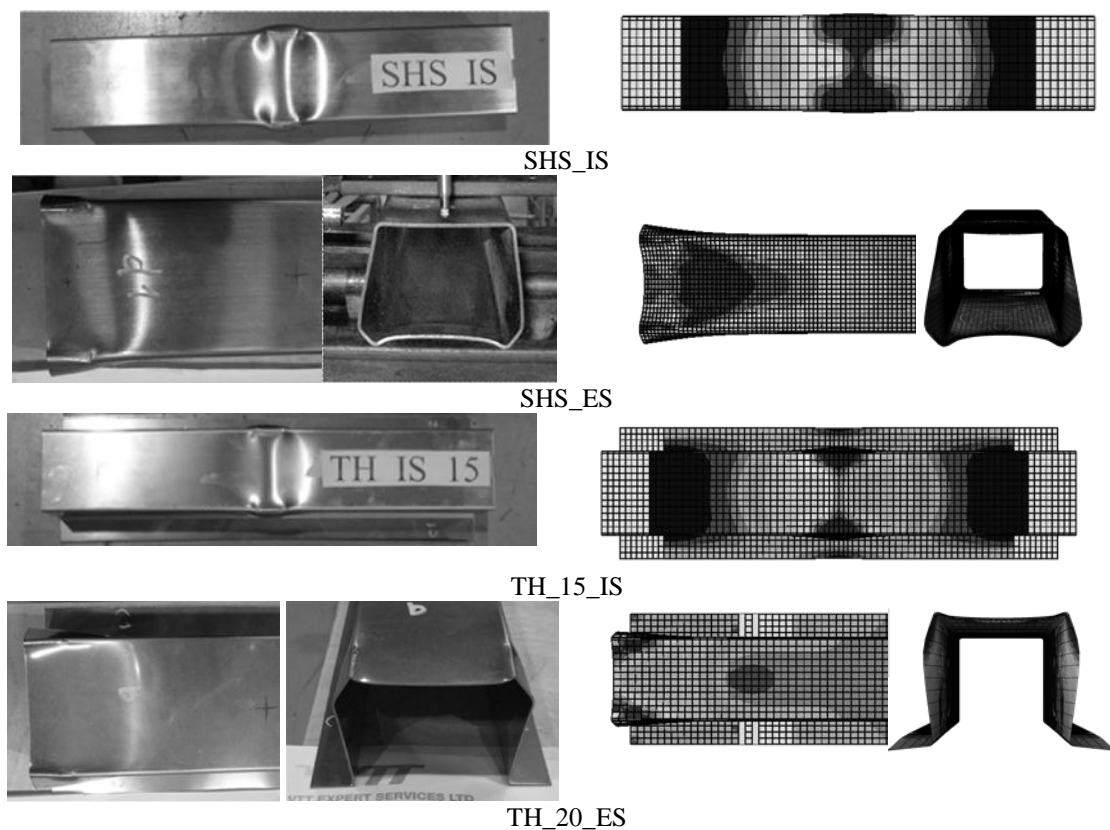


Fig. 2.5 Comparison between experimental and numerical deformed shapes

Table 2.1 Comparison between experimental and numerical results

	Specimen	Grade	$R_{WC,exp}$ (kN)	$M_{BD,exp}$ (kNm)	$R_{u,num}$ (kN)			$R_{u,num}/R_{WC,exp}$		
					t/10	$w_0$	t/100	t/10	$w_0$	t/100
EOF	SHS_ES	1.4509	26.76	-	35.37	35.39	35.36	1.32	1.32	1.32
	TH_10_ES	1.4509	7.16	-	7.02	7.02	7.03	0.98	0.98	0.98
	TH_15_ES	1.4509	15.03	-	15.02	15.05	15.07	1.00	1.00	1.00
	TH_20_ES	1.4509	25.91	-	25.71	25.79	25.82	0.99	1.00	1.00
	TH_30_ES	1.4509	42.06	-	39.55	39.92	39.93	0.94	0.95	0.95
IOF	SHS_IS	1.4509	43.92	8.09	37.74	37.33	37.02	0.86	0.85	0.84
	SHS 100×100×3	1.4318	107.1	23.30	99.96	101.15	101.18	0.93	0.94	0.94
	RHS 120×80×3	1.4318	108.3	29.80	96.6	96.21	96.42	0.89	0.89	0.89
	RHS 140×60×3	1.4318	107.5	34.60	94.95	95.47	95.69	0.88	0.89	0.89
	TH_10_IS	1.4509	10	1.57	9.74	9.75	9.75	0.97	0.98	0.98
	TH_15_IS	1.4509	20.73	3.07	19.56	19.58	19.59	0.94	0.94	0.95
	TH_20_IS	1.4509	34.84	5.03	32.22	32.42	32.41	0.92	0.93	0.93
	TH_30_IS	1.4509	55.01	6.44	49.98	50.08	50.09	0.91	0.91	0.91

## 2.3 Sensitivity study

### 2.3.1 Introduction

Having verified that the FE model successfully predict the behaviour of hollow and hat sections subjected to web crippling, a sensitivity study was performed to investigate the response of the numerical model to key input parameters to analyse. The aim of this section is clearly highlight the differences in specific material parameters and cross-section geometry to study if some changes in the current EN 1993-1-3§6.1.7.3 (2006) web crippling formulation might be considered. Web crippling models on two square hollow sections, one rectangular hollow section and one hat section under IOF and EOF were conducted following the schemes of Fig. 2.6. Section dimensions are shown in Table 2.2 according to parameters described in Fig. 2.1. Thicknesses of 1.5 mm and 3 mm were considered to study the effect of changing slenderness. The length of all the specimens ( $L$ ) was constant and equal to 350 mm. IOF supports length ( $s_{sa}$  and  $s_{sb}$ ) was set to be 50 mm and the bearing length ( $s_{sL}$ ) equal to 25 mm. The length of the support that produces web crippling in EOF ( $s_{sa}$ ) was 25 mm whereas the other one ( $s_{sb}$ ) was 50 mm. The distance from the centre of the bearing plate ( $s_{sL}$ ), which has a length equal to 50 mm, to the edge of the nearest support ( $e$ ) was 100 mm. The initial imperfection considered was the predicted by Eq. (2.5).

Table 2.2 Cross-section dimensions used in the sensitivity study

	Label	b (mm)	$h_w$ (mm)	c (mm)	$r_m$ (mm)
SHS 80×80×t	S1	80	80	-	5
Hat 80×80×30×t	S2	80	80	30	5
SHS 100×100×t	S3	100	100	-	2.5
RHS 80×100×t	S4	80	100	-	6

Table 2.3 Material properties

	E (GPa)	$\sigma_{0.2}$ (MPa)	n	$\sigma_u$ (MPa)	m	$\epsilon_u$	$\sigma_u/\sigma_{0.2}$
N1	200	300	5	600	2.75	0.5	2
N2	200	300	10	600	2.75	0.5	2
N3	200	300	25	600	2.75	0.5	2
F1	200	300	10	420	3.5	0.29	1.4
F2	200	400	10	560	3.5	0.29	1.4
F3	200	500	10	700	3.5	0.29	1.4

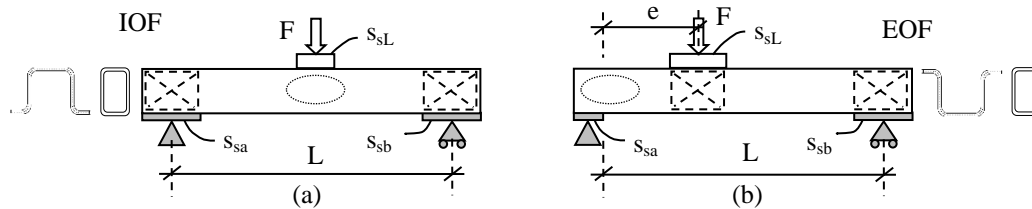


Fig. 2.6 IOF model (a) and EOF model (b) configuration and profile collocation

Table 2.3 shows the values of the six studied materials where group N studies the difference in nonlinear parameter  $n$ . N1 is close to austenitic steels with low  $n$  values whereas N3 is close to carbon steel with high  $n$  values. On the other hand, group F studies the effect of increased strength due to cold-working with lower  $\sigma_u/\sigma_{0.2}$  ratio than group N. In group N this ratio is equal to 2 but in group F is equal to 1.4 which is a typical value for ferritic stainless steels.

### 2.3.2 Results and comparison with EN 1993-1-3 (2006)

Numerical results from ABAQUS are presented herein in Tables 2.4 to 2.7 where  $R_{u,num}$  is the numerical web crippling resistance,  $M_{BD,num}$  is the numerical bending moment resistance,  $R_{w,Rd}$  is the analytical web crippling resistance obtained from applying EN 1993-1-3§6.1.7.2 (2006) and EN 1993-1-3§6.1.7.3 (2006) whereas  $R_{WC-BD}$  is the web crippling strength considering interaction with bending moment according to Eq. (2.3). All partial safety factors have been set to unity to enable a direct comparison. Each specimen has been labeled to be easily identified. The two first characters indicate the material type of the specimens according to Table 2.3, the following two characters correspond to the section type as described in Table 2.2 and finally, the next two numbers are the nominal thickness.

Table 2.4 Numerical results for SHS under IOF loading

Specimen	$R_{u,num}$ (kN)	$M_{BD,num}$ (kNm)	6.1.7.3	6.1.7.2	6.1.7.3	6.1.7.2
			$R_{u,num}/$ $R_{w,Rd}$	$R_{u,num}/$ $R_{w,Rd}$	$R_{u,num}/$ $R_{WC-BD}$	$R_{u,num}/$ $R_{WC-BD}$
N1S115	14.39	3.683	0.903	0.846	0.928	0.885
N1S315	17.49	5.129	1.024	0.943	1.018	0.956
N1S415	16.07	4.727	1.032	1.009	1.025	1.007
N2S115	14.34	3.661	0.900	0.843	0.926	0.883
N2S315	17.68	5.293	1.035	0.953	1.027	0.964
N2S415	15.94	4.788	1.024	1.001	1.018	1.001
N3S115	14.1	3.715	0.885	0.829	0.914	0.872
N3S315	17.76	5.467	1.040	0.958	1.031	0.967
N3S415	15.57	4.893	1.000	0.978	1.000	0.983
F1S115	13.32	3.680	0.836	0.783	0.876	0.835
F1S315	17.42	5.262	1.020	0.939	1.015	0.953
F1S415	14.54	4.769	0.934	0.913	0.948	0.931
F2S115	17.17	4.669	0.934	0.845	0.950	0.883
F2S315	21.8	6.509	1.105	0.984	1.081	0.987
F2S415	18.91	5.979	1.052	0.994	1.041	0.995
F3S115	20.86	5.418	1.014	0.928	1.011	0.947
F3S315	25.19	7.722	1.142	1.028	1.111	1.022
F3S415	23.13	6.959	1.151	1.100	1.117	1.077
N1S130	50.45	10.106	0.876	0.677	0.914	0.775
N1S330	71.63	15.064	1.177	0.960	1.125	0.972
N1S430	55.47	13.543	0.979	0.767	0.984	0.828
N2S130	50.62	9.949	0.879	0.679	0.916	0.778
N2S330	69.89	14.773	1.148	0.937	1.105	0.955
N2S430	55	13.314	0.970	0.760	0.978	0.824
N3S130	49.88	9.590	0.866	0.669	0.908	0.773
N3S330	69.97	14.291	1.150	0.938	1.105	0.957
N3S430	53.7	12.894	0.948	0.742	0.962	0.811
F1S130	47.3	9.686	0.821	0.634	0.875	0.744
F1S330	68.9	14.574	1.132	0.924	1.094	0.946
F1S430	49.13	13.109	0.867	0.679	0.900	0.758
F2S130	61.2	12.538	0.920	0.687	0.944	0.781
F2S330	86.4	18.808	1.230	0.969	1.164	0.978
F2S430	64.4	17.064	0.984	0.745	0.988	0.808
F3S130	74.32	15.443	0.999	0.755	1.000	0.827
F3S330	104.64	22.827	1.332	1.062	1.237	1.044
F3S430	79.24	20.870	1.083	0.829	1.062	0.872
Mean	-	-	1.011	0.869	1.008	0.905
S. D	-	-	0.119	0.128	0.086	0.092

Table 2.5 Numerical results for SHS under EOF loading

Specimen	$R_{u,num}$ (kN)	6.1.7.3	6.1.7.2
		$R_{u,num}/$ $R_{w,Rd}$	$R_{u,num}/$ $R_{w,Rd}$
N1S115	12.057	1.514	2.023
N1S315	17.593	2.060	2.276
N1S415	12.214	1.569	2.465
N2S115	12.057	1.514	2.023
N2S315	17.736	2.076	2.295
N2S415	12.229	1.571	2.468
N3S115	11.821	1.484	1.983
N3S315	17.564	2.056	2.273
N3S415	12.021	1.544	2.427
F1S115	11.579	1.454	1.943
F1S315	16.943	1.984	2.192
F1S415	11.736	1.508	2.369
F2S115	14.929	1.623	2.241
F2S315	21.514	2.181	2.490
F2S415	15.107	1.681	2.728
F3S115	18.114	1.762	2.694
F3S315	25.621	2.323	2.939
F3S415	18.250	1.816	3.265
N1S130	48.071	1.669	1.507
N1S330	58.614	1.926	1.822
N1S430	46.821	1.652	1.573
N2S130	47.650	1.654	1.494
N2S330	58.164	1.912	1.808
N2S430	46.707	1.648	1.570
N3S130	46.479	1.614	1.457
N3S330	56.886	1.870	1.768
N3S430	45.871	1.619	1.541
F1S130	44.507	1.545	1.395
F1S330	53.864	1.770	1.674
F1S430	43.757	1.544	1.470
F2S130	57.814	1.738	1.621
F2S330	69.750	1.985	1.939
F2S430	56.593	1.730	1.701
F3S130	70.650	1.900	1.963
F3S330	85.007	2.164	2.342
F3S430	68.764	1.880	2.048
Mean	-	1.765	2.050
S. D	-	0.228	0.458



Table 2.6 Numerical results for hat sections under IOF loading

Specimen	$R_{u,num}$ (kN)	$M_{BD,num}$ (kNm)	6.1.7.3	6.1.7.2	6.1.7.3	6.1.7.2
			$R_{u,num}/$ $R_{w,Rd}$	$R_{u,num}/$ $R_{w,Rd}$	$R_{u,num}/$ $R_{WC-BD}$	$R_{u,num}/$ $R_{WC-BD}$
N1S215	15.19	1.234	3.415	1.549	0.795	1.551
N2S215	15.05	1.223	3.338	1.535	0.788	1.543
N3S215	14.69	1.194	3.307	1.498	0.769	1.509
F1S215	13.81	1.122	3.296	1.408	0.723	1.420
F2S215	17.95	1.458	4.163	1.585	0.786	1.585
F3S215	21.94	1.783	5.116	1.733	0.869	1.733
N1S230	53.01	4.307	9.398	1.438	0.704	1.545
N2S230	52.57	4.271	9.297	1.426	0.698	1.536
N3S230	49.88	4.053	8.790	1.353	0.662	1.480
F1S230	47.06	3.824	8.965	1.276	0.625	1.389
F2S230	60.92	4.950	11.687	1.431	0.677	1.510
F3S230	73.66	5.985	14.380	1.548	0.740	1.597
Mean	-	-	1.212	0.736	1.312	0.932
S. D	-	-	0.085	0.068	0.063	0.036

Table 2.7 Numerical results for hat sections under EOF loading

Specimen	$R_{u,num}$ (kN)	6.1.7.3	6.1.7.2
		$R_{u,num}/$ $R_{w,Rd}$	$R_{u,num}/$ $R_{w,Rd}$
N1S215	7.843	1.296	1.316
N2S215	7.864	1.299	1.320
N3S215	7.779	1.285	1.305
F1S215	7.486	1.237	1.256
F2S215	9.571	1.369	1.437
F3S215	11.529	1.475	1.715
N1S230	32.579	1.488	1.021
N2S230	32.643	1.491	1.023
N3S230	32.093	1.466	1.006
F1S230	31.079	1.420	0.974
F2S230	39.943	1.580	1.120
F3S230	48.314	1.710	1.343
Mean	-	1.426	1.236
S. D	-	0.138	0.219

Having analyzed the numerical results, the following comments should be pointed out:

- EN 1993-1-3§6.1.7.3 (2006) seems to provide good results for SHS and RHS under IOF configuration as the mean value shows, however, some  $R_{u,num}/R_{w,Rd}$  ratios are below the unity. On the other hand, EN 1993-1-3§6.1.7.2 (2006) seems to be not accurate to predict web crippling resistance providing higher analytical resistances than numerical ones.
- A similar tendency is observed for hat sections under IOF loading but in that case EN 1993-1-3§6.1.7.3 (2006) is quite conservative giving resistances over 30%.
- Both EN 1993-1-3§6.1.7.3 (2006) and EN 1993-1-3§6.1.7.2 (2006) are quite a lot conservative in both sections under EOF loading providing resistances ranging from 20% to 100% over the numerical value.

### 2.3.3 Material influence

The material influence in the web crippling resistance is considered by means of the material proof strength ( $\sigma_{0.2}$ ) because EN 1993-1-3 (2006) is only applicable to carbon steel. Unlike carbon steel, stainless steel has rounded stress-strain behaviour and material nonlinearities must be studied. The effect of the nonlinear parameter 'n' in the ultimate web crippling strength, which has been assessed by comparing N1, N2 and N3 specimen results, is negligible as Tables 2.4 to 2.7 show. Then, the inclusion of that parameter in the web crippling formulation was ruled out. On the other hand, numerical results from N2 and F1 materials, which behaviour is exactly the same before  $\sigma_{0.2}$  but differs beyond that stress, suggest including the ultimate stress,  $\sigma_u$ , since the numerical ultimate load increases when  $\sigma_u$  too. In addition, it can be noticed that thicker sections are more sensitive to that parameter and therefore, the thickness influence should also be considered. It is important to point out that if the  $\sigma_u$  parameter is included, the value of  $\epsilon_u$  must be known. To avoid that calculus, which is not always possible, the stress at 1.0% strain,  $\sigma_{1.0}$ , will be included instead.

### 2.3.4 Internal radius influence

Although the internal radius is considered in the web crippling resistance, the EN 1993-1-3 (2006) formulation is more conservative for small radius as S3 sections show. Additional numerical tests in S1N1 and S1F1 specimens for both IOF (Table 2.8) and EOF (Table 2.9) tests were performed so that the internal radius influence could be studied. They also were labeled by adding the internal radius value to the previous nomenclature. No internal radius variation was considered in hat (S2) sections. The internal radius influence was assessed by means of  $R_{u,num}(r=2.5)/R_{u,num}(r=i)$  ratio and it was found that the ultimate web crippling strength follows an internal radii square root function. Moreover, it can be noticed that the web crippling resistance decreases for increasing radius, which must be taken into account in the new proposal formulation.

Table 2.8 Internal radius assessment. Additional numerical results for IOF loading

Specimen	$r_m$ (mm)	IOF	6.1.7.3	6.1.7.2	IOF	$r_i/2.5^{0.5}$
		$R_{u,num}$ (kN)	$R_{WC-BD}(r=2.5)/$ $R_{WC-BD}(r=i)$	$R_{WC-BD}(r=2.5)/$ $R_{WC-BD}(r=i)$	$R_{u,num}(r=2.5)/$ $R_{u,num}(r=i)$	
N1S13025	2.5	66.89	1	1	1	1
N1S13035	3.5	57.7	1.026	1	1.159	1.163
N1S130	5	50.45	1.056	1.010	1.326	1.366
N1S13060	6	49.04	1.073	1.031	1.364	1.483
F1S13025	2.5	64.52	1	1	1	1
F1S13035	3.5	55.03	1.026	1	1.172	1.163
F1S130	5	47.3	1.056	1.010	1.364	1.366
F1S13060	6	44.04	1.073	1.031	1.465	1.483

Table 2.9 Internal radius assessment. Additional numerical results for EOF loading

Specimen	$r_m$ (mm)	EOF	6.1.7.3	6.1.7.2	EOF	$r_i/2.5^{0.5}$
		$R_{u,num}$ (kN)	$R_{w,Rd}(r=2.5)/$ $R_{w,Rd}(r=i)$	$R_{w,Rd}(r=2.5)/$ $R_{w,Rd}(r=i)$	$R_{u,num}(r=2.5)/$ $R_{u,num}(r=i)$	
N1S13025	2.5	53.736	1	1	1	1
N1S13035	3.5	51.529	1.026	1	1.043	1.163
N1S130	5	48.071	1.056	1.026	1.118	1.366
N1S13060	6	45.264	1.073	1.081	1.187	1.483
F1S13025	2.5	49.143	1	1	1	1
F1S13035	3.5	47.236	1.026	1	1.04	1.163
F1S130	5	44.507	1.056	1.026	1.104	1.366
F1S13060	6	41.993	1.073	1.081	1.170	1.483

### 2.3.5 Bearing length influence

Additional numerical tests were conducted to study the bearing length influence in F1S3 specimen for both IOF (Table 2.10) and EOF (Table 2.11) loading. They also were labeled by adding the bearing length value to the previous nomenclature. No bearing length variation was considered in hat (S2) sections. The bearing length influence was assessed by means of  $R_{u,num}(s_s=25)/R_{u,num}(s_s=i)$  ratio and it was found that EN 1993-1-3 §6.1.7.3 (2006) considers properly the bearing length influence for IOF loading. On the other hand, to predict the ultimate web crippling load for EOF loading, EN 1993-1-3 §6.1.7.3 (2006) sets the bearing length equal to 10 mm whereas article EN 1993-1-3 §6.1.7.2 (2006) specifies that the smaller value of  $s_s$  must be considered. Neither of them considers unequal bearing lengths but numerical results show that significant differences might be obtained. Consequently, some changes should be proposed in the web crippling resistance function for the EOF loading to take into account unequal bearing lengths. Since the ultimate web crippling strength follows a bearing length linear function as the  $\Delta R_{u,numi}/\Delta s_{si}$  ratio shows, it is proposed to include a dimensionless factor for  $l_a$  parameter equal to the slope of the aforementioned function.

Table 2.10 Bearing length assessment. Additional numerical results for IOF loading

Specimen	$s_s$ (mm)	IOF	6.1.7.3	6.1.7.2	IOF
		$R_{u,num}$ (kN)	$R_{WC-BD}(s_s=25)/$ $R_{WC-BD}(s_s=i)$	$R_{WC-BD}(s_s=25)/$ $R_{WC-BD}(s_s=i)$	$R_{u,num}(s_s=25)/$ $R_{u,num}(s_s=i)$
F1S315	25	17.42	1	1	1
F1S31550	50	20.80	0.818	0.905	0.838
F1S31575	75	23.31	0.7184	0.827	0.747
F1S315100	100	25.36	0.651	0.753	0.687
F1S330	25	68.90	1	1	1
F1S33050	50	85.11	0.843	0.948	0.809
F1S33075	75	96.82	0.752	0.901	0.712
F1S330100	100	105.57	0.689	0.8581	0.653

Table 2.11 Bearing length assessment. Additional numerical results for EOF loading

Specimen	$s_s$ (mm)	EOF	6.1.7.3	6.1.7.2	EOF	EOF
		$R_{u,num}$ (kN)	$R_{w,Rd}(s_s=25)/$ $R_{w,Rd}(s_s=i)$	$R_{w,Rd}(s_s=25)/$ $R_{w,Rd}(s_s=i)$	$R_{u,num}(s_s=25)/$ $R_{u,num}(s_s=i)$	$\Delta R_{u,num}/\Delta s_{si}$
F1S315	25	13.993	1	1	1.000	-
F1S31550	50	16.943	1	1	0.826	0.118
F1S31575	75	17.771	1	1	0.787	0.033
F1S315100	100	18.564	1	1	0.754	0.032
F1S330	25	50.557	1	1	1.000	-
F1S33050	50	53.864	1	1	0.939	0.132
F1S33075	75	56.479	1	1	0.895	0.104
F1S330100	100	60.157	1	1	0.840	0.147

### 2.3.6 New proposal

Having studied the parameters influence in the web crippling resistance a new expression given in Eq. (2.6) is proposed based on the one given in EN 1993-1-3§6.1.7.3 (2006) to consider the stainless steel material hardening. Three mainly changes have been proposed: the  $\sigma_{1.0}$  inclusion so that the material hardening that stainless steel shows could be considered, adjustments in the internal radius influence and the bearing length effect for the EOF condition. Every single one of the modifications has been normalised to keep the original expression dimensions and some dimensionless coefficients have been added to obtain better adjustment:  $\beta$ ,  $\delta$ ,  $\xi$ . The calibration of these new constants, together with the existing  $\alpha$ , will be performed in the following section where a parametric study has been conducted to extend the available database.

$$R_{w,Rd} = n_w \alpha t^2 \sqrt{\sigma_{0.2} E} (\xi \sigma_{1.0} / E)^k \sqrt{\beta t / r} (0.5 + \sqrt{0.01 l_a / t}) (2.4 + (\phi / 90)^2) / \gamma_{M1} \quad (2.6)$$

where

$$k = \delta r / t$$

and  $l_a$  must be taken as:  $l_a = 0.01 s_s$  for Category 1 and  $l_a = 2.2 s_s$  for Category 2

## 2.4 Parametric study

### 2.4.1 Introduction

A wider parametric study was conducted to expand the available results over different cross-section typologies and dimensions. Five different cross-sections under IOF and EOF loading were added to the numerical database. The numerical setup followed the schemes of Fig. 2.6 and section properties are described in Table 2.12 according to parameters of Fig. 2.1. Thicknesses of 2 mm and 4 mm in SHS and RHS as well as 1 mm and 2 mm in hat sections were considered to study the effect of changing slenderness. The length of all the specimens (L) was constant and equal to 500 mm. IOF

supports length ( $s_{sa}$  and  $s_{sb}$ ) was set to be 50 mm and the bearing length ( $s_{sL}$ ) equal to 25 mm. The length of the support that produces web crippling in EOF ( $s_{sa}$ ) was 25 mm whereas the other one ( $s_{sb}$ ) was 50 mm. The distance from the centre of the bearing plate ( $s_{sL}$ ), of which length was 50 mm, to the edge of the nearest support ( $e$ ) was 150 mm. The initial imperfection considered was the predicted by Eq. (2.5). Since the previous sensitivity study concluded that it is necessary to add the stress at 1.0% strain value ( $\sigma_{1.0}$ ), different hardening rates will be considered herein keeping other parameters invariable (Table 2.13). The internal radius and the bearing length have an important role in the web crippling formulation and therefore additional models were carried out so that this effect could be studied more accurately. Two more radii per section, 4 mm and 5 mm in S5, S6, S7 and S9, and 5 mm and 6 mm in S8, for materials B1\* and B2\* were considered. On the other hand, three more bearing lengths for IOF ( $s_{sL}=50$  mm, 75 mm and 100 mm), 4 additional lengths of the support that produces web crippling in EOF ( $s_{sa}=40$  mm, 50 mm, 75 mm and 100 mm) and two extra bearing plates ( $s_{sL}=75$  mm and 100 mm) made up the numerical database expansion. Numerical results of these simulations are given in Appendix 2.A.

Table 2.12 Cross-section dimensions used in the parametric study

Cross-section	Label	b (mm)	$h_w$ (mm)	c (mm)	$r_m$ (mm)
SHS 70×70×t	S5	70	70	-	3
RHS 60×120×t	S6	60	120	-	3
Hat 60×60×20×t	S7	60	60	20	3
Hat 120×120×50×t	S8	120	120	50	3
Hat 60×80×25×t	S9	60	80	25	3

Table 2.13 Material properties

Material	E (GPa)	$\sigma_{0.2}$ (MPa)	n	$\sigma_{1.0}$ (MPa)	$\sigma_u$ (MPa)	m	$\epsilon_u$	$\sigma_u/\sigma_{0.2}$
B1	200	250	10	256	275	3	0.4	1.1
B1*	200	250	10	262.2	300	3	0.4	1.2
B2	200	250	10	275	350	3	0.4	1.4
B2*	200	250	10	300	450	3	0.4	1.8

#### 2.4.2 Coefficients adjustment

Once the numerical results from this parametric study were obtained, the four dimensionless coefficients from the new proposal formulation were adjusted. The calibration was performed considering also numerical results from the sensitivity study and the obtained results are presented in Table 2.14. It is important to mention that some EOF models from this parametric study were Category 2 and consequently those were not considered in the adjustment for Category 1 coefficients.

Table 2.14 Values for the dimensionless coefficients

Coefficient	Category 1 (EOF)		Category 2 (IOF)	
	SHS/RHS	Hat section	SHS/RHS	Hat section
$\alpha$	0.07	0.085	0.13	0.14
$\beta$	2.14	1.65	0.59	0.81
$\delta$	0.22	0.13	0.14	0.065
$\xi$	2200	2275	2700	2000

### 2.4.3 Comparison between numerical and analytical predictions

This section presents a graphical comparison of the finite element (FE) results with the studied analytical formulations. Figs 2.7 and 2.8 plot the  $R_{u,num}/R_{WC-BD}$  ratio for hollow sections and hat sections subjected to IOF loading, respectively. On the other hand, Figs 2.9 and 2.10 display the  $R_{u,num}/R_{w,Rd}$  ratio for hollow and hat sections under EOF loading (Category 1), respectively. The comparison has been assessed statistically comparing mean values and standard deviations (S.D.) for all considered formulations. The four figures and all statistical values consider specimens from both sensitive and parametric studies (section 2.3 and 2.4, respectively).

The main conclusions from Figs 2.7 and 2.8 are:

- Both EN 1993-1-3 §6.1.7.3 (2006) and 6.1.7.2 (2006) provide results under the unity with considerably dispersion. However, there are less hat specimens than hollow ones with a ratio below the unity.
- Results from the new proposal are more accurate providing safe values and decreasing the standard deviation of current design provisions.

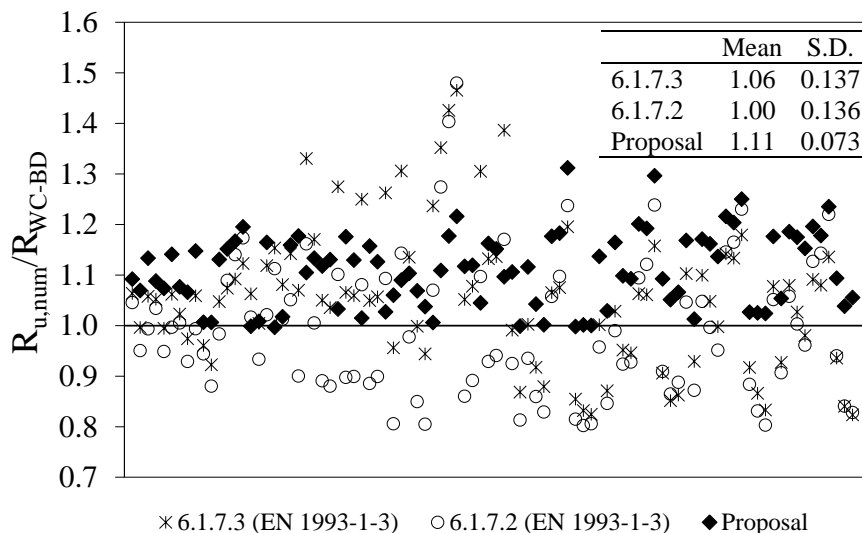


Fig. 2.7 Comparison of the FE results with analytical formulations for SHS/RHS under IOF loading

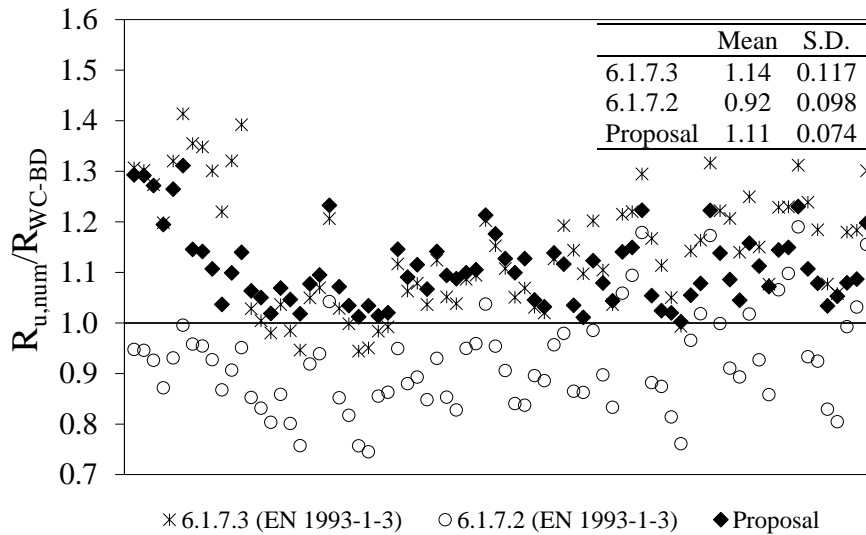


Fig. 2.8 Comparison of the FE results with analytical formulations for hat sections under IOF loading

The most relevant conclusions from Figs 2.9 and 2.10 are:

- Despite EN 1993-1-3§6.1.7.3 (2006) recommends taking 10 mm as the bearing length value, both Figs 2.9 and 2.1 demonstrate that it is more suitable consider the actual plate length which produces crippling ( $s_s$ ). This assumption provides less conservative and less scattered results.
- In general, EN 1993-1-3§6.1.7.2 (2006) presents quite dispersed results but less conservative than current EN 1993-1-3§6.1.7.3 (2006) formulation.
- The new proposal predicts the best adjustment providing the least conservative results and a reasonably dispersion.
- In Fig. 2.9 there are some ultimate loads unsatisfactory predicted with  $R_{u,num}/R_{w,Rd}$  ratios over 2.0 for all the design methods considered and in some cases this value reaches values over three. Despite this, the new proposal gives the most suitable ratios.
- A similar situation is observed in Fig. 2.10. However, It seems that the new formulation improve this imprecise results and relocates the specimens in lower ratios providing the most precise results. This is very satisfactory since it means that the proposed changes allow a better prediction of web crippling strength for hat sections subjected to EOF loading.

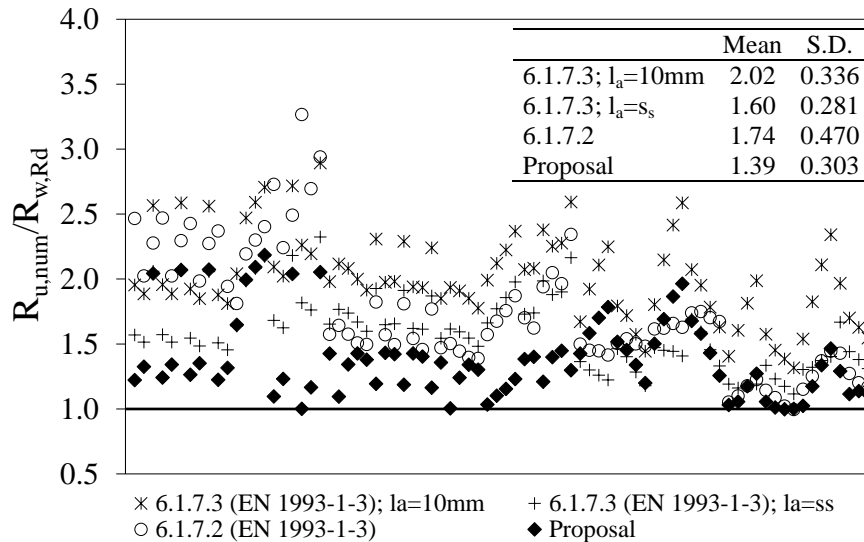


Fig. 2.9 Comparison of the FE results with analytical formulations for SHS/RHS under EOF loading

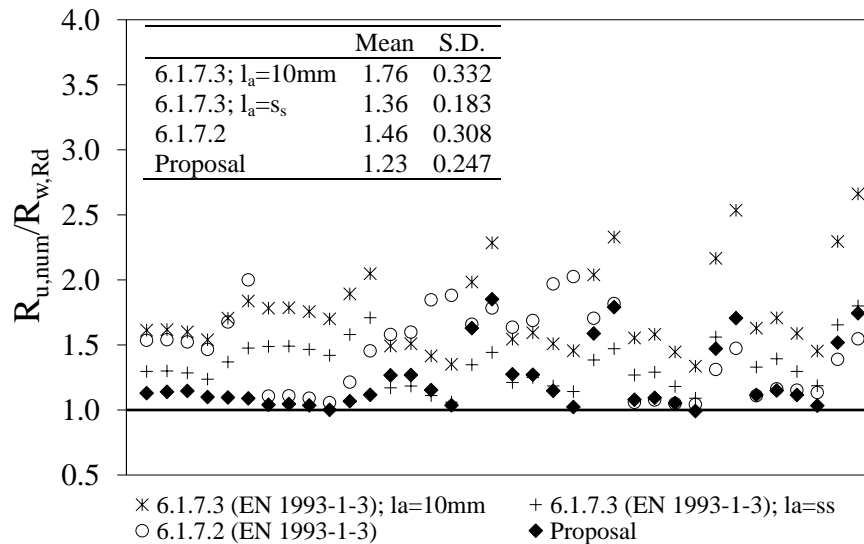


Fig. 2.10 Comparison of the FE results with analytical formulations for hat sections under EOF loading

### 2.5 New proposal validation with experimental results

The new proposal formulation presented in Eq. (2.6) with dimensionless coefficients from Table 2.14 is validated herein by comparing the predictions with all the available experimental results found in the literature (Figs 2.11-2.14). This data gathers documentation from Talja and Salmi (1995), Talja (2004), Zhou and Young (2007a), Gardner et al. (2006), Talja and Hradil (2011). These figures show that EN 1993-1-3 (2006) is quite conservative and how the new proposal provides a better adjustment. The comparison with experimental results is approximately in line with those conducted in the parametric study section.



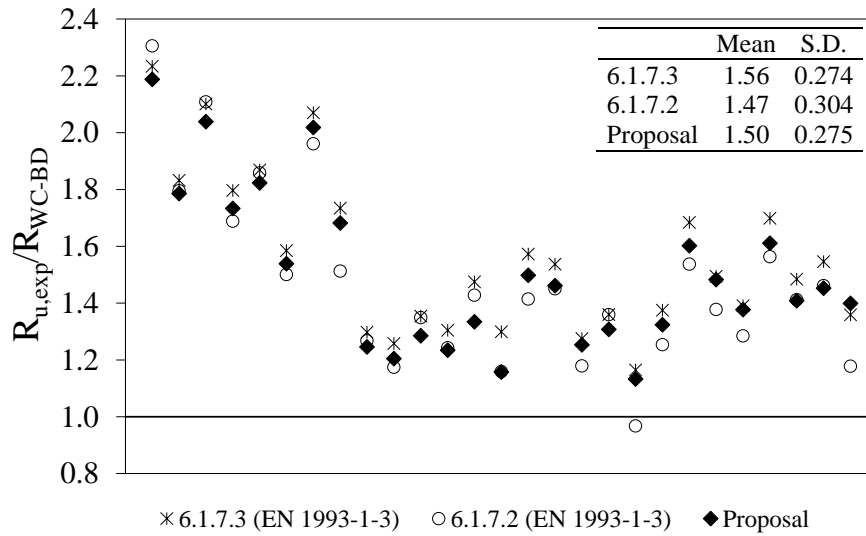


Fig. 2.11 Comparison of experimental results with analytical formulations for SHS/RHS under IOF loading

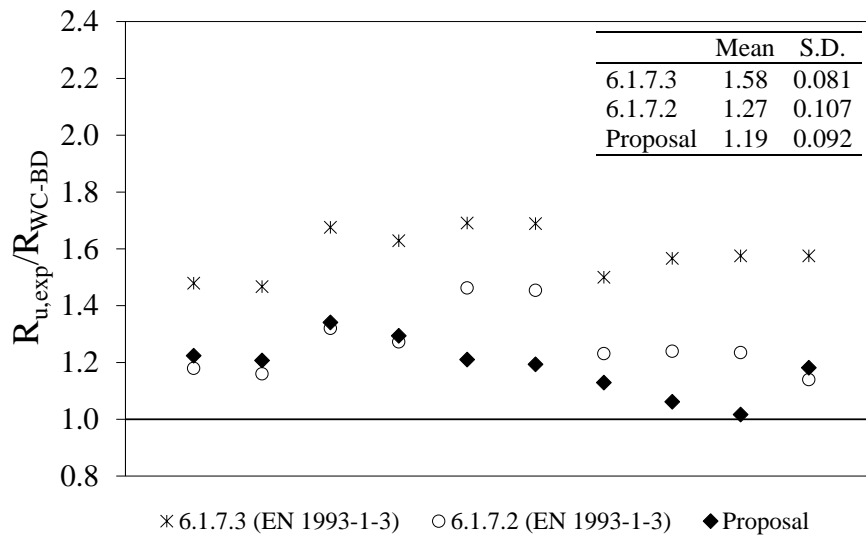


Fig. 2.12 Comparison of experimental results with analytical formulations for hat sections under IOF loading

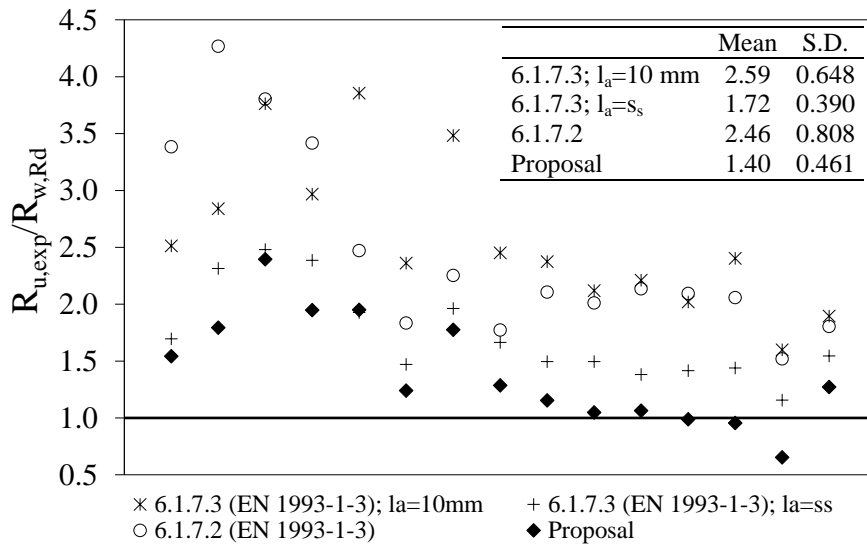


Fig. 2.13 Comparison of experimental results with analytical formulations for SHS/RHS under EOF loading

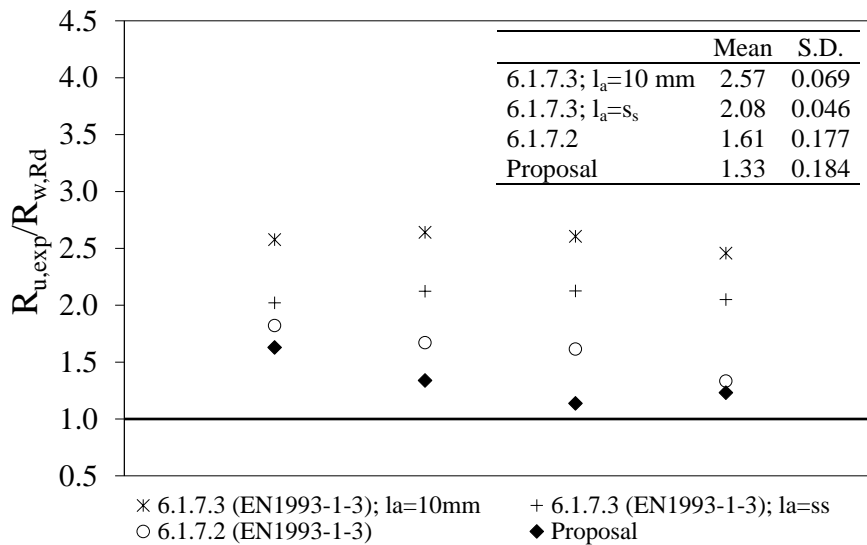


Fig. 2.14 Comparison of experimental results with analytical formulations for hat sections under EOF loading

## 2.6 Conclusions

The urge to provide practising engineers with design rules has motivated researchers to develop several studies in stainless steel sections. One of these design guidance, EN 1993-1-4 (2006), allows the different structural verifications required in a project. However, concerning web crippling resistance, EN 1993-1-4 (2006) refers the user to EN1993-1-3 (2006) which is based on carbon steel providing inaccurate results.

The effect of different materials has been considered in this study so that the applicability of EN 1993-1-3 (2006) could be assessed. The typical rounded stress-strain

relationship of stainless steels has been studied by means of the so-called nonlinear parameter,  $n$ , as well as the hardening ratio  $\sigma_{1.0}/\sigma_{0.2}$ . It has been concluded that the web crippling resistance is not sensitive to the nonlinear parameter but to the hardening ratio. Concerning geometrical and test set up influences, numerical results demonstrate that the internal radius and the bearing length effect slightly differs from that predicted by EN 1993-1-3 (2006) and some changes have been proposed. Having analysed the obtained results throughout this work, a new proposal formula given in Eq. (2.6) with coefficients from Table 2.14 to predict the web crippling resistance has been proposed based on EN 1993-1-3§6.1.7.3 (2006) formulation. This new proposal expression provides safer values, more suitable results and might be applied to any stainless steel.

### **Acknowledgments**

The research leading to these results has received funding from the European Community's Research Fund for Coal and Steel (RFCS) under Grant Agreement No. RFSR-CT-2010-00026, Structural Applications for Ferritic Stainless Steels and from Ministerio de Ciencia e Innovación to the Project BIA2010-11876-E "Acciones complementarias". The first author would like to acknowledge the financial support provided by Universitat Politècnica de Catalunya and from la SUR del DEC de la Generalitat de Catalunya i del FSE as well as El Col·legi d'Enginyers de Camins, Canals i Ports de Catalunya. Special thanks are given to Petr Hradil from VTT Technical Research Centre of Finland for his contribution to ABAQUS plug-in.

---

**Appendix 2.A**

Numerical results of the 332 simulations conducted are presented in this section and compared with the new proposal, EN 1993-1-3§6.1.7.3 (2006) and 6.1.7.2 (2006). According to these two sections, there are some geometrical and configuration ratios that must be previously considered in order to identify the properly equation to apply. The following sections present tables with results where different equations and situations have been considered. Again, all partial safety factors have been set to unity to enable a direct comparison. All specimens were labeled to easily identify load condition, material, section and thickness as well as internal radius and bearing length values of additional simulations. For example, the labels IOFB2\*S615, EOFB2\*S62100 and EOFB2\*S621002 define the following specimens:

- The first three letters define the loading condition, where IOF refers to interior one flange test and EOF to exterior one flange test.
- The notation B2\* indicates the material type.
- The following letter and first number, S6, defines the section.
- The following number indicates the thickness in mm, which is 1 mm in the first specimen and 2 mm in the second one.
- Additional numbers are added when the internal bending radius or the bearing length is varied. For example, 5 (from IOFB2\*S615) means that the internal radius has been changed to 5 mm) and 100 (from EOFB2\*S62100) means that the support length that produces crippling ( $s_{sa}$ ) is 100 mm. The number two is added (EOFB2\*S621002) when the previously number refers to the plate length that applies the load ( $s_{sL}$ ) in EOF loading.

**2.A.1 IOF models for SHS and RHS**

Numerical results from SHS and RHS under IOF loading are presented in Table 2.A.1 where  $R_{u,num}$  is the numerical web crippling resistance,  $M_{BD,num}$  is the numerical bending moment resistance,  $R_{WC-BD}$  is the web crippling strength considering interaction with bending moment and  $R_{w,Rd}$  is the analytical web crippling resistance.

Table 2.A.1 Numerical results, EN 1993-1-3 (2006) and new proposal predicted resistances for SHS/RHS subjected to IOF loading

Specimen	Numerical results		6.1.7.3		6.1.7.2		New proposal	
	$R_{u,num}$ (kN)	$M_{BD,num}$ (kNm)	$R_{w,Rd}$ (kN)	$R_{WC-BD}$ (kN)	$R_{w,Rd}$ (kN)	$R_{WC-BD}$ (kN)	$R_{w,Rd}$ (kN)	$R_{WC-BD}$ (kN)
IOF B1S52	16.94	3.717	25.32	17.092	28.89	18.318	20.842	15.317
IOF B1S62	18.91	7.402	25.32	22.168	27.85	23.678	20.842	19.270
IOF B1*S52	17.22	3.757	25.32	17.176	28.89	18.414	20.947	15.430
IOF B1*S524	15.5	3.720	24.77	16.898	28.00	18.034	19.819	14.871
IOF B1*S525	14.65	3.695	24.29	16.666	27.11	17.675	19.367	14.626
IOF B1*S5250	20.24	3.757	30.76	19.002	31.22	19.141	25.389	17.203
IOF B1*S5275	21.74	3.757	35.04	20.222	33.54	19.814	28.797	18.382
IOF B1*S52100	25.29	3.757	38.73	21.153	35.87	20.441	31.671	19.276
IOF B1*S62	19.34	7.458	25.99	22.632	27.85	23.735	20.947	19.380
IOF B1*S624	18.57	7.382	25.60	22.324	26.99	23.155	19.819	18.549
IOF B1*S625	17.33	7.327	25.27	22.073	26.13	22.591	19.367	18.196
IOF B2S52	17.73	3.800	26.52	17.705	28.89	18.518	21.158	15.594
IOF B2S62	20.16	7.557	26.70	23.150	27.85	23.834	21.158	19.591
IOF B2*S52	18.53	3.887	26.88	18.021	28.89	18.721	21.548	15.910
IOF B2*S524	16.96	3.863	26.48	17.826	28.00	18.364	20.581	15.443
IOF B2*S525	16.64	3.810	26.14	17.590	27.11	17.934	20.302	15.232
IOF B2*S5250	21.31	3.887	33.12	20.046	31.22	19.473	26.118	17.743
IOF B2*S5275	22.61	3.887	37.73	21.308	33.54	20.170	29.624	18.963
IOF B2*S52100	25.78	3.887	41.72	22.269	35.87	20.819	32.579	19.887
IOF B2*S62	21.82	7.723	28.01	24.088	27.85	23.997	21.548	19.971
IOF B2*S624	20.24	7.650	27.59	23.771	26.99	23.413	20.581	19.252
IOF B2*S625	20.3	7.627	27.24	23.541	26.13	22.868	20.302	19.041
IOF B1S54	53.81	7.923	101.61	48.795	117.25	51.430	87.989	46.055
IOF B1S64	65.58	15.747	102.32	70.576	115.19	75.212	87.989	64.756
IOF B1*S54	54.85	8.143	103.04	49.890	117.25	52.348	88.210	46.840
IOF B1*S544	51.79	8.057	102.24	49.414	117.25	51.988	79.848	44.581
IOF B1*S545	48.94	7.993	101.60	49.058	115.49	51.447	74.648	43.053
IOF B1*S5450	60.83	8.143	123.28	53.278	122.16	53.111	103.769	50.026
IOF B1*S5475	62.71	8.143	138.10	55.331	127.08	53.835	115.707	52.100
IOF B1*S54100	67.07	8.143	150.91	56.880	131.99	54.523	125.772	53.646
IOF B1*S64	67.4	16.227	107.47	73.492	115.19	76.289	88.210	65.651
IOF B1*S644	63.13	16.085	106.64	72.893	115.19	75.975	79.848	61.591
IOF B1*S645	60.25	15.932	105.99	72.334	113.46	75.031	74.648	58.845
IOF B2S54	56.81	8.562	109.77	52.721	117.25	54.045	88.652	48.300
IOF B2S64	70.84	17.093	110.55	76.413	115.19	78.152	88.652	67.230
IOF B2*S54	60.44	9.367	111.34	55.986	117.25	57.146	89.466	50.973
IOF B2*S544	57.13	9.317	110.49	55.636	117.25	56.959	81.367	48.625
IOF B2*S545	54.12	9.232	109.82	55.196	115.49	56.309	76.429	46.949
IOF B2*S5450	65.43	9.367	133.25	59.953	122.16	58.056	105.246	54.712
IOF B2*S5475	67.35	9.367	149.29	62.364	127.08	58.923	117.355	57.165
IOF B2*S54100	72.89	9.367	163.16	64.188	131.99	59.748	127.563	59.005
IOF B2*S64	76.84	18.902	116.20	82.134	115.19	81.727	89.466	70.262
IOF B2*S644	68.43	18.723	115.32	81.444	115.19	81.392	81.367	65.907
IOF B2*S645	66.55	18.545	114.62	80.828	113.46	80.364	76.429	63.053

## 2.A.2 IOF models for hat sections

Table 2.A.2 presents numerical results from hat sections subjected to IOF where the same nomenclature of Table 2.A.1 has been used.

Table 2.A.2 Numerical results, EN 1993-1-3 (2006) and new proposal predicted resistances for hat sections subjected to IOF loading

Specimen	Numerical results		6.1.7.3		6.1.7.2		Proposal	
	$R_{u,num}$ (kN)	$M_{BD,num}$ (kNm)	$R_{w,Rd}$ (kN)	$R_{WC-BD}$ (kN)	$R_{w,Rd}$ (kN)	$R_{WC-BD}$ (kN)	$R_{w,Rd}$ (kN)	$R_{WC-BD}$ (kN)
IOF B1S71	4.2	1.002	5.52	4.085	7.76	4.927	6.199	4.369
IOF B1S81	5.47	2.588	5.52	5.447	7.06	6.580	6.199	5.963
IOF B1S91	4.58	1.448	5.52	4.673	7.52	5.702	6.199	5.048
IOF B1*S71	4.25	1.012	5.52	4.102	7.76	4.951	6.248	4.407
IOF B1*S714	3.93	0.993	5.34	3.992	7.76	4.906	6.192	4.350
IOF B1*S715	3.69	0.980	5.18	3.900	7.76	4.874	6.338	4.381
IOF B1*S7150	4.87	1.012	6.86	4.640	8.91	5.302	7.793	4.963
IOF B1*S7175	5.34	1.012	7.89	4.992	10.40	5.688	8.980	5.321
IOF B1*S71100	6.34	1.012	8.75	5.256	12.21	6.084	9.979	5.586
IOF B1*S81	5.59	2.560	5.52	5.434	7.06	6.562	6.248	5.984
IOF B1*S91	4.69	1.473	5.52	4.698	7.52	5.740	6.248	5.104
IOF B1*S914	4.31	1.443	5.34	4.564	7.52	5.694	6.192	5.038
IOF B1*S915	4.28	1.477	5.18	4.503	7.52	5.745	6.338	5.156
IOF B1*S9150	5.33	1.473	6.86	5.419	8.64	6.234	7.793	5.864
IOF B1*S9175	5.86	1.473	7.89	5.906	10.08	6.793	8.980	6.371
IOF B1*S91100	7.01	1.473	8.75	6.278	11.85	7.385	9.979	6.755
IOF B2S71	4.38	1.023	5.52	4.121	7.76	4.978	6.347	4.469
IOF B2S81	5.87	2.582	5.52	5.444	7.06	6.576	6.347	6.069
IOF B2S91	4.88	1.483	5.52	4.709	7.52	5.755	6.347	5.169
IOF B2*S71	4.65	1.033	5.52	4.137	7.76	5.002	6.532	4.561
IOF B2*S714	4.25	1.025	5.34	4.042	7.76	4.982	6.570	4.559
IOF B2*S715	4.11	1.018	5.18	3.959	7.76	4.967	6.825	4.642
IOF B2*S7150	5.09	1.033	6.86	4.685	8.91	5.360	8.148	5.129
IOF B2*S7175	5.52	1.033	7.89	5.045	10.40	5.756	9.388	5.495
IOF B2*S71100	6.39	1.033	8.75	5.314	12.21	6.162	10.433	5.765
IOF B2*S81	6.28	2.593	5.52	5.449	7.06	6.584	6.532	6.210
IOF B2*S91	5.23	1.497	5.52	4.722	7.52	5.775	6.532	5.283
IOF B2*S914	4.84	1.487	5.34	4.607	7.52	5.760	6.570	5.290
IOF B2*S915	4.83	1.493	5.18	4.518	7.52	5.770	6.825	5.430
IOF B2*S9150	5.62	1.497	6.86	5.450	8.64	6.275	8.148	6.060
IOF B2*S9175	6.06	1.497	7.89	5.943	10.08	6.843	9.388	6.577
IOF B2*S91100	7.12	1.497	8.75	6.320	11.85	7.443	10.433	6.969
IOF B1S72	14.66	2.492	19.41	12.292	30.00	14.971	23.724	13.540
IOF B1S82	19.89	7.383	19.41	18.261	28.71	24.151	23.724	21.157
IOF B1S92	16.58	4.007	19.41	15.111	29.57	19.227	23.724	17.042
IOF B1*S72	14.91	2.538	19.41	12.405	30.00	15.138	23.818	13.702
IOF B1*S724	13.41	2.485	18.99	12.141	30.00	14.947	22.066	13.073
IOF B1*S725	12.47	2.492	18.62	12.034	30.00	14.971	21.114	12.817
IOF B1*S7250	16.52	2.538	23.43	13.598	32.42	15.607	28.868	14.901
IOF B1*S7275	17.54	2.538	26.51	14.374	34.83	16.035	32.743	15.667
IOF B1*S72100	19.36	2.538	29.11	14.953	37.25	16.427	36.010	16.231
IOF B1*S82	20.32	7.423	19.41	18.285	28.71	24.194	23.818	21.250
IOF B1*S92	16.9	4.053	19.41	15.177	29.57	19.334	23.818	17.165
IOF B1*S924	14.93	4.023	18.99	14.929	29.57	19.266	22.066	16.364
IOF B1*S925	13.77	3.987	18.62	14.696	29.57	19.181	21.114	15.880
IOF B1*S9250	19.42	4.053	23.43	17.002	31.95	20.118	28.868	19.090
IOF B1*S9275	21.22	4.053	26.51	18.233	34.33	20.845	32.743	20.365
IOF B1*S92100	25.24	4.053	29.11	19.176	36.71	21.523	36.010	21.328

Table 2.A.2 Numerical results, EN 1993-1-3 (2006) and new proposal predicted resistances for hat sections subjected to IOF loading (continuation)

Specimen	Numerical results		6.1.7.3		6.1.7.2		Proposal	
	$R_{u,num}$ (kN)	$M_{BD,num}$ (kNm)	$R_{w,Rd}$ (kN)	$R_{wC-BD}$ (kN)	$R_{w,Rd}$ (kN)	$R_{wC-BD}$ (kN)	$R_{w,Rd}$ (kN)	$R_{wC-BD}$ (kN)
IOF B2S72	15.35	2.605	19.41	12.562	30.00	15.373	24.006	13.945
IOF B2S82	21.13	7.592	19.41	18.386	28.71	24.370	24.006	21.507
IOF B2S92	17.44	4.142	19.41	15.299	29.57	19.533	24.006	17.400
IOF B2*S72	15.96	2.697	19.41	12.771	30.00	15.687	24.353	14.299
IOF B2*S724	14.45	2.668	18.99	12.562	30.00	15.591	22.730	13.760
IOF B2*S725	13.41	2.680	18.62	12.457	30.00	15.631	21.910	13.545
IOF B2*S7250	17.25	2.697	23.43	14.039	32.42	16.192	29.517	15.580
IOF B2*S7275	18.28	2.697	26.51	14.869	34.83	16.653	33.479	16.399
IOF B2*S72100	20.32	2.697	29.11	15.489	37.25	17.076	36.820	17.004
IOF B2*S82	22.9	7.767	19.41	18.487	28.71	24.548	24.353	21.870
IOF B2*S92	18.36	4.295	19.41	15.504	29.57	19.867	24.353	17.815
IOF B2*S924	16.43	4.272	18.99	15.259	29.57	19.817	22.730	17.063
IOF B2*S925	15.94	4.270	18.62	15.064	29.57	19.814	21.910	16.686
IOF B2*S9250	20.54	4.295	23.43	17.413	31.95	20.696	29.517	19.847
IOF B2*S9275	22.14	4.295	26.51	18.707	34.33	21.466	33.479	21.196
IOF B2*S92100	25.63	4.295	29.11	19.700	36.71	22.186	36.820	22.217

### 2.A.3 EOF models for SHS and RHS

Results from SHS and RHS under EOF loading are shown in Table 2.A.3 where numerical ultimate loads ( $R_{u,num}$ ), category (Cat.) and predicted resistances ( $R_{w,Rd}$ ) are presented. Since section EN 1993-1-3§6.1.7.3 (2006) specifies that the  $l_a$  value of specimens for category 1 should be taken as 10 mm, it has been decided asses two values for that parameter: the actual bearing length  $s_s$  and the given of 10 mm.

Table 2.A.3 Numerical results, EN 1993-1-3 (2006) and new proposal predicted resistances for SHS/RHS subjected to EOF loading

Specimen	$R_{u,num}$ (kN)	Cat.	6.1.7.3		6.1.7.2	Proposal
			$R_{w,Rd}$ (kN) ( $l_a=10$ )	$R_{w,Rd}$ (kN) ( $l_a=s_s$ )	$R_{w,Rd}$ (kN)	$R_{w,Rd}$ (kN)
EOF B1S52	15.503	2	20.66	25.32	11.39	12.115
EOF B1S52	17.265	1	10.33	12.66	11.53	12.115
EOF B1*S52	15.968	2	20.66	25.32	11.39	12.211
EOF B1*S524	14.888	2	20.22	24.77	10.47	11.882
EOF B1*S525	13.793	2	19.82	24.29	9.55	11.941
EOF B1*S5240	17.715	2	20.66	28.67	12.15	12.425
EOF B1*S5250	18.615	1	10.33	15.28	13.69	12.545
EOF B1*S5275	19.215	1	10.33	17.29	15.06	12.802
EOF B1*S52100	19.350	1	10.33	18.99	16.42	13.018
EOF B1*S52752	16.688	2	20.66	25.32	11.39	12.211
EOF B1*S521002	17.363	1	10.33	12.66	12.32	12.211
EOF B1*S62	17.745	1	10.33	12.66	11.53	12.211
EOF B1*S624	15.900	1	10.11	12.38	10.60	11.882
EOF B1*S625	14.310	1	9.91	12.14	9.66	11.941
EOF B2S52	16.815	2	20.66	25.32	11.39	12.405
EOF B2S62	18.623	1	10.33	12.66	11.53	12.405
EOF B2*S52	18.308	2	20.66	25.32	11.39	12.766
EOF B2*S524	16.920	2	20.22	24.77	10.47	12.608
EOF B2*S525	15.600	2	19.82	24.29	9.55	12.859
EOF B2*S5240	19.785	2	20.66	28.67	12.15	12.990
EOF B2*S5250	20.790	1	10.33	15.28	13.69	13.116
EOF B2*S5275	22.020	1	10.33	17.29	15.06	13.383
EOF B2*S52100	22.268	1	10.33	18.99	16.42	13.609
EOF B2*S52752	19.088	2	20.66	25.32	11.39	12.766
EOF B2*S521002	20.070	1	10.33	12.66	12.32	12.766
EOF B2*S62	20.160	1	10.33	12.66	11.53	12.766
EOF B2*S624	18.030	1	10.11	12.38	10.60	12.608
EOF B2*S625	16.155	1	9.91	12.14	9.66	12.859
EOF B1S54	48.090	2	76.27	89.97	47.63	56.655
EOF B1S64	53.580	1	38.14	44.98	50.95	56.655
EOF B1*S54	49.860	2	76.27	89.97	47.63	56.879
EOF B1*S544	47.783	2	75.15	88.65	47.63	52.214
EOF B1*S545	44.715	2	74.17	87.49	45.84	49.503
EOF B1*S5440	53.108	2	20.66	28.67	12.15	12.425
EOF B1*S5450	57.353	1	38.14	52.70	55.65	58.001
EOF B1*S5475	60.998	1	38.14	58.63	58.74	58.862
EOF B1*S54100	63.120	1	38.14	63.62	61.83	59.587
EOF B1*S54752	52.845	2	76.27	89.97	47.63	56.879
EOF B1*S541002	56.288	1	38.14	44.98	52.56	56.879
EOF B1*S64	55.358	1	38.14	44.98	50.95	56.879
EOF B1*S644	52.020	1	37.58	44.32	50.95	52.214
EOF B1*S645	48.773	1	37.08	43.74	49.04	49.503



Table 2.A.3 Numerical results, EN 1993-1-3 (2006) and new proposal predicted resistances for SHS/RHS subjected to EOF loading (continuation)

Specimen	$R_{u,num}$ (kN)	Cat.	6.1.7.3		6.1.7.2	Proposal
			$R_{w,Rd}$ (kN) ( $l_a=10$ )	$R_{w,Rd}$ (kN) ( $l_a=s_s$ )	$R_{w,Rd}$ (kN)	$R_{w,Rd}$ (kN)
EOF B2S54	53.348	2	76.27	89.97	47.63	57.328
EOF B2S64	58.635	1	38.14	44.98	50.95	57.328
EOF B2*S54	60.075	2	76.27	89.97	47.63	58.157
EOF B2*S544	56.325	2	75.15	88.65	47.63	53.784
EOF B2*S545	52.838	2	74.17	87.49	45.84	51.371
EOF B2*S5440	62.903	2	20.66	28.67	12.44	58.891
EOF B2*S5450	65.235	1	38.14	52.70	55.65	59.304
EOF B2*S5475	70.980	1	38.14	58.63	58.74	60.184
EOF B2*S54100	74.378	1	38.14	63.62	61.83	60.926
EOF B2*S54752	64.433	2	76.27	89.97	47.63	58.157
EOF B2*S541002	70.328	1	38.14	44.98	52.56	58.157
EOF B2*S64	64.800	1	38.14	44.98	50.95	58.157
EOF B2*S644	61.163	1	37.58	44.32	50.95	53.784
EOF B2*S645	57.300	1	37.08	43.74	49.04	51.371

### 2.A.4 EOF models for hat sections

Finally, Table 2.A.4 presents the results from the parametric study in hat sections subjected to EOF. Again, it has been assessed two values for the  $l_a$  parameter as it was performed for SHS and RHS under EOF loading.

Table 2.A.4 Numerical results, EN1993-1-3 (2006) and new proposal predicted resistances for hat sections subjected to EOF loading

Specimen	$R_{u,num}$ (kN)	Cat.	6.1.7.3		6.1.7.2	Proposal
			$R_{w,Rd}$ (kN) ( $l_a=10$ )	$R_{w,Rd}$ (kN) ( $l_a=s_g$ )	$R_{w,Rd}$ (kN)	$R_{w,Rd}$ (kN)
EOF B1S71	3.338	2	4.33	5.52	2.31	2.529
EOF B1S81	3.203	1	2.15	2.74	2.03	2.529
EOF B1S91	3.248	2	4.33	5.52	2.25	2.529
EOF B1*S71	3.375	2	4.33	5.52	2.31	2.553
EOF B1*S714	2.933	2	4.19	5.34	1.82	2.548
EOF B1*S715	2.625	2	4.07	5.18	1.65	2.627
EOF B1*S7140	4.313	2	4.33	6.38	2.59	2.614
EOF B1*S7150	4.913	2	4.33	6.86	2.78	2.649
EOF B1*S7175	5.850	1	2.15	3.91	3.39	2.723
EOF B1*S71100	6.000	1	2.15	4.34	3.88	2.785
EOF B1*S71752	3.435	2	4.33	5.52	2.31	2.553
EOF B1*S711002	3.818	2	4.33	5.52	2.31	2.553
EOF B1*S81	3.240	1	2.15	2.74	2.03	2.553
EOF B1*S814	2.940	1	2.08	2.65	1.59	2.548
EOF B1*S815	2.723	1	2.02	2.57	1.45	2.627
EOF B1*S91	3.285	2	4.33	5.52	2.25	2.553
EOF B1*S914	2.858	2	4.19	5.34	1.77	2.548
EOF B1*S915	2.543	2	4.07	5.18	1.61	2.627
EOF B1*S9140	4.095	1	2.15	3.16	2.57	2.614
EOF B1*S9150	4.598	1	2.15	3.40	2.75	2.649
EOF B1*S9175	5.820	1	2.15	3.91	3.21	2.723
EOF B1*S91100	6.090	1	2.15	4.34	3.67	2.785
EOF B1*S91752	3.375	1	2.15	2.74	2.29	2.553
EOF B1*S911002	3.788	1	2.15	2.74	2.29	2.553
EOF B2S71	3.450	2	4.33	5.52	2.31	2.601
EOF B2S81	3.315	1	2.15	2.74	2.03	2.601
EOF B2S91	3.353	2	4.33	5.52	2.25	2.601
EOF B2*S71	3.615	2	4.33	5.52	2.31	2.691
EOF B2*S714	3.143	2	4.19	5.34	1.82	2.733
EOF B2*S715	2.888	2	4.07	5.18	1.65	2.868
EOF B2*S7140	4.448	2	4.33	6.38	2.59	2.755
EOF B2*S7150	5.033	2	4.33	6.86	2.78	2.792
EOF B2*S7175	6.270	1	2.15	3.91	3.39	2.870
EOF B2*S71100	6.443	1	2.15	4.34	3.88	2.935
EOF B2*S71752	3.750	2	4.33	5.52	2.31	2.691
EOF B2*S711002	4.163	2	4.33	5.52	2.31	2.691
EOF B2*S81	3.420	1	2.15	2.74	2.03	2.691
EOF B2*S814	3.135	1	2.08	2.65	1.59	2.733
EOF B2*S815	2.933	1	2.02	2.57	1.45	2.868
EOF B2*S91	3.503	2	4.33	5.52	2.25	2.691
EOF B2*S914	3.068	2	4.19	5.34	1.77	2.733
EOF B2*S915	2.820	2	4.07	5.18	1.61	2.868
EOF B2*S9140	4.208	1	2.15	3.16	2.57	2.755
EOF B2*S9150	4.688	1	2.15	3.40	2.75	2.792
EOF B2*S9175	5.880	1	2.15	3.91	3.21	2.870
EOF B2*S91100	6.578	1	2.15	4.34	3.67	2.935

Table 2.A.4 Numerical results, EN1993-1-3 (2006) and new proposal predicted resistances for hat sections subjected to EOF loading (continuation)

Specimen	$R_{u,num}$ (kN)	Cat.	6.1.7.3		6.1.7.2	Proposal
			$R_{w,Rd}$ (kN) ( $l_a=10$ )	$R_{w,Rd}$ (kN) ( $l_a=s_c$ )	$R_{w,Rd}$ (kN)	$R_{w,Rd}$ (kN)
EOF B2*S91752	3.653	1	2.15	2.74	2.29	2.691
EOF B2*S911002	4.110	1	2.15	2.74	2.29	2.691
EOF B1S72	12.780	2	15.84	19.41	11.47	11.307
EOF B1S82	12.203	1	7.85	9.62	11.53	11.307
EOF B1S92	12.525	2	15.84	19.41	11.32	11.307
EOF B1*S72	13.028	2	15.84	19.41	11.47	11.359
EOF B1*S724	11.453	2	15.50	18.99	10.54	10.562
EOF B1*S725	10.328	2	15.20	18.62	9.61	10.142
EOF B1*S7240	16.868	2	15.84	21.98	12.24	11.558
EOF B1*S7250	17.925	2	15.84	23.43	12.75	11.670
EOF B1*S7275	19.425	1	7.85	13.14	15.25	11.909
EOF B1*S72100	20.858	1	7.85	14.43	16.63	12.110
EOF B1*S72752	12.968	2	15.84	19.41	11.47	11.359
EOF B1*S721002	13.425	2	15.84	19.41	11.47	11.359
EOF B1*S82	12.420	1	7.85	9.62	11.53	11.359
EOF B1*S824	11.115	1	7.68	9.41	10.60	10.562
EOF B1*S825	10.065	1	7.53	9.23	9.66	10.142
EOF B1*S92	12.743	2	15.84	19.41	11.32	11.359
EOF B1*S924	11.213	2	15.50	18.99	10.40	10.562
EOF B1*S925	10.140	2	15.20	18.62	9.48	10.142
EOF B1*S9240	16.350	1	7.85	10.89	12.97	11.558
EOF B1*S9250	18.668	1	7.85	11.61	13.51	11.670
EOF B1*S9275	21.203	1	7.85	13.14	14.86	11.909
EOF B1*S92100	21.795	1	7.85	14.43	16.21	12.110
EOF B1*S92752	12.908	1	7.85	9.62	12.16	11.359
EOF B1*S921002	13.890	1	7.85	9.62	12.16	11.359
EOF B2S72	13.470	2	15.84	19.41	11.47	11.465
EOF B2S82	12.795	1	7.85	9.62	11.53	11.465
EOF B2S92	13.155	2	15.84	19.41	11.32	11.465
EOF B2*S72	14.213	2	15.84	19.41	11.47	11.662
EOF B2*S724	12.540	2	15.50	18.99	10.54	10.938
EOF B2*S725	11.340	2	15.20	18.62	9.61	10.596
EOF B2*S7240	18.285	2	15.84	21.98	12.24	11.866
EOF B2*S7250	20.115	2	15.84	23.43	12.75	11.981
EOF B2*S7275	21.443	1	7.85	13.14	15.25	12.225
EOF B2*S72100	22.875	1	7.85	14.43	16.63	12.432
EOF B2*S72752	14.220	2	15.84	19.41	11.47	11.662
EOF B2*S721002	15.263	2	15.84	19.41	11.47	11.662
EOF B2*S82	13.410	1	7.85	9.62	11.53	11.662
EOF B2*S824	12.203	1	7.68	9.41	10.60	10.938
EOF B2*S825	10.950	1	7.53	9.23	9.66	10.596
EOF B2*S92	13.830	2	15.84	19.41	11.32	11.662
EOF B2*S924	12.225	2	15.50	18.99	10.40	10.938
EOF B2*S925	10.808	2	15.20	18.62	9.48	10.596
EOF B2*S9240	17.325	1	7.85	10.89	12.97	11.866
EOF B2*S9250	19.590	1	7.85	11.61	13.51	11.981
EOF B2*S9275	23.340	1	7.85	13.14	14.86	12.225
EOF B2*S92100	24.068	1	7.85	14.43	16.21	12.432
EOF B2*S92752	14.093	1	7.85	9.62	12.16	11.662
EOF B2*S921002	15.390	1	7.85	9.62	12.16	11.662

---

**CHAPTER 3 – Statistical evaluation of a new resistance model for cold-formed stainless steel cross-sections subjected to web crippling**

This chapter has been submitted to the *International Journal of Steel Structures* under the reference:

Bock M, Real E and Mirada FX (2014b). Statistical evaluation of a new resistance model for cold-formed stainless Steel cross-sections subjected to web crippling. *International Journal of Steel Structures* (under review).

**Abstract**

This paper presents a statistical evaluation according to Annex D of EN 1990 (2002) of a new resistance function for web crippling design of cold-formed stainless steel cross-sections. This resistance function was derived in Bock et al. (2013) through the use of carefully validated numerical models with the aim to propose a design expression for stainless steel sections, which are currently designed following the provisions for cold-formed carbon steel sections given in EN 1993-1-3 (2006). Although it was shown that the proposed design equation is appropriate for application to various stainless steels, the statistical uncertainties in material properties that the different types of stainless steels exhibit require an assessment of various partial safety factors. The statistical assessment showed that the proposed resistance function by Bock et al. (2013) requires adjustment to satisfy the safety level set out in EN 1993-1-4 (2006); A recalibration is performed herein. The web crippling design provisions given in EN 1993-1-3 (2006) and SEI/ASCE 8-02 (2002) American standard for application to stainless steel are also statistically evaluated herein. Comparison with test and numerical data showed that the predictions of the recalibrated resistance function are more accurate and consistent than existing design provisions.

**Keywords**

Cold-formed sections, concentrated loads, numerical analyses, stainless steel, statistical validation, web crippling.

### 3.1 Introduction

Cold-formed members exhibit a high strength-to-weight ratio which makes them attractive for a variety of structural applications where the use of less material has profound financial and environmental benefits. In particular, cold-formed stainless steel members possess the additional advantages of excellent corrosion resistance and recyclability which may offset the disadvantage of high material cost when cost is considered on a whole life basis. However, high slenderness of cold-formed member makes them more susceptible to local instabilities such as web crippling where the cross-section becomes unstable under concentrated transverse forces. The web crippling design equations given in existing structural design guidance take into account the type of loading and load location. Forces applied through one side of the cross-section flange are defined as one-flange loading, while those acting on both cross-section flanges are defined as two-flange loading. Depending on the location of the load, distinction is made between interior and exterior loading if the load is applied within the span or at the end of the member, respectively. The combination of these situations defines the four loading cases: IOF (interior one-flange), ITF (interior two-flanges), EOF (exterior one-flange) and ETF (exterior two-flanges). This classification is currently adopted in SEI/ASCE 8-02 (2002) American standard for application to stainless steel while the design expressions given in EN 1993-1-3 (2006) use relevant categories. Category 1 is the EOF, ETF and ITF counterpart while Category 2 is equivalent to IOF loading.

Web crippling is a complex type of local failure because it includes a large number of factors. Because of this, most existing expressions for web crippling design are merely empirical in nature and were calibrated by statistical fitting against experimental data. Winter and Pian (1946) proposed the first curve-fitting expression for carbon steel I-sections under EOF and IOF loading at Cornell University. After that, many empirical equations have been derived and implemented in the design rules for other cross-section geometries and load cases. Relevant research includes the studies performed by Baehre (1975), Hetrakul and Yu (1978), Wing (1981), Packer (1984), Santaputra et al. (1989), Studnicka (1990), Bhakta et al. (1992), Prabhakaran (1993), Cain et al. (1995), and Gerges (1997). In parallel with these studies on carbon steel, research was also conducted by Tsai (1987), Bakker and Stark (1994), Zhao and Hancock (1992, 1995), Hofmeyer et al. (2001) and Young and Hancock (2001) where analytical models for various types of cross-sections are proposed.

---

Given the relatively emergence of the usage of stainless steel in construction and the urge to provide practising engineers and researchers with design rules, the first version of the current SEI/ASCE 8-02 (2002) American standard for stainless steels, the ANSI/ASCE 8-90 (1990) American standard, adopted the web crippling design provisions for carbon steel. The suitability of this assumption was assessed by Korvink et al. (1995) in the Rand Afrikaans University, where some discrepancies were observed.

The aim of following studies was therefore to achieve better understanding of the effect of material behaviour on web crippling response and to develop appropriate design provisions for stainless steels. While research conducted by Zhou and Young (2006a, 2007a, 2007b, 2007c, 2008) focused on the development of web crippling design expressions within the framework of SEI/ASCE 8-02 (2002) American standard and NASPEC-2001 (2001) specifications, Talja and Salmi (1995), Talja (2004), Zilli (2004) and Bock et al. (2013), among other studies, assessed the European code. It is within this latter research, where a new expression adapted from EN 1993-1-3 (2006) was proposed to predict the web crippling resistance of cold-formed stainless steel members. The studied cross-sections were cold-formed square hollow sections (SHS), rectangular hollow sections (RHS) and hat sections. The purpose of this paper is to conduct a statistical evaluation according to Annex D of EN 1990 (2002) to assess the reliability of the proposed design equation by Bock et al. (2013) and provide a safe equation, where recalibration is required, applicable to various stainless steel grades.

## **3.2 Existing design guidance**

### **3.2.1 European design rule EN 1993-1-3 (2006)**

The web crippling design rules for stainless steel cross-sections given in EN 1993-1-4 (2006) are adopted from the specifications for cold-formed carbon steel members provided by EN 1993-1-3 (2006). The current design approach given in EN 1993-1-3 (2006) to determine the web crippling cross-section design resistance per web  $R_{w,Rd}$  provides various empirical equations for various load cases (relevant categories) and takes into consideration the number of webs of the cross-section as well as whether they are stiffened or unstiffened. For the case of cross-sections with two or more unstiffened webs, upon which the proposed equation in Bock et al. (2013) is concerned, the resistance is given by Eq. (3.1) where  $r$  is the internal radius of the corners,  $t$  is the

thickness,  $\phi$  is the relative angle between the web and the flange,  $E$  is the material Young's modulus and  $\sigma_{0.2}$  is the material proof strength. The equation also depends on  $\alpha$  and  $l_a$ , which are a non-dimensional coefficient related to the cross-section geometry and the effective bearing length related to the relevant category, respectively. The values of these parameters for hat sections are given in EN 1993-1-3 (2006) as follows: for Category 1 (EOF)  $\alpha=0.057$  and  $l_a=10$  mm; for Category 2 (IOF)  $\alpha=0.115$  and  $l_a=s_s$  where  $s_s$  is the bearing length over which the transversal load is applied. The design formulation includes a partial safety factor  $\gamma_{M1}$ . Despite EN 1993-1-3 (2006) does not explicitly give design rules for the determination of the web crippling resistance for SHS and RHS, Talja and Salmi (1995) proposed to assume coefficients for sheeting with values of  $\alpha=0.075$  for Category 1 (EOF) and  $\alpha=0.15$  for Category 2 (IOF). This is therefore adopted in the present study; previous investigations have also used this approach (Gardner et al. (2006), Talja and Hradil (2011) and Bock et al. (2013)).

$$R_{w,Rd} = \alpha t^2 \sqrt{\sigma_{0.2} E} \left( 1 - 0.1 \sqrt{\frac{r}{t}} \right) \left( 0.5 + \sqrt{\frac{0.02 l_a}{t}} \right) \left( 2.4 + \left( \frac{\phi}{90} \right)^2 \right) / \gamma_{M1} \quad (3.1)$$

In addition, those cross-sections subjected to the combined action of a bending moment  $M_{Ed}$  and a transverse force  $R_{Ed}$  (i.e. interior supports of continuous spans – IOF or Category 2) should satisfy Eqs (3.2)-(3.4) where  $M_{c,Rd}$  is the moment resistance of the cross-section and  $R_{w,Rd}$  is the sum of the local transverse resistances of the individual webs as given by Eq. (3.1). The web crippling cross-section design resistance for elements under such combination of actions  $R_{WC-BD}$  is given by Eq. (3.5) where  $L$  and  $s_{sL}$  are defined in Fig. 3.1.

$$\frac{R_{Ed}}{R_{w,Rd}} \leq 1 \quad (3.2)$$

$$\frac{M_{Ed}}{M_{c,Rd}} \leq 1 \quad (3.3)$$

$$\frac{R_{Ed}}{R_{w,Rd}} + \frac{M_{Ed}}{M_{c,Rd}} \leq 1.25 \quad (3.4)$$

$$R_{WC-BD} = R_{Ed} = 1.25 / \left( \frac{1}{R_{w,Rd}} + \frac{L - s_{sL}}{4M_{c,Rd}} \right) \leq \min\{R_{Ed}, 4M_{c,Rd}/(L - s_{sL})\} \quad (3.5)$$

### 3.2.2 SEI/ASCE 8-02 American standard

In the American framework, SEI/ASCE 8-02 (2002) provides Eq. (3.6) and (3.7) for web crippling design of shapes having single webs and unstiffened flanges, upon which the proposed equation in Bock et al. (2013) is concerned, under IOF loading while for EOF loading, the expression is given in Eq. (3.8). In these equations, the coefficients  $C_1$ ,  $C_2$ ,  $C_3$ ,  $C_4$  and  $C_\theta$  are defined in Eqs (3.9)-(3.13). Bending and web crippling interaction effects are accounted for as given by Eq. (3.14) which may be rewritten as Eq. (3.15), where  $\phi_w=0.7$  and  $\phi_b=0.85$  are the resistance factor for web crippling and bending, respectively. For consistency reasons, the above mentioned expressions follow EN 1993-1-3 (2006) symbols and SI units.

$$R_{w,Rd} = 6.9\phi_w t^2 C_1 C_2 C_\theta \left(538 - 0.74 \frac{h}{t}\right) \left(1 + 0.007 \frac{s_s}{t}\right) \text{ if } \frac{s_s}{t} \leq 60 \quad (3.6)$$

$$R_{w,Rd} = 6.9\phi_w t^2 C_1 C_2 C_\theta \left(538 - 0.74 \frac{h}{t}\right) \left(0.75 + 0.011 \frac{s_s}{t}\right) \text{ if } \frac{s_s}{t} > 60 \quad (3.7)$$

$$R_{w,Rd} = 6.9\phi_w t^2 C_3 C_4 C_\theta \left(244 - 0.57 \frac{h}{t}\right) \left(1 + 0.01 \frac{s_s}{t}\right) \quad (3.8)$$

$$C_1 = \left(1.22 - 0.22 \frac{f_{yb}}{227.7}\right) \frac{f_{yb}}{227.7} \text{ if } \frac{f_{yb}}{631.35} \leq 1 \text{ or } C_1 = 1.69 \text{ if } \frac{f_{yb}}{631.35} > 1 \quad (3.9)$$

$$C_2 = \left(1.06 - 0.06 \frac{r}{t}\right) \leq 1 \quad (3.10)$$

$$C_3 = \left(1.33 - 0.33 \frac{f_{yb}}{227.7}\right) \frac{f_{yb}}{227.7} \text{ if } \frac{f_{yb}}{458.85} \leq 1 \text{ or } C_3 = 1.34 \text{ if } \frac{f_{yb}}{458.85} > 1 \quad (3.11)$$

$$C_4 = \left(1.15 - 0.15 \frac{r}{t}\right) \leq 1 \text{ but not less than } 0.50 \quad (3.12)$$

$$C_\theta = 0.7 + 0.3(\phi/90)^2 \quad (3.13)$$

$$\frac{1.07R_{Ed}}{\phi_w R_{w,Rd}} + \frac{M_{Ed}}{\phi_b M_{c,Rd}} \leq 1.42 \quad (3.14)$$

$$R_{WC-BD} = R_{Ed} = 1.327 / \left( \frac{1}{\phi_w R_{w,Rd}} + \frac{L - s_{SL}}{4\phi_b M_{c,Rd}} \right) \leq \min\{F_{Ed}, 4M_{c,Rd}/(L - s_{SL})\} \quad (3.15)$$

### 3.3 Summary of the proposed web crippling resistance function for stainless steel cross-sections

The investigation conducted by Bock et al. (2013) examined numerically the web crippling response of ferritic and austenitic stainless steel SHS, RHS and hat sections using the finite element software ABAQUS. In the study, the load cases under consideration were internal and external concentrated loads applied through one flange, IOF and EOF respectively. It is worth to point out that this load cases resemble the web crippling response of continuous spans where the local transverse force satisfy IOF loading (Category 2) at interior supports while EOF loading (Category 1) is given at the



end of the member as shown in Fig. 3.1, where these forces are denoted as  $s_{sL}$  for the former and  $s_{sa}$  for the latter. The obtained models, which had been validated against existing experimental results conducted by Talja and Hradil (2011), were used to analyse key parameters influencing the web crippling resistance. Comparisons presented by Bock et al. (2013) with numerical and test data, highlighted the over conservative and inaccurate predictions of EN 1993-1-3 (2006) and showed that some modifications of the original formula given in the code could improve the predicted strength. Upon this observation, three mainly changes were proposed: the inclusion of the 1% proof strength  $\sigma_{1.0}$  in order to consider the strain hardening of stainless steel, some adjustments of the corner radius and the bearing length influence, and three dimensionless coefficients ( $\beta$ ,  $\delta$  and  $\xi$ ) were added to obtain better fit with numerical data (see Table 3.1). The proposed resistance model is given by Eq. (3.16) where  $k=\delta r/t$  and  $l_a=0.01s_s$  for EOF (or Category 1) while for IOF (or Category 2),  $l_a=2.2s_s$ . Predictions by this proposed resistance model were observed to provide more accurate web crippling resistances than EN 1993-1-3 (2006) enabling a more efficient design. Furthermore, the expression was observed to be suitable for application to both types of stainless steel: austenitic and ferritic stainless steels.

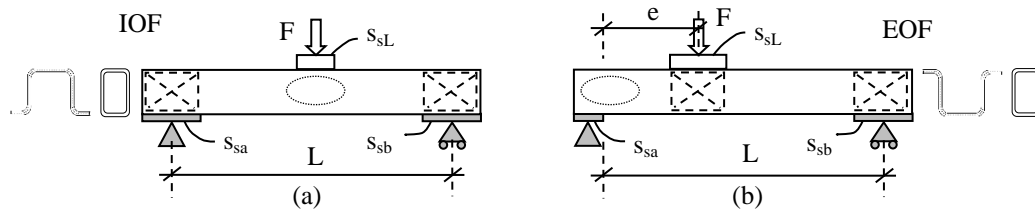


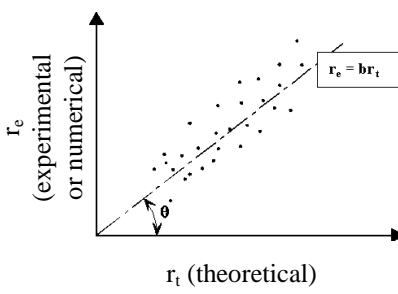
Fig. 3.1 Loading cases considered: (a) interior one-flange (IOF or Category 2) and (b) exterior one-flange (EOF or Category 1)

$$R_{w,Rd} = \alpha t^2 \sqrt{\sigma_{0.2} E} \left( \xi \frac{\sigma_{1.0}}{E} \right)^k \sqrt{\frac{\beta t}{r}} \left( 0.5 + \sqrt{\frac{0.01 l_a}{t}} \right) \left( 2.4 + \left( \frac{\phi}{90} \right)^2 \right) / \gamma_{M1} \quad (3.16)$$

Table 3.1 Non-dimensional coefficient values

Coefficient	Category 1 (EOF)		Category 2 (IOF)	
	SHS/RHS	Hat section	SHS/RHS	Hat section
$\alpha$	0.07	0.085	0.13	0.14
$\beta$	2.14	1.65	0.59	0.81
$\delta$	0.22	0.13	0.14	0.065
$\xi$	2200	2275	2700	2000

Table 3.2 Summary of the discrete steps

Step	Feature	Objective															
1. Develop a design model	$r_t = g_{rt}(\underline{X}_m)$	Develop a design model for the theoretical resistance $r_t$ represented by the resistance function $g_{rt}(\underline{X}_m)$ and to consider all the basic variables $X_i$ through the vector $\underline{X}_m = \sum_{i=1}^m X_i$ , where $m$ is the number of the various basic variables (i.e. geometry, material, coefficients)															
2. Compare experimental (or numerical) and theoretical values		See and study the deviation of all the experimental (or numerical) $r_{e,i}$ and their corresponding theoretical values $r_{t,i}$ . If the resistance function is exact and complete, the points will lie on the line $\theta = \pi/4$ , but in practice the points show some scatter. The vectors $r_{e,i}$ and $r_{e,t}$ must have the same dimension $n$ (population of data taken under consideration)															
3. Estimate the mean value of the correction factor $b$	$b = \frac{\sum_{i=1}^n r_{e,i} r_{t,i}}{\sum_{i=1}^n r_{t,i}^2}$	Represent the probabilistic model of the resistance $r$ in the format $r = b r_{t,i} \delta$ , where $b$ is the least squares best-fit to the slope and $\delta$ is the error term															
4. Estimate the coefficient of variation $V_\delta$ of the $\delta_i$ error terms	$\delta_i = \frac{r_{e,i}}{b r_{t,i}}$ $\bar{\Delta} = \frac{1}{n} \sum_{i=1}^n \Delta_i$ $\Delta_i = \ln(\delta_i) \quad s_\Delta^2 = \frac{1}{n-1} \sum_{i=1}^n (\Delta_i - \bar{\Delta})^2$	Determine the error term $\delta_i$ for each experimental (or numerical) value $r_{e,i}$ to estimate the coefficient of variation of the errors from the values of $\Delta_i$ , $\bar{\Delta}$ and $s_\Delta^2$ through $V_\delta = \sqrt{\exp(s_\Delta^2) - 1}$															
5. Analyse compatibility	Kolmogorov-Smirnov tests	Test the normality of the distribution of the errors $\delta_i$															
6. Define the coefficients of variation $V_{X_i}$ for the basic variables $X_i$ (material and geometry)	<table border="1" style="width:100%; border-collapse: collapse;"> <thead> <tr> <th>Parameter</th> <th>Mean <math>X_i</math></th> <th><math>V_{X_i}</math></th> </tr> </thead> <tbody> <tr> <td><math>M_{ost}\sigma_{0.2}</math> for austenitic</td> <td><math>1.3\sigma_{0.2,nom}</math></td> <td>0.066</td> </tr> <tr> <td><math>M_{ost}\sigma_{0.2}</math> for ferritic</td> <td><math>1.2\sigma_{0.2,nom}</math></td> <td>0.050</td> </tr> <tr> <td><math>M_{ost}\sigma_{0.2}</math> for duplex</td> <td><math>1.1\sigma_{0.2,nom}</math></td> <td>0.049</td> </tr> <tr> <td>Geometry</td> <td>nominal value</td> <td>0.050</td> </tr> </tbody> </table>	Parameter	Mean $X_i$	$V_{X_i}$	$M_{ost}\sigma_{0.2}$ for austenitic	$1.3\sigma_{0.2,nom}$	0.066	$M_{ost}\sigma_{0.2}$ for ferritic	$1.2\sigma_{0.2,nom}$	0.050	$M_{ost}\sigma_{0.2}$ for duplex	$1.1\sigma_{0.2,nom}$	0.049	Geometry	nominal value	0.050	These coefficients of variation $V_{X_i}$ have been recently presented for stainless steel in Baddoo and Francis (2012, 2013) after an extensive statistical study of data collected from the stainless steel suppliers and manufacturers
Parameter	Mean $X_i$	$V_{X_i}$															
$M_{ost}\sigma_{0.2}$ for austenitic	$1.3\sigma_{0.2,nom}$	0.066															
$M_{ost}\sigma_{0.2}$ for ferritic	$1.2\sigma_{0.2,nom}$	0.050															
$M_{ost}\sigma_{0.2}$ for duplex	$1.1\sigma_{0.2,nom}$	0.049															
Geometry	nominal value	0.050															
7. Define the combined coefficient of variation $V_r^2$	$V_{rt}^2 = \frac{var[g_{rt}(\underline{X}_m)]}{g_{rt}^2(\underline{X}_m)} = \frac{1}{g_{rt}^2(\underline{X}_m)} \sum_{i=1}^j \left[ \frac{\partial g_{rt}}{\partial X_i} \cdot V_{X_i} \right]^2$ $V_r^2 = V_\delta^2 + V_{rt}^2 + V_{FEM}^2$	This term is considered to include all possible deviations: errors ( $V_\delta$ ), resistance function ( $V_{rt}^2$ ) and the deviation of the numerical model ( $V_{FEM}^2$ ) proposed by Davaine (2005) given in sub-section 3.3															
8.a Method a) Definition of the characteristic value	$r_k = b C_k g_{rt}(X_m)$ $C_k = \exp(-k_\infty \alpha_{rt} Q_{rt} - k_n \alpha_\delta Q_\delta - 0,5 Q^2)$	$Q_{rt} = \sqrt{\ln(V_{rt}^2 + 1)} \quad Q_\delta = \sqrt{\ln(V_\delta^2 + 1)}$ $Q = \sqrt{\ln(V_r^2 + 1)} \quad \alpha_{rt} = \frac{Q_{rt}}{Q} \quad \alpha_\delta = \frac{Q_\delta}{Q}$															
8.b Method b) Definition of the design value	$r_d = b C_d g_{rt}(X_m)$ $C_d = \exp(-k_{d,\infty} \alpha_{rt} Q_{rt} - k_{d,n} \alpha_\delta Q_\delta - 0,5 Q^2)$	$k_n$ and $k_\infty$ are defined in Table D1 of EN 1990 whereas $k_{d,n}$ and $k_{d,\infty}$ are given in Table D2.															
9. Partial safety factor	$\gamma_{M1} = \frac{r_k}{r_d} = \frac{C_k}{C_d}$	The partial safety factor is obtained dividing $r_k$ by $r_d$															
10. Corrected partial safety factor	$\gamma_{M1}^* = \frac{r_k r_n}{r_d r_k} = \frac{r_n}{r_d}$	To adapt the partial safety factor to better statistical variations															

### 3.4. Statistical analysis

#### 3.4.1 Annex D of EN 1990

When an alternative design rule is proposed, the resulting design model  $r_t$  for the resistance function  $g_{rt}(\underline{X}_m)$ , where  $\underline{X}_m$  refers to all basic variables (i.e. geometry, mechanical material properties and non-dimensional coefficients) that affect the resistance at the relevant limit state, should be in accordance with the principles of EN 1990 (2002). Annex D of EN 1990 (2002) establishes the principles for design assisted by testing, where the reliability of the derived model is assessed on the basis of a statistical interpretation of available test data. The standard evaluation procedure given in Annex D of EN 1990 (2002) considers two methods to statistically evaluate a design model: Method a) by evaluating the characteristic value of the resistance function  $r_k$ ; and Method b) by direct determination of the design value of the resistance function  $r_d$ . Hence, the partial safety factor can be obtained dividing the characteristic value by the design value as given by Eq. (3.17).

$$\gamma_{M1} = \frac{r_k}{r_d} \quad (3.17)$$

Both methods are given in Annex D of EN 1990 (2002) as a number of discrete steps which are summarised in Table 3.2. It is important to mention that the basic variables  $X_i$  (related to material and geometry) for evaluating the design and characteristic resistance functions,  $r_d$  and  $r_k$  respectively, are based on different values. While the material mechanical properties are defined as nominal values ( $\sigma_{0.2,nom}$ ), which could be understood as the minimum (characteristic) value to be satisfied after the steelmaking with an over-strength ratio  $M_{osr}$  (average difference between the true strength of the material and the value used in design), the nominal geometrical values are adopted as mean values with a certain fabrication tolerance. To statistically harmonise these discrepancies and use nominal values for all input parameters, EN 1990 (2002) introduces the nominal resistance function  $r_n$  to correct the partial safety factor  $\gamma_{M1}$  into  $\gamma_{M1}^*$ . The nominal value of this resistance function  $r_n$  is determined evaluating the resistance function using the nominal values for the basic variables (i.e. measured value for the geometry and  $\sigma_{0.2,nom} = \sigma_{0.2}/M_{osr}$  for the material where  $\sigma_{0.2}$  is the measured value of the 0.2% proof strength). Baddoo and Francis (2012, 2013) undertook a large collection of data from steel producers and manufacturers where the over-strength ratio

$M_{osr}$  was found to be 1.3, 1.2 and 1.1 for austenitic, ferritic and duplex stainless steel, respectively. The transformed value of  $\gamma_{M1}^*$  is given by Eq. (3.18) and is used herein to statistically evaluate the proposed resistance function  $r_t$  by Bock et al. (2013) (Eq. (3.19)) and existing design standards.

$$\gamma_{M1}^* = \frac{r_k r_n}{r_d r_k} = \frac{r_n}{r_d} \quad (3.18)$$

$$r_t = g_{rt}(\underline{X}_m) = \alpha t^2 \sqrt{\sigma_{0.2} E} \left( \xi \frac{\sigma_{1.0}}{E} \right)^k \sqrt{\frac{\beta t}{r}} \left( 0.5 + \sqrt{\frac{0.01 l_a}{t}} \right) \left( 2.4 + \left( \frac{\phi}{90} \right)^2 \right) \quad (3.19)$$

### 3.4.2 Adaptation of the procedure to a numerical database

The original procedure given in Annex D of EN 1990 (2002) is intended to statistically evaluate resistance functions (design models) derived through the use of experimental data  $r_e$  (experimental). Due to the fact that the statistical evaluation performed in this study is based on numerical results,  $r_e$  (numerical), an additional term  $V_{FEM}$  was considered for the combined coefficient of variation  $V_r^2$  as given by Eq. (3.20).

$$V_r^2 = V_\delta^2 + V_{rt}^2 + V_{FEM}^2 \quad (3.20)$$

This  $V_{FEM}$  term refers to the coefficient of variation of the numerical model and was proposed to be included in  $V_r^2$  by Davaine (2005) to consider uncertainties and unfavourable deviations between the numerical model and the experimental data considered for its calibration; this approach has also been used by Gabeler (2009) and Chacón et al. (2012) in their studies on plate girders subjected to patch loading. The proposed process by Davaine (2005) to determine the value of  $V_{FEM}$  is given in Eqs (3.21)-(3.26) where  $r_{e,i}$  are experimental values,  $r_{FEM,i}$  are their corresponding numerical values predicted by the numerical model,  $b_{FEM}$  is the average ratio of experimental to numerical based on a least squares fit to the test data,  $\delta_{FEM,i}$  is the error term for each numerical value,  $n_{FEM}$  is the population of numerical analyses taken under consideration and  $r_{FEM,i}$ ,  $\Delta_{FEM,i}$ ,  $\bar{\Delta}_{FEM}$  and  $s_{\Delta,FEM}^2$  are statistical parameters. Note that this notation resembles the one used to determine the coefficient of variation of the error  $V_\delta$  (see Table 3.2).

$$b_{FEM} = \frac{\sum r_{e,i} r_{FEM,i}}{\sum r_{FEM,i}^2} \quad (3.21)$$

$$\delta_{FEM,i} = \frac{r_{e,i}}{b_{FEM} r_{FEM,i}} \quad (3.22)$$

$$\Delta_{FEM,i} = \ln(\delta_{FEM,i}) \quad (3.23)$$

$$\bar{\Delta}_{FEM} = \frac{1}{n_{FEM}} \sum_{i=1}^{n_{FEM}} \ln(\delta_{FEM,i}) \quad (3.24)$$

$$s_{\Delta,FEM}^2 = \frac{1}{n_{FEM} - 1} \sum_{i=1}^n (\Delta_{FEM,i} - \bar{\Delta}_{FEM})^2 \quad (3.25)$$

$$V_{FEM} = \sqrt{\exp(s_{\Delta,FEM}^2) - 1} \quad (3.26)$$

### 3.5 Numerical analyses

#### 3.5.1 Available numerical database

In order to conduct the statistical evaluation of the proposed resistance function (Eq. (3.19)), the generated numerical data by Bock et al. (2013) was considered and split into sub-sets based on their load condition, cross-section geometry and material. Given the fact that most of the numerical analyses were performed on ferritic stainless steel cross-sections and little numerical data for austenitic stainless steel was available, this latter database is expanded in the present paper on the basis of parametric studies by using the finite element package ABAQUS. Further details of the numerical analyses are given in the following sub-sections. Having complemented the original available numerical data, a total of 262 and 182 numerical results for ferritic and austenitic stainless, respectively, steel were involved in the statistical analysis. Details of the amount of numerical data considered in each sub-set are given in Table 3.3.

Table 3.3 Available numerical database

Load case	Cross-Section type	Ferritics	Austenitics
IOF	SHS/RHS	83	53
	Hat sections	74	64
EOF	SHS/RHS	71	41
	Hat sections	34	24
Total		262	182

#### 3.5.2 Parametric study

The additional numerical analyses of the simulations performed by using ABAQUS on austenitic stainless steel cross-sections with material mechanical properties given in Table 3.4 are described herein. The cross-sections considered were SHS, RHS and hat sections with the dimensions given in Table 3.5 with reference to symbols shown in Fig. 3.2. These cross-sections were modelled under IOF and EOF loading. Thicknesses of 2 mm and 4 mm for the SHS and RHS and 1 mm and 2 mm for the hat sections were

considered. The length of all the specimens ( $L$ ) remained constant at 500 mm. The length of the supports ( $s_{sa}$  and  $s_{sb}$ ) for the IOF loading was set to 50 mm while the bearing length through of which the load is applied ( $s_{sL}$ ) was 25 mm. For the EOF loading, the length of the support that produces web crippling (end bearing support,  $s_{sa}$ ) was 25 mm whereas for the further end support ( $s_{sb}$ ) was 50 mm. The load was applied through a plate ( $s_{sL}$ ), which was 50 mm length, and the distance from its centre to the edge of the end bearing support ( $e$ ) was 150 mm. All these abovementioned parameters are depicted in Fig. 3.1. 4-point bending models were also performed on these geometries to determine the moment resistance of the cross-section  $M_{c,Rd}$  and study the combined bending and web crippling interaction effects for IOF loading (Eqs (3.5) and (3.15)). In these models, the load was applied through two plates of 50 mm-wide placed at 1/3 and 2/3 of the total length which was set to 1000 mm. Additional specimens were modelled for materials A1\* and A2\* to study the influence of various parameters on the web crippling strength, including: two more corner radii ( $r_m=4$  mm and 5 mm for S5, S6, S7 and S9 and  $r_m=5$  mm and 6 mm for S8); four more bearing lengths for IOF loading ( $s_{sL}=40$  mm, 50 mm, 75 mm and 100 mm); and four more end bearing lengths ( $s_{sa}=40$  mm, 50 mm, 75 mm and 100 mm) and two plate lengths over which the load is applied ( $s_{sL}=75$  mm and 100 mm) for EOF loading. A total of 44 and 64 numerical analyses were performed on austenitic SHS/RHS and hat sections under IOF loading respectively, while for EOF loading the number of conducted numerical analyses were 31 and 24 for SHS/RHS and hat sections, respectively. Further details of the numerical model used herein are given in Bock et al. (2013) where a carefully validation against experimental results was also undertaken. Recall that the parametric study performed herein on austenitic stainless steel cross-section complements the numerical data reported in Bock et al. (2013) where more focus was given to the web crippling response of ferritic stainless steel cross-sections. The document also reports an assessment of the sensitivity of the numerical model to different key modelling parameters including initial imperfections and mesh studies as well as the influence of various geometries and material properties on the web crippling response.

Table 3.4 Material mechanical properties considered

	E (GPa)	$\sigma_{0.2}$ (MPa)	n	$\sigma_{1.0}$ (MPa)	$\sigma_u$ (MPa)	m	$\epsilon_u$	$\sigma_u/\sigma_{0.2}$
A1	200	250	5	256	275	3	0.4	1.1
A1*	200	250	5	262.2	300	3	0.4	1.2
A2	200	250	5	275	350	3	0.4	1.4
A2*	200	250	5	300	450	3	0.4	1.8

Table 3.5 Basic cross-section geometries considered

	Label	b (mm)	$h_w$ (mm)	c (mm)	$r_m$ (mm)
SHS 70×70×t	S5	70	70	-	3
RHS 60×120×t	S6	60	120	-	3
Hat 60×60×20×t	S7	60	60	20	3
Hat 120×120×50×t	S8	120	120	50	3
Hat 60×80×25×t	S9	60	80	25	3

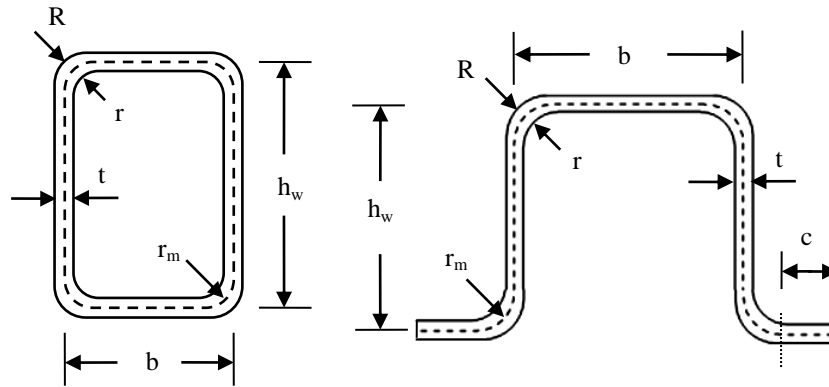


Fig. 3.2 Definition of symbols for the cross-sections

The obtained numerical results of this parametric study performed on austenitic stainless steel cross-sections are presented in Appendix 3.A where all the specimens were labelled following the same criteria used by Bock et al. (2013) so that the austenitic counterpart result could be compared with the ferritic one.

### 3.6. Results of the statistical evaluation

#### 3.6.1 General

In this section, the obtained partial safety factors for the eight sub-sets of considered data (2 load conditions, 2 types of cross-section and 2 materials shown in Table 3) and key results for the steps summarised in Table 3.2 are analysed and used to assess the reliability of the proposed resistance function by Bock et al. (2013). The equations given in EN 1993-1-3 (2006) and SEI/ASCE 8-02 (2002) were also considered in this statistical analysis for comparison purposes.

#### 3.6.2 Estimation of $V_{FEM}$

The coefficient of variation of the numerical model  $V_{FEM}$  was determined preceding the actual statistical analyses since, as mentioned earlier, the data under consideration was based on numerical results. To this end, the results from the validation of the numerical model given by Bock et al. (2013), where existing test performed by Gardner et al.

(2006) and Talja and Hradil (2011) were collected and modelled by using ABAQUS, were considered to determine such parameter. The results are shown in Table 3.6 where  $r_{e,i}$  and  $r_{FEM,i}$  are the reported values in the corresponding documents for the experimental and numerical web crippling strength of the cross-section respectively, and  $b_{FEM}$ ,  $\delta_{FEM,i}$ ,  $\Delta_{FEM,i}$ ,  $\bar{\Delta}_{FEM}$  and  $s_{\Delta,FEM}^2$  are key statistical parameters determined according to Eqs (3.21)-(3.26).

Table 3.6 Determination of the VFEM

Type of load	Specimen	$r_{e,i}$ (kN)	$r_{FEM,i}$ (kN)	$r_{e,i}/r_{FEM,i}$	$r_{e,i}r_{FEM,i}$	$r_{FEM,i}^2$	$\delta_{FEM,i}$	$\Delta_{FEM,i}$	$(\Delta_{FEM,i} - \bar{\Delta}_{FEM})^2$
EOF	SHS_ES <sup>a</sup>	25.76	35.36	0.73	910.9	1250.3	0.671	-0.399	0.1241
	TH_10_ES <sup>a</sup>	7.16	7.03	1.02	50.3	49.4	0.939	-0.063	0.0003
	TH_15_ES <sup>a</sup>	15.03	15.07	1.00	226.5	227.1	0.919	-0.084	0.0015
	TH_20_ES <sup>a</sup>	25.91	25.82	1.00	669.0	666.7	0.925	-0.078	0.0010
	TH_30_ES <sup>a</sup>	42.06	39.93	1.05	1679.5	1594.4	0.971	-0.030	0.0003
IOF	SHS_IS <sup>a</sup>	43.92	37.02	1.19	1625.9	1370.5	1.093	0.089	0.0183
	SHS_100×100×3 <sup>b</sup>	107.10	101.18	1.06	10836.4	10237.4	0.975	-0.025	0.0005
	SHS_120×80×3 <sup>b</sup>	108.30	96.42	1.12	10442.3	9296.8	1.035	0.034	0.0065
	RHS_140×60×3 <sup>b</sup>	107.50	95.69	1.12	10286.7	9156.6	1.035	0.035	0.0065
	TH_10_IS <sup>a</sup>	10.00	9.75	1.03	97.5	95.1	0.945	-0.056	0.0001
	TH_15_IS <sup>a</sup>	20.73	19.59	1.06	406.1	383.8	0.975	-0.025	0.0004
	TH_20_IS <sup>a</sup>	34.84	32.41	1.07	1129.2	1050.4	0.991	-0.009	0.0013
	TH_30_IS <sup>a</sup>	55.01	50.09	1.10	2755.5	2509.0	1.012	0.012	0.0034
<sup>a</sup> Talja and Hradil (2011)				$b_{FEM} = 1.085$					
<sup>b</sup> Gardner et al. (2006)				$\bar{\Delta}_{FEM} = -0.046$					
				$s_{\Delta,FEM}^2 = 0.014$					
				$V_{FEM} = 0.117$					

### 3.6.3 Resulting partial safety factors

The obtained partial safety factors from the statistical evaluations are presented herein. The structural design guidance for stainless steels, the EN 1993-1-4 (2006), employs a partial safety factor  $\gamma_{M1}^*$  of 1.1. Hence, partial safety factors falling below this value of 1.1 reflect that the resistance function is reliable. Above 1.1, the design approach is deemed to be unsafe thereby requiring a recalibration so that the safety level is satisfied. Tables 3.7 and 3.8 show key results of the statistical evaluation for IOF and EOF loading respectively, while Figs 3.3 and 3.4 show the numerical resistances  $r_e$  plotted against the predicted ones  $r_t$  for IOF and EOF loading respectively, where the least squares best-fit to the slope  $b$  is also given (Step 2 from Table 3.2). Table 3.9 show key statistical values concerning mean predictions and coefficient of variation (COV) of the three design approaches relative to the numerical results for IOF loading while for EOF loading, these are given in Table 3.10. From the results for IOF loading given in Table



3.7, it can be observed that the proposed resistance function by Bock et al. (2013) satisfies the safety level recommended in EN 1993-1-4 (2006) for all sets of data. Note also that this proposal provides higher partial safety factors for ferritic stainless steel than the austenitics reflecting that the former ones are designed more efficiently. EN 1993-1-3 (2006) yields similar partial safety factors for hat sections, though the safety level for SHS and RHS is not satisfied. This is associated with the inaccuracy of the approach to predict web crippling strength for such cross-sections, as is highlighted in Fig. 3.3(a) and (c) where it is observed that EN 1993-1-3 (2006) over-estimates the resistance of some specimens. Recall that EN 1993-1-3 (2006) does not make allowance for SHS and RHS, and the approach recommended by Talja and Salmi (1995) was used herein. The assessment for SEI/ASCE 8-02 (2002) shows that this approach is not suitable for the material and cross-sections considered in the present study since the predicted web crippling capacity is too optimistic (see Fig. 3.3)

Table 3.7 Summary of statistical evaluation of various approaches for IOF loading

Material	Cross-section	Design approach	$V_{\delta}$	$V_r$	$\gamma_{M1}$	$\gamma_{M1}^*$
Ferritic	SHS/RHS	EN 1993-1-3	0.132	0.036	1.194	1.147
		ASCE	0.131	0.036	1.193	1.280
		Proposal	0.070	0.024	1.099	0.928
	Hat sections	EN 1993-1-3	0.102	0.029	1.145	0.899
		ASCE	0.090	0.027	1.126	1.188
		Proposal	0.068	0.023	1.098	0.928
Austenitic	SHS/RHS	EN 1993-1-3	0.122	0.036	1.194	1.131
		ASCE	0.125	0.036	1.199	1.232
		Proposal	0.073	0.026	1.119	0.888
	Hat sections	EN 1993-1-3	0.090	0.029	1.141	0.904
		ASCE	0.095	0.030	1.149	1.134
		Proposal	0.062	0.025	1.105	0.892

Table 3.8 Summary of statistical evaluation of various approaches for EOF loading

Material	Cross-section	Design approach	$V_{\delta}$	$V_r$	$\gamma_{M1}$	$\gamma_{M1}^*$
Ferritic	SHS/RHS	EN 1993-1-3	0.177	0.050	1.282	0.763
		ASCE	0.273	0.094	1.488	1.120
		Proposal	0.216	0.066	1.361	1.355
	Hat sections	EN 1993-1-3	0.185	0.053	1.323	0.819
		ASCE	0.226	0.070	1.419	1.188
		Proposal	0.190	0.055	1.334	1.388
Austenitic	SHS/RHS	EN 1993-1-3	0.171	0.050	1.294	0.760
		ASCE	0.208	0.064	1.373	0.933
		Proposal	0.202	0.062	1.360	1.263
	Hat sections	EN 1993-1-3	0.217	0.068	1.436	0.907
		ASCE	0.230	0.074	1.470	1.076
		Proposal	0.206	0.064	1.408	1.244

Regarding the results for EOF loading, which are given in Table 3.8, it is observed that the proposed resistance function by Bock et al. (2013) yields unreliable predictions for the recommended value  $\gamma_{M1}^*$  of 1.1 given in EN 1993-1-4 (2006). Similar results are observed for the approach given in SEI/ASCE 8-02 (2002) when is applied to ferritic stainless steels, however, the safety level for the austenitics is satisfied. Unlike the results for IOF loading, where some approaches over-estimated web crippling capacities, the unsatisfactory partial safety factors obtained for EOF loading are associated with the high scatter (COV) provided by the actual design approach (see Table 3.10). Note that, as shown in Fig. 3.4, the three design methods provide safe values, though the web crippling resistances are overly underestimated as shown the mean prediction given in Table 3.10. This is also highlighted in the results for the statistical evaluation of EN 1993-1-3 (2006) where all partial safety factors are far below 1.1, but satisfying the safety level. Hence, on the basis of these observations, it is concluded that a revised expression of the proposed resistance function is required for EOF loading. This is conducted in the following section.

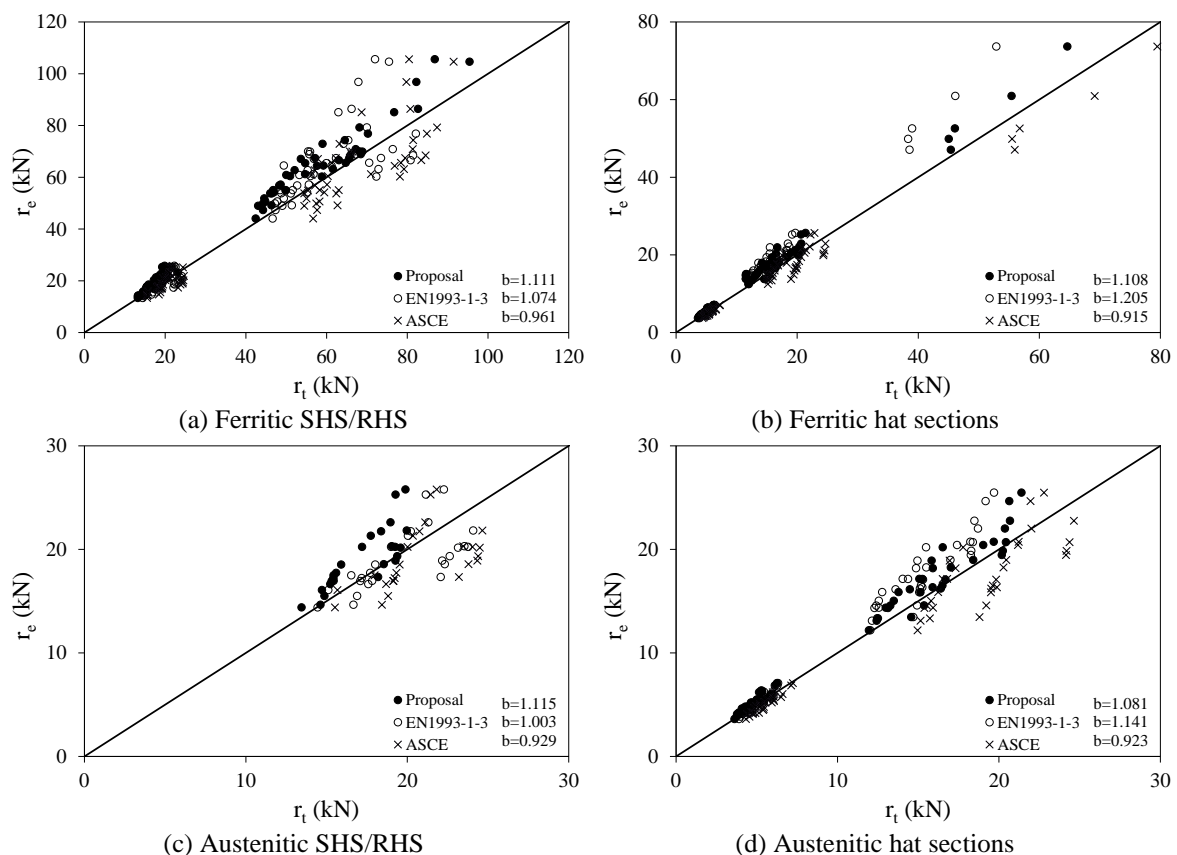


Fig. 3.3 Comparison of numerical loads  $r_e$  and predicted resistances  $r_t$  by EN 1993-1-3 (2006), SEI/ASCE 8-02 (2002) and proposal for IOF loading

Statistical evaluation of a new resistance model for cold-formed stainless steel cross-sections subjected to web crippling

Table 3.9 Key statistical values of the comparison for IOF loading

Material	Cross-section	Design approach	Mean	COV
Ferritic	SHS/RHS	EN 1993-1-3	$r_c/r_t$ 1.048	0.133
		ASCE	$r_c/r_t$ 0.958	0.132
		Proposal	$r_c/r_t$ 1.109	0.070
	Hat sections	EN 1993-1-3	$r_c/r_t$ 1.135	0.102
		ASCE	$r_c/r_t$ 0.931	0.090
		Proposal	$r_c/r_t$ 1.101	0.069
Austenitic	SHS/RHS	EN 1993-1-3	$r_c/r_t$ 1.008	0.120
		ASCE	$r_c/r_t$ 0.938	0.125
		Proposal	$r_c/r_t$ 1.117	0.072
	Hat sections	EN 1993-1-3	$r_c/r_t$ 1.090	0.090
		ASCE	$r_c/r_t$ 0.921	0.095
		Proposal	$r_c/r_t$ 1.078	0.062

Table 3.10 Key statistical values of the comparison for EOF loading

Material	Cross-section	Design approach	Mean	COV
Ferritic	SHS/RHS	EN 1993-1-3	$r_c/r_t$ 2.007	0.173
		ASCE	$r_c/r_t$ 2.218	0.278
		Proposal	$r_c/r_t$ 1.386	0.225
	Hat sections	EN 1993-1-3	$r_c/r_t$ 1.763	0.193
		ASCE	$r_c/r_t$ 1.822	0.219
		Proposal	$r_c/r_t$ 1.241	0.203
Austenitic	SHS/RHS	EN 1993-1-3	$r_c/r_t$ 1.874	0.168
		ASCE	$r_c/r_t$ 1.906	0.211
		Proposal	$r_c/r_t$ 1.358	0.206
	Hat sections	EN 1993-1-3	$r_c/r_t$ 1.742	0.225
		ASCE	$r_c/r_t$ 1.883	0.216
		Proposal	$r_c/r_t$ 1.287	0.209

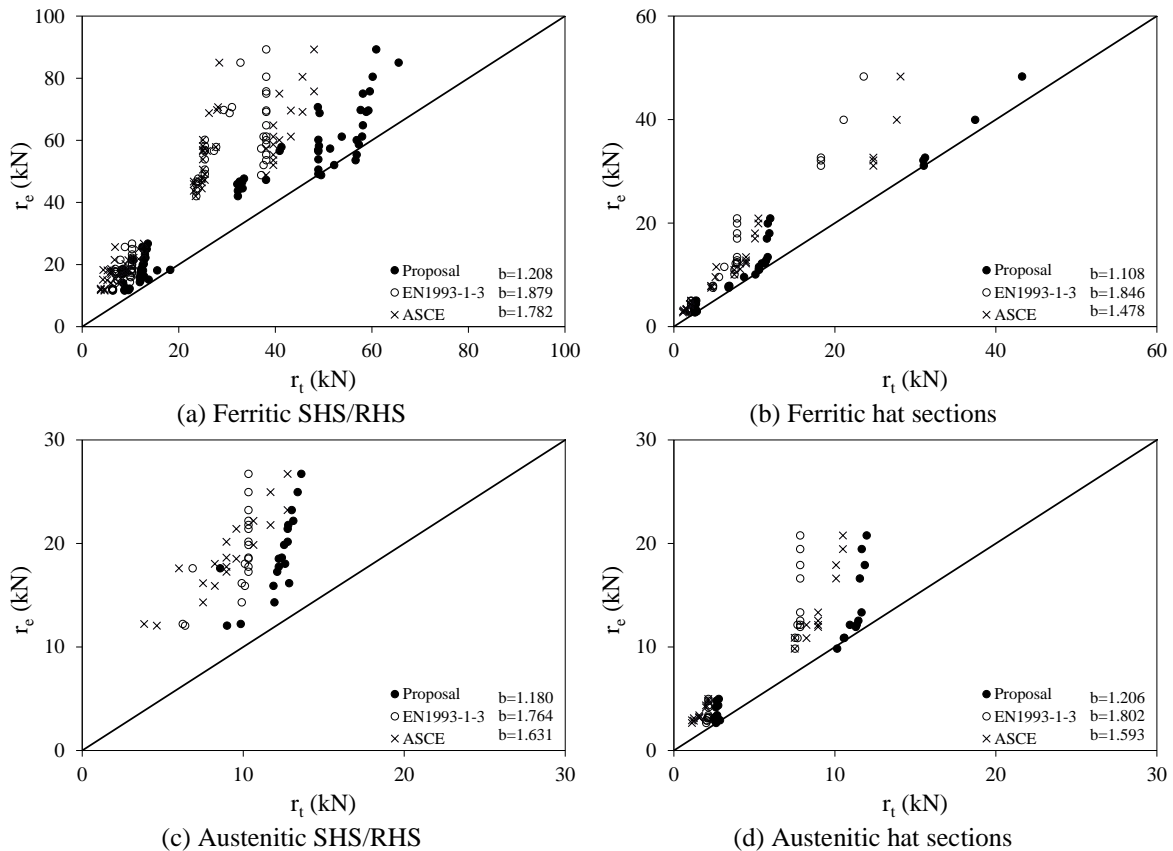


Fig. 3.4 Comparison of numerical loads  $r_c$  and predicted resistances  $r_t$  by EN 1993-1-3 (2006), SEI/ASCE 8-02 (2002) and proposal for EOF loading

### 3.6.4 Recalibration of the proposed resistance function

Having concluded that the proposed resistance function for EOF loading requires further adjustment, a revised value for the new non-dimensional coefficient  $\alpha$  was sought. This was achieved by setting the corrected partial safety factor  $\gamma_{M1}^*$  for the most restrictive set of data (i.e. ferritic stainless steel SHS and RHS) to the required safety level of 1.1 and limiting the number of decimals of the coefficient  $\alpha$ . The coefficients  $\beta$ ,  $\delta$  and  $\xi$  were kept since non-significant improvements were observed. The resulting value for  $\alpha$  is given in Table 3.11 together with the coefficients for IOF loading. The results of the statistical evaluation of the recalibrated resistance function for EOF loading are shown in Table 3.12 where previous resulting partial safety factors for EN 1993-1-3 (2006) and SEI/ASCE 8-02 (2002) are also given. The updated results for the comparison between the numerical resistances  $r_e$  and the predicted ones  $r_t$ , including the least squares best-fit to the slope parameter  $b$  (Step 2 from Table 3.2), and for the key statistical values concerning mean predictions and coefficient of variation (COV) of the three design approaches relative to the numerical results are given in Fig. 3.5 and Table 3.13, respectively. The results show that the recalibrated resistance function satisfies the safety level set out in EN 1993-1-4 (2006). Besides, as it has been observed for IOF loading, higher partial safety factors are achieved for ferritic stainless steels than for the austenitics reflecting that the former ones are designed more efficiently.

Table 3.11 Non-dimensional coefficient values after recalibration

Coefficient	Category 1 (EOF)		Category 2 (IOF)	
	SHS/RHS	Hat section	SHS/RHS	Hat section
$\alpha$	0.057	0.067	0.13	0.14
$\beta$	2.14	1.65	0.59	0.81
$\delta$	0.22	0.13	0.14	0.065
$\xi$	2200	2275	2700	2000

Table 3.12 Partial safety factors for EOF load condition after recalibration

Material	Cross-section	Design approach	$V_\delta$	$V_r$	$\gamma_{M1}$	$\gamma_{M1}^*$
Ferritic	SHS/RHS	EN 1993-1-3	0.177	0.050	1.282	0.763
		ASCE	0.273	0.094	1.488	1.120
		Proposal	0.216	0.066	1.361	1.098
	Hat sections	EN 1993-1-3	0.185	0.053	1.323	0.819
		ASCE	0.226	0.070	1.419	1.188
		Proposal	0.190	0.055	1.334	1.097
Austenitic	SHS/RHS	EN 1993-1-3	0.171	0.050	1.294	0.760
		ASCE	0.208	0.064	1.373	0.933
		Proposal	0.202	0.062	1.360	1.023
	Hat sections	EN 1993-1-3	0.217	0.068	1.436	0.907
		ASCE	0.230	0.074	1.470	1.076
		Proposal	0.206	0.064	1.408	0.983

Statistical evaluation of a new resistance model for cold-formed stainless steel cross-sections subjected to web crippling

Table 3.13 Key statistical values of the comparison for the EOF loading after recalibration

Material	Cross-section	Design approach	Mean	COV
Ferritics	SHS/RHS	EN 1993-1-3	$r_e/r_t$ 2.007	0.173
		ASCE	$r_e/r_t$ 2.218	0.278
		Proposal	$r_e/r_t$ 1.711	0.225
	Hat sections	EN 1993-1-3	$r_e/r_t$ 1.763	0.193
		ASCE	$r_e/r_t$ 1.822	0.219
		Proposal	$r_e/r_t$ 1.571	0.203
Austenitics	SHS/RHS	EN 1993-1-3	$r_e/r_t$ 1.874	0.168
		ASCE	$r_e/r_t$ 1.906	0.211
		Proposal	$r_e/r_t$ 1.676	0.202
	Hat sections	EN 1993-1-3	$r_e/r_t$ 1.742	0.225
		ASCE	$r_e/r_t$ 1.883	0.216
		Proposal	$r_e/r_t$ 1.629	0.209

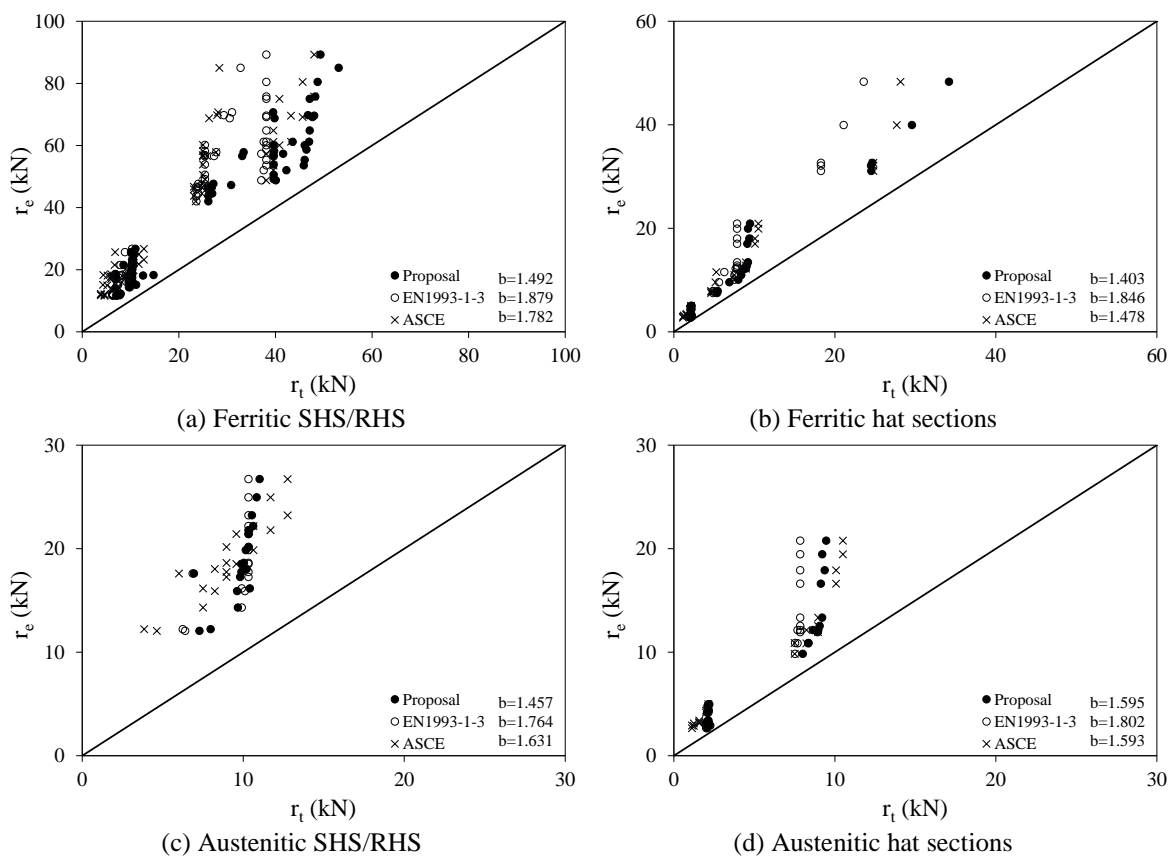


Fig. 3.5 Comparison of numerical loads  $r_e$  and predicted resistances  $r_t$  by EN 1993-1-3 (2006), SEI/ASCE 8-02 (2002) and proposal for EOF loading after recalibration

### 3.7 Validation of the revised design equation with experimental results

The predictions of the proposed formulation by Bock et al. (2013) and given in Eq. (3.16) with revised non-dimensional coefficients from Table 3.11 are compared with existing test results on various stainless steel grades including high strength austenitic and duplex stainless steels (Zhou and Young (2007a, 2007b and 2007c)), austenitic stainless steels (Talja and Salmi (1995) and Gardner et al. (2006)) and ferritic stainless

steels (Talja and Hradil (2011)). Capacity predictions according to EN 1993-1-3 (2006) and SEI/ASCE 8-02 (2002) are also determined. The comparisons for both load cases are given in Fig. 3.6 on the basis of the experimental to predicted ratio  $r_e/r_t$  where it is observed that the recalibrated resistance function (proposal) achieves a reduction of mean prediction with similar scatter compared to existing design guidance, in line with the observations outlined in sub-sections 3.6.3 and 3.6.4 for the numerical data. Key statistical values concerning mean predictions and COV relative to the tests are given in Table 3.14 for the various sets of data.

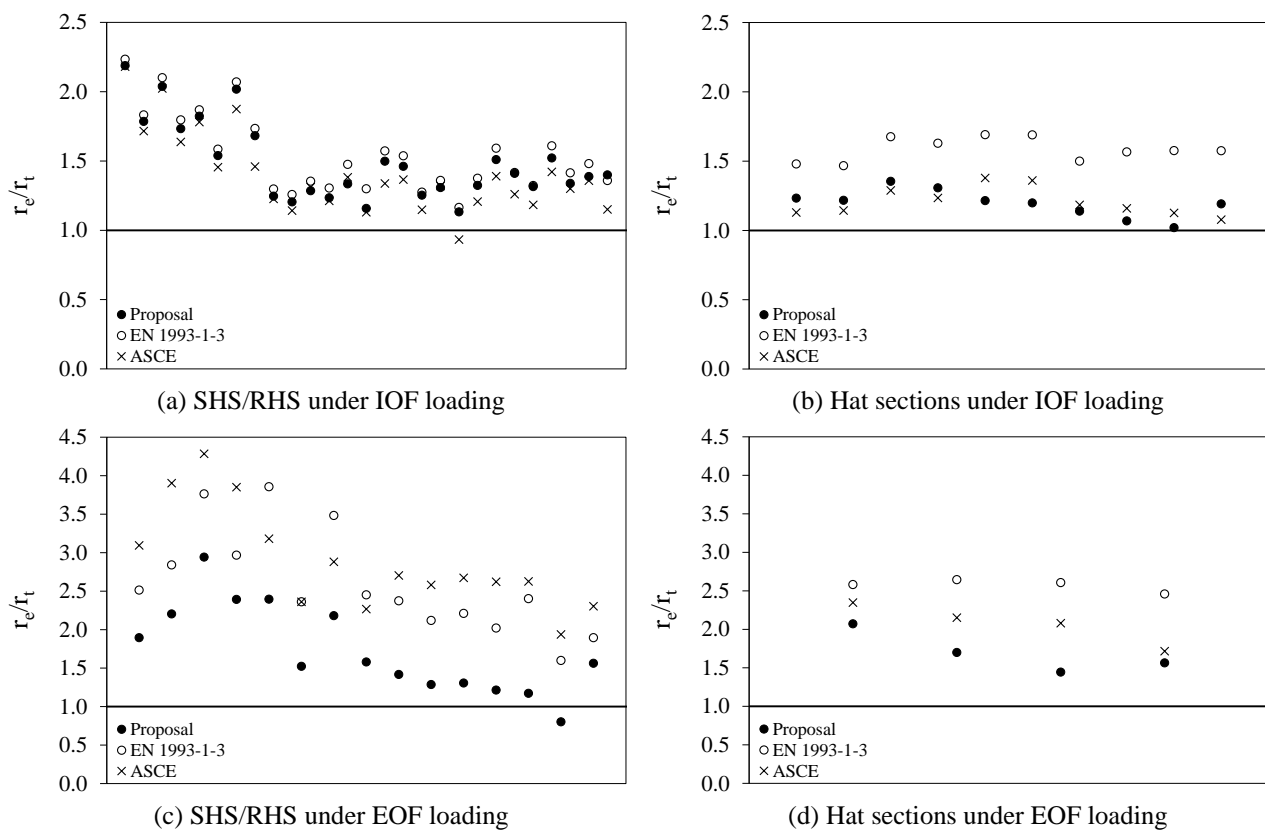


Fig 3.6 Comparison between the revised resistance function and existing provisions

Table 3.14 Statistical results of the ratio  $r_e/r_t$  based on experimental results

Load case	Cross-section	Design approach	Mean	COV
IOF	SHS/RHS	EN 1993-1-3 $r_e/r_t$	1.544	0.179
		ASCE $r_e/r_t$	1.404	0.204
		Proposal $r_e/r_t$	1.486	0.186
	Hat sections	EN 1993-1-3 $r_e/r_t$	1.584	0.051
		ASCE $r_e/r_t$	1.208	0.081
		Proposal $r_e/r_t$	1.194	0.079
EOF	SHS/RHS	EN 1993-1-3 $r_e/r_t$	2.590	0.250
		ASCE $r_e/r_t$	2.884	0.224
		Proposal $r_e/r_t$	1.724	0.328
	Hat sections	EN 1993-1-3 $r_e/r_t$	2.572	0.027
		ASCE $r_e/r_t$	2.073	0.110
		Proposal $r_e/r_t$	1.694	0.139

### 3.8 Conclusions

A statistical evaluation of a proposed resistance model for web crippling design of stainless steel cross-sections under IOF and EOF loading by Bock et al. (2013) has been performed according to Annex D of EN 1990 (2002) to determine its level of reliability. Existing design provisions given in EN 1993-1-3 (2006) and SEI/ASCE 8-02 (2002) were also considered for comparison purposes. To this end, parametric studies on austenitic stainless steel were conducted herein to complement the existing numerical data which was considered to derive the proposed resistance model. The available numerical data was split into various sub-sets according to load case (IOF and EOF loading), cross-section geometry (SHS/RHS and hat sections) and material (austenitic and ferritic stainless steel) upon which the assessment of the resulting partial safety factors was based on.

The results show that the proposed resistance function satisfies the safety level recommended in EN 1993-1-4 (2006) for IOF loading, but required a readjustment for EOF loading to ensure reliable predictions. A new value for the non-dimensional coefficient  $\alpha$  has been proposed. Regarding the assessment of the reliability of existing provisions, SEI/ASCE 8-02 (2002) was observed to be only appropriate for the design of the austenitic set of data under EOF loading generated herein while EN 1993-1-3 (2006) yielded satisfactory results for both load cases, though for IOF loading, the required safety level was not achieved for SHS and RHS.

Predicted web crippling resistances by EN 1993-1-3 (2006), SEI/ASCE 8-02 (2002) and the revised resistance function of numerical data and existing test results on various stainless steel grades showed that the latter provides more accurate predictions enabling a more efficient design for both types of load cases.

Building on the observations regarding the material effect on the partial safety factor and the good agreement achieved between ultimate capacity predictions and existing test results, it is speculated that the proposed formula is also applicable to duplex stainless steel because their stress-strain behaviour lays between the respective values for austenitic and ferritic grades but a formal validation is required.

---

**Acknowledgments**

The research leading to these results has received funding from the European Community's Research Fund for Coal and Steel (RFCS) under Grant Agreement No. RFSR-CT-2010-00026, Structural Applications for Ferritic Stainless Steels and from Ministerio de Ciencia e Innovación to the Project BIA2010-11876-E "Acciones complementarias". The first author would like to acknowledge the financial support provided by the Secretaria d'Universitats i de Recerca del Departament d'Economia i Coneixement de la Generalitat de Catalunya i del Fons Social Europeu. The authors gratefully acknowledge the scholarship provided by AGAUR to Mr Mirada.

**Appendix 3.A**

Tables 3.A.1-3.A.4 present the capacity predictions according to EN 1993-1-3 (2006), SEI/ASCE 8-02 (2002) and proposed resistance model (proposal) of the numerical models generated herein. In these tables,  $R_{u,num}$  is the numerical web crippling resistance of the cross-section,  $M_{c,num}$  is the numerical bending moment resistance obtained in the 4-point bending model,  $R_{w,Rd}$  is the predicted value for the web crippling resistance and  $R_{WC-BD}$  is the combined web crippling and bending strength. All partial safety factors were set to unity to enable a direct comparison.

Specimens were labelled to easily identify load case, material, cross-section and thickness as well as corner radius and bearing length. The first three letters define the load case, where IOF refers to interior one-flange loading and EOF to exterior one-flange loading. The following notation describes the material type (A1, A1\*, A2, A2\*). The following letter and first number defines the section (S5 to S9). And finally, the value of the thickness (either 1 mm or 2 mm for hat sections and either 2 mm or 4 mm for SHS/RHS). Additional numbers were added when the corner radius or the bearing length that produces crippling ( $s_{sL}$  and  $s_{sa}$  for IOF and EOF loading respectively, with their corresponding values) are varied and the number two is attached when the previously number refers to the variation of the plate length that applies the load ( $s_{sL}$ ) for EOF loading. The same labels were used by Bock et al. (2013) for ferritic stainless steel cross-sections and were adopted herein so that the austenitic counterpart could be compared.



Statistical evaluation of a new resistance model for cold-formed stainless steel cross-sections subjected to web crippling

Table 3.A.1 Numerical and predicted resistances for SHS/RHS under IOF loading

Specimen	Numerical result		EN 1993-1-3		SEI/ASCE 8-02		Proposal	
	R <sub>u,num</sub> (kN)	M <sub>c,num</sub> (kNm)	R <sub>w,Rd</sub> (kN)	R <sub>WC-BD</sub> (kN)	R <sub>w,Rd</sub> (kN)	R <sub>WC-BD</sub> (kN)	R <sub>w,Rd</sub> (kN)	R <sub>WC-BD</sub> (kN)
IOF A1S52	16.94	3.72	25.32	17.09	22.42	19.13	20.84	15.32
IOF A1S62	18.91	7.40	25.32	22.17	21.61	24.34	20.84	19.27
IOF A1*S52	17.22	3.76	25.32	17.18	22.42	19.22	20.95	15.43
IOF A1*S524	15.50	3.72	24.77	16.90	21.73	18.82	19.82	14.87
IOF A1*S525	14.65	3.695	24.29	16.67	21.04	18.43	19.37	14.63
IOF A1*S5250	20.24	3.76	30.76	19.00	24.23	20.02	25.39	17.20
IOF A1*S5275	21.74	3.76	35.04	20.22	26.03	20.76	28.80	18.38
IOF A1*S52100	25.29	3.76	38.73	21.15	27.84	21.44	31.67	19.28
IOF A1*S62	19.34	7.46	25.99	22.63	21.61	24.40	20.95	19.38
IOF A1*S624	18.57	7.38	25.60	22.32	20.95	23.79	19.82	18.55
IOF A1*S625	17.33	7.33	25.27	22.07	20.28	23.20	19.37	18.20
IOF A2S52	17.73	3.80	26.52	17.70	22.42	19.33	21.16	15.59
IOF A2S62	20.16	7.56	26.70	23.15	21.61	24.49	21.16	19.59
IOF A2*S52	18.53	3.89	26.88	18.02	22.42	19.53	21.55	15.91
IOF A2*S524	16.96	3.86	26.48	17.83	21.73	19.14	20.58	15.44
IOF A2*S525	16.64	3.81	26.14	17.59	21.04	18.69	20.30	15.23
IOF A2*S5250	21.31	3.89	33.12	20.05	24.23	20.35	26.12	17.74
IOF A2*S5275	22.61	3.89	37.73	21.31	26.03	21.11	29.62	18.96
IOF A2*S52100	25.78	3.89	41.72	22.27	27.84	21.82	32.58	19.89
IOF A2*S62	21.82	7.72	28.01	24.09	21.61	24.65	21.55	19.97
IOF A2*S64	20.24	7.65	27.59	23.77	20.95	24.04	20.58	19.25
IOF A2*S65	20.30	7.63	27.24	23.54	20.28	23.47	20.30	19.04
IOF A1S54	53.81	7.92	101.61	48.79	90.99	54.48	87.99	46.06
IOF A1S64	65.58	15.75	102.32	70.58	89.39	78.43	87.99	64.76
IOF A1*S54	54.85	8.14	103.04	49.89	90.99	55.42	88.21	46.84
IOF A1*S544	51.79	8.06	102.24	49.41	90.99	55.05	79.85	44.58
IOF A1*S545	48.94	7.99	101.6	49.06	89.63	54.47	74.65	43.05
IOF A1*S5450	60.83	8.14	123.28	53.28	94.81	56.27	103.77	50.03
IOF A1*S5475	62.71	8.14	138.1	55.33	98.62	57.09	115.71	52.10
IOF A1*S54100	67.07	8.14	150.91	56.88	102.4	57.86	125.77	53.65
IOF A1*S64	67.40	16.23	107.47	73.49	89.39	79.50	88.21	65.65
IOF A1*S644	63.13	16.085	106.64	72.89	89.39	79.18	79.85	61.59
IOF A1*S645	60.25	15.93	105.99	72.33	88.05	78.19	74.65	58.85
IOF A2S54	56.81	8.56	109.77	52.72	90.99	57.15	88.65	48.30
IOF A2S64	70.84	17.09	110.55	76.41	89.39	81.34	88.65	67.23
IOF A2*S54	60.44	9.37	111.34	55.99	90.99	60.31	89.47	50.97
IOF A2*S544	57.13	9.32	110.49	55.64	90.99	60.12	81.37	48.63
IOF A2*S545	54.12	9.23	109.82	55.20	89.63	59.43	76.43	46.95
IOF A2*S5450	65.43	9.37	133.25	59.95	94.81	61.33	105.25	54.71
IOF A2*S5475	67.35	9.37	149.29	62.36	98.62	62.30	117.35	57.17
IOF A2*S54100	72.89	9.37	163.16	64.19	102.44	63.22	127.56	59.01
IOF A2*S64	76.84	18.90	116.2	82.13	89.39	84.87	89.47	70.26
IOF A2*S644	68.43	18.72	115.32	81.44	89.39	84.54	81.37	65.91
IOF A2*S645	66.55	18.55	114.62	80.83	88.05	83.46	76.43	63.05

Table 3.A.2 Numerical and predicted resistances for hat sections under IOF loading

Specimen	Numerical result		EN1993-1-3		SEI/ASCE 8-02		Proposal	
	R <sub>u,num</sub> (kN)	M <sub>c,num</sub> (kNm)	R <sub>w,Rd</sub> (kN)	R <sub>WC-BD</sub> (kN)	R <sub>w,Rd</sub> (kN)	R <sub>WC-BD</sub> (kN)	R <sub>w,Rd</sub> (kN)	R <sub>WC-BD</sub> (kN)
IOF A1S71	4.11	0.98	5.52	4.09	5.30	4.75	5.22	3.91
IOF A1S81	5.35	2.53	5.52	5.45	4.82	6.06	5.22	5.19
IOF A1S91	4.48	1.42	5.52	4.67	5.14	5.39	5.22	4.47
IOF A1*S71	4.15	0.99	5.52	4.10	5.30	4.77	5.24	3.94
IOF A1*S714	3.84	0.97	5.34	3.99	4.94	4.55	4.83	3.72
IOF A1*S715	3.61	0.96	5.18	3.90	4.57	4.32	4.60	3.59
IOF A1*S7150	4.76	0.99	6.86	4.64	6.09	5.14	6.54	4.47
IOF A1*S7175	5.22	0.99	7.89	4.99	7.10	5.56	7.53	4.82
IOF A1*S71100	6.19	0.99	8.75	5.26	8.34	5.99	8.37	5.08
IOF A1*S81	5.46	2.50	5.52	5.43	4.82	6.05	5.24	5.19
IOF A1*S91	4.58	1.44	5.52	4.70	5.14	5.42	5.24	4.50
IOF A1*S914	4.21	1.41	5.34	4.56	4.79	5.14	4.83	4.23
IOF A1*S915	4.18	1.44	5.18	4.50	4.44	4.92	4.60	4.11
IOF A1*S9150	5.21	1.44	6.86	5.42	5.90	5.93	6.54	5.21
IOF A1*S9175	5.73	1.44	7.89	5.91	6.89	6.51	7.53	5.69
IOF A1*S91100	6.85	1.44	8.75	6.28	8.09	7.13	8.37	6.06
IOF A2S71	4.29	1.00	5.52	4.12	5.30	4.80	5.29	3.98
IOF A2S81	5.75	2.53	5.52	5.44	4.82	6.06	5.29	5.24
IOF A2S91	4.78	1.45	5.52	4.71	5.14	5.44	5.29	4.54
IOF A2*S71	4.62	1.03	5.52	4.14	5.30	4.85	5.38	4.06
IOF A2*S714	4.23	1.02	5.34	4.04	4.94	4.64	5.00	3.88
IOF A2*S715	4.09	1.01	5.18	3.96	4.57	4.42	4.81	3.77
IOF A2*S7150	5.06	1.03	6.86	4.69	6.09	5.24	6.71	4.62
IOF A2*S7175	5.49	1.03	7.89	5.04	7.10	5.67	7.73	4.98
IOF A2*S71100	6.35	1.03	8.75	5.31	8.34	6.12	8.59	5.25
IOF A2*S81	6.24	2.58	5.52	5.45	4.82	6.09	5.38	5.33
IOF A2*S91	5.20	1.49	5.52	4.72	5.14	5.49	5.38	4.63
IOF A2*S914	4.81	1.48	5.34	4.61	4.79	5.22	5.00	4.40
IOF A2*S915	4.80	1.48	5.18	4.52	4.44	4.96	4.81	4.28
IOF A2*S9150	5.59	1.49	6.86	5.45	5.90	6.00	6.71	5.36
IOF A2*S9175	6.02	1.49	7.89	5.94	6.89	6.60	7.73	5.86
IOF A2*S91100	7.08	1.49	8.75	6.32	8.09	7.24	8.59	6.24
IOF A1S72	14.34	2.44	19.41	12.29	22.59	15.39	22.22	12.98
IOF A1S82	19.45	7.22	19.41	18.26	21.61	24.16	22.22	20.06
IOF A1S92	16.21	3.92	19.41	15.11	22.26	19.52	22.22	16.25
IOF A1*S72	14.57	2.48	19.41	12.40	22.59	15.54	22.27	13.11
IOF A1*S724	13.10	2.43	18.99	12.14	21.89	15.15	19.90	12.29
IOF A1*S725	12.18	2.43	18.62	12.03	21.19	14.96	18.36	11.81
IOF A1*S7250	16.14	2.48	23.43	13.60	24.40	16.05	26.99	14.29
IOF A1*S7275	17.14	2.48	26.51	14.37	26.22	16.52	30.61	15.05
IOF A1*S72100	18.91	2.48	29.11	14.95	28.04	16.95	33.67	15.60
IOF A1*S82	19.85	7.25	19.41	18.29	21.61	24.19	22.27	20.11
IOF A1*S92	16.51	3.96	19.41	15.18	22.26	19.62	22.27	16.35
IOF A1*S924	14.59	3.93	18.99	14.93	21.57	19.22	19.90	15.23
IOF A1*S925	13.45	3.89	18.62	14.70	20.88	18.80	18.36	14.44
IOF A1*S9250	18.97	3.96	23.43	17.00	24.05	20.45	26.99	18.22
IOF A1*S9275	20.73	3.96	26.51	18.23	25.84	21.23	30.61	19.46
IOF A1*S92100	24.66	3.96	29.11	19.18	27.64	21.96	33.67	20.40
IOF A2S72	15.03	2.55	19.41	12.56	22.59	15.80	22.37	13.34
IOF A2S82	20.70	7.44	19.41	18.39	21.61	24.37	22.37	20.32
IOF A2S92	17.08	4.06	19.41	15.30	22.26	19.83	22.37	16.55
IOF A2*S72	15.87	2.68	19.41	12.77	22.59	16.24	22.56	13.74
IOF A2*S724	14.37	2.65	18.99	12.56	21.89	15.92	20.25	12.95
IOF A2*S725	13.33	2.66	18.62	12.46	21.19	15.72	18.77	12.48
IOF A2*S7250	17.15	2.68	23.43	14.04	24.40	16.80	27.35	15.02

Statistical evaluation of a new resistance model for cold-formed stainless steel cross-sections subjected to web crippling

Table 3.A.2 Numerical and predicted resistances for hat sections under IOF loading (continuation)

Specimen	Numerical result		EN 1993-1-3		SEI/ASCE 8-02		Proposal	
	R <sub>u,num</sub> (kN)	M <sub>c,num</sub> (kNm)	R <sub>w,Rd</sub> (kN)	R <sub>WC-BD</sub> (kN)	R <sub>w,Rd</sub> (kN)	R <sub>WC-BD</sub> (kN)	R <sub>w,Rd</sub> (kN)	R <sub>WC-BD</sub> (kN)
IOF A2*S7275	18.17	2.68	26.51	14.87	26.22	17.31	31.02	15.85
IOF A2*S72100	20.20	2.68	29.11	15.49	28.04	17.78	34.11	16.46
IOF A2*S82	22.77	7.72	19.41	18.49	21.61	24.65	22.56	20.66
IOF A2*S92	18.25	4.27	19.41	15.50	22.26	20.28	22.56	16.98
IOF A2*S924	16.33	4.25	18.99	15.26	21.57	19.88	20.25	15.86
IOF A2*S925	15.85	4.24	18.62	15.06	20.88	19.51	18.77	15.11
IOF A2*S9250	20.42	4.27	23.43	17.41	24.05	21.18	27.35	18.98
IOF A2*S9275	22.01	4.27	26.51	18.71	25.84	22.01	31.02	20.32
IOF A2*S92100	25.48	4.27	29.11	19.70	27.64	22.79	34.11	21.33

Table 3.A.3 Numerical and predicted resistances for SHS/RHS under EOF loading

Specimen	Numerical result		EN 1993-1-3	SEI/ASCE 8-02	Proposal*
	R <sub>u,num</sub> (kN)	R <sub>w,Rd</sub> (kN)	R <sub>w,Rd</sub> (kN)	R <sub>w,Rd</sub> (kN)	R <sub>w,Rd</sub> (kN)
EOF A1*S1250	19.86	10.33	10.63	10.21	
EOF A1*S5275	21.78	10.33	11.70	10.42	
EOF A1*S52100	23.22	10.33	12.76	10.60	
EOF A1*S521002	18.52	10.33	9.57	9.94	
EOF A1*S62	17.75	10.33	8.96	9.94	
EOF A1*S624	15.90	10.11	8.24	9.68	
EOF A1*S625	14.31	9.91	7.51	9.72	
EOF A2S62	18.62	10.33	8.96	10.10	
EOF A2*S5250	22.18	10.33	10.64	10.68	
EOF A2*S5275	24.96	10.33	11.70	10.90	
EOF A2*S52100	26.72	10.33	12.76	11.08	
EOF A2*S521002	21.41	10.33	9.57	10.40	
EOF A2*S62	20.16	10.33	8.96	10.40	
EOF A2*S624	18.03	10.11	8.24	10.27	
EOF A2*S625	16.16	9.91	7.51	10.47	
EOF A1S64	53.58	38.14	39.59	46.13	
EOF A1*S5450	61.18	38.14	43.23	47.23	
EOF A1*S5475	69.13	38.14	45.64	47.93	
EOF A1*S54100	75.74	38.14	48.04	48.52	
EOF A1*S541002	60.04	38.14	40.83	46.32	
EOF A1*S64	55.36	38.14	39.59	46.32	
EOF A1*S644	52.02	37.58	39.59	42.52	
EOF A1*S645	48.77	37.08	38.10	40.31	
EOF A2S64	58.64	38.14	39.59	46.68	
EOF A2*S5450	69.58	38.14	43.23	48.29	
EOF A2*S5475	80.44	38.14	45.64	49.01	
EOF A2*S54100	89.25	38.14	48.04	49.62	
EOF A2*S541002	75.02	38.14	40.83	47.36	
EOF A2*S64	64.80	38.14	39.59	47.36	
EOF A2*S644	61.16	37.58	39.59	43.79	
EOF A2*S645	57.30	37.08	38.10	41.83	

\*After readjustment

Table 3.A.4 Numerical and predicted resistances for hat sections under EOF loading

Specimen	Numerical result		EN 1993-1-3	SEI/ASCE 8-02	Proposal*
	$R_{u,num}$ (kN)	$R_{w,Rd}$ (kN)	$R_{w,Rd}$ (kN)	$R_{w,Rd}$ (kN)	$R_{w,Rd}$ (kN)
EOF A1S81	3.13	2.15	2.15	1.58	1.99
EOF A1*S81	3.17	2.15	2.15	1.58	2.01
EOF A1*S814	2.87	2.08	2.08	1.24	2.01
EOF A1*S815	2.66	2.02	2.02	1.13	2.07
EOF A1*S9140	4.16	2.15	2.15	2.00	2.06
EOF A1*S9150	4.79	2.15	2.15	2.14	2.09
EOF A2S81	3.25	2.15	2.15	1.58	2.05
EOF A2*S81	3.40	2.15	2.15	1.58	2.12
EOF A2*S814	3.12	2.08	2.08	1.24	2.15
EOF A2*S815	2.92	2.02	2.02	1.13	2.26
EOF A2*S9140	4.35	2.15	2.15	2.00	2.17
EOF A2*S9150	4.97	2.15	2.15	2.14	2.20
EOF A1S82	11.93	7.85	7.85	8.96	8.91
EOF A1*S82	12.13	7.85	7.85	8.96	8.95
EOF A1*S824	10.86	7.68	7.68	8.24	8.33
EOF A1*S825	9.83	7.53	7.53	7.51	7.99
EOF A1*S9240	16.61	7.85	7.85	10.08	9.11
EOF A1*S9250	19.45	7.85	7.85	10.50	9.20
EOF A2S82	12.53	7.85	7.85	8.96	9.04
EOF A2*S82	13.33	7.85	7.85	8.96	9.19
EOF A2*S824	12.13	7.68	7.68	8.24	8.62
EOF A2*S825	10.89	7.53	7.53	7.51	8.35
EOF A2*S9240	17.91	7.85	7.85	10.08	9.35
EOF A2*S9250	20.77	7.85	7.85	10.50	9.44

\*After readjustment



---

**CHAPTER 4 – Strength curves for web crippling design of cold-formed stainless steel hat sections**

This chapter is currently available in the *Thin-Walled Structures* journal under the reference:

Bock M and Real E (2014a). Strength curves for web crippling design of cold-formed stainless steel hat sections. *Thin-Walled Structures*, 85, pp.93-105.

<http://dx.doi.org/10.1016/j.tws.2014.07.021>

**Abstract**

The web crippling design guides are based on empirical adjustments of available test data. These equations differ from the basic concept underpinning most of the other instabilities, the so-called strength curves. This investigation presents a new design approach for web crippling design of stainless steel hat sections based on strength curves controlled by slenderness-based functions  $\chi(\bar{\lambda})$ . The effects of web crippling on such cross-sections were studied numerically and the obtained results were used to derive the design expressions. Comparisons with tests and FE data, and with design guides show that the proposed design approach provides more accurate web crippling resistance.

**Highlights**

- Literature review, including web crippling research and design
- FE simulation of stainless steel hat sections subjected to web crippling
- Development of design expressions for the proposed design approach
- Statistical validation of the proposed design method
- Comparison of the proposed method with design standards

**Keywords**

Hat sections, reduction factor, stainless steel, strength curves, transverse forces, web crippling.

#### **4.1 Introduction**

The use of stainless steel in construction has been permanently increasing during the last years due to its favourable characteristics in terms of strength, durability, formability and aesthetics. Cold-formed stainless steel hat sections are frequently used as secondary structural elements in roof or wall cladding subjected to local transverse loads or reactions which produce local high stresses. These cross-sections present high web-to-thickness ratio, and its web is therefore susceptible to local buckling (localized crushing or crippling of the web).

The first web crippling experimental investigation was conducted at Cornell University by Winter and Pian (1946) and Winter (1952) on cold-formed carbon steel I-sections. Within this investigation, two types of load locations and two types of loading were examined, resulting in the four types of loading cases: interior one-flange (IOF), interior two-flanges (ITF), exterior one-flange (EOF) and exterior two-flanges (ETF). Exterior loading defines a situation when the load is applied at the end of the member whereas in the case of interior loading, the load is applied within the span. Distinction is made between one flange loading or two flange loading if the load is applied through one flange or acting on both flanges, respectively. This classification was adopted in the early versions of the AISI (1968) specification for cold-formed carbon steel and later on, in the first version (ANSI/ASCE 8-90 (1991)) of the current SEI/ASCE 8-02 (2002) standard for application to stainless steel. The European design guidance for stainless steel, EN 1993-1-4 (2006), refers to the European design guidance for cold-formed carbon steel, EN 1993-1-3 (2006), to predict web crippling strength where different empirical equations are given. In this latter, for the particular case of hat sections, two categories are codified: Category 1 which corresponds to EOF, ETF and ITF loading; and Category 2 which is equivalent to IOF loading.

The theoretical treatment of web crippling is rather complex because many parameters are involved (Yu and LaBoube (2010)): cross-section geometry (I-sections, C-sections, Z-sections, hat sections and multi web sections); inclination of the web element; inside bending radius; relative slenderness of the web; the length over which the load is distributed (bearing length); loading case; steel properties; and support conditions. Consequently, current standards (SEI/ASCE 8-02 (2002) and EN 1993-1-3 (2006)) provide various empiric design equations for a given load case and particular cross-

---

section geometry which were derived from regression analysis of existing test on different cold-formed carbon steel sections. Despite accurate plastic mechanism models based on yield line theory were derived for cold-formed carbon steel hat sections (Bakker and Stark (1994) and Hofmeyer et al. (2001)), their application is rather tedious for hand calculation purposes. Relevant research regarding these adjustments is summarized in Table 4.1 for cold-formed carbon steel. The applicability of the aforementioned empiric equations to stainless steel was found to be not always acceptable (Korvink et al. (1995)) and further research was conducted in order to adapt these equations to different stainless steel grades and cross-section types (Talja and Salmi (1995), Zhou and Young (2006a, 2007a and 2007b) and Bock et al. (2013)). Other relevant studies on cold-formed stainless steels are summarized in Table 4.2. Indeed, these adjustments correlate well with the data they allow for but such empiric design approach deviates from the treatment of most of the other instabilities in the European structural design standards, the so-called strength curves controlled by slenderness-based functions  $\chi(\bar{\lambda})$ .

Hence, the purpose of this paper is to develop a new design approach for web crippling design of cold-formed stainless steel hat sections under IOF loading (Category 2) and EOF loading (Category 1) employing strength curves  $\chi(\bar{\lambda})$ . To this end, collected tests on ferritic stainless steel hat sections (Talja and Hradil (2011)) were modelled with ABAQUS to develop and calibrate a comprehensive finite element (FE) model. Since the amount of existing test data is quite scarce and having validated the numerical model, parametric studies were conducted to extend the available database over a large range of hat section geometries and two stainless steel grades: austenitic and ferritic. Following analysis of results, the proposed design equations are derived through semi-empiric analyses and statistically validated according to Annex D of EN 1990 (2002). Finally, the resistances achieved in the generated models and existing tests are compared with predicted resistances using different methods, including the proposed design approach, EN 1993-1-3 (2006) design provisions and the North American SEI/ASCE 8-02 (2002) standard. The design rules for the web crippling design of cold-formed hat sections given in those standards (SEI/ASCE 8-02 (2002) and EN 1993-1-3 (2006)) are also outlined in this paper.



Table 4.1 Relevant research on cold-formed carbon steel members subjected to web crippling

Source	Section	Load case	Relevant Contribution
Winter and Pian (1946)	I-sections (stiffened flanges unfastened)	30 EOF; 10 IOF	First consideration of the four load cases: IOF, EOF, ITF and ETF First study on webs restrained against rotation (I-sections) and on single unreinforced webs (Hat sections)
		27 ETF; 36 ITF	
Winter (1952)	Hat sections (stiffened/unstiffened flanges unfastened)	60 EOF	Derived expressions for computing the web crippling resistance for IOF and EOF which were included in AISI (1968)
		30 IOF	
Baehre (1975)	Multi-web sections (hat type)	IOF	First study on single unreinforced webs of multi-web sections Introduced the web inclination $\phi$ on the web crippling strength Derived expressions for computing the web crippling resistance for IOF
Hetrakul and Yu (1978)	I-sections (stiffened flanges unfastened)	50 EOF; 19 IOF	Collection of existing tests Recalibration of coefficients proposed in previous studies New expressions for IOF, EOF, ITF and ETF suitable for vertical webs and small $r/t$ and $s_w/t$ ratios included in more recent versions of AISI (1968)
		30 ETF; 30 ITF	
	I-sections (unstiffened flanges unfastened)	4 EOF; 2 IOF	
	C-sections (stiffened flanges fastened)	8 EOF	
	C-sections (stiffened flanges unfastened)	34 EOF; 24 IOF 26 ETF; 26 ITF	
Yu (1981)	Multi-web sections (hat type and unfastened)	18 EOF; 4 IOF	Study of combined web crippling and bending on multi-web sections
		4 ETF; 4 ITF	
Wing (1981)	Hat sections (fastened)	18 EOF	Study of combined web crippling and bending effects Derived expressions to predict web crippling resistance for IOF, ITF and ETF
		25 IOF	
	7 ETF; 23 ITF		
Studnicka (1990)	Multi-web sections (hat type and unfastened)	34 IOF	Assessment of the CSA S136-84 (1984) Canadian Standard and AISI (1986). Obtained good agreement for IOF loading but discrepancies for EOF loading
		63 ETF; 57 ITF	
Bhakta et al. (1992)	I-sections (stiffened flanges fastened)	IOF; EOF	Long span roof deck and floor deck tests Flange restraint study (fastened flanges to the support) Provided strength comparisons between different cross-sections and highlighted the influence of flange restraint on the ultimate web crippling resistance for different load cases
		6 IOF	
	I-sections (stiffened flanges unfastened)	6 EOF	
		6 EOF	
	C-sections (stiffened flanges fastened)	6 EOF	
		6 EOF	
	C-sections (stiffened flanges unfastened)	4 EOF	
		4 EOF	
	Z-sections (stiffened flanges unfastened)	4 EOF	
		2 EOF	
	Hat sections (unfastened)	2 EOF	
		2 EOF	
Z-sections (stiffened flanges fastened)	18 ETF; 18 ITF		
	2 EOF		
Multi-web sections (hat type and fastened)	2 EOF		
	2 IOF		
Multi-web sections (hat type and unfastened)	2 IOF		
	2 IOF		

Table 4.1 Relevant research on cold-formed carbon steel members subjected to web crippling (continuation)

Source	Section	Load case	Relevant Contribution
Prabhakaran (1993)	-	-	Collection of all existing tests. A unified expression for web crippling design is derived which was adopted in the CSA S136-94 (1994) Canadian Standard and in the North American Specification NASPEC-2001 (2001)
Langan et al. (1994)	C-sections (stiffened flanges unfastened)	23 EOF 8 IOF	Assessment of available specifications and design recommendations
Cain et al. (1995)	I-sections (stiffened flanges fastened)	12 IOF	Assessment of available specifications and design recommendations
	Z-sections (stiffened flanges fastened)	14 EOF	
	Z-sections (stiffened flanges unfastened)	14 EOF	
Gerges (1997)	C-sections (stiffened flanges fastened)	67 EOF	Studied sections with large inside bending radius-to-thickness ratio. New coefficients for Prabhakaran's (1993) unified equation are derived
Wu et al. (1997)	Hat sections (fastened)	3 EOF	Assessment of available specifications and design recommendations
	Multi-web sections (hat type and unfastened)	16 E'TF 16 ITF	
Young and Hancock (1998)	C-sections (unstiffened flanges unfastened)	14 EOF	Compared test results against AISI (1996) and concluded that its codified equations were too optimistic for C-sections. Proposed a unified expression based on a simple plastic mechanism approach
		16 IOF	
		12 E'TF	
		14 ITF	
Beshara (2000)	C-sections (stiffened flanges fastened)	18 E'TF	Test collection to develop an experimental database Calibration of new coefficients for computing the web crippling strength of cold-formed carbon steel members. Improved coefficients of AISI (1996) and CSA S136-94 (1994) Canadian Standard, and were approved by the AISI committee in the North American Specification for the Design of Cold-Formed Steel Structural Members AISI (2002)
		18 ITF	
Beshara (2000)	Z-sections (stiffened flanges fastened)	18 E'TF	
		18 ITF	

Table 4.2 Relevant research on cold-formed stainless steel members subjected to web crippling

Source	Section	Load case	Grade	Relevant objective
Korvink and van den Berg (1994)	Stiffened C-section (fastened to the support)	98 IOF	1.4016 1.4003	Asses the applicability of ANSI/ASCE 8-90 (1991) to stainless steel. The standard was not always appropriate
Korvink et al. (1995)	Stiffened C-section (fastened to the support)	139 IOF	1.4301 1.4016 1.4003	Asses the Applicability of ANSI/ASCE 8-90 (1991) to stainless steel
Talja and Salmi (1995)	SHS, RHS	6 IOF	1.4301	Provide tests results on austenitic square and rectangular hollow sections (SHS and RHS, respectively) for the development of European design rules. Since EN 1993-1-3 (2006) does not explicitly include coefficients for SHS and RHS, coefficients for sheeting profiles are recommended
Talja (1997)	Multi-web section unstiffened Multi-web section stiffened flanges (1 <sup>st</sup> generation sheets) Multi-web section stiffened flanges and webs (2 <sup>nd</sup> generation sheets)	3 IOF 3 IOF 3 IOF	1.4301	Assess the applicability of EN 1993-1-3 (2006) to austenitic stainless steel
Sélen (2000)	I-sections	5 IOF 4 EOF	1.4301	Assess the applicability of EN 1993-1-3 (2006) to austenitic stainless steel
Zilli (2004)	Trapezoidal section (Hat with inclined webs) Trapezoidal section	8 IOF 3 IOF	1.4318 C700 1.4318 C850	Assess the applicability of EN 1993-1-3 (2006) to high-strength austenitic stainless steel, including web crippling and combined bending and web crippling. A new interaction equation, which is less conservative, is recommended
Talja (2004)	Trapezoidal section stiffened flange Hat sections	6 IOF 6 IOF	1.4318 C700 1.4318 C850	
Zhou and Young [13]	SHS, RHS	17 ETF 16 ITF	1.4301	Proposal of a unified web crippling equation with new coefficients for cold-formed stainless steel sections with single webs
Zhou and Young (2007a)	SHS, RHS	14 EOF; 14 IOF 15 ETF; 15 ITF	HSA, Duplex	Assessment of different design rules and adjustment of new coefficients of Prabhakaran's (1993) and Beshara's (2000) unified formula for high-strength SHS and RHS
Zhou and Young (2007b)	SHS, RHS	32 EL 32 IL	1.4301 HSA Duplex	Floor joints simulation (section supported along its longitudinal axis). Assessment of the suitability of the web crippling design rules in the current specifications for stainless steel SHS and RHS under this load configuration. New coefficients are adjusted
Zhou and Young (2007c)	SHS, RHS	21 IOF	HSA Duplex	Assessment of design rules to investigate the cold-formed stainless steel members subjected to combined bending and web crippling.

Table 4.2 Relevant research on cold-formed stainless steel members subjected to web crippling (continuation)

Source	Section	Load case	Grade	Relevant objective
Gardner et al. (2006)	SHS, RHS	6 IOF	1.4318 C700 1.4318 C850	Comparison between test results and strengths determined using EN 1993-1-3 (2006) assuming coefficients proposed by Talja and Salmi (1995) for SHS and RHS. Extension to the high-strength grades (1.4318 C700 and C800) is recommended.
Talja and Hradil (2011)	Hat sections (unfastened) RHS	4 IOF; 4 EOF 1 IOF; 1 EOF	1.4509 1.4509	Assess the applicability of EN 1993-1-3 (2006) to ferritic stainless steel
Real et al. [62]	Multi-web sections (stiffened flanges and web embossments)	9 IOF; 4 EOF	1.4003	Assess the applicability of EN 1993-1-3 (2006) to ferritic stainless steel

## 4.2 Current design equations

### 4.2.1 EN 1993-1-3

As given in EN 1993-1-3 (2006), the local transverse resistance per web  $R_{w,Rd}$  of a hat section should be determined according to Eq. (4.1) using the symbols illustrated in Fig. 1 where  $r$  is the inside bending radius of the corners,  $t$  is the thickness,  $\phi$  is the relative angle between the web and the flange,  $E$  is the material Young's modulus,  $f_{yb}$  is taken as the material proof strength  $\sigma_{0.2}$  for stainless steel and  $\gamma_{M1}$  is the partial safety factor with a recommended value of 1.1 for stainless steel as specified in EN1993-1-4 (2006). The expression also depends on the effective bearing length  $l_a$  and the non-dimensional coefficient  $\alpha$  which must be taken according to the relevant loading Category and the cross-section shape. The values of these parameters for hat sections are: for Category 1 (EOF)  $l_a=10\text{mm}$  and  $\alpha=0.057$ ; whereas for Category 2 (IOF)  $l_a=s_s$  where  $s_s$  is the bearing length and  $\alpha=0.115$ . Some geometrical limitations to satisfy are also provided in the design standard:  $r/t \leq 10$ ;  $h/t \leq 200 \sin \phi$ ;  $45^\circ \leq \phi \leq 90^\circ$ , where  $h$  is the web height between midlines of the flanges (see Fig. 4.1); and the clear distance from either the support reaction or local load to a free end must be at least 40 mm.

$$R_{w,Rd} = \alpha t^2 \sqrt{f_{yb} E} \left( 1 - 0.1 \sqrt{\frac{r}{t}} \right) \left( 0.5 + \sqrt{\frac{0.02 l_a}{t}} \right) \left( 2.4 + \left( \frac{\phi}{90} \right)^2 \right) / \gamma_{M1} \quad (4.1)$$

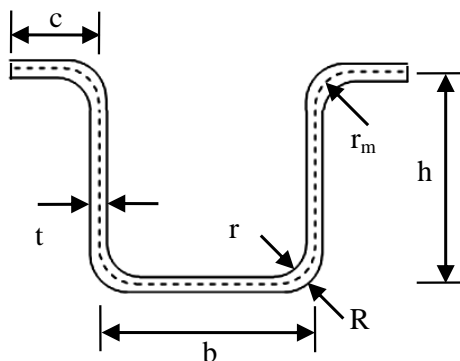


Fig. 4.1 Definition of symbols in the cross-section

In such circumstances where an applied local transverse force  $F_{Ed}$  interacts with a bending moment  $M_{Ed}$  (e.g. intermediate supports - Category 2 or equivalently IOF loading),  $F_{Ed}$  should satisfy Eq. (4.2) where  $M_{c,Rd}$  is the moment resistance of the cross-section and  $R_{w,Rd}$  is the sum of the local transverse resistances of the individual webs as given by Eq. (4.1). Eq. (4.2) results into Eq. (4.3), when the induced bending moment  $M_{Ed}$  by the local load  $F_{Ed}$  is introduced according to  $M_{Ed} = F_{Ed}(L_s - s_s)/4$  where  $L_s$  is the span as shown in Fig. 4.2.

$$\frac{F_{Ed}}{R_{w,Rd}} + \frac{M_{Ed}}{M_{c,Rd}} \leq 1.25 \quad \frac{F_{Ed}}{R_{w,Rd}} \leq 1 \quad \frac{M_{Ed}}{M_{c,Rd}} \leq 1 \quad (4.2)$$

$$F_{Ed} = 1.25 / \left( \frac{1}{R_{w,Rd}} + \frac{L_s - s_s}{4M_{c,Rd}} \right) \leq \min\{F_{Ed}, 4M_{c,Rd}/(L_s - s_s)\} \quad (4.3)$$

#### 4.2.2 ASCE standard SEI/ASCE 8-02

The web crippling resistance equations provided in SEI/ASCE 8-02 (2002) standard for the design of hat sections under IOF loading are given in Eq. (4.4) and Eq.(4.5) for different conditions according to the bearing length-to-thickness ratio whereas the expression for EOF loading is given in Eq. (4.6). In these equations, the coefficients  $C_1$ ,  $C_2$ ,  $C_3$ ,  $C_4$  and  $C_\theta$  are defined in Eqs (4.7)-(4.11). These expressions are given herein following EN 1993-1-3 (2006) symbols and SI units for consistency reasons and apply if:  $s_s/t \leq 210$ ;  $s_s/h \leq 3.5$ ; beams with  $r/t \leq 6$ ; and deck with  $r/t \leq 7$ ;  $h/t \leq 200 \sin \phi$ ;  $45^\circ \leq \phi \leq 90^\circ$ . Interaction effects for the combination of bending and web crippling at intermediate supports (IOF loading) are accounted for by means of Eq. (4.12) which may be rewritten as Eq. (4.13) following the same procedure described for the interaction formula provided in EN 1993-1-3 (2006). The corresponding resistance factor for web crippling and bending should be taken as  $\phi_w=0.7$  and  $\phi_b=0.85$ , respectively.

$$R_{w,Rd} = 6.9\phi_w t^2 C_1 C_2 C_\theta \left( 538 - 0.74 \frac{h}{t} \right) \left( 1 + 0.007 \frac{s_s}{t} \right) \text{ if } \frac{s_s}{t} \leq 60 \quad (4.4)$$

$$R_{w,Rd} = 6.9\phi_w t^2 C_1 C_2 C_\theta \left( 538 - 0.74 \frac{h}{t} \right) \left( 0.75 + 0.011 \frac{s_s}{t} \right) \text{ if } \frac{s_s}{t} > 60 \quad (4.5)$$

$$R_{w,Rd} = 6.9\phi_w t^2 C_3 C_4 C_\theta \left( 244 - 0.57 \frac{h}{t} \right) \left( 1 + 0.01 \frac{s_s}{t} \right) \quad (4.6)$$

$$C_1 = \left( 1.22 - 0.22 \frac{f_{yb}}{227.7} \right) \frac{f_{yb}}{227.7} \text{ if } \frac{f_{yb}}{631.35} \leq 1 \text{ or } C_1 = 1.69 \text{ if } \frac{f_{yb}}{631.35} > 1 \quad (4.7)$$

$$C_2 = \left( 1.06 - 0.06 \frac{r}{t} \right) \leq 1 \quad (4.8)$$

$$C_3 = \left( 1.33 - 0.33 \frac{f_{yb}}{227.7} \right) \frac{f_{yb}}{227.7} \text{ if } \frac{f_{yb}}{458.85} \leq 1 \text{ or } C_3 = 1.34 \text{ if } \frac{f_{yb}}{458.85} > 1 \quad (4.9)$$

$$C_4 = \left( 1.15 - 0.15 \frac{r}{t} \right) \leq 1 \text{ but not less than } 0.50 \quad (4.10)$$

$$C_\theta = 0.7 + 0.3(\phi/90)^2 \quad (4.11)$$

$$\frac{1.07F_{Ed}}{\phi_w R_{w,Rd}} + \frac{M_{Ed}}{\phi_b M_{c,Rd}} \leq 1.42 \quad (4.12)$$

$$F_{Ed} = 1.327 / \left( \frac{1}{\phi_w R_{w,Rd}} + \frac{L_s - s_s}{4\phi_b M_{c,Rd}} \right) \leq \min\{F_{Ed}, 4M_{c,Rd}/(L_s - s_s)\} \quad (4.13)$$

### 4.3 Numerical modelling

#### 4.3.1 Modelled tests

The finite element (FE) software ABAQUS was used to model 8 hat sections in grade EN 1.4509 (ferritic) stainless steel subjected to web crippling, including 4 tests under IOF loading and 4 tests under EOF loading which were performed at VTT Technical Research Centre of Finland by Talja and Hradil (2011). The model was based on centreline dimensions (see Fig. 4.1) determined from measured geometry reported by Talja and Hradil (2011) as given in Table 4.3 where  $h$  is the web height between the midlines of the flanges,  $b$  is the flange width,  $c$  is the flat part of the lip,  $t$  is the thickness and  $r_m$  is the bending radius measured from the midline. Important information is also provided in Table 4.3 by the beam labelling. Considering ITH\_10 as an example, I is the load configuration, TH stands for Top Hat and 10 is ten times the nominal thickness of the cross-section in mm. The overall length  $L$  of all the specimens was 399 mm, the supports  $S$  were 50 mm length, the bearing length  $s_s$  was 25 mm and the clear distance between the steel plate under the applied force and the end support in the EOF loading test,  $e$ , was 75 mm (see Figs 4.2 and 4.3). It should be noted that the configuration of these tests was intended to reproduce the web crippling response of continuous spans where the lips of the hat section are oriented upwards as shown in Fig. 4.1. Hence, the applied local transverse forces satisfy EOF loading at the end of the continuous member (external supports) whereas interior supports are subjected to IOF loading. Table 4.3 also gives the ultimate applied load in the test (Talja and Hradil (2011))  $F_{u,test}$  and the local transverse resistance per web  $R_{w,u,test}$  which was determined according to  $R_{w,u,test} = F_{u,test}/2$  for IOF loading whereas for EOF loading, the expression  $R_{w,u,test} = [(F_{u,test}[L_s - e - (S/2)])/L_s]/2$  applies, where  $L_s$  is the span as shown in Fig. 4.3.

Table 4.3 Geometry (Talja and Hradil (2011)) of the modelled specimens and comparison between test results and FE model

Beam	$h$ (mm)	$b$ (mm)	$c$ (mm)	$t$ (mm)	$r_m$ (mm)	$F_{u,test}$ (kN)	$R_{w,u,test}$ (kN)	$F_{u,num}$ (kN)	$R_{w,u,num}$ (kN)	$F_{u,test}/F_{u,num}$
ITH_10	71.09	72.89	24.17	0.99	1.65	10.01	5.00	10.19	5.09	0.982
ITH_15	70.73	70.56	24.11	1.53	1.9	20.73	10.37	21.04	10.70	0.969
ITH_20	70.08	69.72	24.02	1.99	2.4	34.84	17.42	34.99	17.50	0.996
ITH_30	69.95	68.86	23.82	2.95	4.25	55.01	27.51	57.89	28.95	0.951
ETH_10	71.05	72.85	24.15	0.99	1.65	10.05	3.59	9.96	3.56	1.009
ETH_15	70.84	70.47	24.03	1.53	1.9	21.06	7.52	20.36	7.27	1.034
ETH_20	70.52	69.65	23.98	1.99	2.4	36.29	12.96	33.91	12.11	1.071
ETH_30	69.39	68.86	23.74	2.94	4.25	58.90	21.04	53.72	19.18	1.096
								Mean		1.011
								COV		0.046

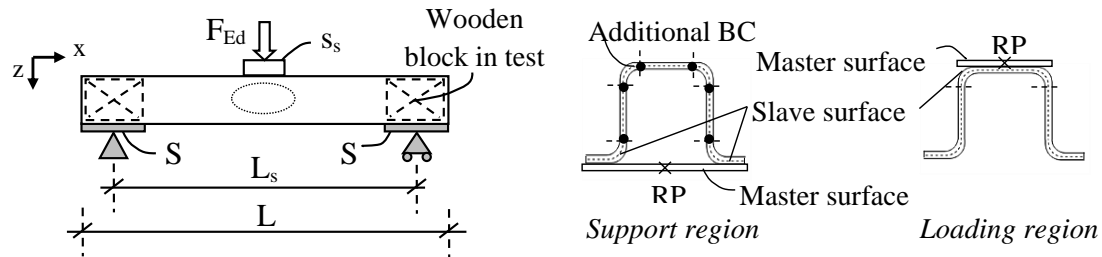


Fig. 4.2 Numerical model for IOF loading

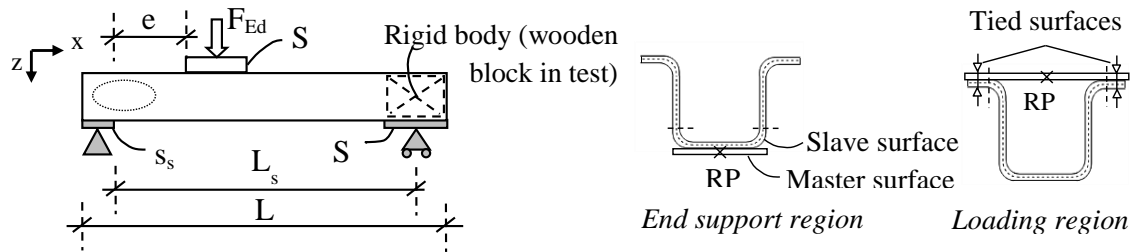


Fig. 4.3 Numerical model for EOF loading

#### 4.3.2 Mesh and material

The geometry of these ferritic stainless steel hat sections was discretized using the four-node doubly curved shell element with reduced integration S4R. The employed mesh size used in the model was optimized to achieve accurate results while minimizing computational time; hence, a mesh size of  $3 \times 3$  mm was used for the flat parts of the cross-sections whereas a number of elements equals to ten times the nominal thickness was employed to model the corners. The material properties of the tested specimens reported by Talja and Hradil (2011) are given in Table 4.4, including the material Young modulus  $E$ , the 0.2% proof stress  $\sigma_{0.2}$ , the ultimate stress and its corresponding ultimate strain,  $\sigma_u$  and  $\epsilon_u$  respectively, and the first and second strain hardening parameters,  $n$  and  $m$  respectively. The whole stress-strain (engineering) curve was obtained using the compound two-stage Mirambell and Real (2000) material model, modified by Rasmussen (2003) and included in Annex C of EN 1993-1-4 (2006). These material properties were incorporated into the FE model converting the stress-strain (engineering) curve into true stress and logarithmic plastic strain.

Table 4.4 Measured material properties (Talja and Hradil (2011)) of the modelled specimens

Nominal thickness (mm)	$E$ (GPa)	$\sigma_{0.2}$ (MPa)	$n$	$\sigma_u$ (MPa)	$m$	$\epsilon_u$
1	200	359	23.1	479	1.46	0.0170
1.5	191	322	26.1	475	1.21	0.0160
2	193	372	23.0	489	1.30	0.0164
3	180	297	23.5	445	1.22	0.0160



### 4.3.3 Boundary conditions and loading

For the case of the IOF loading (Category 2), the transverse load  $F_{Ed}$  was applied through a rigid plate ( $s_s$ ) controlled by a reference point (RP). All the degrees of freedom except the vertical translation were restrained in this RP and a vertical displacement was imposed to represent the loading. Contact pair (surface-to-surface) was used to model the interface between the rigid plate (master surface) and the flange of the cross-section (slave surface, extended up to the corners) assuming frictionless response in the tangential direction and hard response in the normal one. Two supports (S), which were also modelled as rigid plates, were placed on both edges in contact with the lips to model simply supported conditions. Their respective reference points (RP) were provided with appropriate boundary conditions to allow in-plane rotation. In the test arrangement (Talja and Hradil (2011)), wooden blocks were placed within the cross-section to prevent possible local instabilities at the support regions. This was modelled by restraining the vertical and horizontal translations as well as the rotation about the x-axis at the flat regions of the webs and the flange adjacent on either side of the corners over the length of the supports S. All these details are given in Fig. 4.2.

Regarding EOF loading (Category 1), the transverse load  $F_{Ed}$  was also applied through a rigid plate (S), similarly to the IOF loading. While testing (Talja and Hradil (2011)), screw clamps were used to join this plate and the lips of the hat section together, which was modelled by tying the surfaces in contact. The end bearing support ( $s_s$ ) was also modelled as a rigid plate and contact pair was used to model the interface with the specimen. A wooden block was placed within the cross-section at the further end support to prevent distortional deformation in the test (Talja and Hradil (2011)). The geometry of the cross-section over this support was modelled as a rigid body controlled by a reference point (RP) in its center of mass. In-plane rotation was allowed at the bearing support ( $s_s$ ) and in the rigid body (end support). All these details are given in Fig.4.3.

### 4.3.4 Verification of the numerical model

Figs 4.4 and 4.5 present the load-displacement response recorded in the test (Talja and Hradil (2011)) and obtained with the numerical model for IOF and EOF loading, respectively, whereas ultimate applied numerical loads  $F_{u,num}$  and resistances per web  $R_{w,u,num}$  determined as described in sub-section 4.3.1 are given in Table 4.3. Excellent

good agreement between test results and models was achieved, particularly for the ultimate predicted load for both loading configurations with mean test-to-numerical ratio of 1.011 and coefficient of variation (COV) of 0.046. Experimental and numerical failure modes for both IOF and EOF loading are shown in Figs 4.6 and 4.7, respectively. In both cases, the numerical models accurately capture the experimental failure mode. This numerical model is therefore deemed reliable and suitable to perform parametric studies. The discrepancy between the experimental and numerical stiffness, particularly in the EOF curves, was also observed in existing studies (Hofmeyer (2000) and Kaitila (2004)), which was associated with the sensitivity of the FE model to the boundary conditions and initial imperfections of the member owing to the thin-walled nature of the cross-section.

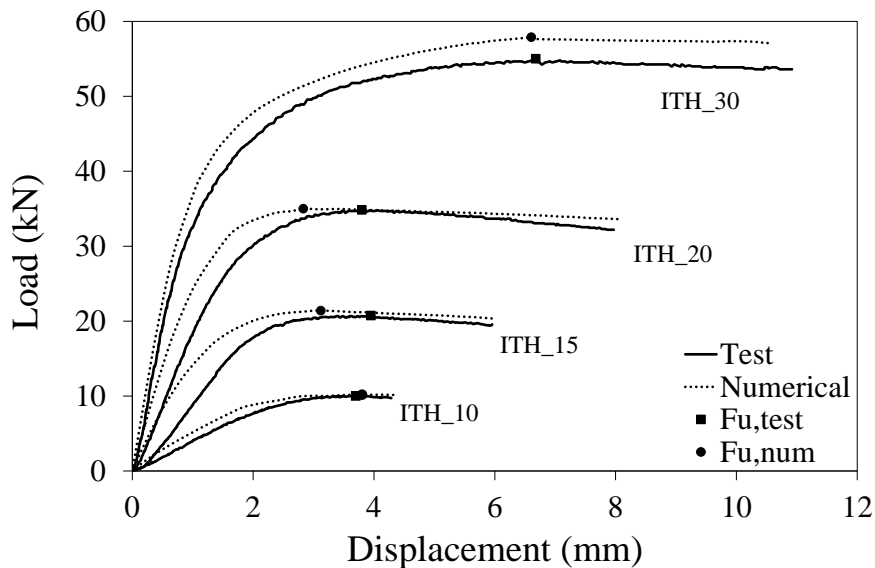


Fig. 4.4 Load-displacement response for beams subjected to IOF loading

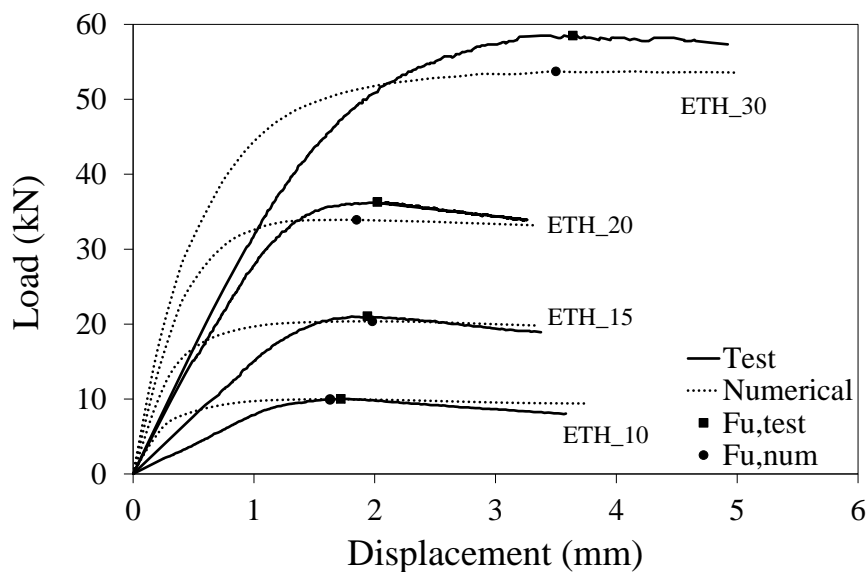


Fig. 4.5 Load-displacement response for beams subjected to EOF loading

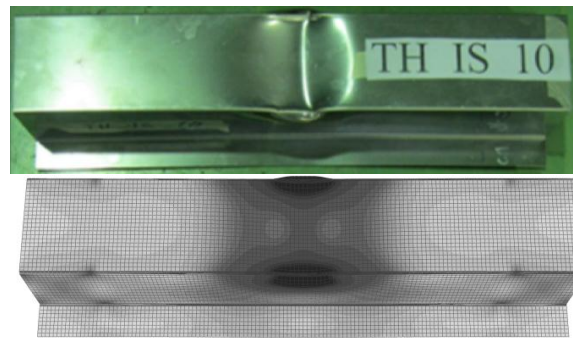


Fig. 4.6 Typical web crippling failure mode for IOF loading (ITH\_10)

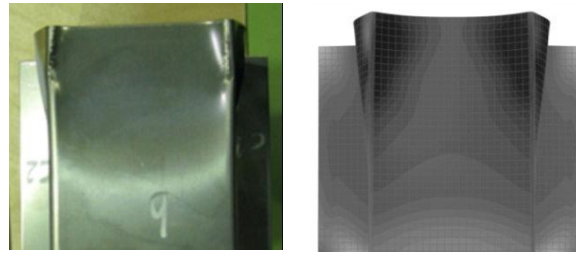


Fig. 4.7 Typical web crippling failure mode for EOF loading (ETH\_10)

#### 4.3.5 Cross-section geometries and load configurations for the parametric study

Having validated the numerical model, an extensive parametric study was conducted to generate numerical data over different geometries and investigate the web crippling behaviour of hat sections under both IOF (Category 2) and EOF (Category 1) loading conditions. The study was performed for ferritic and austenitic stainless steels with the following material properties based on average values given in EN 1993-1-4 (2006):  $E=200$  GPa,  $\sigma_{0.2}=350$  MPa,  $n=15$ ,  $\sigma_u=450$  MPa,  $m=3$  and  $\epsilon_u=0.15$  for ferritic stainless steel, while  $E=193$  GPa,  $\sigma_{0.2}=445$  MPa,  $n=7$ ,  $\sigma_u=700$  MPa,  $m=3.4$  and  $\epsilon_u=0.42$  for austenitic stainless steel. The parametric study included 7 different hat section geometries with the following centreline dimension in mm ( $h \times b \times c \times t \times r_m$ ):  $30 \times 30 \times 17 \times 1 \times 1.5$ ,  $50 \times 50 \times 20 \times 1.5 \times 2$ ,  $80 \times 50 \times 20 \times 1.5 \times 2$ ,  $100 \times 50 \times 20 \times 1.5 \times 2$ ,  $50 \times 80 \times 20 \times 1.5 \times 2$ ,  $100 \times 100 \times 25 \times 1.5 \times 2$  and  $70 \times 70 \times 25 \times 1.5 \times 2$ . For all these geometries, the length of the member  $L$ , the bearing plate  $s_s$ , and the support plates  $S$ , were 400 mm, 25 mm and 50 mm respectively. Regarding the clear distance  $e$  for the EOF loading, this was set out as  $e=75$  mm. Additional specimens were modelled to study the influence of various parameters on the web crippling strength, including: the thickness ( $t=0.5$  mm, 0.75 mm, 1 mm and 2 mm); the bearing length ( $s_s=12.5$  mm and 50 mm for IOF loading, and  $s_s=10$  mm and 35 mm for EOF loading); the bending radius ( $r_m=1.5$  mm, 2.5 mm and 3 mm); the length ( $L=600$  mm and  $L=800$  mm); a clear distance  $e=150$  mm was also studied for the EOF loading.

## 4.4 Strength curves controlled by slenderness-based functions

### 4.4.1 Basis of the method

The concept underpinning the so-called strength curves  $\chi(\bar{\lambda})$  is that structural steel members (or cross-sections) fail in a way involving buckling and yielding relating the reduction factor  $\chi$  to a relative slenderness  $\bar{\lambda}$ . Unlike the current web crippling design equations, which are purely empirical in nature, this slenderness-based design approach combines both theoretical and empirical basis and therefore, leads to a better understanding of the underlying engineering principles involved in the formulation. Various strength curves are currently given in the design codes for the verification of different instabilities including local buckling, shear buckling, patch loading and global buckling among others.

The suitability of this method based on strength curves  $\chi(\bar{\lambda})$  for web crippling design was recently investigated by Duarte and Silvestre (2013) on cold-formed carbon unstiffened C-sections. The success for such sections opens the way for its extension to cover other section typologies and materials. Hence, the method is extended herein for web crippling design of stainless steel hat sections following previous research on the same topic by Bock et al. (2014a).

$$\chi = \frac{A}{\bar{\lambda}^B} \leq 1 \quad (4.14)$$

$$\bar{\lambda} = \sqrt{\frac{R_{w,pl}}{R_{w,cr}}} \quad (4.15)$$

$$R_{w,u} = \chi R_{w,pl} \quad (4.16)$$

The base curve (strength curve) of this method, given in Eq. (4.14) in the general expression where the coefficients A and B may be derived by regression analysis of data, provides a continuous relationship between the reduction factor  $\chi$  and the relative slenderness  $\bar{\lambda}$  given by Eq. (4.15), where  $R_{w,cr}$  and  $R_{w,pl}$  are the elastic critical buckling resistance and the plastic resistance per web, respectively. The web crippling resistance per web  $R_{w,u}$  may be then determined applying the reduction factor  $\chi$  to the plastic resistance  $R_{w,pl}$  as defined by Eq. (4.16).

#### 4.4.2 Data required for the design method

The determination of the coefficients A and B within the strength curve utilises data over a  $\chi - \bar{\lambda}$  space. While Eq. (4.15) is used to obtain values over the horizontal axis, the reduction factor  $\chi$ , taken as Eq. (4.16) and rewritten as  $\chi=R_{w,u}/R_{w,pl}$ , is used for the vertical axis. Consequently, three different resistances are required upon which to base the development of the design method: the web crippling resistance  $R_{w,u}$ ; the elastic critical buckling resistance  $R_{w,cr}$ ; and the plastic resistance  $R_{w,pl}$ . It should be noted that while the web crippling resistance  $R_{w,u}$  may be obtained from tests (or numerical simulations), both elastic critical buckling resistance  $R_{w,cr}$  and plastic resistance  $R_{w,pl}$  may only be determined numerically.

The validated numerical model described previously in section 4.3 was therefore used to obtain such resistances for the aforementioned cross-section geometries and load cases described in sub-section 4.3.5. The three resistances  $R_{w,cr}$ ,  $R_{w,pl}$  and  $R_{w,u}$  were determined performing three types of analyses on every single model (Duarte and Silvestre (2013) and Bock et al. (2014a)): (1) elastic buckling analyses to determine the elastic critical buckling resistances  $R_{w,cr}$ ; (2) first order plastic analyses to obtain the plastic resistances  $R_{w,pl}$ ; and (3) geometrical and material nonlinear analyses for the determination of the ultimate web crippling resistances  $R_{w,u}$ . A total of 350 numerical analyses were conducted.

#### 4.4.3 Results from the analyses

The obtained numerical results, including the generated models in the parametric study and the modelled tests are presented in Figs 4.8 and 4.9 for IOF and EOF loading, respectively. In Figs 4.8 and 4.9, the reduction factor  $\chi$ , determined as the ultimate numerical web crippling resistance  $R_{w,u,num}$  divided by the numerical plastic resistance  $R_{w,pl,num}$ , is plotted against the relative slenderness  $\bar{\lambda}$  obtained as the squared root of the numerical plastic resistance  $R_{w,pl,num}$  to numerical critical resistance  $R_{w,cr,num}$  ratio as given by Eq. (4.15). Strength curves applicable to other cross-sections, including those proposed by Duarte and Silvestre (2013) for cold-formed carbon steel unstiffened C-sections and given in EN 1993-1-5 (2006) for carbon steel plate girders (I-sections) subjected to patch loading are also depicted in Figs 4.8 and 4.9 so that their suitability for application to cold-formed stainless steel hat sections could be assessed.

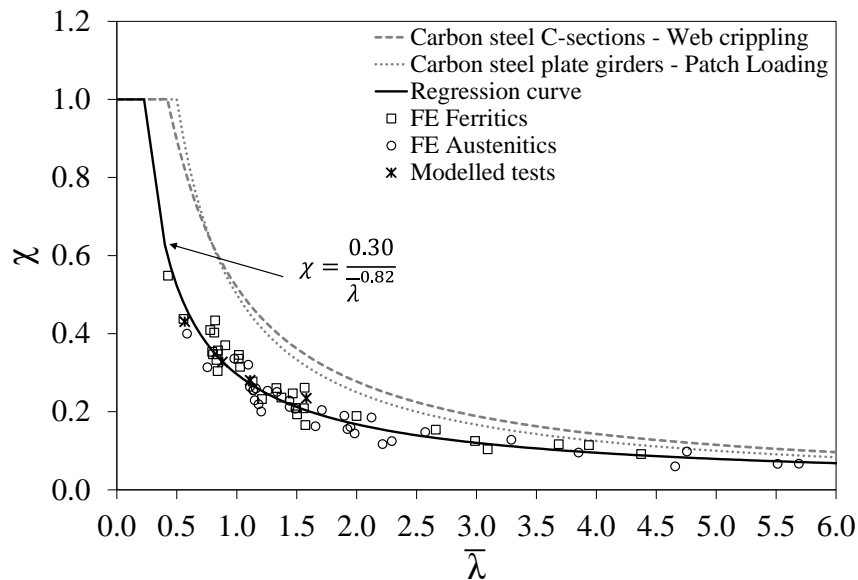


Fig. 4.8 Reduction factor versus relative slenderness (based on numerical results) for IOF loading

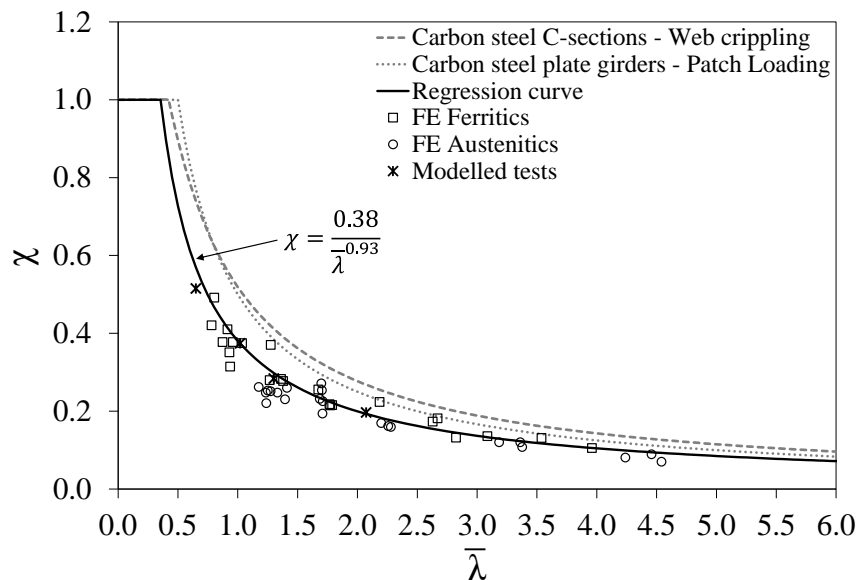


Fig. 4.9 Reduction factor versus relative slenderness (based on numerical results) for EOF loading

Three main conclusions can be drawn from Figs 4.8 and 4.9. Firstly, the resulting points display a curved trend of decreasing reduction factor  $\chi$  with increasing relative slenderness  $\bar{\lambda}$ . The regression curves (strength curves) yielding the equations shown in the corresponding figures represent this continuous relationship between reduction factor  $\chi$  and relative slenderness  $\bar{\lambda}$ . Secondly, all the generated data lay significantly below the strength curves for web crippling design of cold-formed carbon unstiffened C-sections (Duarte and Silvestre (2013)) and patch loading design of plated girders (EN 1993-1-5 (2006)), reflecting a different web crippling response of stainless steel hat sections for both IOF and EOF loading. And finally, regarding the material effect,

austenitic and ferritic stainless steel appeared to perform similarly, thus, there is no need to derive different strength curves for different stainless steels. For practical application of the adjusted strength curves shown in Figs 4.8 and 4.9, predictive models for both elastic critical buckling resistance  $R_{w,cr}$  and the first order plastic load  $R_{w,pl}$  may be derived. Additionally, these strength curves should be statistically validated so that they satisfy the partial safety factor recommended in EN 1993-1-4 (2006) for stainless steels ( $\gamma_{M1}=1.1$ ). Both tasks are developed in the following section.

## 4.5 Proposed strength curves and predictive models

### 4.5.1 Predictive model for $R_{w,cr}$

The proposed predictive model for the elastic critical buckling resistance  $R_{w,cr,pred}$  stems from classical elastic theory of instability for a plate loaded with a concentrated in-plane force at the edge given in Eq. (4.17) where the dimensionless buckling coefficient  $k_F$  may be derived for a given plate geometry and boundary conditions (Duarte and Silvestre (2013), Johansson and Lagerqvist (1995) and Lagerqvist and Johansson (1996)). The derived expression for  $k_F$  is given in Eq. (4.18) where coefficients were determined by regression analysis accounting both generated models in the parametric study and modelled tests. Note that although the key controlling parameters in the dimensionless buckling coefficient  $k_F$  are similar for both IOF and EOF loading, two different expressions are proposed. The symbols of these expressions are defined by reference to Figs 4.1-4.3.

$$R_{w,cr,pred} = k_F \frac{\pi^2 E t^3}{12(1 - \nu^2)h} \quad (4.17)$$

$$k_F = \begin{cases} 4.9 - 1.6 \left(\frac{b}{h}\right) - 0.006 \left(\frac{L}{h}\right)^2 + 6.6 \left(\frac{S_s}{L}\right) & \text{For IOF loading} \\ 1.85 - 0.75 \left(\frac{b}{h}\right) + 1.75 \left(\frac{S_s}{h}\right) & \text{For EOF loading} \end{cases} \quad (4.18)$$

Tables 4.5 and 4.6 compare the numerical elastic critical resistances  $R_{w,cr,num}$  with the predicted ones using this proposed model  $R_{w,cr,pred}$  for the modelled tests alone under IOF and EOF loading, respectively. Table 4.7 presents the results for the generated numerical models in terms of mean numerical-to-predicted ratio. In Tables 4.5-4.7, results show that predicted resistances agree with the numerical results with a mean numerical-to-predicted ratio very close to unity and fairly reduced coefficient of variation (COV). Figs 4.10 and 4.11 show a comparison of the predictions to all the data

for IOF and EOF loading, respectively, where distinction between materials is made (FE Ferritics and FE Austenitics).

Table 4.5 Comparison between numerical results and predictive models for the modelled tests under IOF loading

Beam	$R_{w,cr,num}$ (kN)	$R_{w,cr,pred}$ (kN)	$R_{w,pl,num}$ (kN)	$R_{w,pl,pred}$ (kN)	$R_{w,cr,num}/$ $R_{w,cr,pred}$	$R_{w,pl,num}/$ $R_{w,pl,pred}$
ITH_10	8.62	8.70	21.73	21.28	0.991	1.021
ITH_15	30.94	30.86	38.12	31.61	1.003	1.206
ITH_20	67.70	69.10	53.41	50.41	0.980	1.059
ITH_30	195.97	209.77	67.20	52.41	0.934	1.282
				Mean	0.977	1.142
				COV	0.026	0.093

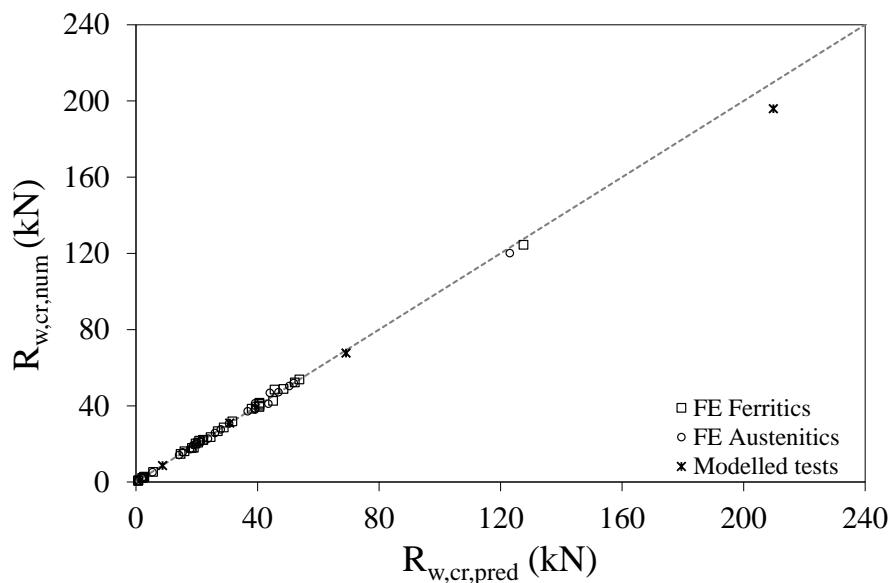


Fig. 4.10 Comparison between numerical and predicted elastic critical resistances for IOF loading

Table 4.6 Comparison between numerical results and predictive models for the modelled tests under EOF loading

Beam	$R_{w,cr,num}$ (kN)	$R_{w,cr,pred}$ (kN)	$R_{w,pl,num}$ (kN)	$R_{w,pl,pred}$ (kN)	$R_{w,cr,num}/$ $R_{w,cr,pred}$	$R_{w,pl,num}/$ $R_{w,pl,pred}$
ETH_10	4.17	4.14	17.91	16.96	1.007	1.056
ETH_15	15.21	15.08	25.71	23.97	1.008	1.072
ETH_20	33.05	33.88	34.29	34.22	0.976	1.002
ETH_30	95.76	104.05	40.48	41.56	0.920	0.974
				Mean	0.978	1.026
				COV	0.036	0.038

Table 4.7 Comparison between numerical results and predictive models for the generated models in the parametric study

	$R_{w,pl,num}/R_{w,pl,pred}$					
	$R_{w,cr,num}/R_{w,cr,pred}$		Ferritics		Austenitics	
	IOF	EOF	IOF	EOF	IOF	EOF
Mean	0.991	1.00	1.134	1.098	1.334	1.334
COV	0.035	0.015	0.176	0.226	0.205	0.241



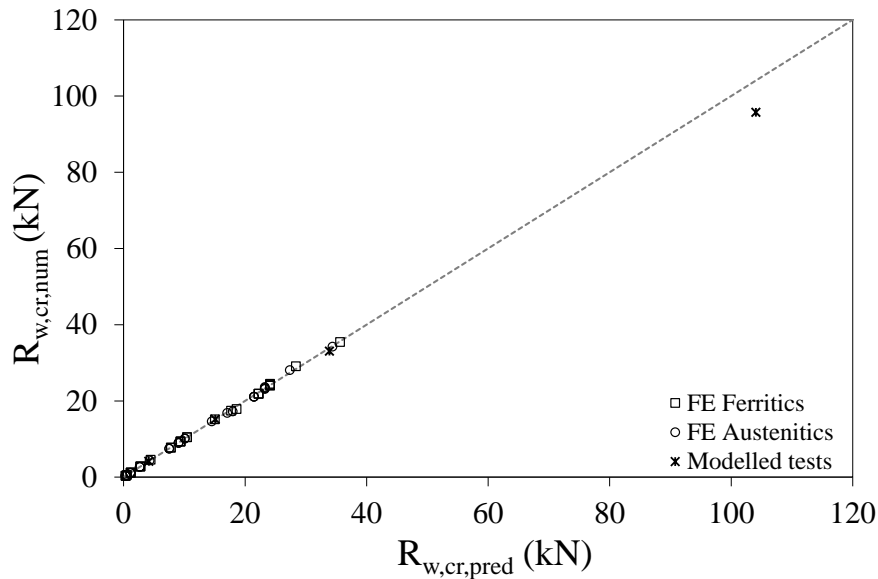


Fig 4.11 Comparison between numerical and predicted elastic critical resistances for EOF loading

#### 4.5.2 Predictive model for $R_{w,pl}$

The plastic mechanism model proposed by Young and Hancock (2001) for cold-formed unstiffened C-sections is adapted herein for cold-formed hat sections as the predictive model of the first order plastic resistance per web  $R_{w,pl,pred}$ . Given the localized nature of the failure mode, the observed plastic mechanisms in the numerical analyses resemble the assumed plastic mechanism model regardless of the cross-sectional geometry. Other plastic mechanism models derived from yield lines for square hollow sections (Zhao and Hancock (1992, 1995) and Zhou and Young (2006b) as well as models based on plastic hinges (Lagerqvist and Johansson (1996) and Roberts and Rockey (1979) are available in the literature.

The basis of the assumed plastic mechanism model, as shown in Fig. 4.12, is that the concentrated load applied over a bearing length on the flange  $s_s$  can be idealized as a local eccentric load  $R_{w,pl,pred}$  given in Eq. (4.19), inducing a plastic hinge per unit length  $M_{pl,l_y}$  along the yield line  $l_y$  as given in Eq. (4.20). Hence, the key parameter to adjust is this yield line length  $l_y$ . A regression analysis accounting all the data lead to Eq. (4.21) where distinction is also made between load conditions and symbols are defined by reference to Figs 4.1-4.3. It should be noted that, unlike the adjusted strength curves and derived elastic critical buckling resistance model, this plastic resistance model includes a material correction factor  $m$ , allowing for the attainment of higher plastic resistances for material with higher ductility. A value of  $m=1$  for ferritic stainless steel and  $m=1.15$

for austenitic stainless steel provided good agreement between predicted  $R_{w,pl, pred}$  and numerical  $R_{w,pl, num}$  resistances as shown in Figs 4.13 and 4.14 for IOF and EOF loading, respectively. Note that in both figures, most of the predicted plastic resistances are placed on the safe side for both materials (FE Ferritics and FE Austenitics) accounted in the study.

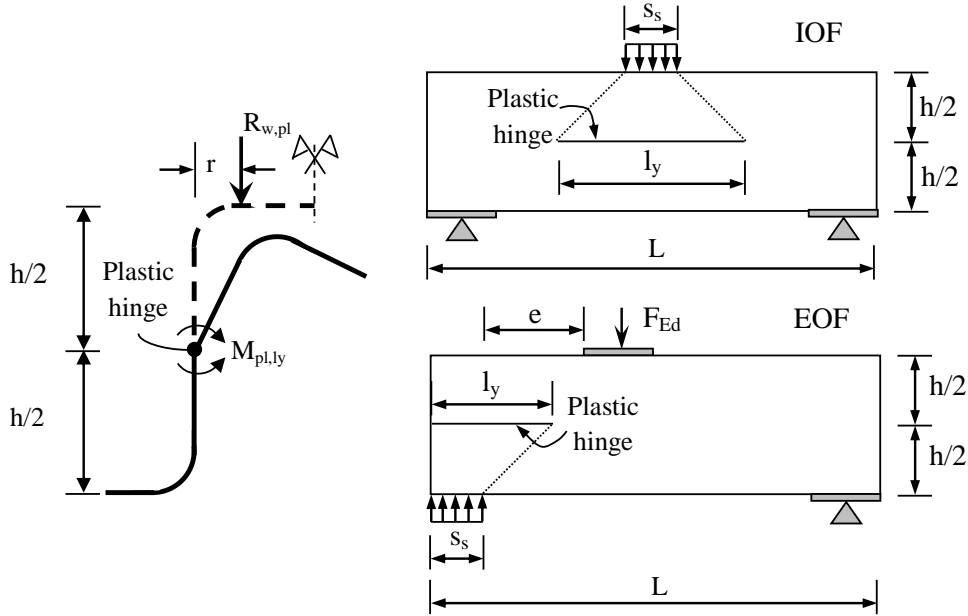


Fig. 4.12 Adopted plastic mechanism model (Young and Hancock (2001)) for hat sections

$$R_{w,pl,pred} = \frac{M_{pl,ly} l_y}{r} \quad (4.19)$$

$$M_{pl,ly} = \frac{\sigma_{0.2} t^2}{4} \quad (4.20)$$

$$l_y = \begin{cases} (s_s + h)m \left[ \frac{2r}{t} + \frac{5b}{L} - 0.55 \right] & \text{For IOF loading} \\ (s_s + h/2)m \left[ 2.2 - 6.2 \frac{\sqrt{r^2 + t^2}}{t} + \frac{6.3r}{t} + \frac{0.6L}{e} \right] & \text{For EOF loading} \end{cases} \quad (4.21)$$

Tables 4.5 and 4.6 give the predicted first order plastic resistances per web  $R_{w,pl, pred}$  determined using this proposed predictive model for the modelled tests alone subjected to IOF and EOF loading, respectively. Regarding generated numerical models in the parametric study, only key statistical results based on mean numerical-to-predicted ratio and coefficient of variation (COV) are shown in Table 4.7 where distinction is made between materials.

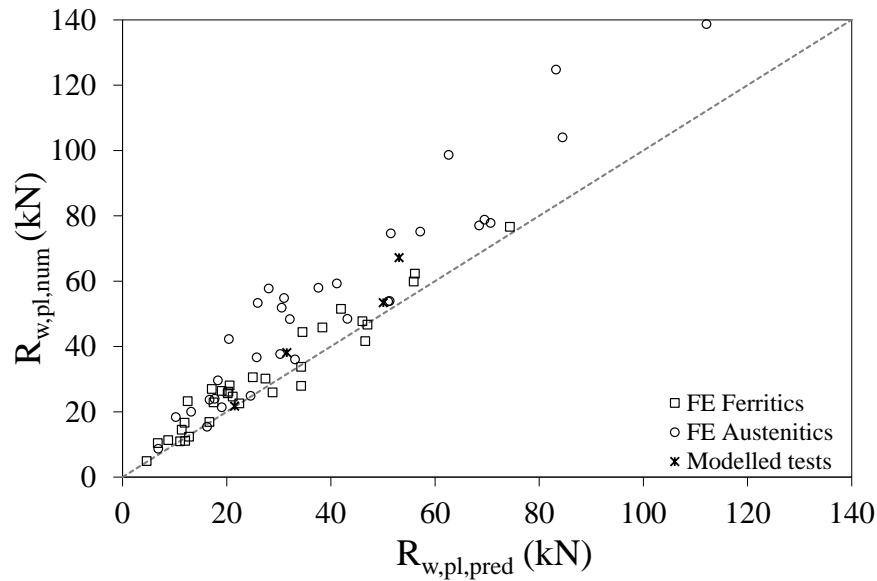


Fig. 4.13 Comparison between numerical and predicted plastic resistances for IOF loading

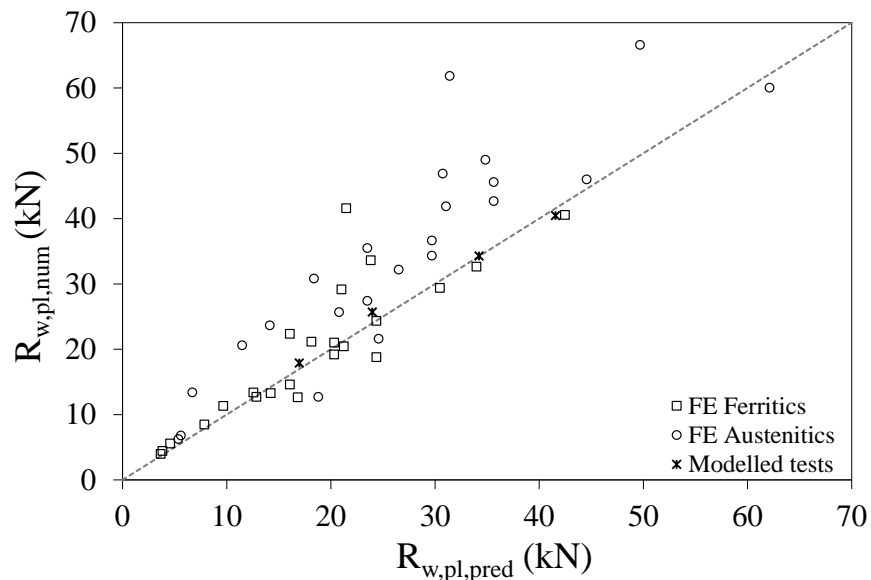


Fig. 4.14 Comparison between numerical and predicted plastic resistances for EOF loading

#### 4.5.3 Proposed strength curves and statistical validation

Having adjusted predictive models for the elastic critical strength  $R_{w,cr,pred}$  and the first order plastic resistance  $R_{w,pl,pred}$  given in the set of Eqs (4.17)-(4.18) and Eqs (4.19)-(4.21), respectively, these models are therefore used to derive practical strength curves for web crippling design of stainless steel hat sections. To this end, the predicted values provided by the corresponding predictive models for the elastic critical strength  $R_{w,cr,pred}$  and the first order plastic resistance  $R_{w,pl,pred}$  are used to replace the corresponding numerical values which had been used to determine the relationship between the reduction factor  $\chi$  and relative slenderness  $\bar{\lambda}$  in previous section (Figs 4.8 and 4.9).

Hence, the new reduction factor  $\chi$  is determined as the ultimate numerical web crippling resistance  $R_{u,w,num}$  divided by the predicted plastic resistance  $R_{w,pl,pred}$ , and plotted against the new relative slenderness  $\bar{\lambda}$  obtained as the squared root of the predicted plastic resistance  $R_{w,pl,pred}$  to predicted critical resistance  $R_{w,cr,pred}$  ratio as given in Eq. (4.15). The new relationship is shown in Figs 4.15 and 4.16 for IOF and EOF loading, respectively, where it is observed that the replacement has not significantly affected the results in comparison with those obtained in Figs 4.8 and 4.9; hence, reflecting the suitability of the proposed predictive models for the elastic critical strength  $R_{w,cr,pred}$  and the first order plastic resistance  $R_{w,pl,pred}$ .

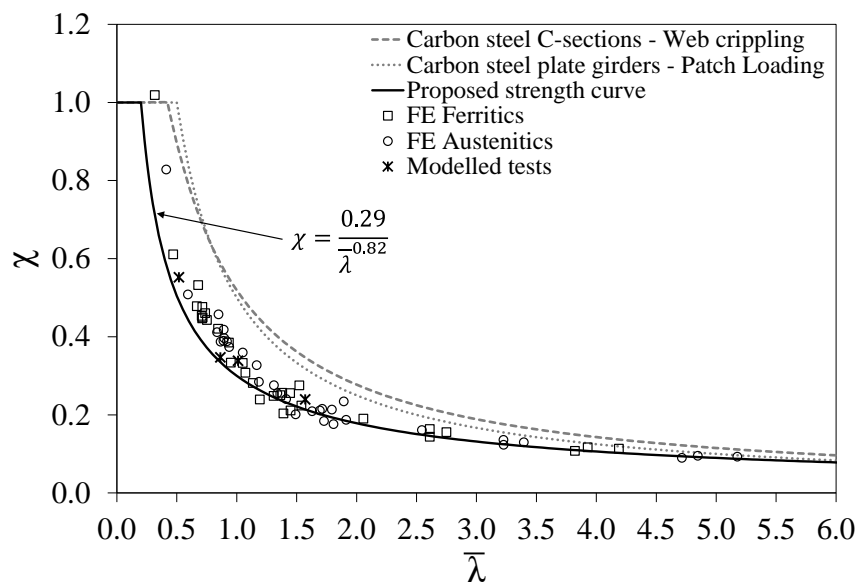


Fig. 4.15 Proposed Strength curve for IOF loading

Finally, following the general expression for a strength curve given in Eq. (4.14), new coefficients A and B were derived for the design approach combining regression analyses and statistical evaluations in accordance with Annex D of EN 1990 (2002) thereby obtaining the optimal values given in Eq. (4.22). The strength curves are shown in Figs 4.15 and 4.16 for IOF and EOF loading, respectively, together with those proposed by Duarte and Silvestre (2013) for cold-formed carbon steel unstiffened C-sections and given in EN 1993-1-5 (2006) for carbon steel plate girders (I-sections) subjected to patch loading.

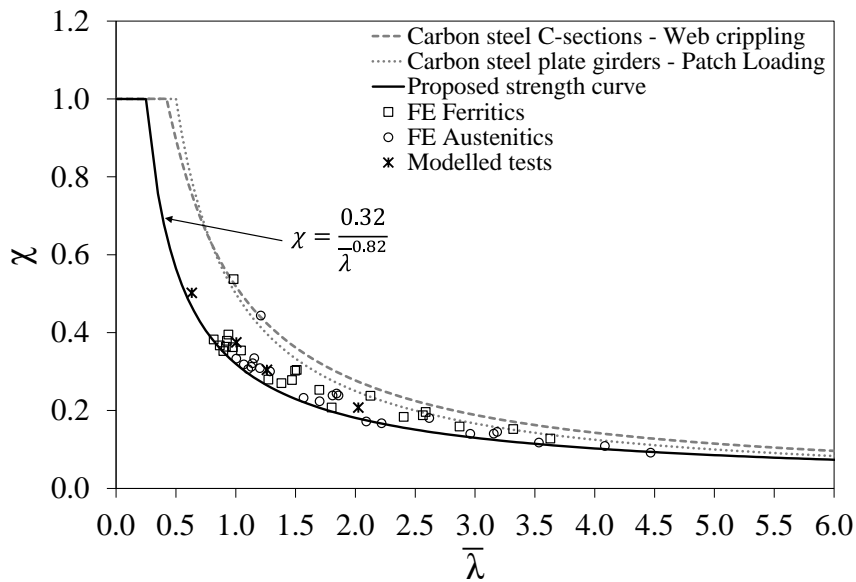


Fig. 4.16 Proposed Strength curve for EOF loading

$$\chi = \begin{cases} \frac{0.29}{\bar{\lambda}^{0.82}} & \text{For IOF loading} \\ \frac{0.32}{\bar{\lambda}^{0.82}} & \text{For EOF loading} \end{cases} \quad (4.22)$$

Table 4.8 Statistical results and partial safety factor for the proposed strength curves

Loading	Material	n	b	$V_{\delta}$	$V_{FEM}$	$V_r$	$\gamma_{M1}$
IOF	Ferritics	32	1.113	0.088	0.020	0.115	1.078
	Austenitics	32	1.129	0.088	0.020	0.122	1.075
EOF	Ferritics	23	1.149	0.120	0.096	0.169	0.977
	Austenitics	23	1.139	0.109	0.096	0.174	1.013

For the statistical evaluation of the proposed design approach (resistance model), the database was split into two sub-sets based on their material grade to consider the difference in over-strength ratio (measured/minimum specified strength) following recommendations by Baddoo and Francis (2013). Details of the procedure to statistically validate a resistance model are given in Bock et al. (2014b). A summary of key statistical parameters is presented in Table 4.8 where n is the population of the data under consideration, b is the mean value of numerical data to predicted resistance ratio,  $V_{\delta}$  is coefficient of variation of the numerical data relative to the resistance model (error of the model) and  $V_r$  is combined coefficient of variation making allowance for the error of the model  $V_{\delta}$ , including the basic variables  $V_{xi}$  and the FE model  $V_{FEM}$  (Davaine (2005)). The adopted coefficients of variation for the basic variables were (Baddoo and Francis (2013)): 0.05 for the coefficient of variation of geometric properties; 0.066 and 0.050 for the coefficient of variation associated with the material strength for austenitic and ferritic stainless steel, respectively; material over-strength of 1.3 for austenitic

stainless steel and 1.2 for ferritic stainless steel. The results of the statistical evaluation show that the proposed design approach is reliable ( $\gamma_{M1} \leq 1.1$  for safe design) for a partial safety factor of  $\gamma_{M1} = 1.1$ .

#### 4.5.4 Comparison with numerical data and design models

The obtained numerical ultimate resistances per web of the generated models in the parametric study  $R_{w,u,num}$  are compared herein with predicted resistances using EN 1993-1-3 (2006)  $R_{w,u,EC}$ , the North American SEI/ASCE 8-02 (2002) standard  $R_{w,u,ASCE}$  and the proposed design approach based on strength curves  $R_{w,u,\chi-\lambda}$  given in Eqs (4.15)-(4.22). The partial safety factor was set to unity to allow direct comparison between resistances which are shown in Figs 4.17 and 4.18 for IOF and EOF loading, respectively. In these figures, the numerical resistances are normalized by the respective predictive methods and plotted against the slenderness parameter  $\bar{\lambda}$  determined in accordance with Eq. (4.15) using predictive models derived in Eqs (4.17)-(4.21). Table 4.9 presents such comparison in terms of mean numerical-to-predicted ratio and coefficient of variation (COV). The results show that both EN 1993-1-3 (2006) and the North American SEI/ASCE 8-02 (2002) standard provide similar results yielding conservative predictions and large scatter whereas the proposed design approach based on strength curves  $\chi(\bar{\lambda})$  offer the most accurate predictions. Note that the accuracy of the proposed method remains constant with increasing relative slenderness  $\bar{\lambda}$  leading to a significant reduction in scatter.

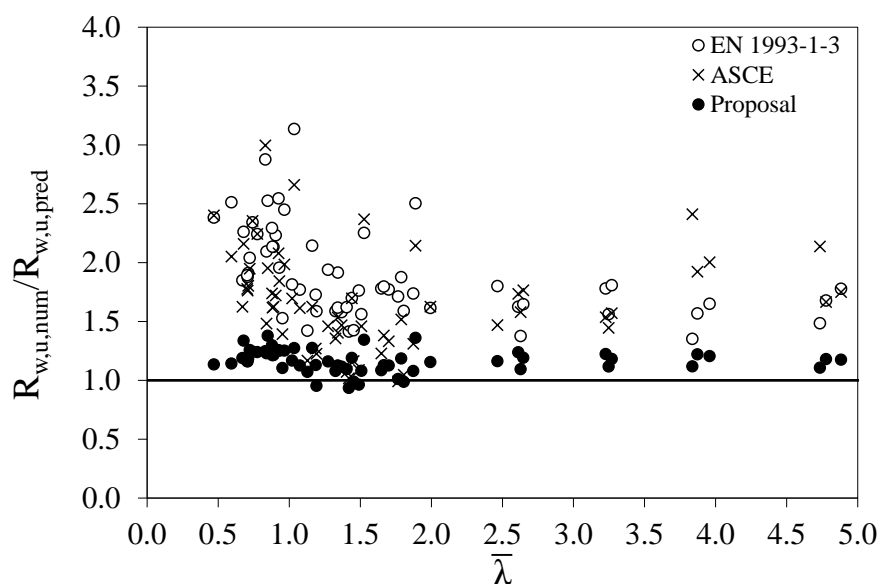


Fig. 4.17 Comparison of numerical web crippling strength with proposed design method and design standards for IOF loading

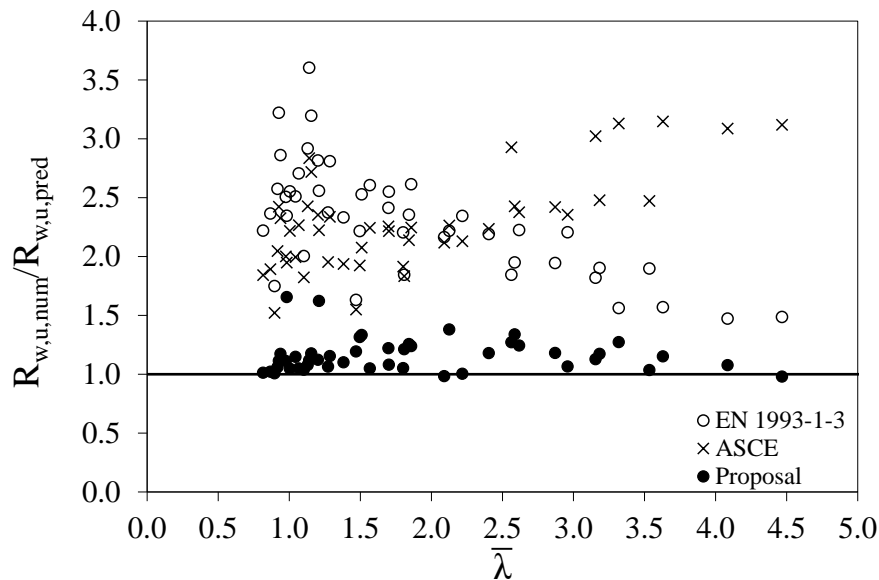


Fig. 4.18 Comparison of numerical web crippling strength with proposed design method and design standards for EOF loading

Table 4.9 Comparison of ultimate web crippling capacity against different formulations for generated models in the parametric study

Load case	Data source	Ratio	Mean	COV
IOF	FE	$R_{w,u,num}/R_{w,u,EC}$	1.931	0.217
		$R_{w,u,num}/R_{w,u,ASCE}$	1.719	0.262
		$R_{w,u,num}/R_{w,u,\gamma-\lambda}$	1.172	0.086
	Tests <sup>a,b</sup>	$R_{w,u,test}/R_{w,u,EC}$	1.709	0.050
		$R_{w,u,test}/R_{w,u,ASCE}$	1.603	0.064
		$R_{w,u,test}/R_{w,u,\gamma-\lambda}$	1.117	0.056
EOF	FE	$R_{w,u,num}/R_{w,u,EC}$	2.303	0.202
		$R_{w,u,num}/R_{w,u,ASCE}$	2.286	0.174
		$R_{w,u,num}/R_{w,u,\gamma-\lambda}$	1.158	0.123
	Tests <sup>a</sup>	$R_{w,u,test}/R_{w,u,EC}$	2.572	0.027
		$R_{w,u,test}/R_{w,u,ASCE}$	2.073	0.110
		$R_{w,u,test}/R_{w,u,\gamma-\lambda}$	1.160	0.037

<sup>a</sup>Talja and Hradil (2011)

<sup>b</sup>Talja (2004)

#### 4.6. Validation of the design approach with test data

The proposed design approach is validated in this section on the basis of available test data, including austenitic hat sections under IOF loading (Talja (2004)) and ferritic hat sections under both IOF and EOF loading (Talja and Hradil (2011)). As commented before, all relevant published test data on stainless steel are summarized in Table 4.2. The mean values and coefficients of variation of the test results  $R_{w,u,test}$  normalized by predicted ultimate resistances using the three considered approaches: EN 1993-1-3 (2006)  $R_{w,u,EC}$ ; the North American SEI/ASCE 8-02 (2002) standard  $R_{w,u,ASCE}$ ; and the proposed design approach based on strength curves  $R_{w,u,\gamma-\lambda}$  given in Eqs (4.15)-(4.22), are shown in Table 4.9, whereas comparisons of the predictions with existing tests are

given in Table 4.10. Similarly to the comparison based on numerical results, the proposed design approach for web crippling design based on strength curves controlled by slenderness-based functions  $\chi(\bar{\lambda})$  achieve a significant reduction in terms of mean and scatter. Figs 4.19 and 4.20 reflect the accuracy of the proposed design approach for IOF and EOF loading, respectively, where it is also observed that all predicted resistances are safe.

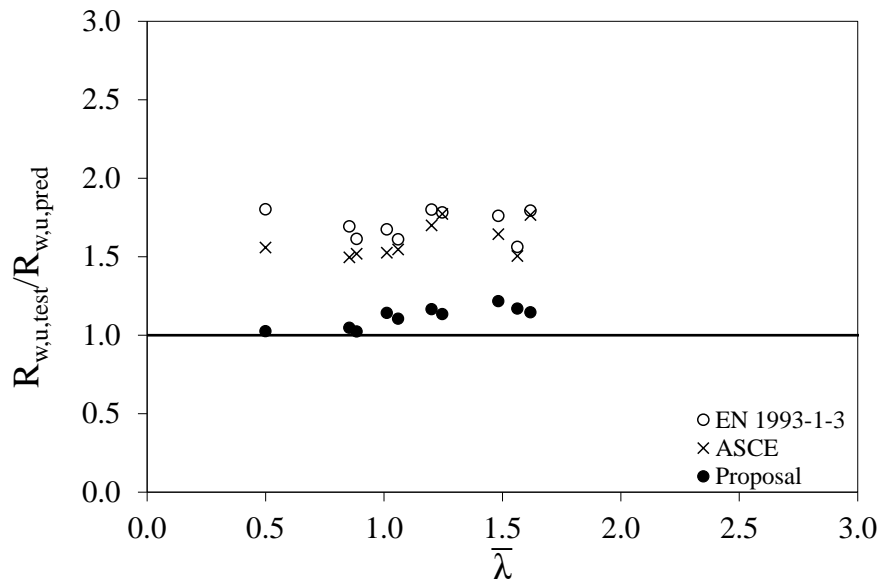


Fig. 4.19 Comparison of test web crippling strength with proposed design method and design standards for IOF loading

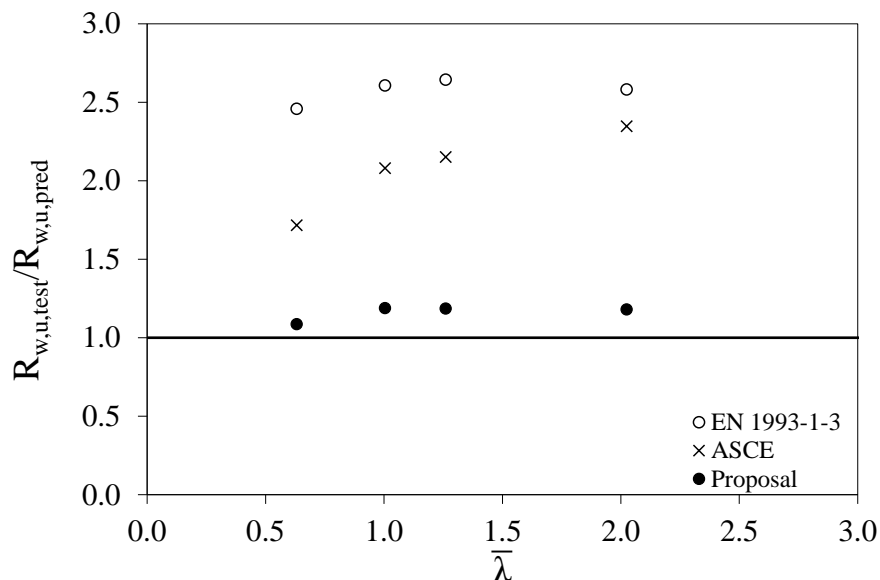


Fig. 4.20 Comparison of test web crippling strength with proposed design method and design standards for EOF loading



Table 4.10 Comparison of ultimate web crippling capacity against different formulations for collected tests

Beam	Load type, Source	$R_{w,u,test}$ (kN)	$R_{w,u,EC}$ (kN)	$R_{w,u,ASCE}$ (kN)	$R_{w,u,\chi-\lambda}$ (kN)	$R_{w,u,test}/R_{w,u,EC}$	$R_{w,u,test}/R_{w,u,ASCE}$	$R_{w,u,test}/R_{w,u,\chi-\lambda}$
ITH_10	IOF <sup>a</sup>	5.00	3.20	3.32	4.28	1.562	1.504	1.169
ITH_15	IOF <sup>a</sup>	10.37	6.19	6.80	9.08	1.674	1.525	1.142
ITH_20	IOF <sup>a</sup>	17.42	10.29	11.65	16.64	1.693	1.496	1.047
ITH_30	IOF <sup>a</sup>	27.51	15.27	17.65	26.84	1.802	1.558	1.025
H100-100×2-C700	IOF <sup>b</sup>	24.75	15.35	16.30	24.19	1.613	1.519	1.023
H150-100×2-C700	IOF <sup>b</sup>	25.01	15.53	16.18	22.64	1.610	1.546	1.104
H100-100×2-C850	IOF <sup>b</sup>	31.20	17.34	18.36	26.77	1.800	1.700	1.165
H150-100×2-C850	IOF <sup>b</sup>	31.02	17.62	18.87	25.51	1.760	1.644	1.216
H100-100×2-C850	IOF <sup>b</sup>	44.34	24.88	25.01	39.08	1.782	1.772	1.134
H150-100×2-C850	IOF <sup>b</sup>	45.67	25.47	25.87	39.87	1.793	1.765	1.146
ETH_10	EOF <sup>a</sup>	3.59	1.39	1.53	3.04	2.581	2.347	1.179
ETH_15	EOF <sup>a</sup>	7.52	2.85	3.50	6.34	2.643	2.151	1.186
ETH_20	EOF <sup>a</sup>	12.96	4.97	6.23	10.91	2.606	2.079	1.188
ETH_30	EOF <sup>a</sup>	21.04	8.56	12.26	19.37	2.458	1.716	1.086

<sup>a</sup>Talja and Hradil (2011)<sup>b</sup>Talja (2004)

#### 4.7 Conclusions

A new design approach based on strength curves  $\chi(\bar{\lambda})$  controlled by slenderness-based equations has been presented in this paper for web crippling design of stainless steel hat sections subjected to IOF and EOF loading. To this end, 8 tests on ferritic stainless steel hat sections under both loading types were modelled to calibrate and validate a comprehensive FE model. Further parametric studies were conducted to extend the available database over a large range of hat section geometries and two types of stainless steels: austenitic and ferritic stainless steel. The parametric study, consist of three different types of analyses performed on every single generated model to determine: the elastic critical resistances  $R_{w,cr}$ ; the first order plastic resistances  $R_{w,pl}$ ; and the web crippling ultimate resistances  $R_{w,u}$ . Following analysis of the results and in order to provide practical design expressions for the proposed design method, predictive models were derived for the elastic critical resistance  $R_{w,cr}$  and the plastic resistance  $R_{w,pl}$ . Having incorporated these predictive models in the  $\chi - \bar{\lambda}$  space, the strength curves for the design of stainless steel hat sections were therefore derived through a combined process of regression analyses and statistical validations. Different expressions were set out for IOF and EOF loading. Comparisons of generated numerical models with design rules show that the proposed design approach fairly improves mean and reduces scatter for both IOF and EOF loading configurations enabling a more accurate and efficient design.

It should be highlighted that the calibration of the proposed design method was based on numerical models. Despite test data on stainless steel hat sections were used to validate the proposed design approach, those tests are limited to a small range of geometries. Hence, building on the limited existing test data and the satisfactory results achieved by the proposed design method, a new line of experimental investigation on the web crippling behaviour of cold-formed stainless steel cross-sections is essential to (1) enable a further validation of the derived strength curves for application to hat sections and (2) extend the methodology of strength design curves to cover the common structural section types and load cases.

### **Acknowledgements**

The research leading to these results has received funding from the European Community's Research Fund for Coal and Steel (RFCS) under Grant Agreement No. RFSR-CT-2010-00026, Structural Applications for Ferritic Stainless Steels and from Ministerio de Ciencia e Innovación to the Project BIA 2012-36373. The first author is grateful to the Secretaria d'Universitats i de Recerca del Departament d'Economia i Coneixement de la Generalitat de Catalunya for their financial contribution. The authors gratefully acknowledge all the experimental information provided by Asko Talja and Petr Hradil from VTT Technical Research Centre of Finland. They would also like to thank Professor Feng Zhou from Tongji University for the provided support in the FE model.



---

**CHAPTER 5 – Material and local buckling response of ferritic stainless steel sections**

This chapter has been submitted to the *Thin-Walled Structures* journal under the reference:

Bock M, Gardner L and Real E (2014c). Material and local buckling response of ferritic stainless steel sections. *Thin-Walled Structures* (under review).

**Abstract**

An investigation into the material response and local buckling behaviour of ferritic stainless steel structural cross-sections is presented in this paper. Particular attention is given to the strain hardening characteristics and ductility since these differ most markedly from the more common austenitic and duplex stainless steel grades. Based on collated stress-strain data on ferritic stainless steel, key aspects of the material model given in Annex C of EN 1993-1-4 (2006) were evaluated and found to require adjustment. Proposed modifications are presented herein.

The local buckling behaviour of ferritic stainless steel sections in compression and bending was examined numerically, using the finite element (FE) package ABAQUS. The studied section types were cold-formed square hollow sections (SHS), rectangular hollow sections (RHS) and channels, as well as welded I-sections. The models were first validated against experimental data collected from the literature, after which parametric studies were performed to generate data over a wide range of section geometries and slendernesses. The obtained numerical results, together with existing experimental data from the literature were used to assess the applicability of the slenderness limits and effective width formulae set out in EN 1993-1-4 (2006) to ferritic stainless steel sections.

The comparisons of the generated FE results for ferritic stainless steel with the design provisions of EN 1993-1-4 (2006), highlighted, in agreement with other stainless steel grades, the inherent conservatism associated with the use of the 0.2% proof stress as the limiting design stress. To overcome this, the continuous strength method (CSM) was developed as an alternative design approach to exploit the deformation capacity and strain hardening potential of stocky cross-sections. An extension of the method to ferritic stainless steels, including the specification of a revised strain hardening slope for the CSM material model, is proposed herein. Comparisons with test and FE data showed that the CSM predictions are more accurate and consistent than existing provisions thus leading to significant material savings and hence more efficient structural design.

### **Highlights**

- Collection of ferritic stainless steel material test data from the literature
- Development of a predictive model for the ultimate strain for ferritic stainless steels
- Nonlinear FE simulations of stub column and 4-point bending tests
- Assessment of current design guidance for ferritic stainless steel
- Extension of the CSM material model for application to ferritic stainless steel

### **Keywords**

Continuous strength method, cross-section classification, ferritic stainless steel, finite element modelling, local buckling, material properties, slenderness limits, stress-strain model.

---

## 5.1 Introduction

Stainless steels fall into five main categories, depending on their microstructure: ferritic, austenitic, martensitic, duplex and precipitation hardening. To date, the austenitic and duplex grades have been the most widely used in construction and have received the most attention from structural engineering researchers. Ferritic stainless steels differ from the austenitic and duplex grades in that they contain no nickel, hence their cost is lower and more stable. The key alloying element remains chromium which gives the material the ability to resist corrosion. In terms of mechanical properties, ferritic stainless steels have higher mechanical strengths than the austenitics in the annealed condition, and display a less rounded stress-strain response with lower ultimate-to-yield strength ratios. In general, ferritic stainless steels possess many of the advantages that the austenitics have over carbon steel but at a lower material cost, making them a more economic and sustainable alternative for a number of structural applications.

Despite the fact that the European structural design guidance for stainless steels, EN 1993-1-4 (2006), includes three ferritic grades (1.4003, 1.4016 and 1.4512) the applicability of all aspects of the code to ferritic stainless steels is yet to be fully validated. With the benefit of a far greater pool of experimental data (Bredenkamp and van den Berg (1995), Stangenberg (2000a, 2000b), Rossi (2010), Talja and Hradil (2011), Manninen and Säynäjäkangas (2012), Real et al. (2013), Arrayago et al. (2013), Afshan and Gardner (2013a) and Afshan et al. (2013)) than was available when EN 1993-1-4 (2006) was published, and through the use of carefully validated finite element models, the applicability of the code to ferritic stainless steel is examined herein. In particular, focus is given to the material model given in Annex C of EN 1993-1-4 (2006) and the slenderness limits and effective width formulations used for cross-section design. For the latter, the revised slenderness limits and effective width formulae proposed by Gardner and Theofanous (2008) are also assessed. Finally, the continuous strength method, which is a deformation-based design approach that allows for the beneficial influence of strain hardening, is extended to cover ferritic stainless steel.

## 5.2 Material response

### 5.2.1 Material modelling

The nonlinear stress-strain response of metallic materials such as stainless steel and aluminum has traditionally been represented by Hill's (1944) modified version of the Ramberg-Osgood (1943) material model. During recent years, structural applications of these materials have increased and so the need to provide practising engineers and researchers with more accurate models to replicate their material response. The current material model presented in Annex C of EN 1993-1-4 (2006) is based on Rasmussen's (2003) modification of the two-stage Ramberg-Osgood model presented by Mirambell and Real (2000) and described in Eq. (5.1), where  $E$  is the Young's modulus,  $E_{0.2}$  is the tangent modulus at the 0.2% proof stress  $\sigma_{0.2}$ ,  $\varepsilon_{0.2}$  is the total strain at the 0.2% proof stress,  $\sigma_u$  is the ultimate tensile stress with its corresponding ultimate strain  $\varepsilon_u$  and  $n$  and  $m$  are strain hardening exponents. Rasmussen (2003) also proposed predictive expressions for some components of the model, reducing the number of required input parameters from six (Mirambell and Real (2000)) to three. These predictive expressions, for  $m$ ,  $\varepsilon_u$  and  $\sigma_u$ , are given by Eqs (5.2)-(5.4), respectively.

$$\varepsilon = \begin{cases} \frac{\sigma}{E} + 0.002 \left( \frac{\sigma}{\sigma_{0.2}} \right) & \text{For } \sigma \leq \sigma_{0.2} \\ \frac{\sigma - \sigma_{0.2}}{E_{0.2}} + \varepsilon_u \left( \frac{\sigma - \sigma_{0.2}}{\sigma_u - \sigma_{0.2}} \right)^m + \varepsilon_{0.2} & \text{For } \sigma > \sigma_{0.2} \end{cases} \quad (5.1)$$

$$m = 1 + 3.5 \frac{\sigma_{0.2}}{\sigma_u} \quad (5.2)$$

$$\varepsilon_u = 1 - \frac{\sigma_{0.2}}{\sigma_u} \quad (5.3)$$

$$\frac{\sigma_{0.2}}{\sigma_u} = \begin{cases} 0.2 + 185(\sigma_{0.2}/E) & \text{For austenitic and duplex alloys} \\ \frac{0.2 + 185(\sigma_{0.2}/E)}{1 - 0.0375(n - 5)} & \text{For all alloys} \end{cases} \quad (5.4)$$

Rasmussen (2003) noted that the accuracy of the predictive model for  $\varepsilon_u$  (Eq. (5.3)) may require further assessment because "it was not clear if the ultimate strain quoted in the references were the uniform elongation at the ultimate tensile strength, as was assumed, or the total strain after fracture including local elongation in the area of necking". A reassessment of Eq. (5.3) was carried out by Afshan et al. (2013), where the accuracy of the predictive expression was confirmed for austenitic and duplex stainless steel, but the predictions were found to be less accurate for ferritic stainless steel. A proposed revision to Eq. (5.3) was made by Arrayago et al. (2013) based on test data on ferritic

stainless steel sheet material. In light of further available experimental data on a broader range of products, a revised expression is proposed herein.

Table 5.1 Summary of the available stainless steel material data

Source	Austenitic	Ferritic	Duplex	Lean duplex
Rasmussen and Hancock (1993b)	2 flat parts (SHS) 1 CHS 1 corner (SHS)	-	-	-
Talja and Salmi (1995)	2 flat parts (SHS) 4 flat parts (RHS)	-	-	-
Stangenberg (2000a)	-	6 CHS 5 welded I-sections	-	-
Olson (2001)	2 sheets	-	1 sheet	-
Burns and Bezkorovainy (2001)	-	-	3 sheet	-
Real (2001)	1 flat parts (SHS) 1 flat part (RHS)	-	-	-
Gardner and Nethercot (2004a)	28 flat parts (SHS) 26 flat parts (RHS) 3 corners (SHS) 2 corners (RHS)	-	-	-
Estrada (2005)	6 sheet	-	-	-
Rossi (2010)	-	9 sheets	-	-
Theofanous and Gardner (2009)	-	-	-	11 flat parts (SHS) 4 flat parts (RHS)
Talja and Hradil (2011)	-	2 flat parts (SHS) 1 flat part (RHS)	-	-
Manninen and Säynäjäkangas (2012)	-	60 sheets	-	-
Real et al. (2013)	-	4 sheets	-	-
Arrayago et al. (2013)	14 sheets	14 sheets	14 sheets	-
Afshan et al. (2013)	10 flat parts (SHS) 4 flat parts (RHS) 10 corners (SHS) 4 corners (RHS) 5 welds (SHS) 2 welds (RHS)	7 flat parts (SHS) 2 flat parts (RHS) 4 welds (SHS) 1 welds (RHS)	2 CHS	2 flat parts (SHS) 1 weld (SHS) 2 corners (SHS)
Afshan and Gardner (2013a)	-	8 flat parts (SHS) 8 flat parts (RHS) 2 corners (SHS) 2 corners (RHS)	-	-
Total	128	135	20	20

### 5.2.2 Collection of experimental data

The results from a total of 135 material tests on ferritic stainless steel (Stangenberg (2000a), Rossi (2010), Talja and Hradil (2011), Manninen and Säynäjäkangas (2012), Real et al. (2013), Arrayago et al. (2013), Afshan and Gardner (2013a) and Afshan et al. (2013)), where the strain at the ultimate tensile stress  $\epsilon_u$  was recorded, have been gathered. Additionally, 128 material tests conducted on austenitic stainless steel (Rasmussen and Hancock (1993b), Talja and Salmi (1995), Olson (2001), Real (2001), Gardner and Nethercot (2004a), Estrada (2005), Arrayago et al. (2013) and Afshan et al.



(2013)), 20 on duplex (Olson (2001), Burns and Bezkorovainy (2001), Arrayago et al. (2013) and Afshan et al. (2013)) and 20 on lean duplex (Theofanous and Gardner (2009) and Afshan et al. (2013)) have also been considered for comparison purposes. A summary of the sources of the test data, the number of results, the product types and the material grades is provided in Table 5.1. Note that the collected experimental data includes results on sheet material as well as material extracted from the flat and corner regions of SHS, RHS, CHS (circular hollow sections) and I-sections.

### 5.2.3 Assessment of the predictive expression for $\epsilon_u$

The collected test data are compared with the existing EN 1993-1-4 predictive model (Eq. (5.3)) in Fig. 5.1, which shows a graph of ultimate strain  $\epsilon_u$  against  $\sigma_{0.2}/\sigma_u$ . The comparison reveals good agreement between the predictive model and the austenitic, duplex and lean duplex data, all of which follow a similar trend. However, the ferritic material data points follow a less inclined path due to their lower ductility and, as a consequence, the current predictive expression given in Annex C of EN 1993-1-4 (2006) is inappropriate. Hence, a revised predictive expression for the ultimate strain  $\epsilon_u$  of ferritic stainless steels, generated by minimizing the error of  $(\epsilon_{u,\text{test}} - \epsilon_{u,\text{pred}})^2$  where  $\epsilon_{u,\text{test}}$  and  $\epsilon_{u,\text{pred}}$  are the experimentally measured and predicted ultimate strain respectively, is proposed, as given by Eq. (5.5). This proposed expression is also displayed in Fig. 5.1 and some relevant statistical results are presented in Table 5.2, where it is shown that the revised model for the ferritics provides good average predictions of the test data with a moderate coefficient of variation (COV). In Table 5.2, the experimentally measured ultimate strain  $\epsilon_{u,\text{test}}$  has been normalized by the predicted ultimate strain  $\epsilon_{u,\text{pred}}$  by either the current model of EN 1993-1-4 (Eq. (5.3)) or the proposal made herein for ferritics (Eq. (5.5)).

Note that the current predictive model given in the Eurocode (Eq. (5.3)) over-estimates the ductility (strain at ultimate stress  $\epsilon_u$ ) of ferritic stainless steel by a factor of around two, and it is therefore recommended that the revised expression (Eq. (5.5)) is adopted for the ferritics in future revisions of EN 1993-1-4 (2006).

$$\epsilon_u = 0.6 - 0.6 \frac{\sigma_{0.2}}{\sigma_u} \quad \text{For ferritic stainless steel} \quad (5.5)$$

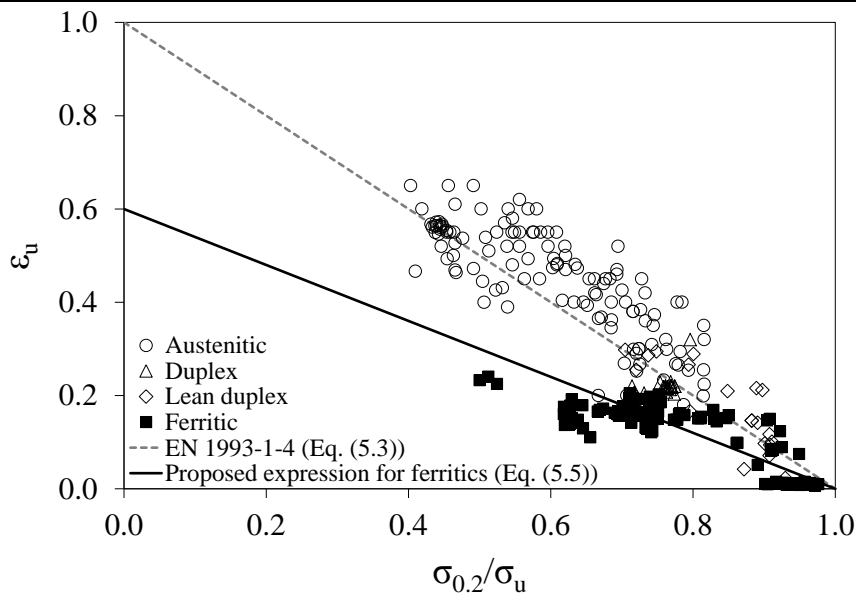


Fig. 5.1 Comparison between ultimate strain  $\varepsilon_u$  from material tests and predictive expressions given in EN 1993-1-4 and proposed herein for ferritics in Eq. (5.5)

Table 5.2 Statistical results of the ratio  $\varepsilon_{u,\text{test}}/\varepsilon_{u,\text{pred}}$  for different predictive models

	Austenitic, Duplex and Lean duplex EN 1993-1-4 model (Eq. (5.3)) $\varepsilon_{u,\text{test}}/\varepsilon_{u,\text{pred}}$	Ferritic EN 1993-1-4 model (Eq. (5.3)) $\varepsilon_{u,\text{test}}/\varepsilon_{u,\text{pred}}$	Ferritic Proposed model (Eq. (5.5)) $\varepsilon_{u,\text{test}}/\varepsilon_{u,\text{pred}}$
Mean	1.041	0.558	0.929
COV	0.277	0.496	0.496

### 5.3 Numerical modelling of ferritic stainless steel cross-section behaviour

#### 5.3.1 Introduction

In this section, the local buckling behaviour of ferritic stainless steel cross-sections is examined. In particular, the applicability of the slenderness limits and effective width formulae for slender cross-sections given in EN 1993-1-4 (2006), as well as those proposed by Gardner and Theofanous (2008), is assessed.

Numerical analyses were performed using the finite element programme ABAQUS. Stub column and 4-point bending models were firstly validated against existing experimental results (Stangenberg (2000a, 2000b), Kuwamura (2003), Gardner and Nethercot (2004a), Saliba and Gardner (2013) and Afshan and Gardner (2013a)), and were subsequently used for parametric studies to expand the numerical data over a wider range of section geometries and slendernesses. The study covers compressed internal elements and outstand flanges in SHS, RHS, channels, and I-sections.

### 5.3.2 FE model

Owing to the thin-walled nature of the modelled cross-sections, and based on previous studies concerning numerical analyses of metallic structures (Rasmussen et al. (2003), Gardner and Nethercot (2004b), Ellobody and Young (2005), Ashraf et al. (2006) and Rossi et al. (2010)), the general-purpose shell element S4R was used to discretise the models. Following the recommendations given by Schafer (1998) concerning the minimum number of elements to employ in such buckling based problems, mesh convergence studies were conducted to determine an appropriate mesh density to achieve suitably accurate results while minimizing computational time. Hence, an element size equal to one twentieth of the largest plate width that makes up the cross-section was used for the flat parts, while the curved geometry of the corner regions of the cold-formed sections was approximated by 2 or 3 elements. Sharp corners were specified in the case of the I-sections.

Regarding the stub column models, all degrees of freedom were restrained at the end of cross-sections except vertical displacement at the loaded end, where a vertical deformation was applied to represent the loading. For the beam models, which featured SHS, RHS and I-sections, the cross-sections at the supports were defined as rigid bodies with boundary conditions applied at their centre to allow appropriate movement and rotation to simulate simple support conditions. The loads were evenly applied at third points to simulate 4-point bending; the cross-sections at the load points were also defined as rigid bodies to avoid web crippling.

The nonlinear material behaviour of stainless steel was introduced into ABAQUS by defining a multi-linear stress–strain curve based on the compound two-stage Ramberg-Osgood model (Mirambell and Real (2000) and Rasmussen (2003)) included in Annex C of EN 1993-1-4 (2006), specified in terms of true stresses  $\sigma_{true}$  and logarithmic plastic strains  $\varepsilon_{pl,true}$  as given by Eq. (5.6) where  $E$  is the Young's modulus, and  $\sigma_{nom}$  and  $\varepsilon_{nom}$  are the engineering stress and strain, respectively.

$$\begin{aligned}\sigma_{true} &= \sigma_{nom}(1 + \varepsilon_{nom}) \\ \varepsilon_{pl,true} &= \ln(1 + \varepsilon_{nom}) - \frac{\sigma_{true}}{E}\end{aligned}\tag{5.6}$$

Initial geometric imperfections were incorporated into the FE models in the form of the lowest elastic eigenmode, with an amplitude  $w_0$  derived from the predictive expression of Eq. (5.7) (Dawson and Walker (1972) and Gardner and Nethercot (2004b)), where  $t$

is the plate thickness,  $\sigma_{0.2}$  is the material 0.2% proof stress and  $\sigma_{cr}$  is the elastic buckling stress of the cross-section plate elements assuming simply supported conditions. The influence of other imperfection amplitudes on the structural response of the generated models was studied by Bock et al. (2011). The geometrically and materially nonlinear analyses employed the modified Riks algorithm to trace the pre- and post-ultimate equilibrium response of the models.

$$w_0 = 0.023 \left( \frac{\sigma_{0.2}}{\sigma_{cr}} \right) t \quad (5.7)$$

Residual stresses were not explicitly incorporated into the FE models due to their inherent partial (i.e. bending residual stresses) presence in the material properties extracted from manufactured profiles in the case of cold-formed sections (Rasmussen (1993), Jandera et al. (2008), Cruise and Gardner (2008a) and Gardner and Cruise (2009)) and their limited influence on the behaviour of similar studied sections (Young and Lui (2005), Cruise and Gardner (2008a), Theofanous and Gardner (2010) and Saliba and Gardner (2013)). For simplicity, and with little influence when the results are considered on a normalised basis, corner strength enhancements (Ashraf et al. (2005), Cruise and Gardner (2008b), Rossi (2008) and Rossi et al. (2013)) were also omitted from the models.

### 5.3.3 Validation of the FE model

The ability of the FE model to replicate observed physical behaviour was assessed by comparison with existing experimental results on different stainless steel grades. The ultimate reported axial load  $N_{u,test}$  from the previous stub column tests (Stangenberg (2000a, 2000b), Kuwamura (2003), Gardner and Nethercot (2004a), Saliba and Gardner (2013) and Afshan and Gardner (2013a)) as well as the ultimate experimental bending moment  $M_{u,test}$  and rotation capacity  $R_{u,test}$  from existing 4-point bending tests (Saliba and Gardner (2013) and Afshan and Gardner (2013a)) were compared with the equivalent numerical values  $N_{u,num}$ ,  $M_{u,num}$  and  $R_{u,num}$  predicted by the FE model. The rotation capacity was defined by Eq. (5.8) where  $\kappa_u$  is the sectional curvature at the point at which the falling branch of the moment–curvature curve falls below the plastic moment resistance of the cross-section  $M_{pl}$ , and  $\kappa_{pl} = M_{pl}/EI$  is the elastic portion of the total curvature corresponding to the plastic moment  $M_{pl}$ , as illustrated in Fig. 5.2. The curvature  $\kappa$  was determined (Rasmussen and Hancock (1993b) and Afshan and Gardner (2013a)) from the central uniform moment region of the 4-point bending models

through Eq. (5.9), where  $u_{ms}$  is the deflection at mid-span,  $u_{av}$  is the average of the two vertical displacements at third points ( $u_{av}=(u_1+u_2)/2$ ), and  $L$  is the distance between those points, as shown in Fig. 5.3.

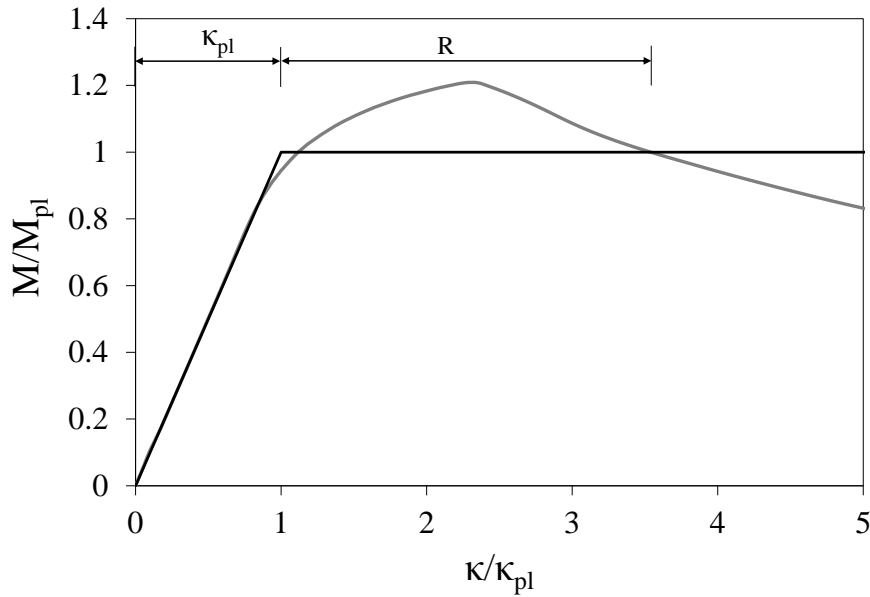


Fig. 5.2 Non-dimensionalized moment-curvature diagram and definition of rotation capacity  $R$

$$R = \frac{\kappa_u}{\kappa_{pl}} - 1 \quad (5.8)$$

$$\kappa = \frac{8(u_{ms} - u_{av})}{4(u_{ms} - u_{av})^2 + L^2} \quad (5.9)$$

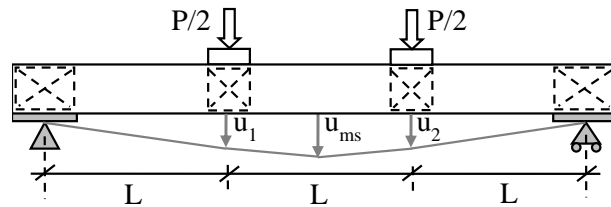


Fig. 5.3 Loading arrangement in the 4-point bending model

The comparisons between the test and FE results are presented in Tables 5.3 and 5.4 for the stub columns and beams, respectively. Overall, the FE models show excellent ability to predict ultimate load-carrying capacity, with mean test-to-numerical ratios very close to unity and with small scatter, though the rotation capacity  $R$  is less accurately, but acceptably, predicted. Typical comparison between test and FE failure modes for stub columns are shown in Fig. 5.4 where the observed test failure modes can be seen to be accurately captured by the FE models. FE failure models for the beams are shown in Fig. 5.5, which also mirror those observed in the corresponding tests (Saliba and Gardner (2013) and Afshan and Gardner (2013a)). Hence, it is concluded that the FE models are appropriate to perform parametric studies.

Table 5.3 Comparison between numerical and experimental results for the stub column models

Stainless steel	Reference	Cross-section	$N_{u,test}$ (kN)	$N_{u,num}$ (kN)	$N_{u,num}/N_{u,test}$
Ferritic	ISC140×80 <sup>a</sup>	I-section	680	695	1.022
Austenitic	I-160×160-SC <sup>b</sup>	I-section	1440	1510	1.049
Austenitic	SC-2C2 <sup>c</sup>	Channel	134	127	0.948
Austenitic	SC-2C4 <sup>c</sup>	Channel	156	166	1.064
Austenitic	SC-4C1 <sup>c</sup>	Channel	186	173	0.930
Austenitic	SC-4C3 <sup>c</sup>	Channel	234	219	0.936
Austenitic	RHS100×50×2-SC2 <sup>d</sup>	RHS	181	175	0.967
Austenitic	SHS100×100×4-SC2 <sup>d</sup>	SHS	774	761	0.983
Lean duplex	I-200×140×6×6 <sup>e</sup>	I-section	1473	1464	0.994
Lean duplex	I-200×140×8×6 <sup>e</sup>	I-section	1849	1807	0.977
Lean duplex	I-200×140×10×8 <sup>e</sup>	I-section	2540	2495	0.982
Lean duplex	I-200×140×12×8 <sup>e</sup>	I-section	2978	2859	0.960
Ferritic	80×80×3-1 <sup>f</sup>	SHS	392	381	0.972
Ferritic	60×60×3-1 <sup>f</sup>	SHS	376	372	0.989
Ferritic	120×80×3-1 <sup>f</sup>	RHS	449	468	1.042
Ferritic	60×40×3-1 <sup>f</sup>	RHS	278	268	0.964
<sup>a,b</sup> Stangenberg (2000a, 2000b)	<sup>e</sup> Saliba and Gardner (2013)			Mean	0.986
<sup>c</sup> Kuwamura (2003)	<sup>f</sup> Afshan and Gardner (2013a)			COV	0.038
<sup>d</sup> Gardner and Nethercot (2004a)					

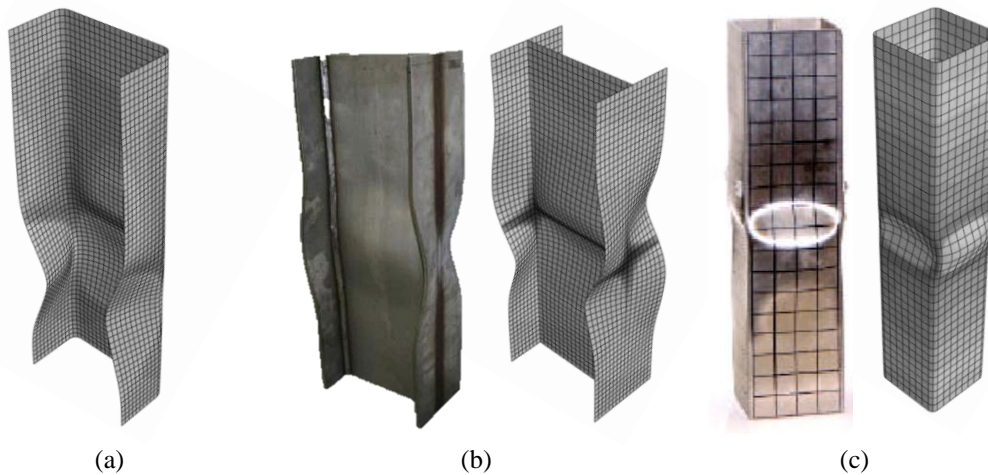


Fig. 5.4 Typical deformed shapes from FE models for (a) a channel, (b) an I-section (Saliba and Gardner (2013)) and (c) an SHS (Gardner and Nethercot (2004a)) under compression (stub column models), including comparisons, where available, with corresponding experimental failure modes

Table 5.4 Comparison between numerical and experimental results for the 4-point bending models

Stainless steel	Reference	Cross-section	$M_{u,test}$ (kNm)	$R_{test}$	$M_{u,num}$ (kNm)	$R_{num}$	$M_{u,num}/M_{u,test}$	$R_{num}/R_{test}$
Ferritic	120×80×3-4PB <sup>f</sup>	RHS	20	1.45	19.21	3.81	0.961	2.628
Ferritic	60×40×3-4PB <sup>f</sup>	RHS	5.3	>4.9	5.1	(12.3)	0.962	-
Ferritic	80×80×3-4PB <sup>f</sup>	SHS	11.3	1.86	10.95	2.13	0.969	1.145
Ferritic	60×60×3-4PB <sup>f</sup>	SHS	7.9	2.85	7.43	7.1	0.941	2.491
Lean duplex	I-200×140×6×6-2 <sup>e</sup>	I-section	132	2.22	128.25	2.06	0.972	0.928
Lean duplex	I-200×140×8×6-2 <sup>e</sup>	I-section	169	6.79	163.64	6.81	0.968	1.003
Lean duplex	I-200×140×10×8-2 <sup>e</sup>	I-section	219	14.2	213.37	16.4	0.974	1.155
Lean duplex	I-200×140×12×8-2 <sup>e</sup>	I-section	259	9.98	257.53	18.71	0.994	1.875
<sup>e</sup> Saliba and Gardner (2013)						Mean	0.968	1.604
<sup>f</sup> Afshan and Gardner (2013a)						COV	0.015	0.418

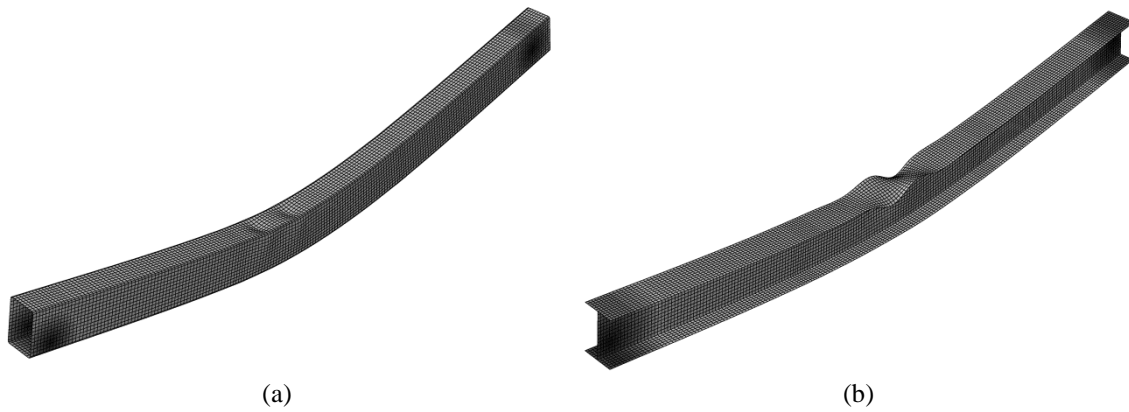


Fig. 5.5 Typical deformed shapes of (a) an RHS and (b) an I-section under bending (4-point bending models)

### 5.3.4 Parametric studies

Having validated the FE models, further numerical analyses were conducted to generate results over a wider range of geometries and local slendernesses to assess the applicability of the slenderness limits and effective width formulae for the treatment of local buckling of compressed internal elements and outstand flanges given in EN 1993-1-4 (2006), as well as those proposed by Gardner and Theofanous (2008), to ferritic stainless steel. The parametric study included 320 stub column models and 108 4-point bending models. For the stub column models, the overall length of all the specimens was set equal to three times the largest cross-section dimension whereas for the 4-point bending models, the span remained constant at 1000 mm. The cross-section geometries were chosen, as detailed below, to cover all four cross-section classes.

A total of 21 different SHS and 12 RHS were modelled. The height of the SHS ranged from 40 to 140 mm, whereas for the RHS, cross-section aspect ratios from 1.3 to 2 were considered by varying the width from 60 to 80 mm and the height between 80 and 120 mm. For both types of cross-sections (SHS and RHS), the thickness was varied between 1.5 and 3 mm, giving internal element width-to-thickness ratios  $c/t\varepsilon$  from 8.8 to 77.9 where  $\varepsilon = [(235/\sigma_{0.2})(E/210000)]^{0.5}$ . The range of channel section geometries was generated by varying the height from 37 to 155 mm, the flange width from 28.5 to 80 mm and the thickness from 1 to 5 mm. For the I-sections, the web height ranged from 40 to 100 mm, the flange width was varied from 70 and 100 mm, and the considered thicknesses ranged from 3 to 4 mm and from 0.95 to 6 mm for the web and the flange, respectively. A total of 46 outstand flange width-to-thickness ratios  $c/t\varepsilon$  were covered with values ranging from 7.8 to 45.7.

The material properties adopted in the FE models to simulate the behaviour of ferritic stainless steel sections were based on the average material properties given in EN 1993-1-4 (2006) with the following values: Young's modulus  $E=200\text{GPa}$ , 0.2% proof stress  $\sigma_{0.2}=250\text{MPa}$ , strain hardening parameters  $n=10$  and  $m=3$  and finally, in order to study the influence of material strain hardening, four different ultimate stresses  $\sigma_u$  were considered ( $\sigma_u=275, 300, 350$  and  $450\text{MPa}$ ) which provided  $\sigma_u/\sigma_{0.2}$  ratios ranging from 1.1, which is the lower limit of the ductility requirement in EN 1993-1-1 (2006), up to 1.8. Discussion of the numerical results is presented in the following section.

## 5.4 Analysis of cross-section resistance results

### 5.4.1 General

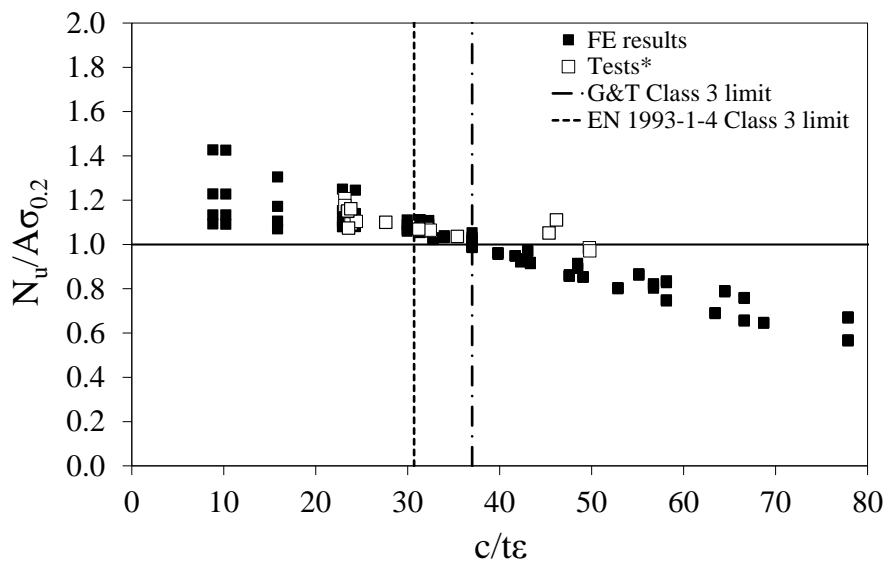
In the following sub-sections, the obtained numerical results, combined with existing experimental data on ferritic stainless steels (Bredenkamp and van den Berg (1995), Stangenberg (2000) and Afshan and Gardner (2013a)), are analysed and used to assess the applicability of the slenderness limits and effective width formula (i.e. local buckling reduction factor  $\rho$ ) provided in EN 1993-1-4 (2006) to ferritic stainless steel internal elements and outstand flanges. In addition, the revised slenderness limits and effective width formula proposed by Gardner and Theofanous (2008) are also considered (labelled as G&T in Figs (5.6)-(5.14)). The reported weighted average material properties were used in the analysis of the existing experimental results.

### 5.4.2 Class 3 slenderness limit and effective width formulation

The obtained numerical results from the stub column models and existing tests (Bredenkamp and van den Berg (1995), Stangenberg (2000) and Afshan and Gardner (2013a)) are used in this sub-section to assess the Class 3 limits and effective width formulae given in EN 1993-1-4 (2006) and Gardner and Theofanous (2008) for application to ferritic stainless steel elements. Figs 5.6 and 5.7 show the relevant response characteristic  $N_u/A\sigma_{0.2}$  for internal and outstand elements respectively, where  $N_u$  is the ultimate load achieved in the FE models or tests,  $A$  is the gross cross-sectional area and  $\sigma_{0.2}$  is the 0.2% proof strength, plotted against the slenderness of the most slender constituent element of the cross-section, expressed by the parameter  $c/t\varepsilon$  where  $c$  is the compressed flat element width,  $t$  is the element thickness and  $\varepsilon$  is the material factor  $\varepsilon=[(235/\sigma_{0.2})(E/210000)]^{0.5}$  given in EN 1993-1-4 (2006). The corresponding Class 3 limits given in EN 1993-1-4 (2006) and Gardner and Theofanous (2008) are

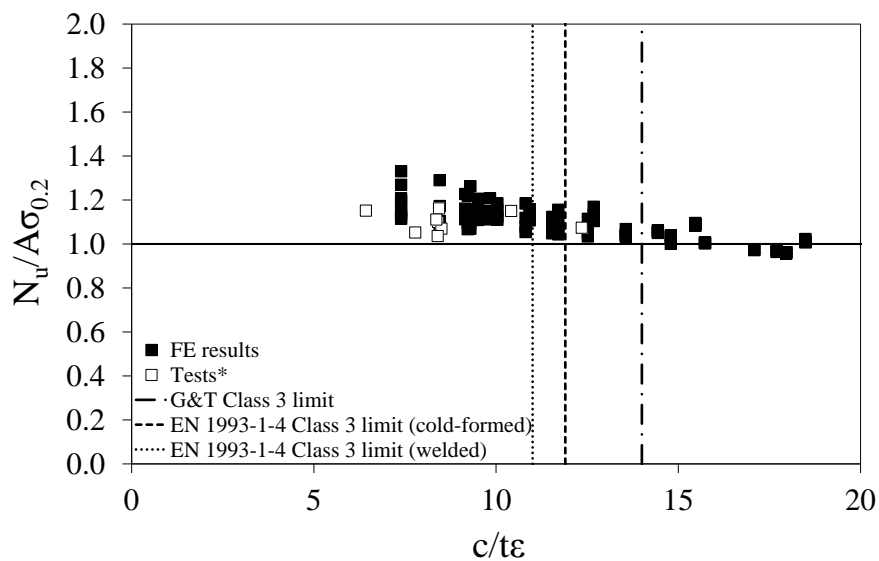


also shown. Note that a cross-section is deemed to be Class 3 (or better) if  $N_u$  exceeds  $A\sigma_{0.2}$ . Results from the 4-point bending models could also have been used for the assessment of the Class 3 limits where the relevant response characteristic is the ultimate bending moment  $M_u$  normalised by the elastic moment capacity  $M_{el}$ , defined as the product of the elastic section modulus  $W_{el}$  and the 0.2% proof strength  $\sigma_{0.2}$ . A value of  $M_u/W_{el}\sigma_{0.2}$  greater than unity would indicate a Class 3 (or lower) section. However, as shown in Fig. 8, assessment based on compression data leads to a stricter Class 3 limit, and this is therefore used in the present study; as it was also used in previous investigations (Gardner et al. (2010)).



Tests\*: Bredenkamp and van den Berg (1995), Stangenberg (2000) and Afshan and Gardner (2013a)

Fig. 5.6 Assessment of Class 3 slenderness limits for internal elements



Tests\*: Bredenkamp and van den Berg (1995), Stangenberg (2000)

Fig. 5.7 Assessment of Class 3 slenderness limits for outstand elements

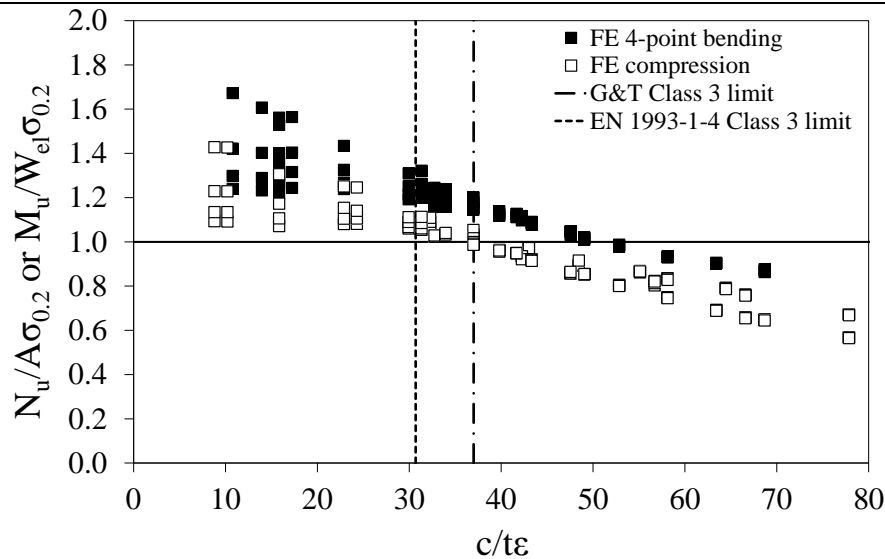


Fig. 5.8 Comparison between compression and bending data for the assessment of Class 3 slenderness limits

From Figs 5.6 and 5.7, it may be concluded that the current Class 3 limits for stainless steel given in EN 1993-1-4 (2006) ( $c/t\epsilon=30.7$  for internal elements and  $c/t\epsilon=11.0$  and  $11.9$  for welded and cold-formed outstand flanges, respectively) are slightly conservative, while the limits of  $c/t\epsilon=37$  and  $c/t\epsilon=14$  proposed by Gardner and Theofanous (2008) for internal elements and outstand flanges respectively, more closely match the numerical and test results. Note also that no distinction is made between welded and cold-formed elements in Gardner and Theofanous (2008), which is consistent with EN 1993-1-1 (2006). It is therefore concluded that the proposed limits given by Gardner and Theofanous (2008), which have been previously verified for application to austenitic and duplex stainless steel, may also be applied to ferritic grades.

The effective width formulae given in EN 1993-1-4 (2006) and Gardner and Theofanous (2008) to allow for local buckling prior to the attainment of the 0.2% proof stress are also evaluated on the basis of the generated compression data and existing test results. The results are illustrated in Figs 5.9 and 5.10 for internal elements and outstand flanges, respectively, together with the local buckling reduction factor  $\rho$  from EN 1993-1-4 (2006) and Gardner and Theofanous (2008). The relationships between  $\rho$  and non-dimensional plate slenderness  $\bar{\lambda}_p$  which is defined in EN 1993-1-5 (2006), are given by Eqs (5.10)-(5.12) for EN 1993-1-4 (2006) and Eqs (5.13) and (5.14) for Gardner and Theofanous (2008).

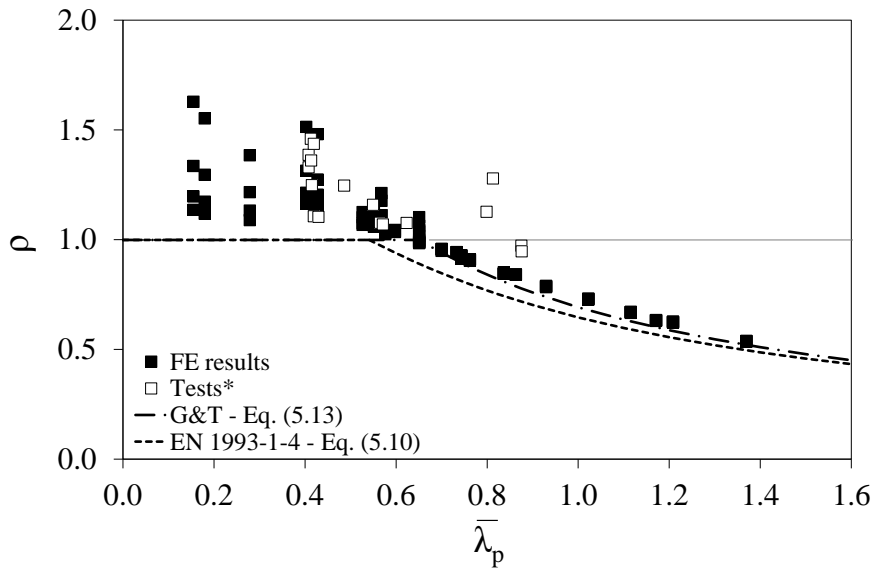
$$\rho = \frac{0.772}{\bar{\lambda}_p} - \frac{0.125}{\bar{\lambda}_p^2} \leq 1 \text{ For internal elements with } \bar{\lambda}_p \geq 0.541 \quad (5.10)$$

$$\rho = \frac{1}{\bar{\lambda}_p} - \frac{0.231}{\bar{\lambda}_p^2} \leq 1 \text{ For cold-formed outstand flanges with } \bar{\lambda}_p \geq 0.637 \quad (5.11)$$

$$\rho = \frac{1}{\bar{\lambda}_p} - \frac{0.242}{\bar{\lambda}_p^2} \leq 1 \text{ For welded outstand flanges with } \bar{\lambda}_p \geq 0.589 \quad (5.12)$$

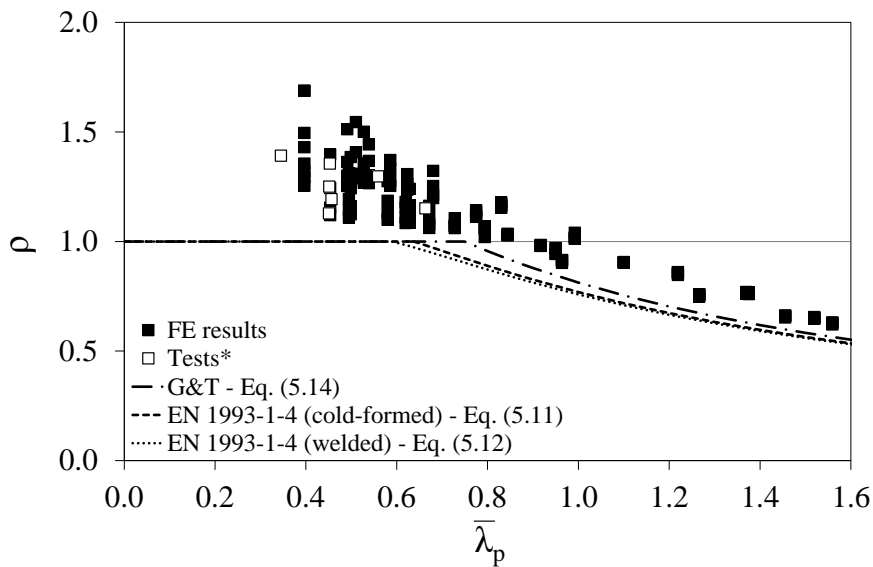
$$\rho = \frac{0.772}{\bar{\lambda}_p} - \frac{0.079}{\bar{\lambda}_p^2} \leq 1 \text{ For internal elements with } \bar{\lambda}_p \geq 0.651 \quad (5.13)$$

$$\rho = \frac{1}{\bar{\lambda}_p} - \frac{0.188}{\bar{\lambda}_p^2} \leq 1 \text{ For outstand flanges with } \bar{\lambda}_p \geq 0.748 \quad (5.14)$$



Tests\*: Bredenkamp and van den Berg (1995), Stangenberg (2000) and Afshan and Gardner (2013a)

Fig. 5.9 Assessment of effective width formulations for internal elements



Tests\*: Bredenkamp and van den Berg (1995)

Fig. 5.10 Assessment of effective width formulations for outstand flanges

From Figs 5.9 and 5.10, it can be concluded that both sets of effective width formulations (EN 1993-1-4 (2006) and Gardner and Theofanous (2008)) are adequate for ferritic stainless steels, though those proposed in Gardner and Theofanous (2008) (Eqs (5.13) and (5.14)) enable more efficient structural design.

### 5.4.3 Class 2 and Class 1 slenderness limits

The obtained numerical ultimate capacities from the 4-point bending models, together with previous (Afshan and Gardner (2013a)) bending test results, have been used to assess the applicability of the Class 2 slenderness limits specified in EN 1993-1-4 (2006) and those proposed by Gardner and Theofanous (2008) to ferritic stainless steel. The ultimate bending moment  $M_u$  achieved in the FE models and tests has been normalized by the plastic moment capacity  $M_{pl}$ , defined as the plastic section modulus  $W_{pl}$  multiplied by the material 0.2% proof stress  $\sigma_{0.2}$  and plotted against the slenderness parameter  $c/t\epsilon$  of the compression flange of the beams in Figs 5.11 and 5.12 for internal elements and outstand flanges, respectively. From Fig. 5.11, the EN 1993-1-4 (2006) Class 2 limit for internal elements ( $c/t\epsilon=26.7$ ) is observed to be safe, but the proposed slenderness limit by Gardner and Theofanous (2008) ( $c/t\epsilon=35$ ) may be more appropriate. For outstand flanges (Fig. 5.12), the EN 1993-1-4 (2006) Class 2 limits of  $c/t\epsilon=9.4$  (welded) and 10.4 (cold-formed) and the single proposed limit (Gardner and Theofanous (2008)) of  $c/t\epsilon=10$  are very similar, and both provide a good representation of the ferritic stainless steel data.

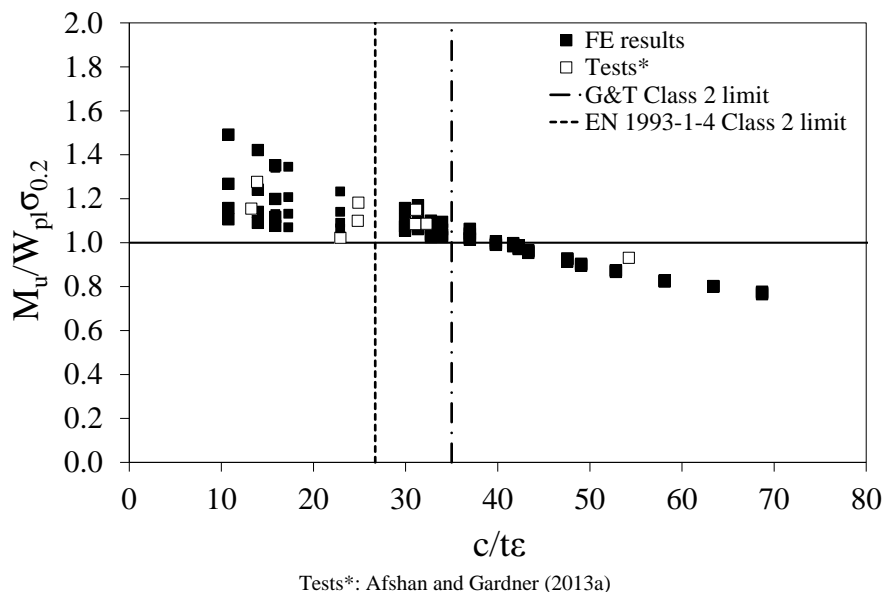


Fig. 5.11 Assessment of Class 2 slenderness limits for internal elements

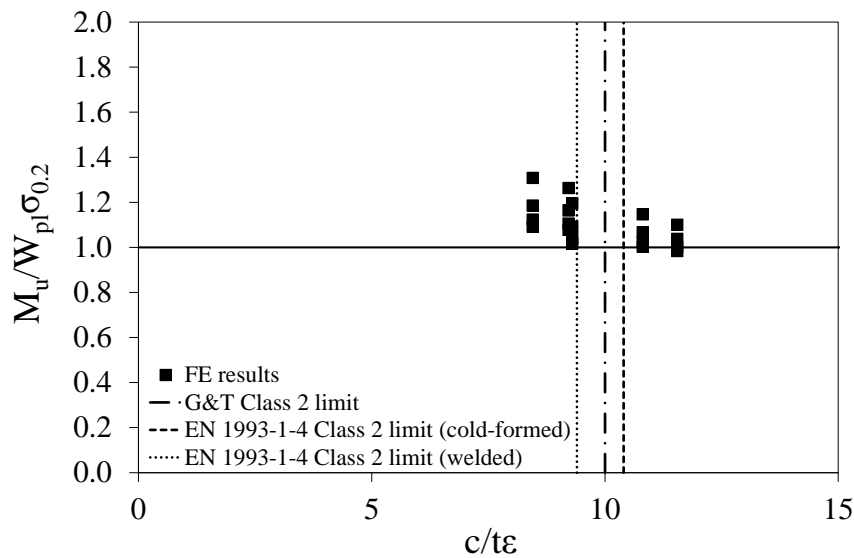


Fig. 5.12 Assessment of Class 2 slenderness limits for outstand flanges

For the appraisal of the Class 1 slenderness limits, the rotation capacity  $R$ , defined by Eq. (8), obtained from the FE models and tests is plotted against the  $c/\epsilon$  ratio of the compression flange of the beams, as shown in Figs 5.13 and 5.14 for internal elements and outstand flanges, respectively. The rotation capacity requirement for plastic design of carbon steel structures of  $R=3$  (Sedlacek and Feldman (1995)) is also shown in the figures, and assumed to apply to stainless steel structures, though it should be noted that EN 1993-1-4 (2006) does not currently permit plastic design. One of the key controlling parameters of the rotation capacity response is the ultimate-to-yield stress ratio  $\sigma_u/\sigma_{0.2}$  of the material (Sedlacek and Feldman (1995)); this point is emphasized in Fig. 5.13, where the trends of the FE results for varying  $\sigma_u/\sigma_{0.2}$  ratios are shown. From the figure, it can be observed that the proposed Class 1 limit by Gardner and Theofanous (2008) ( $c/\epsilon=33$ ) is appropriate for ferritic stainless steel exhibiting higher  $\sigma_u/\sigma_{0.2}$  ratios but optimistic when  $\sigma_u/\sigma_{0.2} \leq 1.2$ . In the latter case, the EN 1993-1-4 (2006) limit of  $c/\epsilon=25.7$  may be more appropriate. For outstand flanges (Fig. 5.14), both the EN 1993-1-4 (2006) Class 1 limits of  $c/\epsilon=9$  (welded) and 10 (cold-formed) and the proposed limit by Gardner and Theofanous (2008) of  $c/\epsilon=9$  are suitable for ferritic stainless steel.

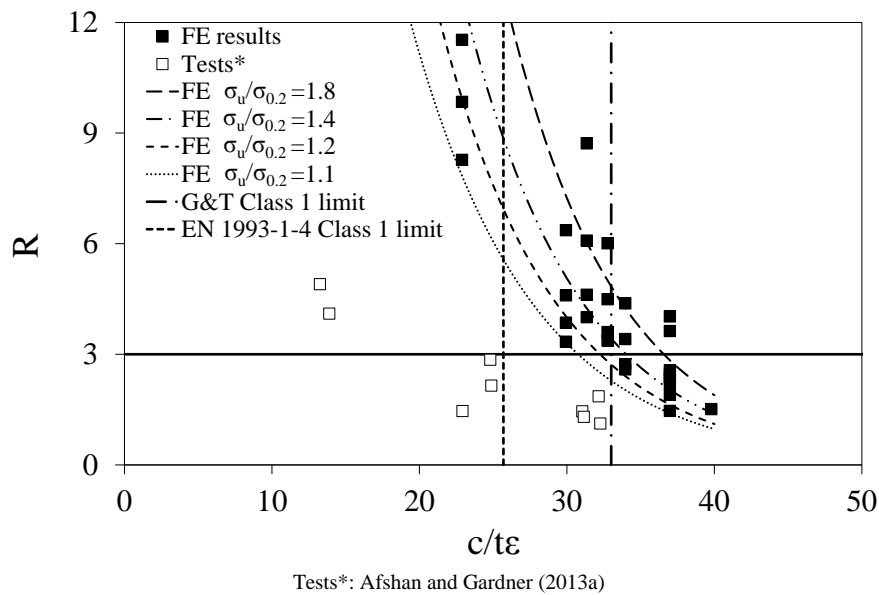


Fig. 5.13 Assessment of Class 1 slenderness limits for internal elements

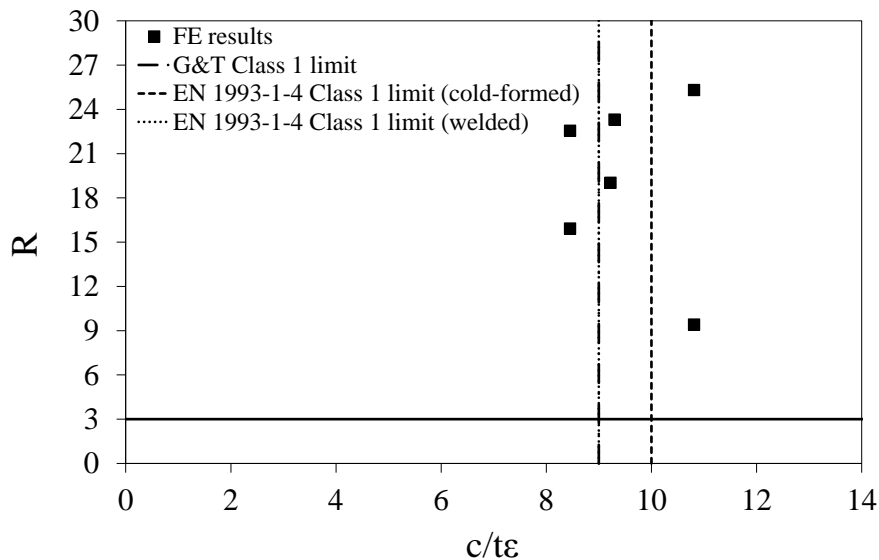


Fig. 5.14 Assessment of Class 1 slenderness limits for outstand flanges

## 5.5 The Continuous Strength Method

### 5.5.1 General

The current European design rules for stainless steel given in EN 1993-1-4 (2006) assume elastic, perfectly plastic material behavior with the maximum attainable stress limited to the 0.2% proof stress; this idealized material model clearly deviates substantially from the actual material response of stainless steel. As a consequence, the concept of cross-section classification which is underpinned by the elastic, perfectly plastic material behaviour is not ideally suited for application to nonlinear materials and

can lead to significant underestimates of ultimate capacity, particularly for stocky cross-sections, which are able to attain stresses far beyond the 0.2% proof stress  $\sigma_{0.2}$ .

The continuous strength method (CSM) has been developed as an alternative design approach (Gardner (2008), Gardner et al. (2011), Su et al. (2013) and Afshan and Gardner (2013b)) that enables material strain hardening properties to be exploited. The key features of the CSM are (1) the base curve, which defines the limiting CSM strain  $\varepsilon_{csm}$  that a cross-section can endure and (2) the strain hardening material model. These two components have been developed for austenitic and duplex stainless steels Afshan and Gardner (2013b), for which the method is included in the AISC Design Guide 30 (2012), but not yet verified for ferritic stainless steel.

$$\frac{\varepsilon_{csm}}{\varepsilon_y} = \frac{0.25}{\bar{\lambda}_p^{3.6}} \quad \text{but} \quad \frac{\varepsilon_{csm}}{\varepsilon_y} \leq \min\left(15, \frac{0.1\varepsilon_u}{\varepsilon_y}\right) \quad \text{For austenitic and duplex grades} \quad (5.15)$$

$$\bar{\lambda}_p = \sqrt{\frac{\sigma_{0.2}}{\sigma_{cr}}} \quad (5.16)$$

### 5.5.2 CSM base curve

The CSM base curve, given by Eq. (5.15), provides a continuous relationship between the normalized cross-section deformation capacity  $\varepsilon_{csm}/\varepsilon_y$ , where  $\varepsilon_y = \sigma_{0.2}/E$  is the material yield strain, and the cross-section slenderness,  $\bar{\lambda}_p$ , given by Eq. (5.16) where  $\sigma_{cr}$  is the elastic buckling stress of either the full cross-section or its most slender constituent plate element. The elastic buckling stress may be determined by numerical methods (Schafer and Ádány (2006)) or approximate analytical methods (Seif and Schafer (2010)) for the full cross-section or by the classical analytical expression for individual plates (EN 1993-1-4 (2006) and EN 1993-1-5 (2006)). The two former procedures, which are used in the direct strength method (DSM, Schafer (2008)), allow for interaction between the elements within the cross-section whereas the latter assumes simple support conditions at the plate edges resulting in a lower-bound (conservative) prediction of  $\sigma_{cr}$ . Clearly more favourable results will be achieved by considering element interaction, and this is therefore recommended but not mandatory within the CSM.

The base curve (Eq. (5.15)) is illustrated in Fig. 5.15 and applies when  $\bar{\lambda}_p \leq 0.68$ , which is the boundary between slender and non-slender sections (Afshan and Gardner (2013b)). The CSM normalised deformation capacity  $\varepsilon_{\text{CSM}}/\varepsilon_y$  is limited to the minimum of either 15, which is related to the material ductility requirement according to EN 1993-1-1 (2006) and prevents excessive strains, or  $0.1\varepsilon_u/\varepsilon_y$ , where  $\varepsilon_u$  is the strain at the ultimate stress of the material. This latter boundary relates to the adopted bilinear material model and was set to avoid over-predictions of CSM material strength for austenitic and duplex stainless steel (Afshan and Gardner (2013b)). A revised value may be required for ferritic stainless steels, as discussed later. The collected experimental data shown in Fig. 5.15 represents maximum strains achieved in stub column and bending tests on a variety of materials. The comparisons show that the base curve provides good predictions of cross-section deformation capacities for all the considered materials, including ferritic stainless steel.

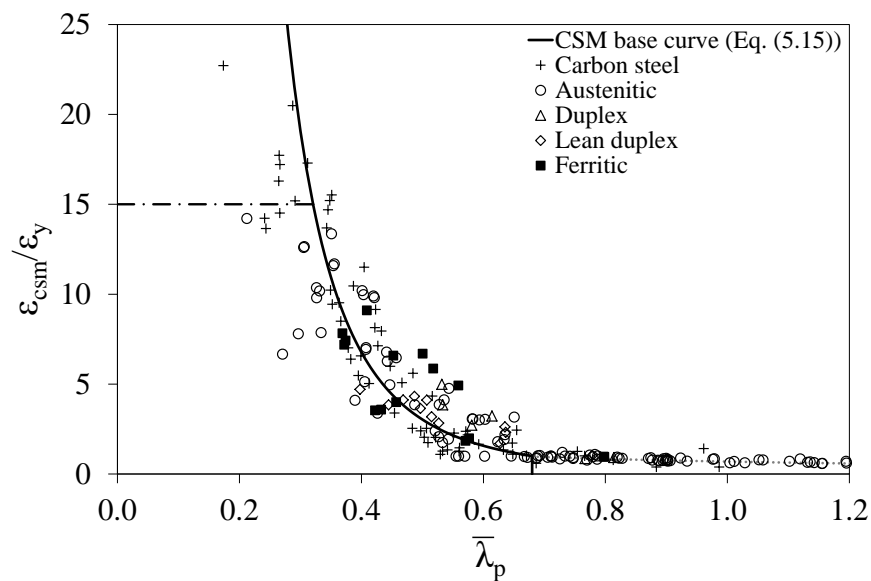


Fig. 5.15 Current design base curve for the CSM

### 5.5.3 CSM material model

The CSM elastic, linear hardening stress-strain model has been previously verified for austenitic and duplex stainless steels (Afshan and Gardner (2013b)). Below  $\sigma_{0.2}$ , elastic behaviour is assumed, though note that the influence of material nonlinearity has been accounted for by deducting 0.2% strain from test cross-section deformation capacity for the development of the base curve. Above  $\sigma_{0.2}$ , the linear hardening behaviour defined



by Eq. (5.17) applies, where  $E_{sh}$  is the material strain hardening slope given, for austenitic and duplex stainless steels, by Eq. (5.18).

$$\sigma_{csm} = \sigma_{0.2} + E_{sh} \varepsilon_y \left( \frac{\varepsilon_{csm}}{\varepsilon_y} - 1 \right) \quad (5.17)$$

$$E_{sh} = \frac{\sigma_u - \sigma_{0.2}}{0.16\varepsilon_u - \varepsilon_y} \quad \text{For austenitic and duplex stainless steel} \quad (5.18)$$

The determination of the material strain hardening slope within the CSM utilises two definition points: the yield stress point ( $\varepsilon_y, \sigma_{0.2}$ ) and a maximum stress point ( $\varepsilon_{max}, \sigma_{max}$ ), as shown in Fig. 5.16. The maximum stress is taken as the ultimate tensile stress  $\sigma_u$ , while the maximum strain is taken, for austenitic and duplex stainless steel as 16% of the ultimate tensile strain  $\varepsilon_u$ . Note that  $\varepsilon_{max}$  is not simply taken as  $\varepsilon_u$  since, for the adopted linear hardening material model, this would result in a significant under-estimation of the strain hardening slope for the strain levels of interest in the design of structural elements such as beams and columns. However, due to the lower ductility and the different characteristic shape of the stress-strain curve (see Fig. 5.1), the previously determined value for  $\varepsilon_{max}$  ( $=0.16\varepsilon_u$ ) was found to be unsuitable for ferritic stainless steels. Thus, a revised value for  $\varepsilon_{max}$  upon which to base the determination of the strain hardening slope  $E_{sh}$  for the ferritic grades was sought. This was achieved through a process of least squares regression based on the available material test data, which was summarised in Table 5.1. Note that the linear hardening slope was initially fitted through the points ( $\varepsilon_y+0.002, \sigma_{0.2}$ ) and ( $\varepsilon_{max}+0.002, \sigma_u$ ) and then translated by 0.002 to give the final CSM material model, as shown in Fig. 5.16. Recall that a revised predictive model for the ultimate strain for ferritic stainless steel (Eq. (5.5)) was developed in Section 5.2.3; this is also utilised here. The resulting expression for  $E_{sh}$  is given by Eq. (5.19) on the basis of  $\varepsilon_{max}=0.45\varepsilon_u$ , with a cut-off of  $0.4\varepsilon_u$ , applied to avoid over-prediction of the material strength, and included in the base curve – Eq. (5.20).

$$E_{sh} = \frac{\sigma_u - \sigma_{0.2}}{0.45\varepsilon_u - \varepsilon_y} \quad \text{if} \quad \frac{\varepsilon_y}{\varepsilon_u} < 0.45, \text{ else } E_{sh} = 0 \quad \text{For ferritic stainless steels} \quad (5.19)$$

$$\frac{\varepsilon_{csm}}{\varepsilon_y} = \frac{0.25}{\bar{\lambda}_p^{3.6}} \quad \text{but} \quad \frac{\varepsilon_{csm}}{\varepsilon_y} \leq \min \left( 15, \frac{0.4\varepsilon_u}{\varepsilon_y} \right) \quad \text{For ferritic stainless steels} \quad (5.20)$$

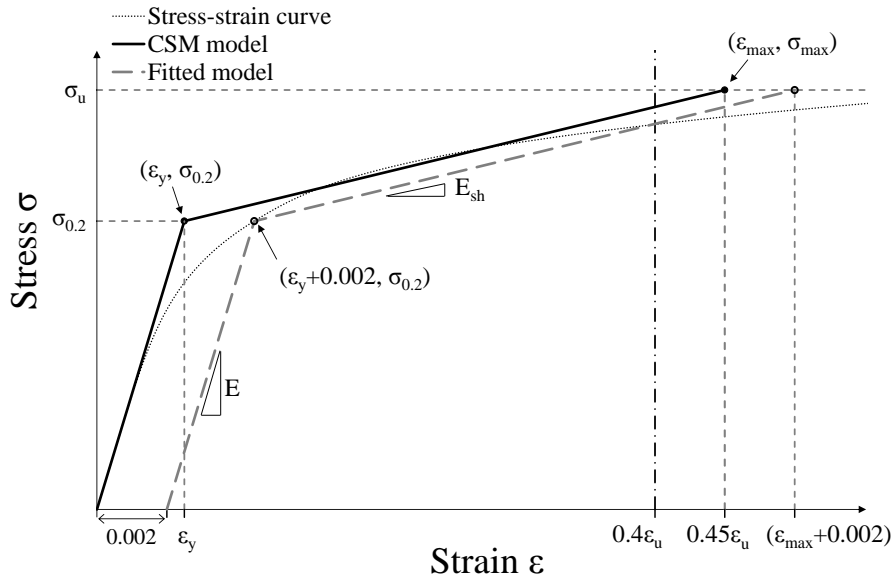


Fig. 5.16 CSM elastic, linearly hardening material model for ferritic stainless steel

#### 5.5.4 CSM resistance functions

The CSM characteristic resistance functions for I-shaped and SHS/RHS cross-sections under pure compression  $N_{csm,Rk}$  and pure bending ( $M_{y,csm,Rk}$  for major axis bending and  $M_{z,csm,Rk}$  for minor axis bending) are given by Eqs (5.21)-(5.23), respectively (Gardner et al. (2011) and Afshan and Gardner (2013b)). In Eq. (5.23)  $\alpha$  is a dimensionless coefficient taken as 2 for SHS/RHS and 1.2 for I-sections.

$$N_{csm,Rk} = \sigma_{csm} A \quad (5.21)$$

$$M_{y,csm,Rk} = W_{pl,y} \sigma_{0.2} \left[ 1 + \frac{E_{sh}}{E} \frac{W_{el,y}}{W_{pl,y}} \left( \frac{\varepsilon_{csm}}{\varepsilon_y} - 1 \right) - \left( 1 - \frac{W_{el,y}}{W_{pl,y}} \right) / \left( \frac{\varepsilon_{csm}}{\varepsilon_y} \right)^2 \right] \quad (5.22)$$

$$M_{z,csm,Rk} = W_{pl,z} \sigma_{0.2} \left[ 1 + \frac{E_{sh}}{E} \frac{W_{el,z}}{W_{pl,z}} \left( \frac{\varepsilon_{csm}}{\varepsilon_y} - 1 \right) - \left( 1 - \frac{W_{el,z}}{W_{pl,z}} \right) / \left( \frac{\varepsilon_{csm}}{\varepsilon_y} \right)^\alpha \right] \quad (5.23)$$

In the following sub-section, the predictions from the CSM resistance functions, together with the revised strain hardening slope  $E_{sh}$ , are compared with test and FE data on ferritic stainless steel cross-sections.

#### 5.5.5 Comparison with design rules

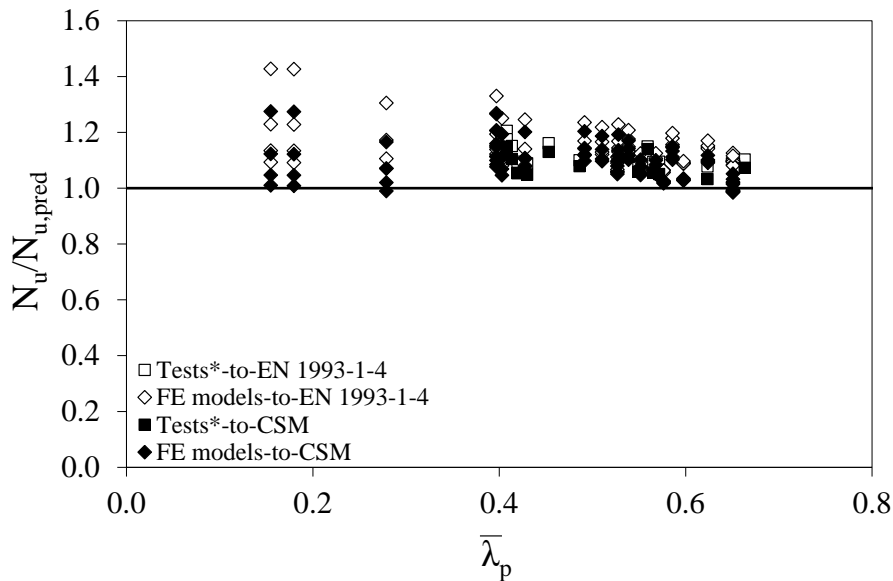
The predictions of the CSM with the revised strain hardening slope  $E_{sh}$  for application to ferritic stainless steel are compared with both existing test results (Bredenkamp and van den Berg (1995), Stangenberg (2000) and Afshan and Gardner (2013a)) and the numerical results generated in the present study. Capacity predictions according to EN 1993-1-4 (2006) are also determined. All comparisons utilise the measured geometric

and material properties with all partial safety factors set to unity, while  $N_{u,pred}$  and  $M_{u,pred}$  represent the predicted axial and bending resistances from the two design methods. The comparisons are presented in Figs. 5.17 and 5.18 for compression and bending, respectively, where the CSM may be seen to provide an improved mean prediction and a reduced scatter compared to EN 1993-1-4 (2006). Key statistical values concerning mean predictions and coefficient of variation (COV) of the CSM and EN 1993-1-4 (2006) relative to the tests (Bredenkamp and van den Berg (1995), Stangenberg (2000) and Afshan and Gardner (2013a)) and numerical results are given in Tables 5.5 and 5.6 for compression and bending, respectively. The reliability of the CSM for ferritic stainless steel is assessed in the following sub-section.

Table 5.5 Key statistical values of the comparison for stub columns

	Tests*		FE models	
	EN 1993-1-4	CSM	EN 1993-1-4	CSM
	$N_{u,test}/N_{u,pred}$	$N_{u,test}/N_{u,pred}$	$N_{u,FE}/N_{u,pred}$	$N_{u,FE}/N_{u,pred}$
Mean	1.125	1.079	1.141	1.090
COV	0.045	0.037	0.064	0.059

\* Bredenkamp and van den Berg (1995), Stangenberg (2000) and Afshan and Gardner (2013a)



\* Bredenkamp and van den Berg (1995), Stangenberg (2000) and Afshan and Gardner (2013a)

Fig. 5.17 Comparison of predicted resistances by CSM and EN 1993-1-4 for stub columns

Table 5.6 Key statistical values of the comparison for beams

	Tests*		FE models	
	EN 1993-1-4	CSM	EN 1993-1-4	CSM
	$M_{u,test}/M_{u,pred}$	$M_{u,test}/M_{u,pred}$	$M_{u,FE}/M_{u,pred}$	$M_{u,FE}/M_{u,pred}$
Mean	1.372	1.141	1.296	1.112
COV	0.074	0.040	0.092	0.062

\* Afshan and Gardner (2013a)

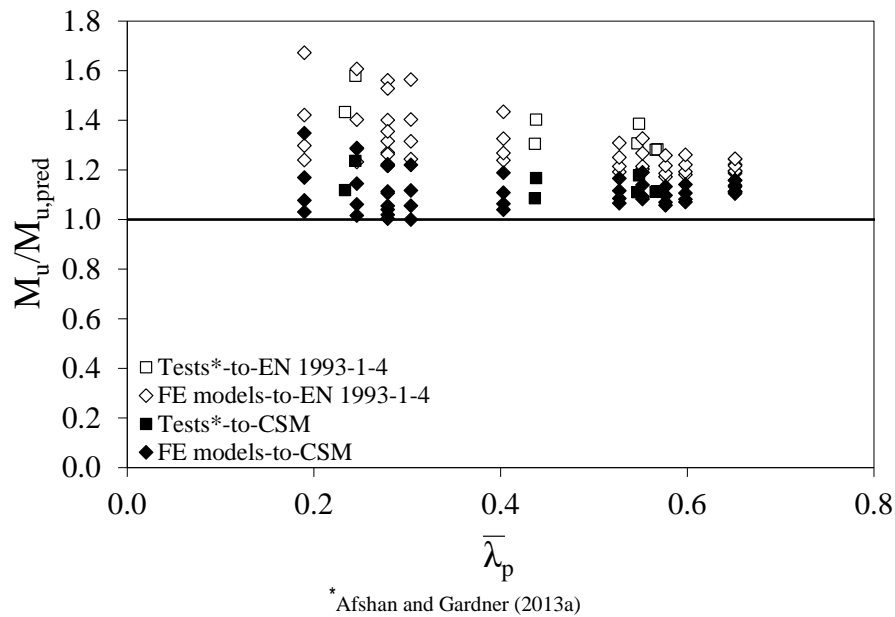


Fig. 5.18 Comparison of predicted resistances by CSM and EN 1993-1-4 for beams

### 5.5.6 Reliability analysis

A statistical analysis was conducted according to EN 1990 Annex D (2002) to assess the reliability of the CSM proposals for ferritic stainless steels. Tables 5.7 and 5.8 summarise the key statistical parameters for the CSM comparisons with experimental and FE results, respectively, including the number of tests and FE simulations  $n$ , the design (ultimate limit state) fractile factor  $k_{d,n}$ , the average ratio of test (or FE)-to-model resistance based on a least squares fit to all the data  $b$ , the coefficient of variation of the tests and FE simulations relative to the resistance model  $V_{\delta}$ , the combined coefficient of variation incorporating both model and basic variable uncertainties  $V_r$ , and the partial safety factor  $\gamma_{M0}$ . The material overstrength was taken as 1.2 for the ferritic material with a COV of material strength 0.05, in accordance with Baddoo and Francis (2013). Variation in geometric properties also followed the recommendation by Baddoo and Francis (2013). The analysis showed that the required partial factors are all less than the currently adopted value of  $\gamma_{M0}=1.1$  used in EN 1993-1-4 (2006). This partial factor may therefore be safely applied.

Table 5.7 Summary of CSM reliability analysis based on ferritic stainless steel experimental results

Specimens	No. of tests	$k_{d,n}$	$b$	$V_{\delta}$	$V_r$	$\gamma_{M0}$
Stub columns	13	4.078	1.079	0.036	0.080	1.00
Beams	8	5.076	1.137	0.043	0.083	0.99

Table 5.8 Summary of CSM reliability analysis based on ferritic stainless steel FE simulations

Specimens	No. of FE simulations	$k_{d,n}$	$b$	$V_{\delta}$	$V_r$	$\gamma_{M0}$
Stub columns	112	3.179	1.093	0.058	0.091	1.02
Beams	68	3.240	1.127	0.061	0.093	0.99

## 5.6 Conclusions

An investigation into the material response and structural performance of ferritic stainless steel structural elements has been conducted. Collected material data on ferritic stainless steel (Stangenberg (2000a), Rossi (2010), Talja and Hradil (2011), Manninen and Säynäjäkangas (2012), Real et al. (2013), Arrayago et al. (2013), Afshan and Gardner (2013a) and Afshan et al. (2013)) has been analysed and used to assess the predictive expression given in Annex C of EN 1993-1-4 (2006) for ultimate strain  $\epsilon_u$ . The results show that the current predictive model is inappropriate for ferritics and yields unconservative results. A revised expression suitable for ferritic stainless steels has been proposed.

The structural response of cold-formed ferritic stainless steel cross-sections has also been examined and the applicability of the current slenderness limits and effective width formulae of EN 1993-1-4 (2006) and those proposed by Gardner and Theofanous (2008) to ferritic stainless steel has been assessed. To this end, a finite element model was developed in ABAQUS, validated against existing test results from the literature (Stangenberg (2000a, 2000b), Kuwamura (2003), Gardner and Nethercot (2004a), Saliba and Gardner (2013) and Afshan and Gardner (2013a)) and subsequently used to perform parametric studies. The assessments were made on the basis of both existing experimental data on ferritic stainless steels (Bredenkamp and van den Berg (1995), Stangenberg (2000) and Afshan and Gardner (2013a)) and the FE results generated herein. It was shown that the Class 2 and Class 3 slenderness limits and the effective width formulae of EN 1993-1-4 (2006) are adequate for application to ferritic stainless steel internal elements and outstand flanges, though those proposed by Gardner and Theofanous (2008) more closely represent the numerical and test results enabling more efficient design. For the Class 1 slenderness limit, it was observed that the proposed value by Gardner and Theofanous (2008) is satisfactory for ferritic stainless steel sections when  $\sigma_u/\sigma_{0.2} > 1.2$ , but the stricter EN 1993-1-4 (2006) Class 1 slenderness limit may be more appropriate when  $\sigma_u/\sigma_{0.2} \leq 1.2$ . Table 5.9 summarises the slenderness limits given in EN 1993-1-4 (2006), those revised by Gardner and Theofanous (2008) and the recommendations given herein for ferritic stainless steel internal elements and outstand flanges in compression.

Table 5.9 Summary of the slenderness limits based on the  $c/t\epsilon$  values for compressed elements

Type of element		EN 1993-1-4 (2006)			Revised limits by Gardner and Theofanous (2008)			Recommended value for ferritics		
		Class 1	Class 2	Class 3	Class 1	Class 2	Class 3	Class 1	Class 2	Class 3
Internal elements	$\sigma_u/\sigma_{0.2} > 1.2$	25.7	26.7	30.7	33	35	37	33	35	37
	$\sigma_u/\sigma_{0.2} \leq 1.2$	25.7	26.7	30.7	33	35	37	25.7	35	37
Outstand flanges	welded	9	9.4	11	9	10	14	9	10	14
	cold-formed	10	10.4	11.9	9	10	14	9	10	14

The results from the above assessment highlighted the conservatism associated with the usage of an elastic, perfectly plastic material model, limited to the 0.2% proof stress, which is assumed in EN 1993-1-4 (2006). The continuous strength method (CSM), which is a deformation-based design approach that allows for the beneficial influence of strain hardening beyond the 0.2% proof strength, and was extended herein to ferritic stainless steel. The available material data on ferritic stainless steel was used to determine new values for the slope  $E_{sh}$  of the linear hardening material model adopted in the CSM, suitable for this type of material. A reliability analysis was also conducted to statistically verify the applicability of the method. Ultimate capacity predictions by EN 1993-1-4 (2006) and the CSM of existing test results (Bredenkamp and van den Berg (1995), Stangenberg (2000) and Afshan and Gardner (2013a)) and the numerical results generated in the present study showed that the latter achieves more precise predictions enabling a more efficient design.

### Acknowledgements

The research leading to these results has received funding from the European Community's Research Fund for Coal and Steel (RFCS) under Grant Agreement No. RFSR-CT-2010-00026, Structural Applications for Ferritic Stainless Steels, from Ministerio de Ciencia e Innovación to the Project BIA 2010-11876-E "Acciones complementarias" and from Ministerio de Economía y Competitividad to the Project BIA 2012-36373 "Estudio del comportamiento de estructuras de acero inoxidable ferrítico". The first author would like to acknowledge the financial support provided by the Secretaria d'Universitats i de Recerca del Departament d'Economia i Coneixement de la Generalitat de Catalunya i del Fons Social Europeu. Special thanks are given to Petr Hradil from VTT Technical Research Centre of Finland who has contributed in the FE modelling.



---

**CHAPTER 6 – Experiments on cold-formed ferritic stainless steel slender sections**

This chapter has been submitted to the *Journal of Constructional Steel Research* under the reference:

Bock M, Arrayago I and Real E (2014d). Experiments on cold-formed ferritic stainless steel slender sections *Journal of Constructional Steel Research* (under review).

**Abstract**

The usage of stainless steel in construction has been increasing owing to its corrosion resistance, aesthetic appearance and favourable mechanical properties. The most common stainless steel grades used for structural applications are austenitic steels. The main drawback of these grades relies on their nickel content (around 8-10%), resulting in a relatively high initial material cost. Other stainless steel grades with lower nickel content such as the ferritic steels offer the benefits of stainless steels in terms of functional qualities and design but within a limited cost frame. Hence, ferritic stainless steels may be a viable alternative for structural applications. Given the fact that little experimental information on ferritic stainless steels is currently available, the purpose of this investigation is to report a series of material and cross-section tests on ferritic grade EN 1.4003 (similar to 3Cr12) stainless steel square and rectangular hollow sections to enable a better understanding of their material response and structural performance. Four different cross-section geometries have been tested under pure compression and in-plane bending. Measurements of geometric imperfections and material properties are also presented. The obtained test results are used to assess the adequacy of the slenderness limits and effective width formula given in EN 1993-1-4 (2006) to ferritic stainless steel, those proposed by Gardner and Theofanous (2008) and Zhou et al. (2013) design approach.

**Highlights**

- Experimental study of ferritic stainless steel stub columns and beams
- Behaviour of cross-sections with different aspect ratios
- Assessment of various design methods for application to ferritic stainless steel
- Design recommendations

**Keywords**

Cross-section behaviour, element interaction, experiments, ferritic stainless steel, hollow section, local buckling



## 6.1 Introduction

What particularly features stainless steels is the amount of chromium present within their internal structure which forms a passivation layer of chromium oxide ( $\text{Cr}_2\text{O}_3$ ) when exposed to oxygen preventing surface corrosion. Other alloying elements are added to meet specific needs in terms of strength, corrosion resistance and ease of fabrication. Depending on their chemical composition, stainless steels can be classified into main five categories: ferritic, austenitic, martensitic, duplex and precipitation hardening. The most commonly used ones in construction are the austenitic grades which have reasonable mechanical strength with 0.2% proof stress of 210-240  $\text{N/mm}^2$  and display high ductility with ultimate strains  $\epsilon_u$  laying between 50 and 60%. These positive features, however, may be inhibited by the high initial material cost and considerable price fluctuations associated with the amount of nickel involved in austenitic stainless steels (8-11%). Ferritic stainless steels, on the other hand, contain little nickel remaining chromium as the main alloying element (min. 10.5%); hence, they are an attractive alternative for structural applications due to their lower cost and price stability in comparison with the austenitics. Despite their low nickel content, which may reduce ductility and increase risk of pitting corrosion, ferritic stainless steels offer a good combination of mechanical and corrosion-resistance properties with higher 0.2% proof stress of 250-330  $\text{N/mm}^2$  in the annealed condition and they are easier to work and machine in comparison with the austenitics. Moreover, by increasing the chromium content (10.5-30%) and including establishing alloying elements such as molybdenum and niobium, similar corrosion resistance to some austenitics grades can be achieved without compromising the initial material cost.

The viability of ferritic stainless steels for structural applications has been recently investigated within the framework of a RFCS European project (Cashell and Baddoo (2014)) where the applicability of various aspects of the European design guidance for stainless steels, EN 1993-1-4 (2006), to this material was examined. Despite the pool of experimental and numerical data generated in this project, and available in the literature (Bredenkamp and van den Berg (1995), Stangenberg (2000a), Afshan and Gardner (2013a) and Bock et al. (2014c)), the suitability of EN 1993-1-4 (2006) to ferritic stainless steel requires further experimental verification, particularly to assess the applicability of current slenderness limits and effective width formulations used for cross-section design. Hence, the purpose of this paper is to describe a comprehensive

laboratory testing program on grade 1.4003 stainless steel slender tubular sections featuring square and rectangular hollow sections (SHS and RHS, respectively) conducted at the Universitat Politècnica de Catalunya. A total of 8 stub column tests and 9 beam tests, including 3-point bending and 4-point bending configurations were carried out. The mechanical material properties were determined at Acerinox Europa S.A.U where 16 tensile coupon tests, including both flat and corner specimens, were performed. The obtained test results have been used to assess the applicability of the slenderness limits and the accuracy of the effective width equations for slender elements given in EN 1993-1-4 (2006). The revised slenderness limits and effective width formula proposed by Gardner and Theofanous (2008) as well as the design approach derived by Zhou et al. (2013) have also been considered herein. Relevant conclusions regarding various appraisals are presented and design recommendations are proposed.

## 6.2 Experimental investigation

### 6.2.1 Introduction

An experimental investigation including 8 stub column tests and 9 beam tests was performed on ferritic stainless steel SHS and RHS in the Laboratori de Tecnologia d'Estructures Luis Agulló, in the Department of Construction Engineering at Universitat Politècnica de Catalunya. Four section sizes were examined ( $h \times b \times t$ ): SHS  $60 \times 60 \times 2$ , RHS  $70 \times 50 \times 2$ , RHS  $80 \times 40 \times 2$  and RHS  $100 \times 40 \times 2$ , see Fig. 6.1. The investigated sections provided height to width ratios of 1, 1.4, 2 and 2.5. The specimens were cold-rolled from annealed flat strips of 1.4003 stainless steel and were delivered by the manufacturer in appropriate lengths to perform material and structural tests. The chemical composition and the tensile properties of the coil material used to form the various specimens are given in Table 6.1 and 6.2, respectively, as provided by the steelmaker in the mill certificates.

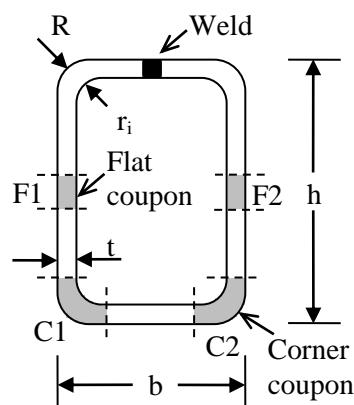


Fig. 6.1 Definition of symbols and location of coupon in cross-section

Table 6.1 Chemical composition of grade EN 1.4003 stainless steel from mill certificates

Section	C %	Si %	Mn %	P %	S %	Cr %	Ni %	N %	CO %
SHS 60×60×2	0.012	0.250	1.440	0.029	0.002	11.300	0.400	0.016	0.010
RHS 70×50×2	0.012	0.290	1.440	0.030	0.001	11.200	0.400	0.009	0.010
RHS 80×40×2	0.012	0.280	1.400	0.030	0.001	11.400	0.400	0.010	0.010
RHS 100×40×2	0.015	0.370	1.480	0.027	0.002	11.200	0.400	0.009	0.010

Table 6.2 Mechanical properties from mill certificates

Section	$\sigma_{0.2}$ (MPa)	$\sigma_{1.0}$ (MPa)	$\sigma_u$ (MPa)	$\epsilon_f$
SHS 60×60×2-T1	355	379	491	0.41
SHS 60×60×2-T2	342	363	479	0.40
RHS 70×50×2-T1	349	371	496	0.38
RHS 70×50×2-T2	350	368	484	0.40
RHS 80×40×2-T1	353	377	501	0.38
RHS 80×40×2-T2	351	372	496	0.37
RHS 100×40×2-T1	373	408	529	0.23
RHS 100×40×2-T2	350	379	498	0.24

### 6.2.2 Material tests

A series of tensile coupon tests were conducted at Acerinox Europa S.A.U to determine the basic stress-strain response of the ferritic stainless steel specimens. All the tested coupons were extracted from the batch of the specimens selected for the tests. Two tensile flat coupons were taken from two faces of the SHS and RHS specimens in the longitudinal direction, resulting in a total of 8 tensile coupon tests. All tensile flat coupons were machined into parallel necked specimens with a standard gauge length of  $5.65\sqrt{A_c}$ , where  $A_c$  is the cross-sectional area of the coupon, and width of 15 mm. Additional corner coupons were extracted from the curved portions of each of the cross-sections extended two times the thickness through the flat region in order to quantify the corner strength enhancements induced by the cold-forming process (Cruise and Gardner (2008b) and Ashraf et al. (2005)). A total of 16 material tests were performed.

Having extracted both flat and corner coupon tests, it was observed a longitudinal curving of all coupon specimens. This was due to the release of the through-thickness bending residual stresses present in the finished cross-section. All the coupons almost returned to their flat state during gripping in the testing machine's jaws (Rasmussen and Hancock (1993a) and Cruise and Gardner (2008a)). Hence, the obtained stress-strain responses inherently include the effect of longitudinal through-thickness bending residual stresses. Membrane residual stresses were not explicitly measured since previous studies (Jandera et al. (2008) and Huang and Young (2012)) concluded that their effect is relatively small compared to bending residual stresses.

The coupons were placed in a hydraulic machine (see Fig. 6.2 (a)) and were tested according to EN ISO6892-1 (2006). The test were conducted at uniform strain rate of  $0.00025 \text{ s}^{-1}$  up to the 0.2% proof stress and then increased up to  $0.008 \text{ s}^{-1}$  until fracture. A data acquisition system was employed to record load and displacement at regular intervals while testing using a data logger piece of software. Typical tensile coupon fractures are presented in Fig. 6.2 (b) and 6.2 (c) for the flat and the corner coupons, respectively.

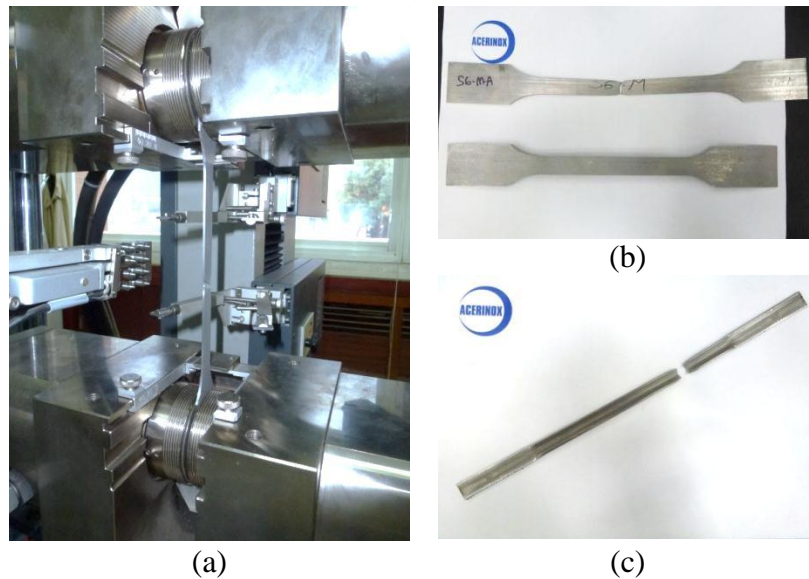


Fig. 6.2 Material test hydraulic machine (a) and typical coupon fractures in (b) flat coupons and (c) corner coupons

The material properties obtained from the coupon tests are summarized in Table 6.3 where the coupons have been labelled beginning with the section geometry e.g. SHS  $60 \times 60 \times 2$ , followed by the coupon type, F for tensile flat, C for tensile corner, and finally the section face number (1, 2), as given in Fig. 6.1. The material parameters reported in Table 6.3 are the Young's modulus  $E$ , the dynamic 0.01%, 0.05% and 0.2% proof stresses  $\sigma_{0.01}$ ,  $\sigma_{0.05}$  and  $\sigma_{0.2}$  respectively, and the maximum achieved ultimate tensile stress  $\sigma_u$  with its corresponding ultimate strain  $\epsilon_u$ . These material properties values can be used to replicate the whole stress-strain curve on the basis of the compound Ramberg-Osgood material models available in the literature (Ramberg and Osgood (1943), Mirambell and Real (2000), Rasmussen (2003) and Gardner and Nethercot (2004)). The weighted average material properties based on face width and corner properties extended two times the thickness through the flat region of each section are given in Table 6.4. Typical stress-strain response of tensile flat and tensile corner ferritic stainless steel material are depicted in Fig. 6.3.

Table 6.3 Material properties for the tensile coupons

Coupon	E (Gpa)	$\sigma_{0.01}$ (MPa)	$\sigma_{0.05}$ (MPa)	$\sigma_{0.2}$ (MPa)	$\sigma_u$ (MPa)	$\epsilon_u$
60×60×2-F1	173	331	396	437	484	0.108
60×60×2-F2	161	324	382	425	473	0.114
70×50×2-F1	178	323	378	418	479	0.137
70×50×2-F2	175	325	381	419	480	0.138
80×40×2-F1	182	321	379	416	484	0.138
80×40×2-F2	172	330	383	419	486	0.147
100×40×2-F1	181	332	382	416	481	0.134
100×40×2-F2	174	334	385	416	484	0.132
60×60×2-C1	172	361	475	552	571	0.008
60×60×2-C2	163	360	468	544	564	0.009
70×50×2-C1	180	394	489	556	576	0.011
70×50×2-C2	178	370	479	554	573	0.012
80×40×2-C1	184	364	456	552	580	0.010
80×40×2-C2	177	396	492	592	611	0.006
100×40×2-C1	182	378	482	558	578	0.012
100×40×2-C2	177	363	445	548	580	0.008

Table 6.4 Weighted average tensile material properties

Section	E (Gpa)	$\sigma_{0.01}$ (MPa)	$\sigma_{0.05}$ (MPa)	$\sigma_{0.2}$ (MPa)	$\sigma_u$ (MPa)	$\epsilon_u$
SHS 60×60×2	167	335	409	459	499	0.086
RHS 70×50×2	176	337	404	450	502	0.108
RHS 80×40×2	177	338	400	451	508	0.113
RHS 100×40×2	178	341	399	443	501	0.109

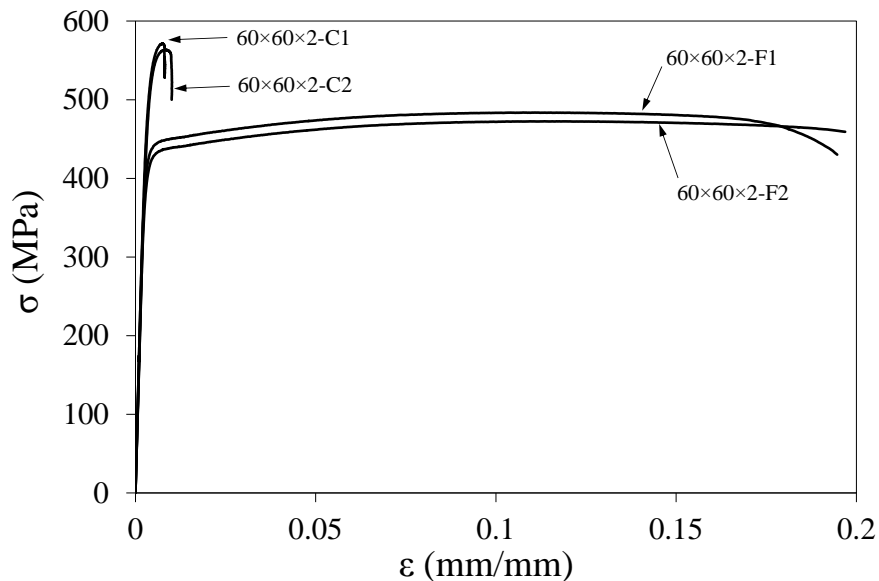


Fig. 6.3 Stress-strain curves for flat tensile and corner tensile material taken from SHS 60×60×2

### 6.2.3 Stub Column tests

Two repeated concentric stub column tests were performed on four ferritic stainless steel slender cross-sections: SHS 60×60×2, RHS 70×50×2, RHS 80×40×2 and RHS 100×40×2. All the specimens were selected to be short enough to avoid global flexural buckling but with enough length to include a representative pattern of residual stresses

and geometric imperfections according to Galambos (1998). Hence, stub column lengths were equal to three times the largest nominal cross-sectional dimension. Prior to testing, measurements of each cross-section dimensions and initial geometric imperfections were conducted, which were measured at the location  $180^\circ$  (opposite face) and  $90^\circ$  angles from the weld. A linear variable differential transformer (LVDT) was used to obtain readings along the middle half of these faces of each specimen. The data was collected by passing the specimen, which was placed on a table of a milling machine, under the LVDT via an automatic feed at a fixed rate of 30 cm per minute. All the data was recorded at  $2 \text{ s}^{-1}$  intervals using the data acquisition system MGCplus and logged using the Catman Easy computer package. The obtained imperfection spectrums exhibited the expected half sine wave. The maximum measured imperfection from both faces was then averaged to determine the imperfection magnitude  $w_0$  given in Table 6.5. This table also reports the measured geometry (see Fig. 6.1) of each stub column specimen where  $L$  is the stub column length,  $h$  is the section depth,  $b$  is the section width,  $t$  is the thickness,  $r_i$  is the internal corner radius and  $A$  is the area of the cross-section.

Table 6.5 Measured dimensions of the stub column specimens and imperfection magnitudes

Specimen	L (mm)	h (mm)	b (mm)	t (mm)	$r_i$ (mm)	A (mm <sup>2</sup> )	$w_0$ (mm)
60×60×2-SC1	179.5	60.3	60.3	2.00	2.4	454	0.02
60×60×2-SC2	180.0	60.3	60.4	2.02	2.3	460	0.02
70×50×2-SC1	210.0	70.1	49.9	2.00	2.3	451	0.03
70×50×2-SC2	210.0	70.0	49.8	1.99	2.2	450	0.03
80×40×2-SC1	240.0	80.0	40.5	2.00	1.3	457	0.06
80×40×2-SC2	240.0	80.0	40.3	1.99	1.9	453	0.06
100×40×2-SC1	299.5	100.1	40.0	2.05	2.1	546	0.07
100×40×2-SC2	299.5	100.1	40.5	1.99	2.2	532	0.07

The specimens were tested in compression between parallel flat platens in an Instron 1000kN hydraulic testing machine as shown in Fig. 6.4. The test was driven by displacement control at 0.5 mm/min. The instrumentation consisted of three LVDTs to measure the end shortening between both flat platens, a load cell to accurately record the compressive load and two strain gauges affixed at mid-height of the largest plate width of the cross-section and at a distance two times the material thickness from mid-width of the face. The strain readings, which were taken from the first set of tests (SC1), were used to verify the concentricity of the loading distribution and to remove the elastic deformation of the flat platens. All the data, including load, displacement,

voltage and strain were recorded at  $2 \text{ s}^{-1}$  intervals using the data acquisition system MGCplus and logged using the Catman Easy computer package.



Fig. 6.4 Stub column test setup – Specimen SHS  $60 \times 60 \times 2$

The experimental ultimate loads  $N_{u,\text{test}}$  of the test specimens and their corresponding end shortenings  $\delta_u$  are given in Table 6.6. The full end-shortening response for all the specimens is shown in Fig. 6.5. Note that the similarity between the first (SC1) and the repeated test (SC2) for all the tested sections demonstrates the reliability of the test results. The reported end-shortening measurements given in Table 6.6 and Fig. 6.5 refer to the true stub column shortening  $\delta$ , which was determined eliminating the elastic deformation of the end platens following the guidelines of the Centre for Advanced Structural Engineering (1990), as given by Eq. (6.1) where  $\delta_{\text{LVDT}}$  is the LVDT end shortening and  $\delta_{\text{platen}}$  is the end platen deformation given in Eq. (6.2) where  $L$  is the length of the stub column specimen,  $\sigma$  is the applied stress, and  $E_{0,\text{LVDT}}$  and  $E_{0,\text{true}}$  are Young's moduli of the LVDTs and strain gauge response, respectively. All the specimens failed by local buckling and typical failure modes are shown in Fig. 6.6.

Table 6.6 Summary of test results for the stub columns

Specimen	$N_{u,\text{test}}$ (kN)	End shortening at ultimate load $\delta_u$ (mm)
60×60×2-SC1	211.37	1.02
60×60×2-SC2	212.31	1.03
70×50×2-SC1	190.15	0.87
70×50×2-SC2	190.05	0.84
80×40×2-SC1	178.21	0.80
80×40×2-SC2	179.52	0.82
100×40×2-SC1	184.23	0.97
100×40×2-SC2	183.99	0.92

$$\delta = \delta_{LVDT} - 2\delta_{platen} \quad (6.1)$$

$$\delta_{platen} = \frac{L}{2} \sigma \left( \frac{1}{E_{0,LVDT}} - \frac{1}{E_{0,true}} \right) \quad (6.2)$$

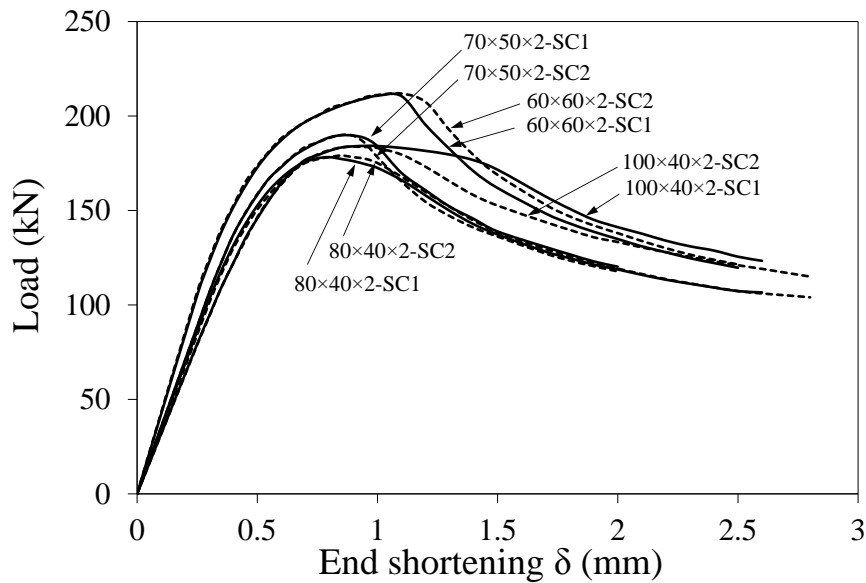


Fig. 6.5 Load-end shortening response for the tested stub columns

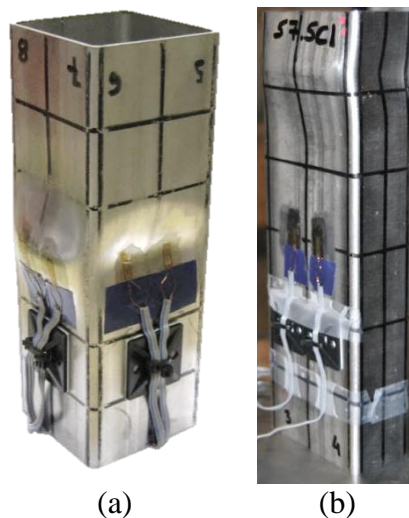


Fig. 6.6 Stub column failure modes: Specimens (a) SHS 60×60×2-SC1 and (b) RHS 80×40×2-SC1

#### 6.2.4 Beam tests

A total of 9 in-plane bending tests, including 3-point (3P) and 4-point (4P) load configurations were conducted to determine the flexural response of ferritic stainless steel SHS and RHS. All four sections SHS 60×60×2, RHS 70×50×2, RHS 80×40×2 and RHS 100×40×2 were tested under 4-point bending configuration about both major (Mj) and minor (Mi) axis while specimens SHS 60×60×2 and RHS 80×40×2 were tested



under 3-point bending configuration about minor axis. All the beams were simply supported with spans of 1500 mm and extended 100 mm beyond the simple supports at each end resulting in a total length of 1700 mm. The supports, which were steel rollers, allowed axial displacement of the beam. Although the tubular geometry of the specimens precluded lateral torsional buckling, possible lateral displacement was prevented placing stabilizers at both supports in contact with the beam through teflon plates provided with a layer of grease to minimize friction and allow in-plane rotation.

Prior to testing, measurements of each cross-section dimensions and initial geometric imperfections were taken following the same procedure conducted in section 2.2 for the stub column specimens. The measured geometry and imperfection magnitudes  $w_0$  of each beam are reported in Table 6.7 where  $W_{el}$  and  $W_{pl}$  are the elastic and the plastic section modulus, respectively.

Table 6.7 Measured dimensions of the beam specimens and imperfection magnitudes

Specimen	Axis of bending	L (mm)	H (mm)	B (mm)	t (mm)	$r_i$ (mm)	$W_{el}$ (mm <sup>3</sup> )	$W_{pl}$ (mm <sup>3</sup> )	$w_0$ (mm)
60×60×2-3P	-	1700.0	60.1	60.1	2.10	2.2	8741	10233	0.02
80×40×2-3P	Minor	1700.0	80.0	40.3	2.08	2.0	6621	7483	0.06
60×60×2-4P	-	1700.0	60.1	60.1	2.05	2.5	8532	9983	0.02
70×50×2-4P	Major	1700.0	70.1	49.8	1.93	2.4	8625	10358	0.03
70×50×2-4P	Minor	1700.0	70.1	49.9	2.03	2.2	7548	8638	0.03
80×40×2-4P	Major	1699.5	80.0	40.5	2.02	2.4	9422	11712	0.06
80×40×2-4P	Minor	1699.0	79.9	40.3	2.08	2.1	6598	7458	0.06
100×40×2-4P	Major	1699.5	100.1	40.0	2.05	1.9	13400	16967	0.07
100×40×2-4P	Minor	1699.5	100.1	39.9	2.05	2.0	7931	8846	0.07

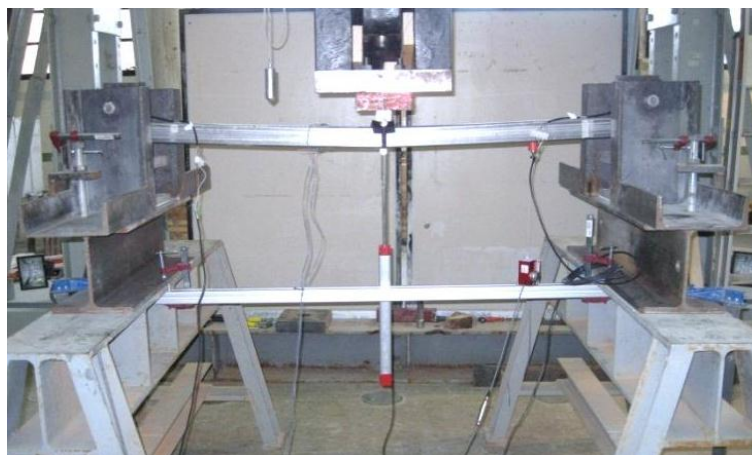


Fig. 6.7 Test arrangement for the 3-point bending test (3P) – Specimen 60×60×2



Fig. 6.8 Test arrangement for the 4-point bending test (4P) – Specimen 80×40×2

The tested beams were loaded symmetrically in a 1000 kN hydraulic testing machine at mid-span for the 3-point configuration while for the 4-point bending tests, the load was applied at two points (510 mm from each support) as shown in Figs 6.7 and 6.8, respectively. Load cells were placed under both supports to verify symmetry of loading while testing. Position sensors (Temposonic) were located at loading points to measure vertical deflections in both test arrangements while a string potentiometer was additionally placed at mid-span for the 4-point bending tests. In order to determine the end rotation of the beams, two inclinometers were positioned at each end of the beams. Strain gauges were affixed at the top and bottom flanges of the beams at 60 mm from the mid-span for the 3-point bending tests and at mid-span for the 4-point bending tests. Specimen RHS 80×40×2-3P tested about minor axis under 3-point bending configuration was monitored with four strain gauges at both top flange and web to recode the onset of local buckling as well as material and post-buckling nonlinear effects. Wooden blocks were placed within the tubes and were carefully located under the loading points to prevent web crippling failure for the 4-point configuration and the specimen 80×40×2 tested about minor axis under the 3-point configuration. The load was applied through elastomeric bearing plates and the test was driven by displacement control at a rate of 3 mm/min. All the data, including load, displacement, voltage and strain was recorded at 2 s<sup>-1</sup> intervals using the data acquisition system MGCplus and logged using the Catman Easy computer package.

The experimental ultimate bending moment  $M_{u,\text{test}}$ , together with other key experimental results are presented in Table 6.8. Recall that specimen 60×60×2-3P was not provided

with wooden blocks and consequently, interaction web crippling and bending effects were observed in the test result. In determining the corrected value for the ultimate bending moment given in Table 6.8, the effective moment resistance of the cross-section determined deducting the ineffective areas according to the reduction factor  $\rho$  given in EN 1993-1-4 (2006) and the interaction bending moment and local load equation given in EN 1993-1-3 (2006) was used. Full moment-rotation and moment-curvature curves from the 3-point bending tests and the 4-point bending tests are presented in Figs 6.9 and 6.10, respectively, where  $\theta$  is the mid-span rotation determined as the sum of the measurements taken by the two inclinometers and  $\kappa$  is the curvature calculated according to Rasmussen and Hancock (1993b) and as given by Eq. (6.3) where  $u_{ms}$  is the deflection at mid-span measured by the string potentiometer,  $u_{av}$  is the average of the vertical displacement at loading points defined as  $u_{av}=(u_1+u_2)/2$  and taken from the tempersonic sensors measurements, and  $L$  is the distance between the loading points.

Table 6.8 Summary of test results for the beams

Specimen	Axis of bending	Ultimate moment $M_{u,test}$ (kNm)	$\theta_{pl}$ or $\kappa_{pl}$	R
60×60×2-3P	-	3.90*	8.04E-02	-
80×40×2-3P	Minor	2.87	1.08E-01	-
60×60×2-4P	-	4.22	1.07E-04	-
70×50×2-4P	Major	4.90	8.74E-05	1.90
70×50×2-4P	Minor	3.50	1.17E-04	-
80×40×2-4P	Major	5.60	7.97E-05	0.72
80×40×2-4P	Minor	2.76	1.44E-04	-
100×40×2-4P	Major	6.29	6.30E-05	-
100×40×2-4P	Minor	3.08	1.40E-04	-

\*Corrected value

$$\kappa = \frac{8(u_{ms} - u_{av})}{4(u_{ms} - u_{av})^2 + L^2} \quad (6.3)$$

The rotation capacity  $R$  reported in Table 6.8 was determined as  $R=(\theta_u/\theta_{pl})-1$  and  $R=(\kappa_u/\kappa_{pl})-1$  for the 3-point bending tests and the 4-point bending tests, respectively, where  $\theta_u$  ( $\kappa_u$ ) is the rotation (curvature) at which the moment-rotation (moment-curvature) curve falls below  $M_{pl}$  on the descending branch and  $\theta_{pl}$  ( $\kappa_{pl}$ ) is the elastic part of the total rotation (curvature) corresponding to  $M_{pl}$  in the ascending branch determined as  $\theta_{pl}=M_{pl}L/2EI$  ( $\kappa_{pl}=M_{pl}L/EI$ ), which is also given in Table 6.8, where  $I$  is the second moment of area of the section. Note that, given the slenderness nature of the cross-sections, most of the failures are achieved prior to the attainment of the plastic moment  $M_{pl}$  exhibiting no or little rotation capacity.

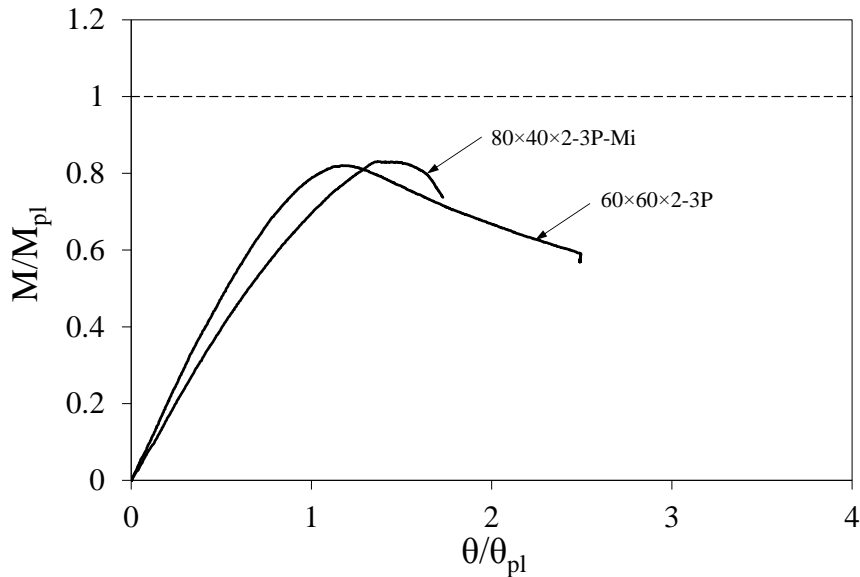


Fig. 6.9 Normalised moment-rotation curves for the three-point bending tests

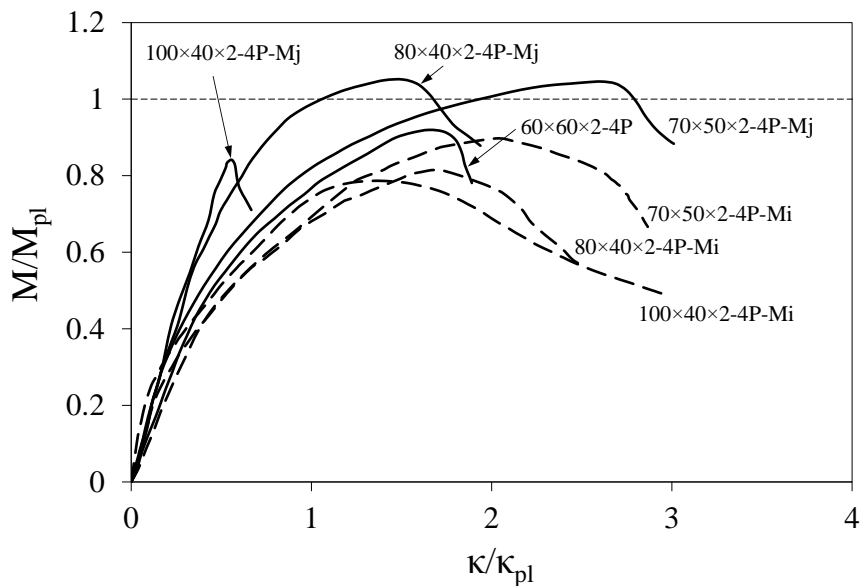


Fig. 6.10 Normalised moment-rotation curves for the four-point bending tests

Typical local buckling modes were observed for all the specimens under both test arrangements as depicted in Fig. 6.11 (a) and 6.11 (b) for the 3-point bending and 4-point bending test configurations, respectively.

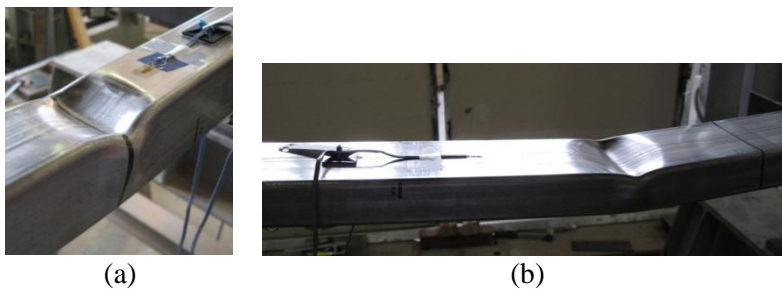


Fig. 6.11 Typical (a) 3-point bending failure mode - Specimen 60x60x2-3P and (b) 4-point bending failure mode - Specimen 100x40x2-4P-Mi

For the specimen 80×40×2-3P-Mi, which was monitored affixing additional strain gauges as mentioned earlier, the evolution of the stresses along the compressed flange and the web under bending is presented in Fig. 6.12 (a) and 6.12 (b), respectively. For the former, strain measurements were taken at coordinates 15, 30, 50 and 65 mm while for the latter the gauges were placed at 10, 16, 23 and 30 mm from the bottom flange. In these figures it is observed a linear stress distribution up to the onset of local buckling in the compressed flange, which is the most slender element, for an applied moment of  $M=2.81\text{kNm}$ . Beyond this point, the stresses in the compressed flange (Fig. 6.12 (a)) are transferred to the edge portion of the plate resulting in the typical non-uniform stress distribution pattern assumed by the effective width theory (post-buckling behaviour) for slender cross-sections. Consequently, the neutral axis (N.A.) of the web subjected to bending (Fig. 6.12 (b)) is shifted downwards. Note that the stress distribution in the web does not remain linear due to the actual non-linear material response exhibited by stainless steel.

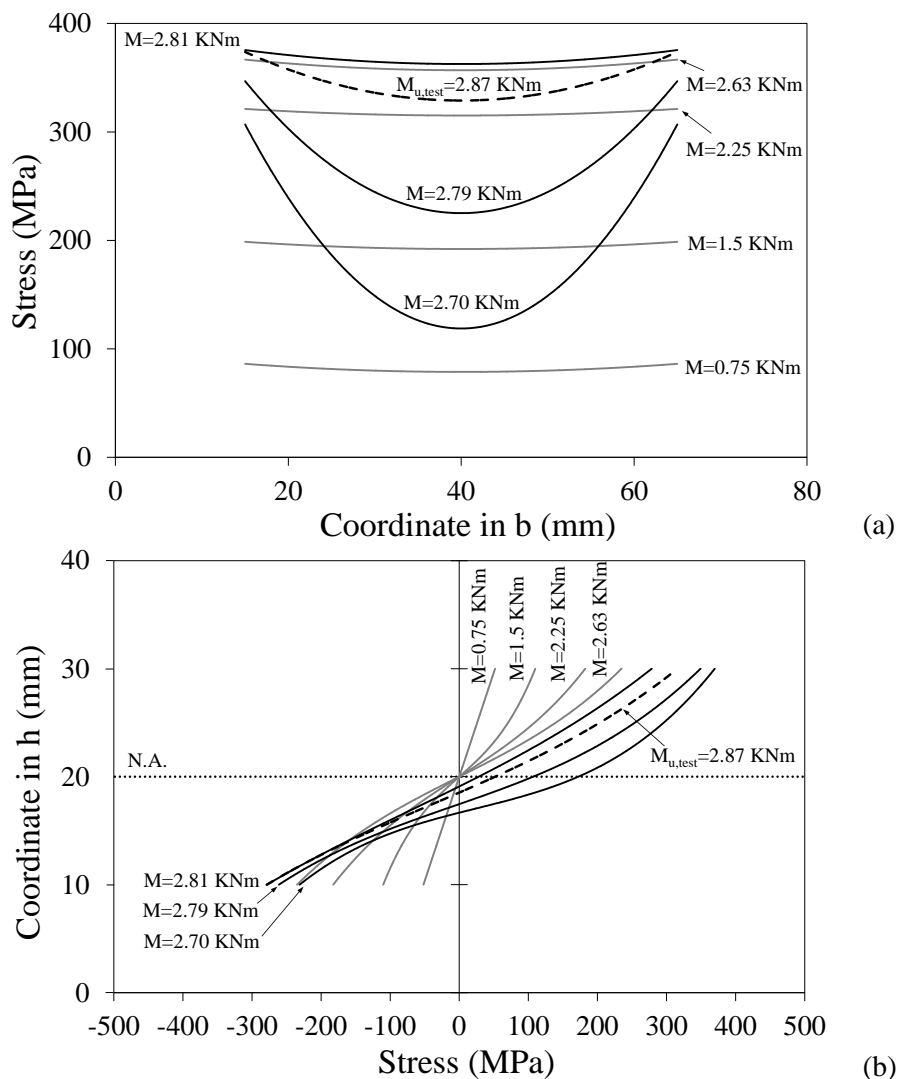


Fig. 6.12 Local buckling response in the specimen RHS 80×40×2-3P-Mi

---

### 6.3 Analysis of results and design recommendations

#### 6.3.1 General

The European structural stainless steel design standard, EN 1993-1-4 (2006), accounts for the effects of local buckling through the cross-section classification concept given in EN 1993-1-1 (2005). The procedure to classify a cross-section is based on the determination of the slenderness parameter  $c/t\varepsilon$ , where  $c$  is the flat width,  $t$  is the element thickness and  $\varepsilon$  is the material factor defined as  $\varepsilon=[(235/\sigma_{0.2})(E/210000)]^{0.5}$ . This parameter is then compared to different slenderness limits defining the different cross-sectional classes which depend on the manufacturing process (cold-formed or welded), the boundary conditions (internal or outstand elements) and the stress gradient (fully compressed, bending or combined compression and bending). In this procedure, all the constituent elements of the cross-section are assumed to be under simply supported conditions, hence neglecting the effect of element interaction. The whole cross-section classification relates to its most slender constituent element. Local buckling effects on slender cross-sections are accounted for by means of the effective width method applying a reduction factor  $\rho$  to the various plate widths that make up the cross-section so that the ineffective areas are deducted.

With the benefit of a far greater pool of experimental data than was available when EN 1993-1-4 (2006) was published, Gardner and Theofanous (2008) proposed new slenderness limits and revised the effective width formulae which have been experimentally verified for a variety of stainless steels and cross-sections (Afshan and Gardner (2013a), Theofanous and Gardner (2009, 2010) and Saliba and Gardner (2013)) but still require further assessment, particularly for ferritic stainless steel slender sections. Slender sections are significantly influenced by the effects of element interaction, performing a higher structural response for higher aspect ratios  $\alpha=h/b$  due to the degree of restraint provided by the flanges to the webs. Zhou et al. (2013) derived a new design procedure to account for element interaction effects by proposing different Class 3 slenderness limits and reduction factor  $\rho$  equations for a given aspect ratio  $\alpha$ . This approach was derived on the basis of generated numerical models on high strength stainless steel sections and its applicability to other grades might be examined.

The obtained experimental results on ferritic SHS and RHS stub column and beam tests are therefore used through this sections to assess the slenderness limits and effective width formula used for cross-section design given in the current European specification

for stainless steel, EN 1993-1-4 (2006), those proposed by Gardner and Theofanous (2008) as well as Zhou et al. (2013) design approach to ferritic stainless steel. The assessment covers internal elements in compression and bending.

### 6.3.2 Assessment of Class 3 slenderness limit and cross-section resistance

#### 6.3.2.1 Elements in compression

Both results from stub column and bending tests have been employed to assess the Class 3 slenderness limit for internal elements in compression. To this end, the relevant response  $N_{u,\text{test}}/A\sigma_{0.2}$  or  $M_{u,\text{test}}/W_{el}\sigma_{0.2}$ , where  $A$  is the area of the gross cross-section,  $W_{el}$  is the elastic section modulus,  $\sigma_{0.2}$  is the 0.2% proof stress and  $N_{u,\text{test}}$  and  $M_{u,\text{test}}$  are the ultimate test load and moment, respectively, has been plotted against the slenderness parameter  $c/t\epsilon$  of the most slender constituent element controlling the local buckling response as shown in Figs 6.13 and 6.14 for the stub columns and the beams, respectively. The corresponding Class 3 limits given in EN 1993-1-4 (2006), revised in Gardner and Theofanous (2008) and proposed in Zhou et al. (2013) are also shown. Note that a cross-section is deemed to be Class 3 (or better) if  $N_{u,\text{test}}$  (or  $M_{u,\text{test}}$ ) exceeds  $A\sigma_{0.2}$  (or  $W_{el}\sigma_{0.2}$ ). In determining the most slender element in terms of the relevant slenderness  $\bar{\lambda}_p$ , simply supported conditions and appropriate stress distribution under which the flat elements of the cross-section are subjected were assumed to calculate the buckling factor  $k_\sigma$  as given by EN 1993-1-5 (2006). Table 6.9 shows the values of the relevant response together with the slenderness of the web  $\bar{\lambda}_{p,w}$  and the flange  $\bar{\lambda}_{p,f}$ , and the slenderness parameter  $c/t\epsilon$  for the cross-sectional plate elements of all the specimens, where  $c_f$  and  $c_w$  are the flat portion of the flange and the web, respectively.

From Figs 6.13 and 6.14, it might be concluded that the current EN 1993-1-4 (2006) Class 3 limit of 30.7 is appropriate for application to ferritic stainless steel, but conservative, while the revised slenderness value of 37 proposed by Gardner and Theofanous (2008) better fits the test results. Zhou et al. (2013) slenderness limiting values given in Eq. (6.4) provide good agreement with test data for an aspect ratio of  $\alpha=1$  (SHS) except for the specimen  $60\times 60\times 2$  tested under 3-point bending configuration which failed by bending and web crippling interaction. For aspect ratios  $\alpha>1$  (RHS) there are not enough representative data to draw a conclusion and further research is required to trace the trend of the structural response of the tested sections over the slenderness axis. However, the experimental results seem to achieve higher ultimate

response with increasing aspect ratio and decreasing slenderness thereby reflecting the benefits of the element interaction effects and allowing less restrictive slenderness limits which is in line with the basis of Zhou et al. (2013) design approach. It is therefore recommended the Class 3 limit of 37 proposed by Gardner and Theofanous (2008) for ferritic stainless steel cross-sections in light of the available resources which indicate the necessity to research on the effects of element interaction to extend Zhou et al. (2013) proposal for application to ferritic steels.

$$\frac{c}{t\epsilon} = \begin{cases} 30.5 + 10.2\alpha - 1.7\alpha^2 & 1 \leq \alpha \leq 3 \\ 45.8 & \alpha > 3 \end{cases} \quad \begin{matrix} \text{For } 488 \leq \sigma_{0.2} \leq 707 \text{ MPa} \\ \text{and } 1 \leq \alpha \leq 6 \end{matrix} \quad (6.4)$$

Table 6.9 Relevant response and slenderness parameters for all the specimens

Specimen	$N_{u,test}/A\sigma_{0.2}$	$M_{u,test}/W_{el}\sigma_{0.2}$	$M_{u,test}/W_{pl}\sigma_{0.2}$	$c_w/t\epsilon$	$c_f/t\epsilon$	$\bar{\lambda}_{p,w}$	$\bar{\lambda}_{p,f}$	Controlling element	Stress distribution
60×60×2-SC1	1.02	-	-	39.97	40.01	0.70	0.70	Web/flange	Compressed
60×60×2-SC2	1.01	-	-	40.36	40.36	0.71	0.71	Web/flange	Compressed
60×60×2-3P	-	0.97	0.83	38.41	38.41	0.28	0.67	Flange	Compressed
60×60×2-4P	-	1.08	0.92	39.05	39.05	0.28	0.69	Flange	Compressed
70×50×2-SC1	0.94	-	-	48.30	32.47	0.85	0.57	Web	Compressed
70×50×2-SC2	0.94	-	-	46.76	31.45	0.82	0.55	Web	Compressed
70×50×2-4P-Mj	-	1.26	1.05	48.11	32.23	0.35	0.57	Flange	Compressed
70×50×2-4P-Mi	-	1.03	0.90	30.91	46.01	0.22	0.81	Flange	Compressed
80×40×2-SC1	0.88	-	-	55.14	25.49	0.97	0.45	Web	Compressed
80×40×2-SC2	0.89	-	-	54.49	24.49	0.96	0.43	Web	Compressed
80×40×2-3P-Mi	-	0.96	0.85	23.39	52.32	0.17	0.92	Flange	Compressed
80×40×2-4P-Mj	-	1.31	1.05	53.24	23.64	0.38	0.42	Flange	Compressed
80×40×2-4P-Mi	-	0.92	0.82	23.25	52.16	0.17	0.92	Flange	Compressed
100×40×2-SC1	0.76	-	-	68.97	24.17	1.21	0.43	Web	Compressed
100×40×2-SC2	0.78	-	-	67.01	23.18	1.18	0.41	Web	Compressed
100×40×2-4P-Mj	-	1.06	0.84	67.13	23.36	0.48	0.41	Web	Bending
100×40×2-4P-Mi	-	0.88	0.79	23.08	66.88	0.17	1.18	Flange	Compressed

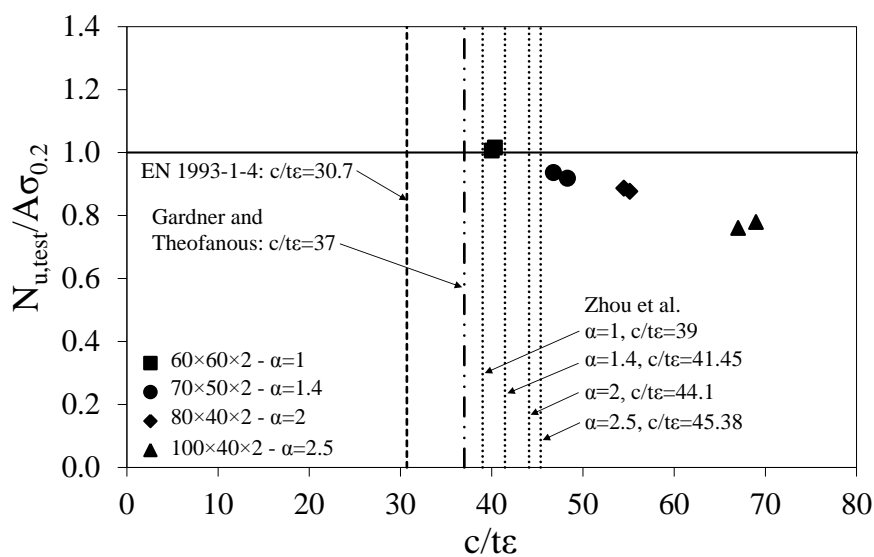


Fig. 6.13 Assessment of Class 3 limit for internal elements in compression (stub column test results)



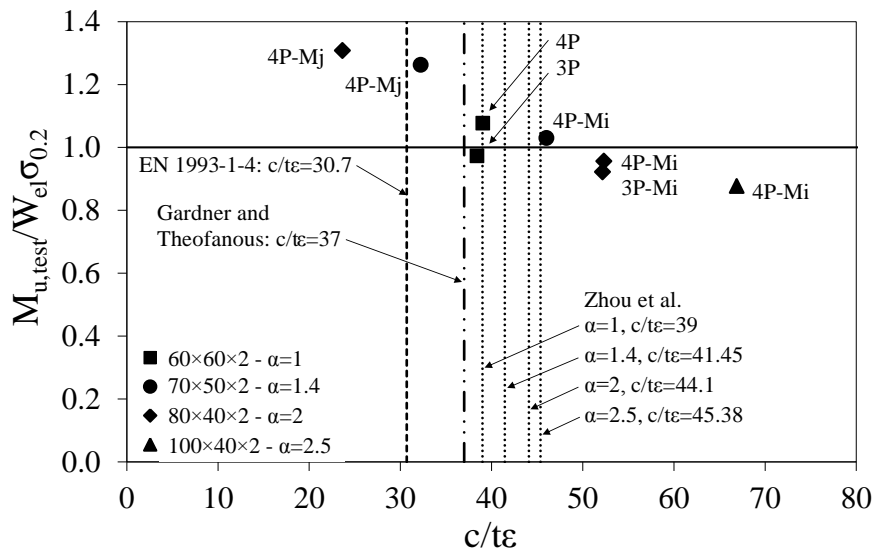


Fig. 6.14 Assessment of Class 3 limit for internal elements in compression (bending test results)

Another aspect that should be mentioned in Figs 6.13 and 6.14 is that, ignoring the combined bending and web crippling interaction failure of specimen  $60 \times 60 \times 2$  tested under 3-point bending configuration, an assessment based on compression data leads to a stricter Class 3 limit, Bock et al. (2014c), Gardner et al. (2010). Thereby, the results from the stub column tests are used herein to assess the effective width formula for internal elements in compression used for cross-section design specified in EN 1993-1-4 (2006) given in Eq. (6.5), and those proposed by Gardner and Theofanous (2008) given in Eq. (6.6) and by Zhou et al. (2013) given in Eqs (6.7) and (6.8). It is worth noting that the two former approaches apply the reduction factor  $\rho$  to the cross-sectional areas of the flat part of the elements of the cross-section classified as Class 4 while in the latter approach  $\rho$  is applied to the whole cross-section. Therefore, for the assessment of EN 1993-1-4 (2006) and revised Gardner and Theofanous (2008) proposal presented in Fig. 6.15, the reduction factor  $\rho$  determined as  $\rho = (N_{u,num} / \sigma_{0.2} - A_r - 2 \cdot t \cdot c_f) / 2 \cdot t \cdot c_w$  where  $N_{u,test}$  is the ultimate load achieved in the tests,  $\sigma_{0.2}$  is the 0.2% proof strength,  $A_r$  is the area of the corners,  $t$  is the thickness and  $c_f$  and  $c_w$  are the flat portion of the flange and the web respectively, has been plotted against the relevant slenderness  $\bar{\lambda}_p$  of the most slender element, while for Zhou et al. approach the relevant response  $N_{u,test} / A \sigma_{0.2}$  has been used in the vertical axis as shown in Fig. 6.16.

The predicted cross-section capacities  $N_{u,pred}$  by these three design approaches and key statistical values concerning mean predictions and coefficient of variation (COV) relative to the test results are given in Table 6.10. As shown in Fig. 6.15, EN 1993-1-4

(2006) is the lowest effective width curve and underestimates the test results, while Gardner and Theofanous (2008) revised equation is more accurate. Overall, Zhou et al. (2013) proposed curves provide a better approximation to the test results as observed in Fig. 6.16 and Table 6.10 with the lowest mean and coefficient of variation (COV).

$$\rho = \frac{0.772}{\bar{\lambda}_p} - \frac{0.125}{\bar{\lambda}_p^2} \leq 1 \text{ with } \bar{\lambda}_p \geq 0.541 \quad (6.5)$$

$$\rho = \frac{0.772}{\bar{\lambda}_p} - \frac{0.079}{\bar{\lambda}_p^2} \leq 1 \text{ with } \bar{\lambda}_p \geq 0.651 \quad (6.6)$$

$$\rho = \begin{cases} \frac{0.772}{\bar{\lambda}_p} \phi(\alpha) - \frac{0.059}{\bar{\lambda}_p^2} \phi(\alpha)^2 + 0.01\alpha\bar{\lambda}_p^{-2} & 1 \leq \alpha \leq 3 \\ \frac{0.907}{\bar{\lambda}_p} - \frac{0.081}{\bar{\lambda}_p^2} + 0.03\bar{\lambda}_p^{-2} & \alpha > 3 \end{cases} \quad (6.7)$$

$$\phi(\alpha) = \frac{30.5 + 10.2\alpha - 1.7\alpha^2}{39} \text{ with } 1 \leq \alpha \leq 3 \quad (6.8)$$

Table 6.10 Comparison of predicted resistances by different approaches for the stub columns

Specimen	EN 1993-1-4	Gardner and	Zhou et al.	Comparison		
	(2006)	Theofanous	(2013)	EN 1993-1-4	Gardner and	Zhou et al.
	$N_{u,pred}$ (kN)	$N_{u,pred}$ (kN)	$N_{u,pred}$ (kN)	$N_{u,test}/N_{u,pred}$	$N_{u,test}/N_{u,pred}$	$N_{u,test}/N_{u,pred}$
60×60×2-SC1	177.76	194.96	202.90	1.189	1.084	1.042
60×60×2-SC2	181.18	198.97	207.20	1.172	1.067	1.025
70×50×2-SC1	186.94	175.55	187.25	1.017	1.083	1.015
70×50×2-SC2	186.38	174.54	186.11	1.020	1.089	1.021
80×40×2-SC1	159.32	165.69	172.47	1.119	1.076	1.033
80×40×2-SC2	159.98	166.41	174.21	1.122	1.079	1.030
100×40×2-SC1	169.66	175.18	181.78	1.086	1.052	1.013
100×40×2-SC2	169.66	175.18	181.78	1.086	1.052	1.013
			Mean	1.123	1.065	1.030
			COV	0.033	0.019	0.015

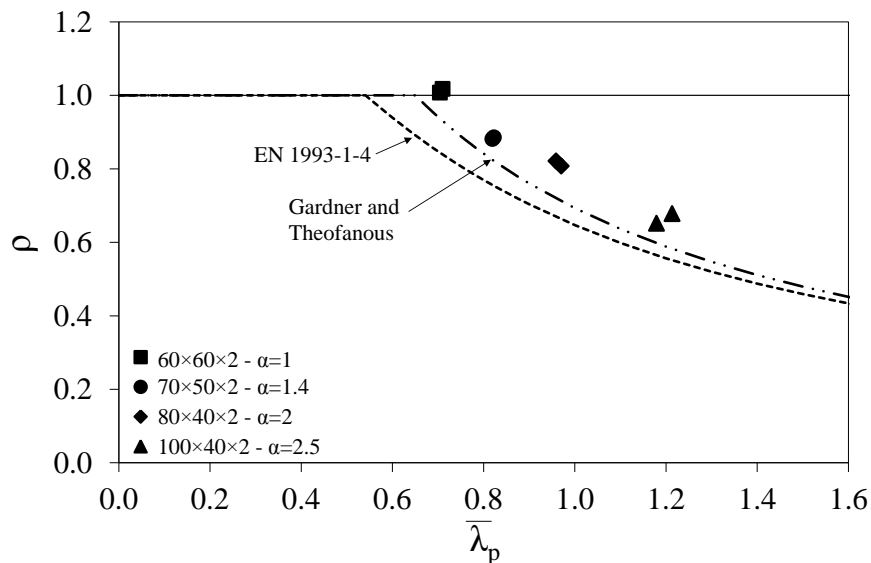


Fig. 6.15 Assessment of effective width formulae given in EN 1993-1-4 (2006) and proposal in Gardner and Theofanous (2008) for internal compressed elements

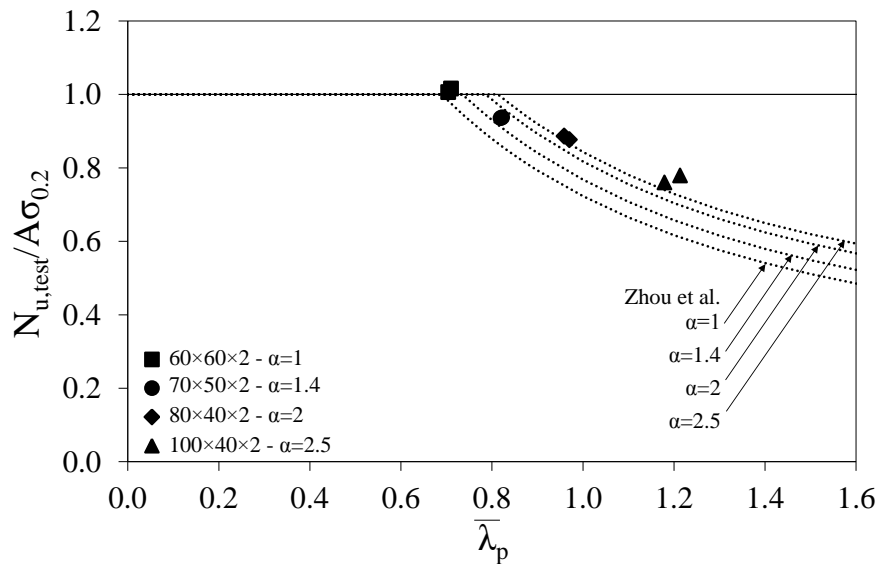


Fig. 6.16 Assessment of the reduction factor for Zhou et al. (2013) approach for internal compressed elements

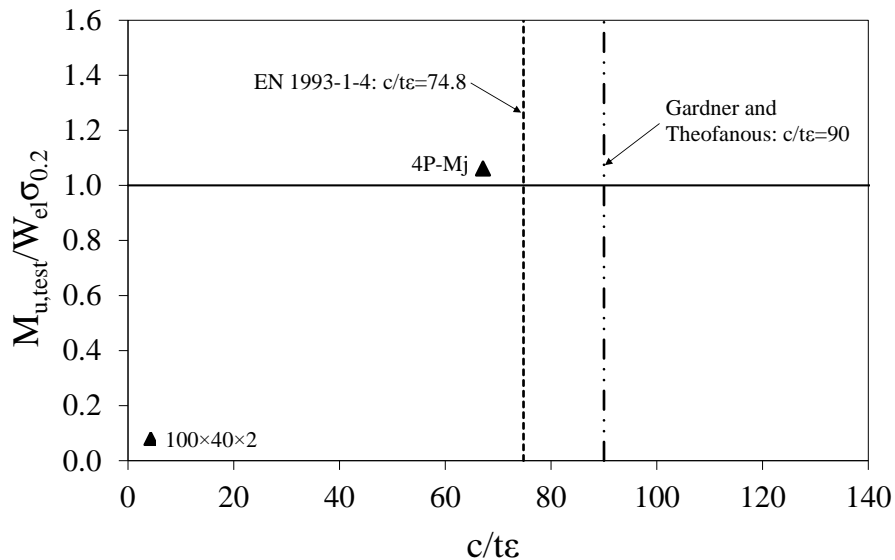


Fig. 6.17 Assessment of Class 3 limit for internal elements in bending (bending test results)

### 6.3.2.2 Elements in bending

The Class 3 slenderness limits for elements in bending specified in EN 1993-1-4 (2006) and proposed by Gardner and Theofanous (2008), together with the bending test results, are assessed in Fig. 6.17, where the test ultimate bending capacity  $M_{u,test}$  has been normalised by the product of the elastic section modulus  $W_{el}$  and the 0.2% proof stress  $\sigma_{0.2}$  and plotted against the slenderness parameter  $c/t_e$  of the most slender constituent element in the cross-section controlling the local buckling response. Note that Fig. 6.15 includes only one piece of data corresponding to the specimen  $100 \times 40 \times 2$ -4P tested about major axis, of which the element in bending (web) controlled the local buckling response; hence, exhibiting higher relevant slenderness  $\bar{\lambda}_p$  than the uniformly

compressed flange, see Table 6.9. From Fig. 6.17, it may be concluded that EN 1993-1-4 (2006) slenderness limit of 74.8 is appropriate for ferritic stainless steel while no conclusions can be drawn for the proposed limit of 90 by Gardner and Theofanous (2008).

### 6.3.3 Assessment of Class 2 and 1 slenderness limits

#### 6.3.3.1 Elements in compression

In Fig. 6.18, the experimental ultimate bending moment  $M_{u,test}$  is normalized by the product of the plastic section modulus  $W_{pl}$  and the 0.2% proof stress  $\sigma_{0.2}$  and plotted against the slenderness parameter  $c/t\epsilon$  of the most slender constituent element in the cross-section to assess the Class 2 slenderness limit for internal elements in compression specified in EN 1993-1-4 (2006) and the proposed by Gardner and Theofanous (2008). This relevant response is also given in Table 6.9. From Fig. 6.18, it might be concluded that the current EN 1993-1-4 (2006) Class 2 limit of 26.7 is applicable to ferritic stainless steel, but conservative, while the revised slenderness value of 35 proposed by Gardner and Theofanous (2008) is more appropriate.

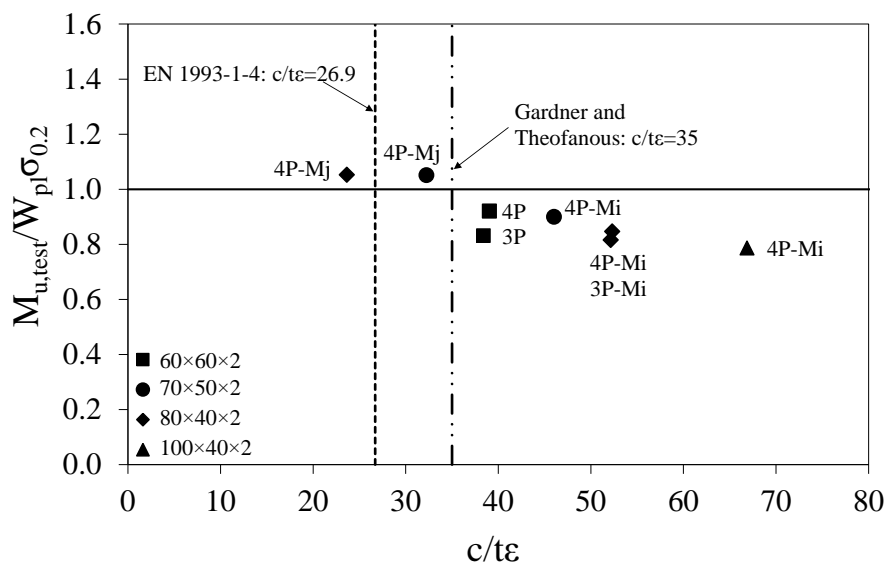


Fig. 6.18 Assessment of Class 2 limit for internal elements in compression (bending test results)

The rotation capacity of the bending test results reported in Table 6.8 is plotted against the flange slenderness in Fig. 6.19 to assess the Class 1 limit. Given the fact that there is no codified deformation capacity requirement for Class 1 stainless steel sections, the rotation capacity requirement of  $R=3$  (Sedlacek and Feldmann (1995)) for carbon steel is adopted herein, as has been assumed in existing investigations, Afshan and Gardner (2013a), Theofanous and Gardner (2010) and Saliba and Gardner (2013). Even though

the European standard for stainless steel do not allow plastic design, a Class 1 limit of 25.7 is given in EN 1993-1-4 (2006). This limit as well as Gardner and Theofanous (2008) proposed value of 33 appear unsafe in Fig. 6.19 under the assumption of that this rotation capacity requirement of  $R=3$  is appropriate for stainless steel. Previous studies reported the influence of the material response on the rotation capacity  $R$  for various stainless steels (Bock et al. (2014c) and Theofanous and Gardner (2010)) which are believed to significantly reduce the ductility demands on stainless steel structures for plastic design, particularly the gradual yielding and considerable strain hardening. To date, there is neither enough available experimental data nor research on stainless steel regarding plastic design to conduct an accurate assessment for the Class 1 slenderness limit.

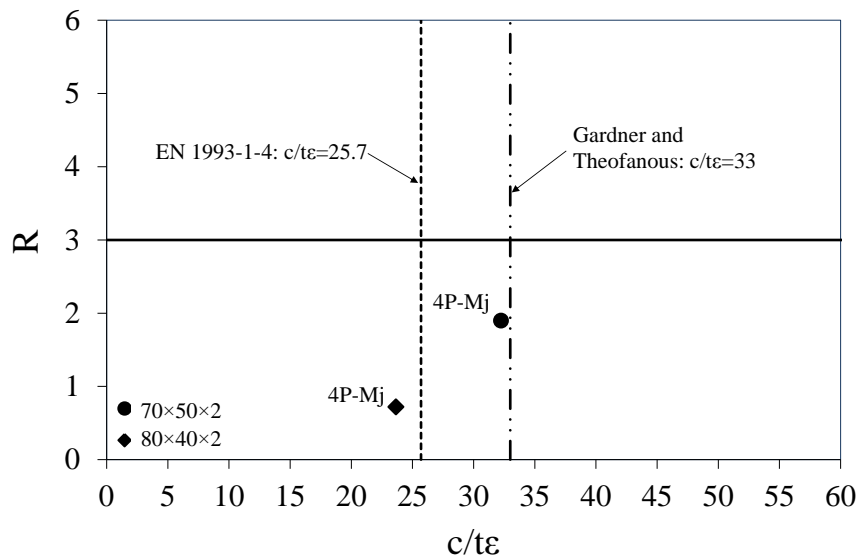


Fig. 6.19 Assessment of Class 1 limit for internal elements in compression (bending test results)

### 6.3.3.2 Elements in bending

The assessment of the Class 2 limit for internal elements in bending is shown in Fig. 6.20, where the experimental ultimate bending moment  $M_{u,test}$  is normalized by the product of the plastic section modulus  $W_{pl}$  and the 0.2% proof stress  $\sigma_{0.2}$  (plastic moment capacity  $M_{pl}$ ) and plotted against the slenderness parameter  $c/t_e$  of the most slender constituent element subjected to bending in the cross-section and controlling the local buckling response, see Table 6.9. In Fig. 6.20 it is observed that the slenderness limit of 76 proposed by Gardner and Theofanous (2008) is too optimistic, and the EN 1993-1-4 (2006) value of 58.2 might be adopted for the design of ferritic stainless steel elements in bending.

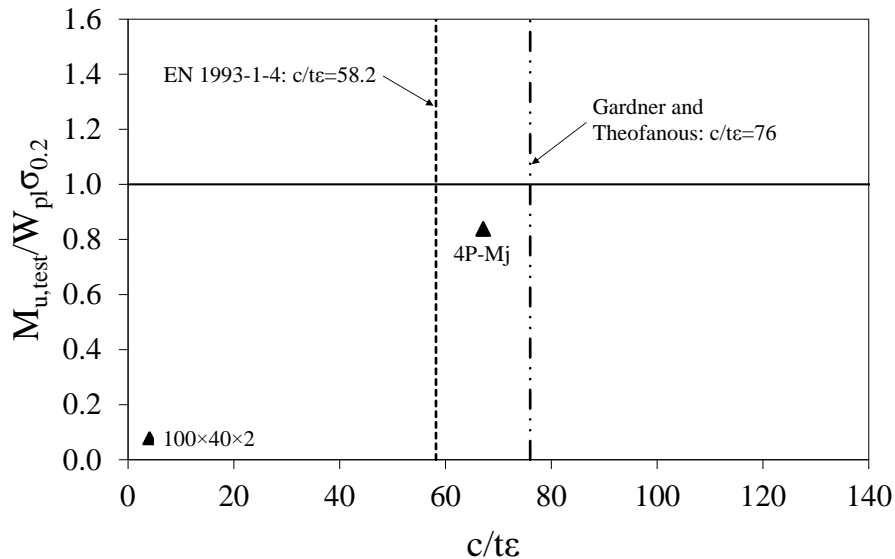


Fig. 6.20 Assessment of Class 2 limit for internal elements in bending (bending test results)

#### 6.4 Conclusions

An experimental investigation on the structural performance of cold-formed SHS and RHS structural elements on grade 1.4003 (similar to 3Cr12) ferritic stainless steel has been described in detail in the present paper. Tests were undertaken on 4 section geometries with different aspect ratios  $\alpha=h/b$  ranging from 1 to 2.5 and featuring slender elements. A total of 16 tensile coupon tests, including flat parts and corners, 8 stub column tests, 2 3-point bending tests and 7 4-point bending tests about major and minor axis have been presented. The obtained test data were used to assess the applicability of the slenderness limits and effective width formulae of the current European specification for stainless steel, EN 1993-1-4 (2006), those proposed by Gardner and Theofanous (2008) and the design approach proposed by Zhou et al. (2013), which accounts for the benefits of element interaction effects, to ferritic stainless steel. The assessment covered internal elements in compression (Class 1 to 4 and effective width method) and internal elements in bending (Class 2 and 3).

The results showed that the Class 3 slenderness limit and effective width equation for elements in compression given in EN 1993-1-4 (2006) are applicable to ferritic stainless steel, though those proposed by Gardner and Theofanous (2008) are more appropriate and this is the recommended approach for cross-section classification of slender elements. The proposed Class 3 limit by Zhou et al. (2013) for aspect ratios of 1 (SHS) is also well suited for ferritic stainless steels but for aspect ratios  $>1$  (RHS) the amount of tested sections, of which the achieved loads were consistent with the basis of this

design method, is not representative to validate the applicability of this design approach to ferritic stainless steel sections and further research is essential to study the effects of element interaction in such sections. On the other hand, the cross-section resistance predicted by Zhou et al. (2013) design method, using the reduction factor  $\rho$  as a function of the aspect ratio, more closely matched the test data in comparison with EN 1993-1-4 (2006) and Gardner and Theofanous (2008) approaches. Regarding the assessment of elements in bending, it was observed that the current Class 3 slenderness limit given in EN 1993-1-4 (2006) is safe for application to ferritic stainless steel while no conclusion could be drawn for the Gardner and Theofanous (2008) slenderness limiting value. The results also showed the adequacy of the Class 2 slenderness limits given in EN 1993-1-4 (2006) for both internal elements in compression and bending, though the proposed slenderness value by Gardner and Theofanous (2008) for the formers reflects better the cross-sectional behaviour. For internal elements in bending, however, the proposed Class 2 limit by Gardner and Theofanous (2008) was observed to be unsafe for application to ferritic stainless steels and it is therefore recommended the value given in EN 1993-1-4 (2006). The necessity to conduct further research on plastic design was also highlighted to derive appropriate ductility demands and Class 1 slenderness limiting values for application to ferritic stainless steels.

### **Acknowledgements**

The research leading to these results has received funding from Ministerio de Economía y Competitividad to the Project BIA 2012-36373 “Estudio del comportamiento de estructuras de acero inoxidable ferrítico”. The authors are grateful to Acerinox Europa S.A.U for their contribution to the material experimental tests. We also want to thank Tomàs Garcia, Carlos Hurtado, Jorge Cabrerizo and Jordi Lafuente for their technical assistance and Toni Sastre for his contribution in the laboratory. The first and second authors would like to acknowledge the financial support provided by the Secretaria d’Universitats i de Recerca del Departament d’Economia i Coneixement de la Generalitat de Catalunya i del Fons Social Europeu.

---

**CHAPTER 7 – Effective width equations accounting for element interaction for cold-formed stainless steel square and rectangular hollow sections**

This chapter has been submitted to the *Structures* journal under the reference:

Bock M and Real E (2014b). Effective width equations accounting for element interaction for cold-formed stainless steel square and rectangular hollow sections. *Structures* (under review)

**Abstract**

Square and rectangular hollow sections (SHS and RHS, respectively) featuring high height-to-width (aspect) ratios have shown to offer improved ultimate capacity due to the effects of the interaction between the elements within the cross-section which are particularly significant for slender cross-sections (class 4) undergoing local buckling. The European design rule dealing with stainless steel, EN 1993-1-4 (2006), utilises the concept of cross-section classification and the effective width method for the design of slender cross-sections susceptible to local buckling neglecting such interaction effects, hence yielding over conservative predictions. This paper examines the benefits of element interaction effects on cold-formed ferritic stainless steel compressed sections on the basis of carefully validated finite element models. Following parametric studies, the applicability of various alternative design approaches accounting for element interaction to ferritic stainless steel is assessed and effective width curves, as well as a Class 3 limiting slenderness equation, are derived herein as an explicit function of the aspect ratio. Comparisons with the loads achieved in the FE models have shown that the proposed effective width equations allowing for the benefits of element interaction improve capacity predictions making design more cost-effective.

**Highlights**

- Numerical modelling of cold-formed ferritic stainless steel stub columns
- Study of the influence of some key parameters on the numerical response
- Successful validation of the scope of various methods to cover ferritic steel
- Incorporation of element interaction effects into the effective width formulation
- Reliability analysis and validation of the proposed method against existing tests

**Keywords**

Cold-formed, effective width equation, element interaction, numerical modelling, local buckling, slender cross-sections, slenderness limits, stainless steel



## 7.1 Introduction

One disincentive to use stainless steel in construction is its initial material cost owing to the expense of the alloying elements. However, stainless steel's favourable properties may result in decreased expenditure through its life when, from a project viewpoint, they are designed efficiently, Gardner (2005). Thereby, a better understanding of their structural behaviour is essential to use stainless steel more wisely. Structural research programmes conducted across the world have caused a significant impact on usage of stainless steel in construction and design guidance development, Baddoo (2008). Notable experimental studies concerning local buckling response of hollow sections include those performed by Rasmussen and Hancock (1993a), Gardner and Nethercot (2004a) and Young and Liu (2003) covering austenitic stainless steel and Young and Lui (2005) and Gardner et al. (2006) on high-strength stainless steel (high-strength austenitic and duplex stainless steel) among others. The nickel content of these grades, however, particularly affects their costs which lead to investigate more price-stable alternatives such as lean duplex grades (Theofanous and Gardner (2009)) and ferritic grades (Afshan and Gardner (2013a)). The structural applications of these latter ones have been recently investigated within a European Project framework and comprehensive design guidance for construction applications has been developed, Cashell and Baddoo (2014). For the local buckling proposed design provisions, which were firstly based on numerical analyses (Bock et al. (2011, 2014c)), experimental research was undertaken to complement those aspects requiring further verification by Bock et al. (2014d) and follow in the present investigation.

The purpose of this paper is to investigate the element interaction effects on cold-formed ferritic stainless steel sections comprising slender elements in compression. The sections taken into account were SHS and RHS. Owing to the cross-sectional shape of the formers and when subjected to uniform compression, the four constituent plate elements are equally restrained to one another and simply supported conditions can be assumed at the interconnected boundaries between these plates. However, in a uniformly compressed RHS, the two short plate elements provide additional edge restraints to the longest ones and the boundary conditions tend to fixed supports as the aspect ratio increases. This element interaction effects turn into higher cross-section capacity and are especially notable in RHS comprising slender elements. The benefits of such additional restraints are examined herein numerically by using the finite element

---

model (FE) package ABAQUS. The results were used to assess the suitability and performance of various design methods that were developed or used for carbon steel and/or other stainless steel to ferritic stainless steel. These include the classic effective width method and Class 3 slenderness limit given in EN 1993-1-4 (2006) and those revised by Gardner and Theofanous (2008), which neglect such interaction effects, as well as alternative design approaches that account for element interaction. For these latter methods, the Direct Strength Method (DSM) developed by Schafer (2008) and adapted for stainless steel by Becque et al. (2008), the regression analysis method proposed by Kato (1989) and modified by Theofanous and Gardner (2011), and the effective cross-section method proposed by Zhou et al. (2013) were considered. One additional design approach worthy of mention, but not detailed here further as its potential is exploited for more complex cross-sections than those considered herein, is the Generalised Beam Theory (GBT) pioneered by Schardt (1989) in Germany, extended by Davies and Leach (1994) and Davies et al. (1994) in Britain, and actively upgraded over the last years by Camotim and his colleagues in Portugal, Gonçalves and Camotim (2004) and Abambres et al. (2014).

Finally, a modification is set out to level the effective width method with those alternative design approaches inserting the aspect ratio within both the reduction factor  $\rho$  equation and the Class 3 limiting slenderness value. The proposed amendment is statistically validated following the guidelines given in Annex D of EN 1990 (2002) and compared with existing test results to verify its applicability to all stainless steel families.

## 7.2 Numerical investigation

### 7.2.1 Modelled stub column tests

The experimental investigation conducted by Bock et al. (2014d) on cold-formed ferritic stainless steel tubular sections is considered herein to develop and validate a comprehensive FE model using the FE package ABAQUS. Bock et al. (2014d) reported the results of 8 stub column tests performed on 4 different section geometries (two repeated tests on each cross-section), including the measurements of such geometries and initial local imperfections  $w_0$ , as given in Table 7.1 where  $L$  is the length of the specimen,  $H$  is the overall height,  $B$  is the overall width,  $t$  is the thickness,  $r_i$  is the internal corner radius and  $A$  is the gross cross-sectional area, see Fig. 7.1. Note that

these tests were particularly suitable to validate the FE model owing to the various aspect ratios of the specimens.

Material properties were derived from coupon tests in Bock et al. (2014d), including tensile flat and corner coupons. The formers were extracted from flat faces of the specimens whereas the latters were taken from the curved portions of each of the cross-sections to quantify the corner strength enhancements induced by the cold-forming process, Ashraf et al. (2005).

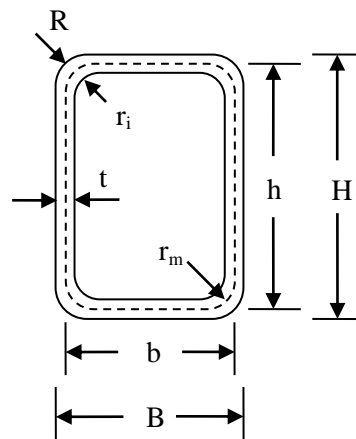


Fig. 7.1 Definition of symbols

Table 7.1 Measured dimensions and test results given in Bock et al. (2014d)

Specimen	L (mm)	H (mm)	B (mm)	t (mm)	R (mm)	$r_i$ (mm)	A (mm <sup>2</sup> )	$w_0$ (mm)	$N_{u,tests}$ (kN)	$\delta_u$ (mm)
60×60×2-SC1	179.5	60.3	60.3	2.00	4.4	2.4	454	0.02	211.37	1.02
60×60×2-SC2	180.0	60.3	60.4	2.02	4.4	2.3	460	0.02	212.31	1.03
70×50×2-SC1	210.0	70.1	49.9	2.00	4.3	2.3	451	0.03	190.15	0.87
70×50×2-SC2	210.0	70.0	49.8	1.99	4.2	2.2	450	0.03	190.05	0.84
80×40×2-SC1	240.0	80.0	40.5	2.00	3.3	1.3	457	0.06	178.21	0.80
80×40×2-SC2	240.0	80.0	40.3	1.99	3.9	1.9	453	0.06	179.52	0.82
100×40×2-SC1	299.5	100.1	40.0	2.05	4.1	2.1	546	0.07	184.23	0.97
100×40×2-SC2	299.5	100.1	40.5	1.99	4.2	2.2	532	0.07	183.99	0.92

Experimental observations in the corner regions performed by Cruise and Gardner (2008b) concluded that this enhanced strength extends into the flat regions by a distance equal to two times the material thickness. This remark has been used in previous numerical studies on other stainless steel grades (Gardner and Nethercot (2004b) and Ashraf and Gardner (2006)) and adopted herein. Measurements of residual stresses were not explicitly taken in Bock et al. (2014d) since they are inherently present (i.e. through-thickness residual stresses) in material properties extracted from cold-formed sections (Rasmussen and Hancock (1993b)) and have shown little influence on the cross-

sectional response, Cruise and Gardner (2008b). The material properties determined in Bock et al. (2014d) are summarized in Table 7.2 for the four sections where the reported parameters are the Young's modulus  $E$ , the 0.01%, 0.05% and 0.2% proof stress  $\sigma_{0.01}$ ,  $\sigma_{0.05}$  and  $\sigma_{0.2}$ , respectively, and the ultimate stress  $\sigma_u$  with its corresponding ultimate strain  $\epsilon_u$ . Table 7.3 gives the weighted average values based on face width and corner properties extended two times the thickness through the flat region for all the tested specimens while Table 7.4 shows the average material properties of all the flat and corner tensile coupon tests. These sets of material properties are used in the following sections to assess their influence on the numerical response.

Table 7.2 Measured material properties for the sections given in Bock et al. (2014d)

Section	Portion	E (Gpa)	$\sigma_{0.01}$ (MPa)	$\sigma_{0.05}$ (MPa)	$\sigma_{0.2}$ (MPa)	$\sigma_u$ (MPa)	$\epsilon_u$
SHS 60×60×2	Flat	167	327	389	431	478	0.111
	Corner	167	360	471	548	568	0.008
RHS 70×50×2	Flat	176	324	380	419	480	0.138
	Corner	179	382	484	555	574	0.012
RHS 80×40×2	Flat	177	326	381	418	485	0.143
	Corner	181	380	474	572	595	0.008
RHS 100×40×2	Flat	178	333	384	416	483	0.133
	Corner	180	371	463	553	579	0.001

Table 7.3 Weighted average tensile material properties given in Bock et al. (2014d)

Specimen	E (Gpa)	$\sigma_{0.01}$ (MPa)	$\sigma_{0.05}$ (MPa)	$\sigma_{0.2}$ (MPa)	$\sigma_u$ (MPa)	$\epsilon_u$
60×60×2-SC1	167	335	409	458	499	0.087
60×60×2-SC2	167	335	409	458	499	0.087
70×50×2-SC1	176	337	404	450	502	0.108
70×50×2-SC2	176	337	404	450	501	0.109
80×40×2-SC1	177	338	399	449	507	0.116
80×40×2-SC2	177	339	399	452	509	0.113
100×40×2-SC1	178	340	399	443	502	0.109
100×40×2-SC2	178	341	399	442	501	0.109

Table 7.4 Average material properties based on all tensile coupons for the portions

Portion	E (Gpa)	$\sigma_{0.01}$ (MPa)	$\sigma_{0.05}$ (MPa)	$\sigma_{0.2}$ (MPa)	$\sigma_u$ (MPa)	$\epsilon_u$
Flat	174	328	383	421	481	0.131
Corner	177	373	473	557	579	0.009

All the specimens were uniformly compressed between flat platens in an Instron 1000kN hydraulic testing machine which was driven by displacement control. The achieved test load  $N_{u,test}$  and its corresponding specimen's end shortening  $\delta_u$  is given in Table 7.1.

### 7.2.2 Finite element model

The FE analysis package ABAQUS was used to simulate the cross-sectional response of the 8 ferritic stainless steel compression SHS and RHS tested in Bock et al. (2014d). The measured geometric properties given in Table 7.1 were used in the FE model, which was based on the centreline dimensions of the cross-sections  $h \times b \times r_m$  (see Fig. 7.1). The geometry of all the specimens was discretized using the four-noded doubly curved shell element with reduced integration S4R (Rasmussen et al. (2003) and Ellobody and Young (2005)), including both flat parts and curved regions of the cross-sections. The geometry of these latter ones was approximated by 3 linear elements. The flat regions adjacent on either side of the corners, which are affected by the cold-forming process exhibiting enhanced strength, were discretized using two elements, each of them with size equal to the thickness of the cross-section. For the remainder flat portion, mesh studies were conducted to achieve accurate results while minimizing computational time obtaining a suitable mesh size of  $8 \times 8$  mm.

Owing to the double symmetry of the geometry, boundary conditions, applied loads and observed failure modes in the experimental investigation undertaken by Bock et al. (2014d), only a quarter of the section with suitable boundary conditions applied along the symmetry axes was modelled thereby saving computational cost. The full length of the stub column was modelled for all the cross-sections. Both ends of the cross-section were restrained against all degrees of freedom except the vertical displacement at the top loaded end, which was constrained using kinematic coupling to ensure the uniform vertical compression represented by a vertical displacement applied to the reference point of the constraint.

An assessment of the influence of material properties on the structural response of the ferritic stainless steel stub column models was conducted by assigning various material properties to the different regions of the models. Three cases were considered: case I uses the material properties of each specimen, as given in Table 7.2, assigning corner material properties to the corresponding corner regions of the models and to the adjacent flat region extended up to two times the thickness of the cross-section while assigning flat material properties to the remainder regions; case II assigns the weighted average material properties of each specimen, as given in Table 7.3, to all the regions of the cross-section; and case III uses average material properties based on all the corner

coupons and the flat coupons, as given in Table 7.4, assigning the former to the corner regions of all the stub column models, including the extended adjacent flat region, and the latter to the remainder regions of all the stub column models. Each particular case of study enables the identification of various situations commonly assumed in numerical modelling. While case I concerns the most realistic case involving the knowledge of the actual material properties of the cross-section, cases II and III resemble a theoretical situation and are particularly appropriate to assess the accuracy of the FE model for a theoretical material (e.g. the material adopted in further parametric studies). Despite case II may be considered the least realistic one; it is simpler to incorporate into the FE and may reduce the computational time associated with models assembled with different materials. This latter approach was used in previous numerical investigations on ferritic stainless steels and showed to accurately match test data, Bock et al. (2014c).

For each set of assumed material properties, the whole stress-strain response of ferritic stainless steel was simulated employing a compound version of the original Ramberg and Osgood (1943) material model proposed by Mirambell and Real (2000), modified by Rasmussen (2003) and given in Annex D of EN 1993-1-4 (2006) in terms of a multi-linear curve with parameters given in Tables 7.2-7.4. The elastic part of the multi-linear curve was described by measured Young's modulus and Poisson's ratio of 0.3 whereas the plastic part was incorporated into the FE converting the nominal (engineering) stress-strain curve into true stress  $\sigma_{true}$  and logarithmic plastic strain  $\varepsilon_{pl}$  curve, as given by Eqs (7.1) and (7.2), respectively.

$$\sigma_{true} = \sigma_{nom}(1 + \varepsilon_{nom}) \quad (7.1)$$

$$\varepsilon_{pl} = \ln(1 + \varepsilon_{nom}) - \frac{\sigma_{true}}{E} \quad (7.2)$$

Initial geometric imperfections were incorporated into the FE models as the lowest local buckling mode shape. The shape was determined through a linear eigenvalue buckling analyses and the amplitude was limited to a certain magnitude. In order to assess the influence of such limiting magnitudes on the structural response, various local imperfection amplitudes were considered: the maximum measured local imperfection  $w_0$  reported in Table 7.1; 1/100 of the cross-sectional thickness; and the value derived from the predictive model (Dawson and Walker (1972) and Gardner and Nethercot

(2004)) of Eq. (7.3), where  $t$  is the plate thickness,  $\sigma_{0.2}$  is the material 0.2% proof stress and  $\sigma_{cr}$  is the elastic buckling stress of the cross-section plate elements assuming simply supported conditions. The modified Riks method was used for the geometrically and materially nonlinear analyses to determine the load-end shortening response and failure modes of all the stub column models.

$$w_0 = 0.023 \left( \frac{\sigma_{0.2}}{\sigma_{cr}} \right) t \quad (7.3)$$

### 7.2.3 Validation of the numerical model

The obtained ultimate numerical loads  $N_{u,num}$  and corresponding end shortenings  $\delta_{u,num}$  of the specimens are compared with the test counterparts  $N_{u,test}$  and  $\delta_{u,test}$  reported in Bock et al. (2014d) to assess the sensitivity of the FE model to different some key modelling parameters and the precision to reproduce the actual structural response. The comparisons are given in Table 7.5 where the influence of the various imperfection amplitudes on the numerical response for the studied cases with different material properties (cases I, II and III) is presented.

The results show that for case I, the numerical model better matches the actual structural behavior when the measured imperfection amplitude is used with normalised mean test to numerical ratios of 1.00 and small coefficient of variation (COV) of 0.03. The ultimate end shortening displacement is less precise yet accurately predicted. It is also observed excellent good agreement between test and numerical results for the imperfection amplitude given by Eq. (7.3) thereby reflecting the accuracy of its predictions. All the models generated in case I failed by local buckling at mid height as shown in Fig. 7.2 where it is observed that the numerical model successfully replicates structural behavior. However, for specimen  $80 \times 40 \times 2$ , the achieved deformed shape for the imperfection amplitude  $t/100$  did not resembled typical local buckling failure mode displaying out of plane deformations near to the edges. This was associated with the small values provided by this imperfection value of  $t/100$  which also derived in slightly over-predictions of the test results. Hence, on the basis of this comparison, the suitability of the predictive model for the imperfection amplitude given in Eq. (7.3) was assessed for cases II and III. The results given in Table 7.5 show the reliability of the numerical model for this imperfection amplitude with normalised mean values of 1.01 and 1.01, and COV of 0.03 and 0.02 for case II and III, respectively. Given their

accuracy, both approaches could be used in further parametric studies but it is believed that case III provides the models with more realistic material properties. Recall that this case differentiates the material properties of the flat portions and the corners of the cross-section while case II incorporates uniform cross-sectional material properties based on weighted average estimation. Thereby, an approach based on case III material properties and imperfection amplitude predicted by Eq. (7.3) was used in the parametric study.

The full load-displacement curves predicted by this approach together with the experimental ones are compared in Figs 7.3 and 7.4 for the first (SC1) and second (SC2) set of test results, respectively

Table 7.5 Comparison between test results and FE predictions for various materials and imperfection amplitudes

Specimen	Case I				Case II				Case III	
	Measured $w_0$		Model Eq. (7.3)		$t/100$		Model Eq. (7.3)		Model Eq. (7.3)	
	$N_{u,test}/N_{u,num}$	$\delta_{u,test}/\delta_{u,num}$	$N_{u,test}/N_{u,num}$	$\delta_{u,test}/\delta_{u,num}$	$N_{u,test}/N_{u,num}$	$\delta_{u,test}/\delta_{u,num}$	$N_{u,test}/N_{u,num}$	$\delta_{u,test}/\delta_{u,num}$	$N_{u,test}/N_{u,num}$	$\delta_{u,test}/\delta_{u,num}$
60×60×2-SC1	1.03	1.33	1.04	1.36	1.03	1.34	1.04	1.36	1.03	1.34
60×60×2-SC2	1.02	1.32	1.02	1.35	1.02	1.33	1.02	1.35	1.05	1.33
70×50×2-SC1	1.01	1.02	1.01	1.02	0.99	1.02	1.01	1.02	0.99	0.96
70×50×2-SC2	0.97	1.05	0.96	1.05	0.95	1.03	0.96	1.05	0.99	1.09
80×40×2-SC1	0.96	1.13	0.96	1.10	0.91 <sup>a</sup>	0.94	0.96	1.10	1.00	1.12
80×40×2-SC2	0.98	1.14	1.02	1.40	0.96 <sup>a</sup>	1.09	1.02	1.40	1.02	1.13
100×40×2-SC1	1.04	1.03	1.04	1.01	1.01	1.49	1.04	1.01	0.97	1.28
100×40×2-SC2	1.00	1.21	1.00	1.24	0.97	1.47	1.00	1.24	1.01	1.17
Mean	1.00	1.15	1.01	1.19	0.98	1.21	1.01	1.19	1.01	1.18
COV	0.03	0.10	0.03	0.13	0.04	0.17	0.03	0.13	0.02	0.10

<sup>a</sup> Failure at both edges

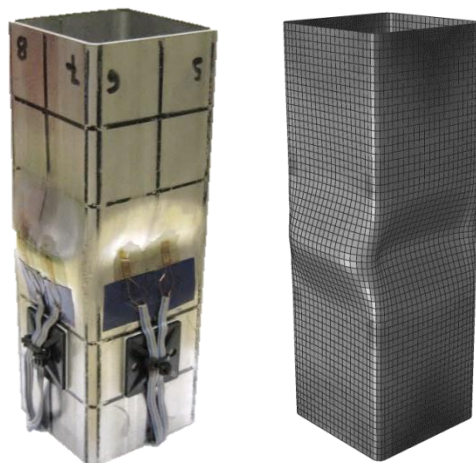


Fig. 7.2 Comparison between test (left) and FE (right) failure mode for specimen 60×60×2-SC1



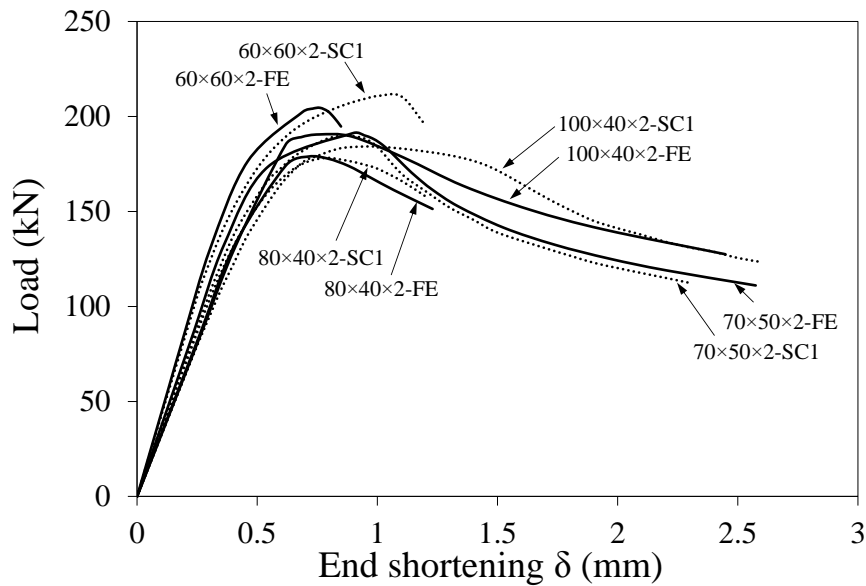


Fig. 7.3 Load-displacement response based on case III and initial imperfection of Eq. (7.3) for the first set of tests

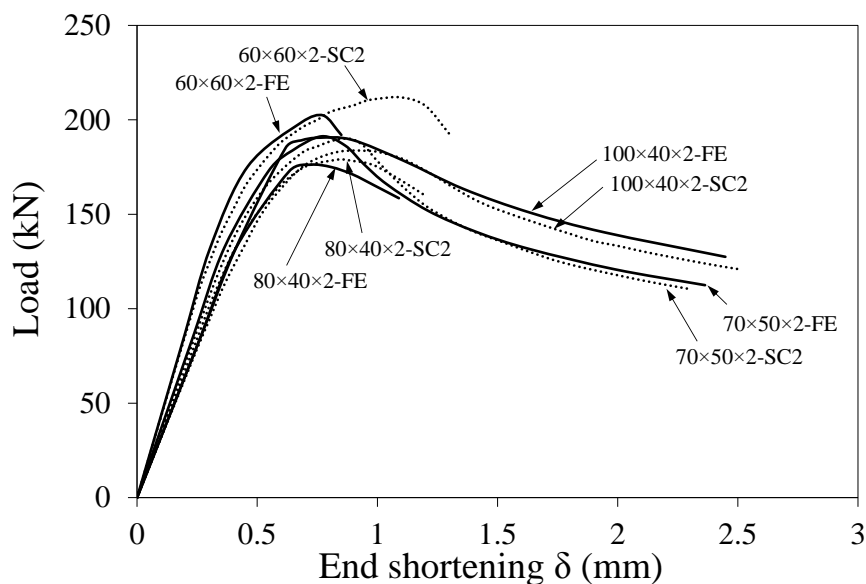


Fig. 7.4 Load-displacement response based on case III and initial imperfection of Eq. (7.3) for the second set of tests

#### 7.2.4 Parametric studies

Once the FE model was deemed reliable, parametric studies were performed for the extrapolation of the test data to investigate the effects of element interaction in square and rectangular sections comprising slender elements and assess the applicability of various approaches for the treatment of local buckling to ferritic stainless steel. The cross-sections under consideration were 3 SHS and 9 RHS with aspect ratios ranging from 1 to 4. The cross-section geometry of the RHS was carefully taken so that local buckling behaviour and ultimate capacity of the section is controlled by at most two

cross-sectional elements. The cross-section geometries were (h×b): 60×60, 80×80 and 100×100 for the SHS; and 100×80, 80×60, 80×50, 100×60, 80×40, 100×50, 100×40, 120×40 and 160×40. The thickness was varied between 6 to 1 mm for the 160×40 cross-sections, between 4 to 1 for the 120×40 cross-sections, between 3.5 to 1 for the 100×40 and 100×50 cross-sections, and between 3 and 1 for the remain cross-sections thereby covering a spectrum of slendernesses defined by the parameter  $c/t\epsilon$  from 24.6 to 236.6, where  $c$  is the flat width of the cross-section plate element,  $t$  is the thickness and  $\epsilon = [(235/\sigma_{0.2})(E/210000)]^{0.5}$ . The length of all the models was set equal to three times the largest cross-section dimension as recommended in EN 1993-1-4 (2006). The material properties adopted are given in Table 7.4, which were appropriately assigned to the different regions of the models as discussed above, and the local imperfection amplitude was predicted through Eq. (7.3). A total number of 124 models were generated.

### **7.3 Methods for cross-section design and discussion of results**

#### **7.3.1 General**

In the following sub-sections, the obtained numerical results are used to assess the applicability of available design approaches for cross-section design that were developed for carbon steel and/or other stainless steel to ferritic stainless steel. Various methods have been considered: methods based on effective width theory and cross-section classification concept which neglect interaction effects and include the approach given in EN 1993-1-4 (2006) and revised by Gardner and Theofanous (2008); the regression analysis method proposed by Kato (1989) and modified by Theofanous and Gardner (2011) which explicitly compute the local buckling resistance and allow for element interaction; and methods based on gross cross-section that also allow element interaction including the Direct Strength Method (DSM) developed by Schafer (2008) and adapted for stainless steel by Becque et al. (2008) and the effective cross-section method proposed by Zhou et al. (2013). These design approaches are first outlined and their performance and application to ferritic stainless steel is assessed thereafter. A comparison of the predicted cross-section resistances by those methods is given and discussed. For the various appraisals, all partial safety factors were set to unity to allow a direct comparison between predicted  $N_{u,pred}$  and numerical loads achieved in the models  $N_{u,num}$ .

### 7.3.2 Available methods for cross-section design

#### 7.3.2.1 The effective width method

The treatment of local buckling within the European design rules for application to stainless steel, EN 1993-1-4 (2006), is underpinned by the concept of cross-section classification and the effective width method. The slenderness of each compression part in a cross-section expressed by the parameter  $c/te$ , where  $c$  is the flat width of the cross-section plate element,  $t$  is the thickness and  $\varepsilon = [(235/\sigma_{0.2})(E/210000)]^{0.5}$ , is compared with limiting slenderness values and placed into four discrete behavioural classes (Class 1-4) and the whole cross-section adopts the behaviour of the most unfavorable (slender) plate element. These slenderness limits depend on the nature of the cross-section, the type of the plate elements (internal elements or outstand flanges) and their stress gradient. The Class 3 limiting value mark the boundary between fully effective or stocky cross-sections (Class 1-3) and those that lose effectiveness due to local buckling effects (Class 4). The cross-sectional design of Class 4 or slender cross-sections is dealt with the effective width method which applies a reduction factor  $\rho$  to determine the effective widths of the individual plate elements. Eqs (7.4) and (7.5) provide the current expression of this reduction factor  $\rho$  for internal elements given in EN 1993-1-4 (2006) and the one revised by Gardner and Theofanous (2008), respectively, where  $\bar{\lambda}_p = \sqrt{\sigma_{0.2}/\sigma_{cr}}$  is the non-dimensional plate slenderness. This parameter requires the elastic buckling stress  $\sigma_{cr}$  of the most slender constituent plate element for its computation which can be determined by using the classical analytical expressions for individual plates  $\sigma_{cr} = k_\sigma \pi^2 E (t/h)^2 / 12(1 - \nu^2)$  as given by EN 1993-1-5 (2006). The stress distribution of the plate element is considered through the buckling factor  $k_\sigma$  which assumes simply support conditions at the plate edges thereby neglecting the above mentioned element interaction effects in RHS.  $k_\sigma$  is taken as 4.0 for internal elements in compression.

$$\rho = \frac{0.772}{\bar{\lambda}_p} - \frac{0.125}{\bar{\lambda}_p^2} \leq 1 \text{ For internal elements with } \bar{\lambda}_p \geq 0.541 \quad (7.4)$$

$$\rho = \frac{0.772}{\bar{\lambda}_p} - \frac{0.079}{\bar{\lambda}_p^2} \leq 1 \text{ For internal elements with } \bar{\lambda}_p \geq 0.651 \quad (7.5)$$

The application limit of the effective width method is established setting the reduction factor  $\rho$  to unity and deducting the non-dimensional slenderness  $\bar{\lambda}_p$ . The resulting boundaries are given in Eqs (7.4) and (7.5) for the approaches under consideration

which can also be expressed in terms of the slenderness parameter through  $c/t\varepsilon=56.8\bar{\lambda}_p$  to define the Class 3 slenderness limiting value. Hence, for internal elements in compression, EN 1993-1-4 (2006) establishes a Class 3 slenderness limit of 30.7 while the revised equation by Gardner and Theofanous (2008) sets a less restrictive value of 37. It should be mentioned that this revised equation for  $\rho$  proposed in Gardner and Theofanous (2008) as given by Eq. (7.5) has been considered in the present study as it showed to improve cross-section resistance predictions, Bock et al. (2014d).

The cross-sectional properties are determined for the effective cross-section and a simple bi-linear elastic-perfectly plastic stress strain material model is assumed with attainable maximum stresses of  $\sigma_{0.2}$ . This simplification, which is a merely adoption of the structural carbon steel material response deviates of the actual stress-strain behavior of stainless steel which display considerable strain hardening and might lead to over-conservative predictions especially for stocky cross-sections where failure occurs at stress levels beyond  $\sigma_{0.2}$ . Unlike slender sections, where local buckling occurs prior to yielding, the effects of element interaction are of little significance in stocky cross-sections since material strain hardening strongly influences and controls their structural response. Exploitation of the material strain hardening properties has been examined elsewhere, Afshan and Gardner (2013b) and Bock et al. (2014c).

Although EN 1993-1-4 (2006) currently includes three ferritic grades (1.4003, 1.4016 and 1.4512), the applicability of the cross-section design provisions for the treatment of local buckling is yet to be validated. This has been performed in existing investigations conducted by Bock et al. (2014c, 2014d) and extended herein for cross-sections with different aspect ratios.

### 7.3.2.2 The regression analysis design method

The regression analysis design method was firstly proposed by Kato (1989, 1990) while examining the flange-web interaction and the material strain hardening influence on the rotation capacity response. Through regression analysis of available test data on stub columns, it was proposed a semi-empiric design method to determine the normalised local buckling strength in terms of the  $\sigma_{0.2}/\sigma_{cr}$  ratio, upon which to base rotation capacity predictions. The general form of this equation is given by Eq. (7.6), where  $\alpha_f$  and the web  $\alpha_w$  are slenderness parameters of the flange and the web respectively, and A, B and C are coefficients to fit in with data. Owing to its simplicity and

appropriateness coupled with its explicit nature to allow for both element interaction effects and material strain hardening therefore also suitable for cross-section design of stocky sections, this versatile model, has been adapted to predict ultimate capacities of various section types and materials including, carbon and high strength steel I-section beams in flexure (Daali and Korol (1995) and Beg and Hladnik (1995)) as well as stainless steel cross-sections in compression. This latter study was performed by Theofanous and Gardner (2011), where regression analyses of numerical data on austenitic and duplex stainless steels compressed RHS resulted in the expression given in Eq. (7.7) where  $\sigma_{LB}=N_u/A$  is the stress at which local buckling occurs and  $\bar{\lambda}_{p,f}$  and  $\bar{\lambda}_{p,w}$  are the flange and web non-dimensional slenderness, respectively. The suitability of this method for application to ferritic stainless steel needs to be verified.

$$\frac{\sigma_{0.2}}{\sigma_{cr}} = A + \frac{B}{\alpha_f} + \frac{C}{\alpha_w} \quad (7.6)$$

$$\frac{\sigma_{0.2}}{\sigma_{LB}} = 0.53 + 0.1\bar{\lambda}_{p,f} + 0.6\bar{\lambda}_{p,w} \quad (7.7)$$

### 7.3.2.3 The direct strength method (DSM)

Slender cross-sections are well-established construction products that offer optimum dimensions to suit structural requirements. Due to the resulting optimized cross-section geometry, which often involves the usage of edge and/or intermediate stiffeners, leads the designers to deal with complex failure modes and interaction effects thereof. The direct strength method (DSM) has been pioneered by Schafer (2008) and is based upon the idea that when all the elastic buckling instabilities for the gross cross-section are determined, the strength can be computed through a slenderness based reduction factor  $\rho$  related to the type of buckling applied to the axial load (or moment if it is a beam) that causes the section to yield. A specific piece of software based on the constrained Finite Strip Method named CUFSM has been developed (Schafer and Ádány (2006)) to determine the elastic buckling instabilities. Its usage within the DSM is not mandatory but highly recommended to account for the non-linear behavior of cold-formed steel members and exploit the potential of the DSM. The DSM was adopted in the North American AISI S100-12 (2012) design rules and the Australian AS/NZS 4600 (2005) specifications for cold-formed steel as an alternative design approach for cross-section and beam design of structural steel when the effective width method turns into tedious calculations owing to the complexity of the geometry of the cross-section.

Investigation towards the adaptation of the DSM for stainless steel was performed by Becque et al. (2008), where direct strength curves for flexural, torsional and flexural-torsional buckling were derived based on a database of experimental and numerical studies on stainless steel SHS, RHS, I-section and lipped channel sections. The DSM curve considered in the present paper for local buckling design is the proposed curve by Becque et al. (2008) for flexural buckling given in Eq. (7.8) where  $\bar{\lambda}_{cs} = \sqrt{\sigma_{0.2}/\sigma_{cr,cs}}$  is the non-dimensional slenderness of the cross-section computed by using the open source software CUFSM to determine the elastic critical stress of the cross-section  $\sigma_{cr,cs}$ . The cross-section resistance is therefore determined multiplying this reduction factor by the yield resistance  $A\sigma_{0.2}$ . Note that the DSM also limits the 0.2% proof stress as the maximum attainable stress thereby neglecting the strain hardening effects. Moreover, the method turns into conservative predictions for very slender cross-sections since the cross-section is treated as a single element assuming that if a small slender element locally buckles, the whole cross-section undergoes local buckling. Its performance for design of ferritic stainless steel slender SHS and RHS is assessed in the present study.

$$\rho = \frac{0.95}{\bar{\lambda}_{cs}} - \frac{0.22}{\bar{\lambda}_{cs}^2} \quad \text{For } \bar{\lambda}_{cs} > 0.55 \quad (7.8)$$

#### 7.3.2.4 The effective cross-section method

The underlying concept of the effective cross-section method proposed by Zhou et al. (2013) steams from the same principles of the effective width method in terms of cross-section classification deducting the ineffective areas of the cross-section due to local buckling effects. What differentiates the method is that the reduction factor  $\rho$  given in Eq. (7.9) is applied to the gross cross-sectional area instead of to the individual plate elements. Moreover, this design method incorporates a function  $\phi(\alpha)$  of the aspect ratio  $\alpha$  thereby enabling to consider explicitly interaction effects as given by Eq. (7.10). The non-dimensional slenderness is determined in the same way as within the effective width method. In order to ensure continuity with this reduction factor  $\rho$ , Zhou et al. (2013) also derived a Class 3 slenderness limit function of the aspect ratio  $\alpha$  as given by Eq. (7.11). The coefficients of Eqs (7.9)-(7.11) were determined through regression analyses of numerical data on high strength stainless steel compressed SHS and RHS and the method applies when  $1 \leq \alpha \leq 6$ ,  $448 \leq \sigma_{0.2} \leq 707$  MPa and  $27.3 \leq c/t \leq 91$  (or

$0.48 \leq \bar{\lambda}_p \leq 1.6$ ). The suitability of this method for application to ferritic stainless steel was first experimentally examined in Bock et al. (2014d) where it was stated the necessity to undertake further research on this topic and this is conducted herein.

$$\rho = \begin{cases} \frac{0.772}{\bar{\lambda}_p} \phi(\alpha) - \frac{0.059}{\bar{\lambda}_p^2} \phi(\alpha)^2 + 0.01\alpha \bar{\lambda}_p^{-2} \leq 1 & \text{For } \bar{\lambda}_p > 0.686 \text{ and } 1 \leq \alpha \leq 3 \\ \frac{0.907}{\bar{\lambda}_p} - \frac{0.081}{\bar{\lambda}_p^2} + 0.03\bar{\lambda}_p^{-2} \leq 1 & \text{For } \bar{\lambda}_p > 0.686 \text{ and } \alpha > 3 \end{cases} \quad (7.9)$$

$$\phi(\alpha) = \frac{30.5 + 10.2\alpha - 1.7\alpha^2}{39} \quad \text{For } 1 \leq \alpha \leq 3 \quad (7.10)$$

$$\frac{c}{t\varepsilon} = \begin{cases} 30.5 + 10.2\alpha - 1.7\alpha^2 & \text{For } 1 \leq \alpha \leq 3 \\ 45.8 & \text{For } \alpha > 3 \end{cases} \quad (7.11)$$

### 7.3.3 Assessment of the design methods

#### 7.3.3.1 Methods based on plate width

For this assessment, the reduction factor of the most slender constituent element of the cross-section defined as  $\rho = (N_{u,num}/\sigma_{0.2} - A_r - 2 \cdot t \cdot c_f)/2 \cdot t \cdot c_w$ , where  $N_{u,num}$  is the ultimate load achieved in the numerical models,  $\sigma_{0.2}$  is the 0.2% proof stress,  $A_r$  is the area of the corners,  $t$  is the thickness and  $c_f$  and  $c_w$  are the flat portion of the flange and the web, respectively, is plotted against the non-dimensional slenderness  $\bar{\lambda}_p$  of the element controlling local buckling behaviour in Fig. 7.5 where the trends of the numerical results for varying aspect ratios  $\alpha=h/b$  are shown. The corresponding effective width equation given in EN 1993-1-4 (2006) and proposed in Gardner and Theofanous (2008) are also depicted. In Fig. 7.5 it is observed that the trends of the numerical results for  $\alpha>1$  (RHS) display higher values for the reduction factor to their SHS ( $\alpha=1$ ) counterparts of equal non-dimensional slenderness  $\bar{\lambda}_p$  exhibiting the higher level of restraint provided by the narrow parts to the slender elements of the RHS cross-sections. The trends corresponding to the various RHS curves converge towards the SHS curve at higher slenderness values for higher aspect ratios reflecting the plate slenderness up to which the effects of element interaction are beneficial for the various aspect ratios. Fig. 7.5 also shows that the effective width equation for internal compressed elements given in EN 1993-1-4 (2006) is safe for application to ferritic stainless steel, though the expression proposed by Gardner and Theofanous (2008) falls closer to the numerical data thereby leading to improved cross-section resistance predictions.

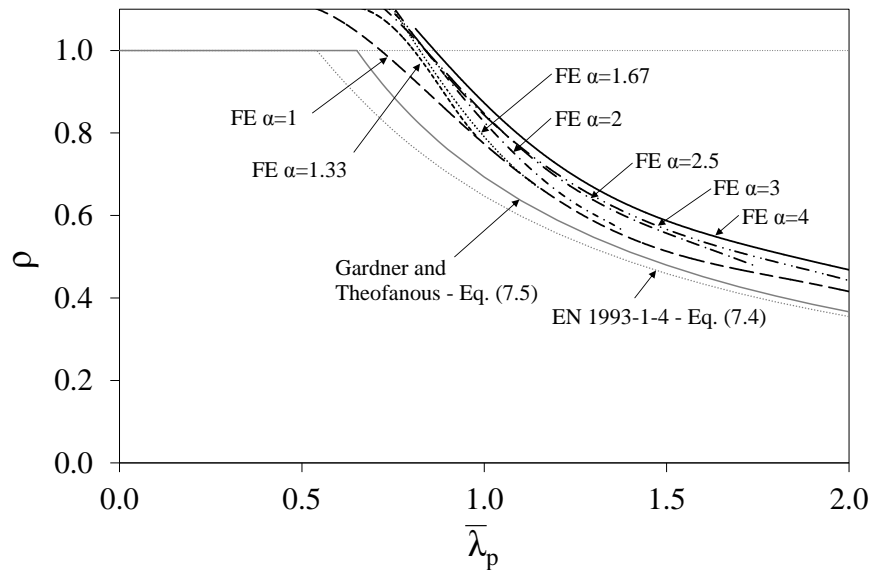


Fig. 7.5 Assessment of methods based on effective plate width (EN 1993-1-4 (2006) and Gardner and Theofanous (2008))

### 7.3.3.2 Regression analysis method

The appraisal of the equation given in Eq. (7.7) (Theofanous and Gardner (2011)) is shown in Fig. 7.6 in terms of normalized ultimate load by the yield resistance  $A\sigma_{0.2}$ . The results show that the equation to allow for element interaction effects for austenitic and duplex stainless steels proposed by Theofanous and Gardner (2011) is applicable to ferritic stainless steel providing fairly appropriate predictions. A maximum unsafe discrepancy of 3%, yet acceptable, is observed between the predicted values and the limiting partial safety factor line of  $\gamma_{M0}=1.1$ , which is the value recommended in EN 1993-1-4 (2006), for the points falling below this line as shown in Fig. 7.6.

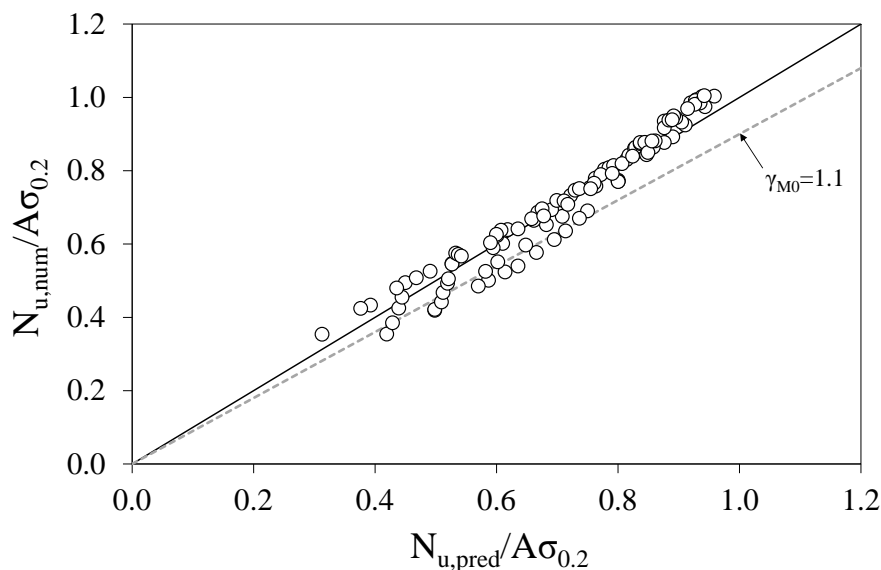


Fig. 7.6 Comparison between numerical and predicted resistances for the regression analysis method proposed in Theofanous and Gardner (2011)



### 7.3.3.3 Methods based on gross cross-section

The methods assessed herein are the DSM for stainless steel developed by Becque et al. (2008) and the effective cross-section method proposed by Zhou et al. (2013). The ultimate numerical load normalised by the squash load has been plotted against the non-dimensional cross-section slenderness  $\bar{\lambda}_{cs}$  determined by using the CUFSM for the former approach and the slenderness of the most slender plate  $\bar{\lambda}_p$  for the latter method in Figs 7.7 and 7.8, respectively.

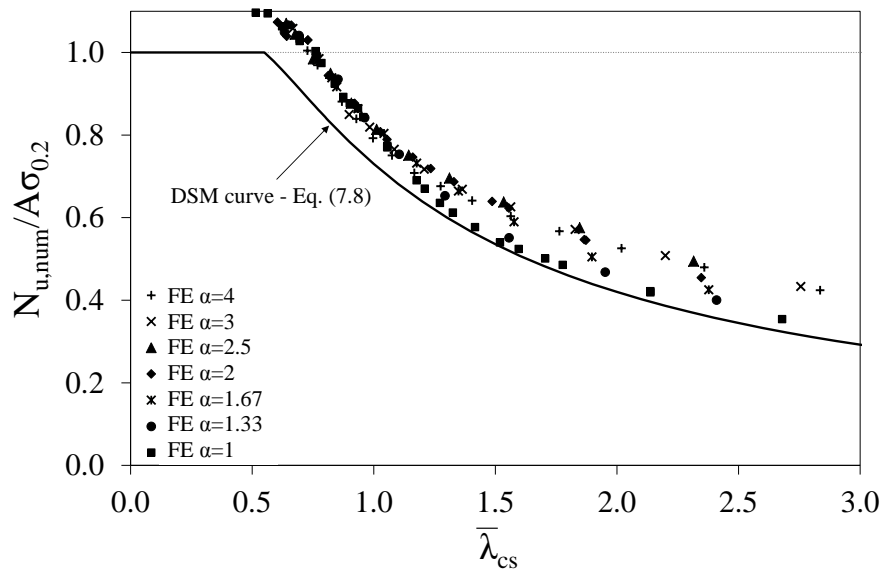


Fig. 7.7 Performance of the DSM (Becque et al. (2008)) when applied to ferritic stainless steel

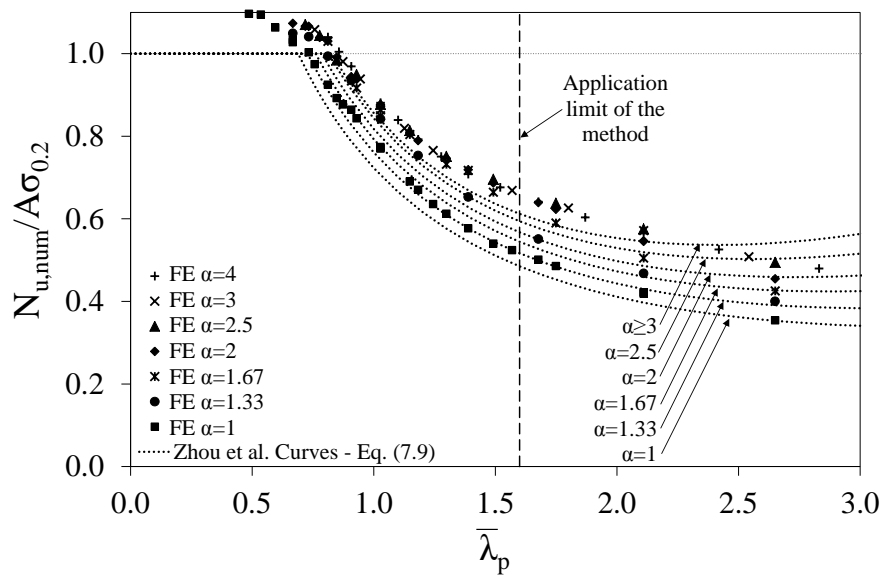


Fig. 7.8 Assessment of the method proposed by Zhou et al. (2013)

The results depicted in Fig. 7.7 show that the DSM curve (Becque et al. (2008)) falls below the numerical results thereby providing safe predictions for ferritic stainless steel, though the method is slightly conservative for  $\alpha > 1$  when  $\bar{\lambda}_{cs}$  increases. Fig. 7.8 show that the curves proposed by Zhou et al. (2013) better match the numerical results for  $\bar{\lambda}_p \leq 2.11$  but might provide optimistic results when  $\bar{\lambda}_p > 2.11$ . This is associated with the application limit of the method in terms of  $\bar{\lambda}_p$  which was set out as  $0.48 \leq \bar{\lambda}_p \leq 1.6$ . Note that despite this, the method provides safe predictions for the numerical data falling between  $1.6 \leq \bar{\lambda}_p \leq 2.11$ . In assessing the suitability of the Class 3 slenderness limits as a function of the aspect ratio proposed by Zhou et al. (2013) for application to ferritic stainless steel, the normalized ultimate numerical load has been plotted against the slenderness parameter  $c/t\epsilon$  of the most slender constituent plate element in Fig. 7.9, together with the Class 3 limit given in EN 1993-1-4 (2006) and revised value proposed by Gardner and Theofanous (2008) for comparison purposes. From Fig. 7.9, it is observed good agreement between the numerical data and the various slenderness limiting values related to their corresponding aspect ratios. Hence, it can be concluded that Zhou et al. (2013) approach is suitable for the design of ferritic stainless steel cross-sections when  $\bar{\lambda}_p \leq 2.11$  but provides optimistic predictions when  $\bar{\lambda}_p > 2.11$ .

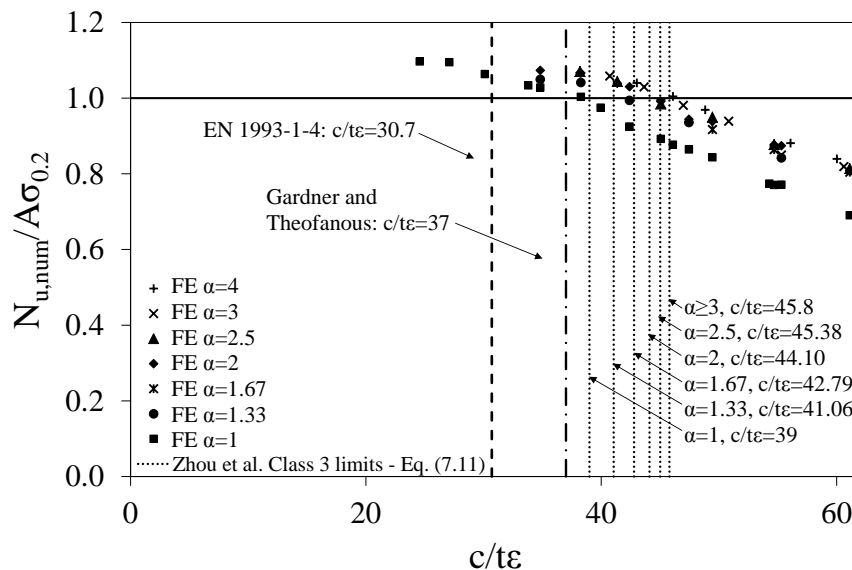


Fig. 7.9 Assessment of the Class 3 slenderness limits proposed by Zhou et al. (2013)

### 7.3.3.4 Discussion

Overall, all the methods assessed along the previous sub-sections showed safe predictions for application to ferritic stainless steel. This is summarized in Table 7.6 where the mean predictions and coefficient of variation (COV) of the various design approaches relative to the numerical results are given. This table provides the results for various sets of data where only those cross-sections failing prior to the attainment of the yield resistance ( $N_{u,num} < A\sigma_{0.2}$ ) were considered to enable a more representative comparison among the various methods. The results show that the most accurate mean predictions are provided by the regression analysis method adapted for stainless steel by Theofanous and Gardner (2011) with mean values of 1.004, though the method is too optimistic for SHS. Conversely, the results do not highlight the potential of the DSM adapter for stainless steel by Becque et al. (2008) owing to the slenderness nature of the modeled RHS but provides good predictions for SHS with relatively small scatter. Table 7.6 also shows the significant improvement proposed by Gardner and Theofanous (2008) for the effective width equation given in EN 1993-1-4 (2006), though it is not as accurate as the proposed method by Zhou et al. (2013). Hence, building on the proposed curve by Gardner and Theofanous (2008) which is in line with the essence of the effective width theory currently employed in EN 1993-1-4 (2006) for cross-section design, a revised expression explicitly accounting for element interaction is proposed in the present study to bring this design approach to the same level of these alternative design methods considering such interaction effects.

Table 7.6 Comparison between numerical results and various design approaches

		EN 1993-1-4 (2006)	Gardner and Theofanous (2008)	Theofanous and Gardner (2011)	DSM Becque e et al. (2008)	Zhou et al. (2013)
		$N_{u,num}/$ $N_{u,pred}$	$N_{u,num}/$ $N_{u,pred}$	$N_{u,num}/$ $N_{u,pred}$	$N_{u,num}/$ $N_{u,pred}$	$N_{u,num}/$ $N_{u,pred}$
SHS	Mean	1.153	1.093	0.927	1.081	1.069
	COV	0.028	0.020	0.076	0.038	0.019
RHS	Mean	1.159	1.108	1.024	1.153	1.056
	COV	0.033	0.036	0.048	0.064	0.093
SHS and	Mean	1.158	1.105	1.004	1.138	1.059
RHS	COV	0.032	0.034	0.067	0.065	0.083

### 7.4 Proposed design approach allowing for the benefits of element interaction

A new design approach is developed herein based on the cross-section classification concept and the effective width theory so as to explicitly account for the benefits of

interaction effects. The method adopts the Class 3 slenderness limit of 37 and effective width equation given in Eq. (7.5) proposed by Gardner and Theofanous (2008) and seeks appropriate functions of the aspect ratio  $\alpha$  to incorporate into them.

### 7.4.1 Development of the Class 3 limit as a function of the aspect ratio

To start with, the numerical results from the parametric study were used to generate analytical equations following the generalised Winter based function  $\rho = A/\bar{\lambda}_p^B$ . These equations are shown in Fig. 7.10 for the various aspect ratios  $\alpha$  and were fit through a process of least squares regression exhibiting  $R^2$  coefficient values around 0.99. The non-dimensional slenderness  $\bar{\lambda}_p$  values providing reduction factors of  $\rho=1$  were deducted thereafter and expressed in terms of the slenderness parameter  $c/t\epsilon$ , as given in Table 7.7. Recall that the relationship between  $\bar{\lambda}_p$  and  $c/t\epsilon$  is determined by the expression  $c/t\epsilon = 56.8\bar{\lambda}_p$ . The slenderness parameter  $c/t\epsilon$  has been plotted against the aspect ratio  $\alpha$  in Fig. 7.11 where the continuous line, which was generated through a process of least squares regression, depicts the proposed Class 3 limit expression incorporating the aspect ratio  $\alpha$  as given by Eq. (7.12). In Fig. 7.11, note that this proposed equation resembles that proposed by Zhou et al. (2013) for high strength steel which has been validated in the present study for application to ferritic stainless steel.

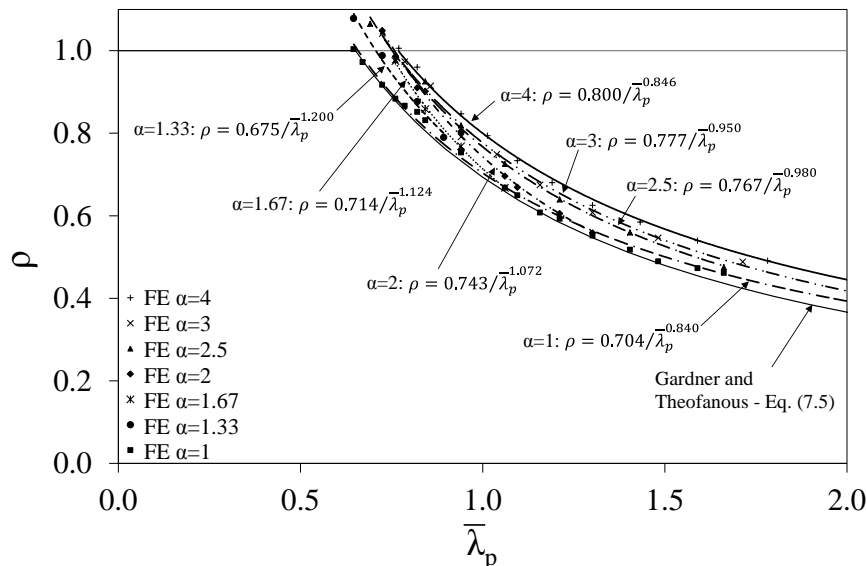


Fig. 7.10 Translation and generated analytical equations for the various aspect ratios

Table 7.7  $\bar{\lambda}_p$  and  $c/t\epsilon$  values providing  $\rho=1$  for the various aspect ratios

$\alpha$	1	1.33	1.67	2	2.5	3	4
$\bar{\lambda}_p$	0.651	0.721	0.741	0.758	0.763	0.767	0.768
$c/t\epsilon$	37	40.94	42.09	43.05	43.33	43.55	43.63

$$\frac{c}{t\varepsilon} = \begin{cases} 28.3 + 10.4\alpha - 1.8\alpha^2 & \text{For } 1 \leq \alpha \leq 3 \\ 43.3 & \text{For } \alpha > 3 \end{cases} \quad (7.12)$$

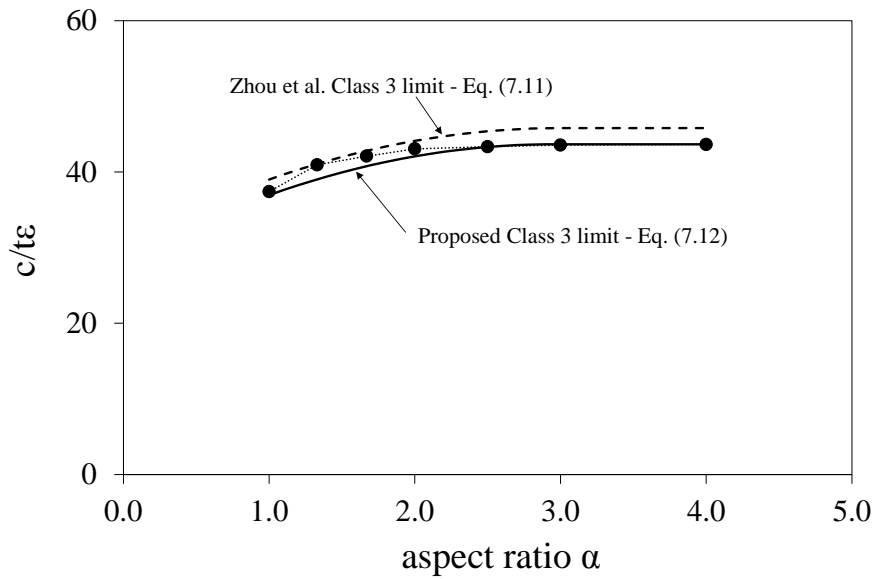


Fig. 7.11 Relationship between the Class 3 limit and the aspect ratio  $\alpha$

#### 7.4.2 Incorporation of the aspect ratio $\alpha$ within the reduction factor $\rho$

The values of the coefficients A and B for the various curves generated in Fig. 7.10 are plotted against the corresponding aspect ratio of the curve in Fig. 7.12 so as to derive appropriate equations as a function of the aspect ratio  $\alpha$  for the parameters A and B of the generalised Winter based function  $\rho = A/\bar{\lambda}_p^B$ . The equations for such coefficients are depicted in Fig. 7.11 and incorporated within the effective width equation proposed by Gardner and Theofanous (2008). This results in the proposed equation for cross-section design allowing for the benefits of element interaction given in Eq. (7.13).

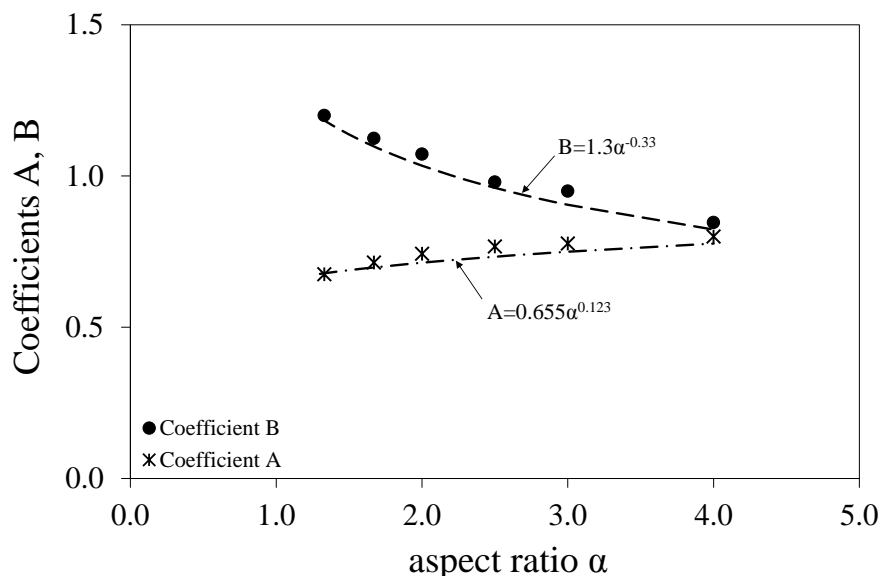


Fig. 7.12 Coefficients A and B as a function of the aspect ratio  $\alpha$

$$\rho = \begin{cases} 1 & \text{For } \bar{\lambda}_p \leq 0.651 \text{ and } \forall \alpha \\ \frac{0.772}{\bar{\lambda}_p} - \frac{0.079}{\bar{\lambda}_p^2} \leq 1 & \text{For } \bar{\lambda}_p > 0.651 \text{ and } \alpha = 1 \\ \frac{0.655\alpha^{0.123}}{\bar{\lambda}_p^{1.3\alpha-0.33}} \leq 1 & \text{but } > \frac{0.772}{\bar{\lambda}_p} - \frac{0.079}{\bar{\lambda}_p^2} \text{ For } \bar{\lambda}_p > 0.651 \text{ and } \alpha > 1 \end{cases} \quad (7.13)$$

### 7.4.3 Reliability analysis

The proposed effective width equation accounting for the benefits of element interaction given in Eq. (7.13) is statistically validated in this section following guidelines of Annex D of EN 1990 (2002). The results are shown in Table 7.8 where  $k_{d,n}$  is the design fractile factor (ultimate state) for the number of tests  $n$  taken into consideration,  $b$  is the slope of the least squares regression that reflects the relationship between the numerical and predicted resistances,  $V_\delta$  is the coefficient of variation of the numerical values relative to the resistance model,  $V_{FEM}$  is the coefficient of variation of the FE model (Davaine (2005) and Bock et al. (2014b)) and  $V_r$  is the combined coefficient of variation including all the uncertainties. The results show that for a material overstrength of 1.2 and values of  $V_{xi}=0.05$  for the geometry and material uncertainties (Baddoo and Francis (2013)), the proposed effective width equations allowing for element interaction provide a partial safety factor  $\gamma_{M0}$  of 0.96. The partial safety factor  $\gamma_{M0}$  given in EN 1993-1-4 (2006) for stainless steel is 1.1, hence the proposed design equation is reliable for this value.

Table 7.8 Results of the reliability analysis

$n$	$k_{d,n}$	$b$	$V_\delta$	$V_{FEM}$	$V_r$	$\gamma_{M0}$
82	3.213	1.077	0.025	0.026	0.079	0.96

### 7.4.4 Applicability of the method to the generated models and other stainless steel

The predictions of the proposed design method are given together with those of the EN 1993-1-4 in Fig. 7.13 for the generated FE models and existing test results collected from the literature (Gardner and Nethercot (2004a), Young and Liu (2003), Young and Lui (2005), Gardner et al. (2006), Afshan and Gardner (2013a) and Bock et al. (2014d)) on various stainless steel. Only Class 4 cross-sections with aspect ratios  $\alpha$  over 1 were considered for both sets of data to enable a better assessment of the proposed design approach. In Fig. 7.13 it is observed a reduction in scatter and translation of the points downwards reflecting a decreasing mean with all the values for both sets of data falling

on the safe side. Table 7.9 shows the predicted resistances on the basis of mean and COV relative to the numerical or test results. In this Table 7.9, the predictions of the proposed equation by Gardner and Theofanous (2008) were also considered. The results show that the proposed effective width equation accounting for element interaction achieves better predictions than current EN 1993-1-4 (2006) and proposed effective width equation in Gardner and Theofanous (2008) reducing mean and scatter, hence leading to a more efficient design and allowing to confirm its applicability to any stainless steel grade.

Table 7.9 Comparison between numerical results, collected tests and various design approaches

	FE models			collected tests		
	EN 1993-1-4 (2006)	Gardner and Theofanous (2008)	Proposed Eq. (7.13)	EN 1993-1-4 (2006)	Gardner and Theofanous (2008)	Proposed Eq. (7.13)
	$N_{u,num}/N_{u,pred}$	$N_{u,num}/N_{u,pred}$	$N_{u,num}/N_{u,pred}$	$N_{u,test}/N_{u,pred}$	$N_{u,test}/N_{u,pred}$	$N_{u,test}/N_{u,pred}$
Mean	1.159	1.108	1.075	1.168	1.123	1.107
COV	0.033	0.036	0.025	0.064	0.068	0.061

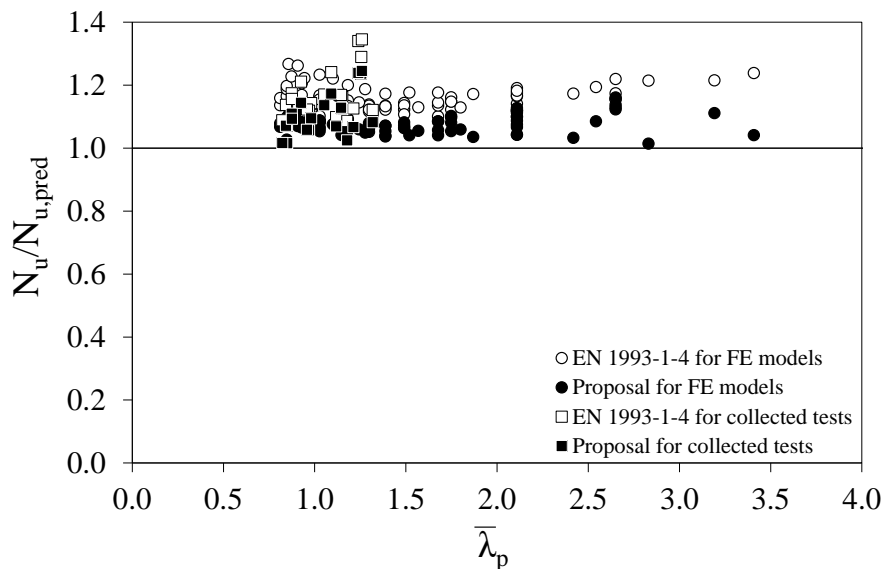


Fig. 7.13 Comparison between EN 1993-1-4 and proposed effective width equation for collected tests and generated numerical models

## 7.5 Conclusions

The effects of element interaction on cold-formed ferritic stainless steel sections (SHS and RHS) have been studied herein on the basis of a comprehensive FE model using ABAQUS. Upon benchmarking the FE models against existing tests and having assessed their sensitivity to some key input parameters including material properties and

---

initial local imperfections, parametric studies were performed. The obtained numerical results were used to derive Winter-based equations allowing for the benefits of element interaction effects and to assess various design methods for the treatment of local buckling in ferritic stainless steel cross-section. Two types of design approaches were considered for the assessment: design methods accounting for element interaction effects and those neglecting these effects. The current effective width equation for compressed internal elements given in EN 1993-1-4 (2006) and that proposed in Gardner and Theofanous (2008), which fall in the latter group, provided conservative results in comparison with the design methods making allowance for the benefits of interaction effects. This included the regression analysis method adapted for austenitic and duplex stainless steel by Theofanous and Gardner (2011), the direct strength curves derived by Becque et al. for stainless steel (2008) and the effective cross-section method proposed by Zhou et al. (2013) for application to high strength steel. The assessment of the applicability of these methods to ferritic stainless steel showed good agreement with the numerical loads achieved in the FE models providing a better representation of the results in comparison with EN 1993-1-4 (2006) and Gardner and Theofanous (2008). Hence, the effective width equation proposed in Gardner and Theofanous (2008) was adapted to explicitly capture the benefits of element interaction effects to amend this design method. A new Class 3 slenderness limit equation incorporating those benefits was also set out herein. The proposed design equation was statistically validated and assessed against the loads achieved in the FE models and collected tests from the literature on various stainless steel. The results showed that the proposed design method is applicable to any stainless steel and significantly improves cross-section capacity predictions and reduces scatter, thereby providing a more accurate and cost saving design.

### **Acknowledgements**

The research leading to these results has received funding from Ministerio de Economía y Competitividad to the Project BIA 2012-36373 “Estudio del comportamiento de estructuras de acero inoxidable ferrítico”. The first author would like to acknowledge the financial support provided by the Secretaria d’Universitats i de Recerca del Departament d’Economia i Coneixement de la Generalitat de Catalunya.





---

**CHAPTER 8 – Conclusions and suggestions for future research**

This chapter summarises the key research findings and most relevant conclusions of this research project. Based on that conducted in this thesis, suggestions for future research are given thereafter.

**8.1 Conclusions**

The first part of this thesis comprising Chapters 2 to 4 investigated the web crippling response of cold-formed stainless steel sections under interior one-flange (IOF) and exterior one-flange (EOF) loading. As frequently mentioned throughout this thesis, web crippling design guidance in EN 1993-1-4 (2006) is missing and the user is consequently conveyed to EN 1993-1-3 (2006) which deals with the design of cold-formed carbon steel members and sheeting. Building on the usage of comprehensive numerical models supported by existing tests collected from the literature and performance of parametric studies, two design methods were developed for stainless steel.

Departing from various cross-sections and the two above mentioned loading types, the influence of those on the web crippling response of square hollow sections (SHS), rectangular hollow sections (RHS) and hat sections was numerically investigated in Chapter 2. The geometrical parameters most affecting the web crippling structural response were observed to be the bearing length  $s_b$  over which the local transverse load is applied, the internal bending radius of the cross-section  $r_i$ , and the geometry of the cross-section itself besides the type of loading (IOF and EOF). On the other hand and regarding the impact of material properties which was assessed considering two types of stainless steel: austenitic and ferritic steels; it was observed that the roundness of the stress-strain response defined by the first strain hardening parameter  $n$  has no significant effect on the web crippling resistance while the hardening ratio  $\sigma_{1.0}/\sigma_{0.2}$  provided higher web crippling capacity for higher values of  $\sigma_{1.0}/\sigma_{0.2}$ . This first study, led to derive an empiric equation to improve current EN 1993-1-3 (2006) predictions for stainless steel. Moreover, various web crippling design provisions given in this code including those applicable to cross-sections with a single web and those applicable to cross-sections with two or more webs were assessed and design recommendations were suggested. The proposed equation showed to improve web crippling predictions in comparison with EN

1993-1-3 (2006) and provide appropriate resistances for both numerical models and existing tests. It was also concluded that this proposed equation is suitable for application to any stainless steel. Chapter 2 is nowadays available as a research article, Bock et al. (2013).

Complementary to the parametric study performed in Chapter 2, Chapter 3 extended the numerical models to undertake a statistical evaluation of the proposed empiric equation and formally assess its applicability to austenitic and ferritic stainless steel according to the guidelines given in Annex D of EN 1990 (2002). The numerical database, upon which the study was based on, was split into four sets of data so that the statistical uncertainties in material properties of austenitics and ferritics could be evaluated for the two load conditions considered: IOF and EOF; and two types of cross-sections: SHS and RHS, and hat sections. Hence, the sets of data consisted of: (a) ferritic SHS and RHS under IOF loading, (b) ferritic hat sections under IOF loading, (c) austenitic SHS and SHS under EOF loading and (d) austenitic hat sections under EOF loading. For comparison purposes, design provisions codified in EN 1993-1-3 (2006) and SEI/ASCE 8-02 (2002) were also statistically assessed. The statistical evaluation showed that the proposed empiric equation for web crippling design of cold-formed stainless steel sections satisfies the safety level established in EN 1993-1-4 (2006) for the sets of data involving IOF loading while for EOF loading, the results highlighted the necessity to readjust the equation. Regarding the statistical evaluations of EN 1993-1-3 (2006) and SEI/ASCE 8-02 (2002), the former yielded satisfactory results for EOF loading while for the latter approach, only the set of data (c) satisfied the safety level. Overall, higher partial safety factors were achieved for ferritics than for austenitics reflecting a more efficient design for the former. The proposed equation by Bock et al. (2013) was therefore revised and its predictions were also compared with those provided by existing design guides.

The resulting revised equation given in Bock et al. (2014b), which is currently under review, keeps the empiric nature of the existing design provisions for web crippling design and results in favourable strength predictions, though provides a relatively high scatter, yet more appropriate than that provided by existing design guides. Hence, it represents a modest improvement within the framework of Eurocode.

---

Building on the necessity to develop a more comprehensible design approach for web crippling design and the willingness to reduce the high scatter associated with that empiric nature so that more consistent predictions are achieved, a new design approach was developed in Chapter 4. The method is based on the use of strength curves  $\chi(\bar{\lambda})$  which are employed in the treatment of most of the instabilities of existing design guides and consist of determining the strengths by applying a reduction factor  $\chi$  expressed as a function of the relative slenderness  $\bar{\lambda}$  to the plastic resistance  $R_{w,pl}$ . With the usage of a refined numerical model, the method was developed to cover cold-formed austenitic and ferritic stainless steel hat sections, and user friendly predictive models to determine the web crippling reduction factor  $\chi$  and the relative slenderness  $\bar{\lambda}$  were also derived. These included expressions for the plastic resistance  $R_{w,pl}$ , the elastic critical resistance  $R_{w,cr}$  and the strength curve  $\chi(\bar{\lambda})$  for IOF and EOF loading. The proposed method, which is currently available as a research article (Bock and Real (2014a)), was statistically validated and verified against numerical and experimental results. The results showed that EN 1993-1-3 (2006) predicted, on average, the 58% and the 39% of the IOF and EOF test load, respectively, whereas the proposed method predicted the 89% and 86% of the test failure load for IOF and EOF loading, respectively. This provides an average increase in resistance of 49% and 45% for IOF and EOF loading, respectively, leading to a more optimum and precise design hence cost saving.

Overall, the objective of achieving a more rational and efficient structural design method for web crippling of stainless steel hat sections has been met. The proposed approach brings greater efficiency and consistency promoting the use of strength curves  $\chi(\bar{\lambda})$ . Thereby, a new line of investigation has emerged, details of which are provided in the following section which addresses the suggestions for further work.

The high material cost of stainless steel relative to carbon steel largely associated with the high nickel content, has led to look for alternative solutions. Ferritic stainless steel, with very low or no nickel content, have a significantly lower initial material cost in comparison with the more commonly used austenitic and duplex stainless steel grades. The importance of a better understanding of its structural behaviour to verify the applicability of existing design guides and alternative methods to ferritic stainless steel has been emphasised throughout Chapters 5 to 7 with the focus lying on cross-section behavior, for which test and numerical data was collected and generated.

Chapter 5 starts with an assessment of the suitability of the EN 1993-1-4 (2006) Annex C predictive expression to determine the strain at ultimate tensile stress  $\epsilon_u$  based on collected test data. It was found that the ferritic set of data had less ductility hence lowest values of  $\epsilon_u$  than the austenitic, the duplex and the lean duplex grades which is not reflected in the current codified equation providing too optimistic values; a revised expression suitable for ferritics was therefore proposed.

The structural behavior of cold-formed ferritic stainless steel sections was investigated numerically through the use of a comprehensive finite element model validated against test data. The generated stub column and bending models, which included SHS, RHS, channels and I-sections, allowed the assessment of EN 1993-1-4 (2006) provisions for cross-section design of fully compressed ferritic internal and outstand elements. The results showed that current slenderness limits and effective width equation given in EN 1993-1-4 (2006) can safely be applied, though those revised by Gardner and Theofanous (2008), which are less restrictive, are more appropriate enabling a more efficient design. An exception was observed for the Class 1 slenderness limit proposed by Gardner and Theofanous (2008) which appeared to be not suitable for ferritic internal elements with  $\sigma_u/\sigma_{0.2} \leq 1.2$ .

Following research on cross-section design of stainless steel, the Continuous Strength Method (CSM) which unlike the existing stainless steel design methods in the standards allows for exploitation of material nonlinearities assuming an elastic, linear hardening material model in its formulation, was extended to cover ferritic stainless steel in Chapter 5. Upon observations of the material test data, ferritic stainless steel displayed a flatter strain hardening response in comparison with the common austenitic and duplex grades, for which the CSM has been validated. A suitable strain hardening slope  $E_{sh}$  for ferritic stainless steel requiring the revised  $\epsilon_u$  model to be computed was proposed. The extension of the method was validated on the basis of stub column and beam models and collected tests, after which a statistical validation was successfully met. As observed for other stainless steel grades, this extension of the CSM for ferritic stainless steel offered improved mean and scatter than EN 1993-1-4 (2006), which represents a decrease of material usage leading to cost saving solutions.

---

Building on existing test data on the structural response of ferritic stainless steel sections most of which was observed to fall within Class 1 to Class 3 sections in Chapter 5, a laboratory testing programme on grade EN 1.4003 ferritic steel SHS and RHS comprising slender elements, was undertaken. Full details of this experimental programme are given in Chapter 6 where the results of 16 tensile coupon tests, 8 stub column tests and 9 beam tests are reported. The stub column and beam test results allowed the assessment of the applicability of the slenderness limits (Class 1 to 3) and effective width equation for internal elements in compression and the Class 2 and Class 3 limiting values for internal elements in bending given in EN 1993-1-4 (2006) and those revised by Gardner and Theofanous (2008) to ferritic stainless steel. The suitability of EN 1993-1-4 (2006) was again confirmed, though overall, Gardner and Theofanous (2008) recommended slenderness limits and effective width equation offered improved design; however, the revised Class 1 slenderness limit for internal elements in compression and the Class 2 slenderness limit for elements in bending were deemed to be too optimistic for application to ferritic stainless steel and those values given in EN 1993-1-4 (2006) for such cases were recommended. In assessing the suitability of the effective width equation and Class 3 slenderness limit for internal elements in compression and, given the shape and slenderness nature of the tested cross-sections, the approach proposed by Zhou et al. (2013) allowing for element interaction was also assessed. In view of the results, this approach seemed to provide a better representation of the actual cross-sectional behavior, though the number of tests were not representative enough to achieve a formal conclusion regarding its applicability to ferritic stainless steel.

This issue was addressed in Chapter 7, where parametric studies were carried out on the basis of a comprehensive numerical model carefully validated with the tested stub columns. The loads achieved in the generated models, which consisted of cold-formed ferritic stainless steel slender SHS and RHS, were compared with the cross-section resistances predicted by EN 1993-1-4 (2006) and by Gardner and Theofanous (2008) employing the effective width theory as well as those provided by alternative design approaches which take into consideration the benefits of element interaction effects. These methods under consideration were the regression analysis method proposed by Kato (1989) and modified by Theofanous and Gardner (2011) for stainless steel, the Direct Strength Method (DSM) pioneered by Schafer (2008) and adapted by Becque et

al. (2008) for stainless steel and the above mentioned design approach proposed by Zhou et al. (2013). Overall, all these methods were deemed to safely be applicable to ferritic stainless steel. The motivation to improve the capacity predictions for cross-sections comprising slender elements within the context of EN 1993-1-4 (2006) lead to proposed a modification of the effective width equation revised by Gardner and Theofaouns (2008) so that the benefits of element interaction effects are allowed for. The equation was derived by using the generated models and showed to provide what was sought to achieve. This modification, which also showed good agreement for other stainless steel types, offers the merits of those alternative design approaches allowing for element interaction but keeping the basis of the effective width theory employed in EN 1993-1-4 (2006).

The contributions provided in this thesis enable to verify the applicability of current EN 1993-1-4 (2006) design provisions and alternative novel design methods for the treatment of local buckling to ferritic stainless steel. Moreover, the extension of the continuous strength method (CSM) set out herein to cover ferritic stainless steel and the proposed modification for the effective width method based on the equation revised by Gardner and Theofanous (2008), offer a significantly improvement on capacity predictions for local buckling design covering the full range of cross-sectional slenderness when both methods are appropriately applied. This leads to material saving solutions which is a key aspect in the design of stainless steel to counterbalance its initial material cost.

## **8.2 Suggestions for further research**

The suggestions and ideas emerged throughout the development of this thesis are proposed herein and believe to follow two distinct paths. The first relate to the extension of the method based on strength curves for web crippling design, and the second to more focused on the structural performance of ferritic stainless steel.

The proposed design method based on strength curves for web crippling of stainless steel is currently limited to cold-formed hat sections. The development of the method for application to structural carbon steel is currently underway elsewhere as the amount of test on that material is larger and covers more aspects in comparison with that available for stainless steel, hence it is essential to undertake a wide experimental

---

programme comprising various cross-section geometries, load cases and stainless steel grades to expand the scope of the method and/or verify its applicability. More specific ideas to start with the extension include testing the same hat section geometries upon which the numerical model was calibrated but under ITF and ETF loading to complement the load cases already tested and investigate the differences in web crippling response of stainless steel among the four load cases. Further recommended sections to test include channels and Z-sections often employed in light construction, as well as linear trays used for cladding systems.

During the last years, the interest in the performance of stainless steel members in fire has arosed. While this issue has been investigated on sections under the more fundamental loading cases (i.e. compression and bending) the web crippling response of members at elevated temperatures remained unexplored. Derivation of a method for web crippling design of stainless steel at the fire limit state following the same underlying principles of the proposed approach could be investigated.

The extension of the CSM for ferritic stainless steel sections presented in Chapter 5 should be further verified for other loading configurations and cross-sections for which the method allows for or is being extended to. In particular, cross-sections under combined loading, which is currently underway elsewhere, or subjected to shear.

Ferritic stainless steel offer similar advantatges in terms of corrosion resistance, though its stress-strain response differ from the more common austenitic and duplex grades offering flatter strain hardening and less ductility which particularly affect plastic response. This issue involves the derivation of appropriate Class 1 (or ductility demans) and Class 2 slenderness limits for which further experimental investigation is necessary and being conducted elsewere.

The differences in stress-strain behaviour desplyed among different grades of stainless steel belonging to the same family may lead to a different structural response. Further experimental and numerical research on the structural response of other ferritic grades such as EN 1.4016 should also be conctued to verify the current scope of EN 1993-1-4 (2006).





---

**REFERENCES**

Abambres M, Camotim D and Silvestre N (2014). GBT-based elastic-plastic post-buckling analysis of stainless steel thin-walled members. *Thin-Walled Structures*; 83:85-02.

ABAQUS 6.9 (2010). Documentation, Simulia, USA.

Ádány S and Schafer BW (2008). A full modal decomposition of thin-walled, single-branched open cross-section members via the constrained finite strip method. *Journal of Constructional Steel Research*; 64:12-29.

Afshan S and Gardner L (2013a). Experimental study of cold-formed ferritic stainless steel hollow sections. *Journal of Structural Engineering (ASCE)* 2013; 139:717-728.

Afshan S and Gardner L (2013b). The Continuous Strength Method for structural stainless steel design. *Thin-Walled Structures*; 68:42-49.

Afshan S, Rossi B and Gardner L (2013). Strength enhancements in cold-formed structural sections – Part I: Material testing. *Journal of Constructional Steel Research*; 83:177-88.

AISC Design Guide 30 (2012): Structural Stainless Steel. American Institute of Steel Construction.

AISI (1968) Edition. Specification for the design of cold-formed steel structural members. Washington, DC: American Iron and Steel Institute.

AISI (1986) Edition. Specification for the design of cold-formed steel structural members. Washington, DC: American Iron and Steel Institute.

AISI (1996) Edition. Specification for the design of cold-formed steel structural members. Washington, DC: American Iron and Steel Institute.

## REFERENCES

---

AISI (2002) Edition. Specification for the design of cold-formed steel structural members. Washington, DC: American Iron and Steel Institute.

AISI S100-12 (2012). North American Specification for the design of cold-formed steel structural members. Washington, D.C: American Iron and Steel Institute.

ANSI/ASCE 8-90 (1991). Specification for the design of cold-formed stainless steel structural members. Reston, VA: American Society of Civil Engineers.

AS/NZS 4600 (2005). Cold-formed steel structures. Sydney, Australia: Standards Australia.

Arrayago I, Real E and Mirambell E (2013). Constitutive equations for stainless steels: Experimental tests and new proposal. Proceedings of the 5th international conference on structural engineering, mechanics and computation (SEMC 2013); 2013 Sep 2-4; Cape Town, South Africa: CRC Press; 2013. p. 1435-40.

Arrayago I, Gardner L and Real E (2014). Material modelling of stainless steel alloys. Materials & Design (under review).

Ashraf M, Gardner L and Nethercot DA (2005). Strength enhancement of the corner regions of stainless steel cross-sections. Journal of Constructional Steel Research; 61:37-52.

Ashraf M, Gardner L and Nethercot DA (2006). Finite element modelling of structural stainless steel cross-sections. Thin-Walled Structures; 44:1048-62.

Baddoo NR (2008). Stainless steel in construction: A review of research, applications, challenges and opportunities. Journal of Constructional Steel Research; 64:1199-1206.

Baddoo NR (2013). 100 years of stainless steel: A review of structural applications and the development of design rules. The Structural Engineer; 91:10-18.

---

Baddoo N, Chinen VL, Gozzi J, Clarin M, Conrad F, Talja A, Ala-Outinen T, Viherma R, Nilimaa H, Gardner L, Zili G, Riscifuli S, Fattorini F, Kasper R, Stangenberg H, Blanguernon A and Zhao B (2004). RFCS Project - Structural design of cold-worked austenitic stainless steel. Contract no. 7210 PR/ 318. Brussels: European Commission.

Baddoo NR and Francis P (2012). Development of design rules in the AISC Design Guide for Structural Stainless Steel. 4th International Stainless Steel Experts Seminar; Dec 6-7; Ascot, UK.

Baddoo NR and Francis P (2013). Re-evaluation of EN 1993-1-4 partial resistance factors for stainless steel. UK: The Steel Construction Institute.

Baehre R (1975). Sheet metal panels for use in building construction-Recent research projects in Sweden. Proceedings of the 3rd International specialty conference on cold-formed steel structures; 1975 Oct; Missouri, USA. p. 383-455.

Bakker MCM (1992). Web crippling of cold-formed steel members [dissertation]. The Netherlands: Eindhoven University of Technology.

Bakker MCM and Stark JWB (1994). Theoretical and experimental research on web crippling of cold-formed flexural steel members. *Thin-Walled Structures*; 18:261-90.

Becque J, Lecce M and Rasmussen KJR (2008). The direct strength method for stainless steel compression members. *Journal of Constructional Steel Research*; 64:1231-38.

Beg D and Hladnik L (1996). Slenderness limit of Class 3 I cross-sections made of high strength steel. *Journal of Constructional Steel Research*; 38:201-17.

Beshara B and Schuster M (2000). Web crippling data and calibrations of cold-formed steel members. AISI Research Report RP00-2. Washington, DC.

Bhakta BH, LaBoube RA and Yu WW (1992). The effect of flange restraint on web crippling strength. Final Report, Civil Engineering Study 92-1. Missouri, USA.

## REFERENCES

---

Bock M, Real E (2014a). Strength curves for web crippling design of cold-formed stainless steel hat sections. *Thin-Walled Structures*; 85:93-105.

Bock M, Real E (2014b). Effective width equations allowing for element interaction effects for cold-formed stainless steel square and rectangular hollow sections. *Structures* (under review).

Bock M, Real E and Mirambell E (2011). Work package 2: Structural performance of steel members - Report on preliminary FEM study: Local buckling. Report to the RFCS Project - Structural applications of ferritic stainless steel (SAFSS). Contract no. RFSR-CT-2010-00026. Spain: Universitat Politècnica de Catalunya (UPC).

Bock M, Arrayago I, Real E and Mirambell E (2013). Study of web crippling in ferritic stainless steel cold-formed sections. *Thin-Walled Structures*; 69:29-44.

Bock M, Real E and Mirambell E (2014a). Strength curves for web crippling design: First approach for stainless steel hat sections based on numerical analyses. *Proceedings of the 7th European conference on steel and composite structures (Eurosteel 2014)*; Sep 10-12; Naples, Italy. p. 41-2.

Bock M, Real E and Mirada FX (2014b). Statistical evaluation of a new resistance model for cold-formed stainless steel cross-sections subjected to web crippling. *International Journal of steel structures* (under review).

Bock M, Gardner L and Real E (2014c). Material and local buckling response of ferritic stainless steel sections. *Thin-Walled Structures* (under review).

Bock M, Arrayago I and Real E (2014d). Experiments on cold-formed ferritic stainless steel slender sections *Journal of Constructional Steel Research* (under review).

Bredenkamp PJ and van den Berg GJ (1995). The strength of stainless steel built-up I-section columns. *Journal of Constructional Steel Research*; 34:131-144.

---

Burns T and Bezkorovainy P (2001). Buckling of stiffened stainless steel plates [dissertation]. Sydney: University of Sydney.

Cashell K and Baddoo NR (2014). Ferritic stainless steels in structural applications. *Thin-Walled Structures*; 83:169-181.

Cain DE, LaBoube RA and Yu WW (1995). The effect of flange restraint on web crippling strength of cold formed steel Z-and I-Sections. Final Report, Civil Engineering Study 95-3. Missouri, USA.

Chacón R, Braun B, Kuhlman U and Mirambell E (2012). Statistical evaluation of the new resistance model for steel plate girders subjected to patch loading. *Steel Construction*; 5:10-15.

Coetzee JS, Van den Berg GJ and Van der Merwe P (1990). The effect of work hardening and residual stresses due to cold-work of forming on the strength of cold-formed stainless steel lipped channel section. Proceedings of the 10th international specialty conference on cold-formed steel structures; 1990 Oct; Missouri, USA. p. 143-62.

Cruise RB and Gardner L (2008a). Residual stress analysis of structural stainless steel sections. *Journal of Constructional Steel Research*; 64:352-66.

Cruise RB and Gardner L (2008b). Strength enhancements induced during cold forming of stainless steel sections. *Journal of Constructional Steel Research*; 64:1310-6.

Cruise RB and Gardner L (2009). Modeling of residual stresses in structural stainless steel sections. *Journal of Structural Engineering (ASCE)*; 135:42-53.

CSA S136-84 (1984). Cold-formed steel structural members. Ontario: Canadian Standards Association (CSA) Group.

CSA S136-94 (1994). Cold-formed steel structural members. Toronto: Canadian Standards Association (CSA) Group.

## REFERENCES

---

Daali ML and Korol RM (1995). Prediction of local buckling and rotation capacity at maximum moment. *Journal of Constructional Steel Research*; 32:1-13.

Davaine L (2005). Formulations de la résistance au lancement d'une âme métallique de pont raidie longitudinalement – Résistance dite de “Patch Loading” [dissertation]. France: L'Institut National des Sciences Appliquées de Rennes. French.

Davies JM and Leach P (1994). First-order generalised beam theory. *Journal of Constructional Steel Research*; 31:187-220.

Davies JM, Leach P and Heinz D (1994). Second-order generalised beam theory. *Journal of Constructional Steel Research*; 31:221-41.

Dawson RG and Walker AC (1972). Post-buckling of geometrically imperfect plates. *Journal of the Structural Division*; 98(ST1):75-94.

Duarte APC and Silvestre N (2013). A new slenderness-based approach for the web crippling design of plain channel steel beams. *International Journal of Steel Structures*; 3:421-34.

Ellobody E and Young B (2005). Structural performance of cold-formed high strength stainless steel columns. *Journal of Constructional Steel Research*; 61:1631-49.

EN 1990 (2002). Eurocode – basis of structural design. Brussels: European Committee for Standardization (CEN).

EN 10088-1 (2005). Stainless steels – Part 1: List of stainless steels. Brussels: European Committee for Standardization (CEN).

EN 1993-1-2 (2005). Eurocode 3: Design of steel structures – Part 1–2: General rules – Structural fire design. Brussels: European Committee for Standardization (CEN).

---

EN 1993-1-3 (2006). Eurocode 3: Design of steel structures – Part 1–3: General rules – Supplementary rules for cold-formed members and sheeting. Brussels: European Committee for Standardization (CEN).

EN 1993-1-4 (2006). Eurocode 3: Design of steel structures – Part 1–4: General rules – Supplementary rules for stainless steels. Brussels: European Committee for Standardization (CEN).

EN 1993-1-5 (2006). Eurocode 3: Design of steel structures – Part 1–5: General rules – Plated structural elements. Brussels: European Committee for Standardization (CEN).

EN 1993-1-8 (2005). Eurocode 3: Design of steel structures – Part 1–8: Design of joints. Brussels: European Committee for Standardization (CEN).

EN 1993-1-9 (2005). Eurocode 3: Design of steel structures – Part 1–9: Fatigue. Brussels: European Committee for Standardization (CEN).

EN 1993-1-10 (2005). Eurocode 3: Design of steel structures – Part 1–10: Material toughness and through-thickness properties. Brussels: European Committee for Standardization (CEN).

EN ISO6892-1 (2006). Eurocode 3: Metallic materials – tensile testing – Part1: Method of test at room temperature. Brussels: European Committee for Standardization (CEN).

Estrada I (2005). Shear design of stainless steel plate girders [dissertation]. Spain: Universitat Politècnica de Catalunya (UPC).

Euro Inox (2006). Design manual for structural stainless steel. 3rd ed. The European Stainless Steel Development Association.

Fielder N (2013). 100 years of stainless steel. 1st ed. Sheffield: British Stainless Steel Association.



## REFERENCES

---

Gabeler L (2009). Statistical evaluation of patch loading resistance models for welded steel girders [Diploma Thesis]. Germany: Institute of Structural Design, University of Stuttgart.

Galambos TV (1998). Guide to stability design criteria for metal structures. 5<sup>th</sup> ed. New York: J. Wiley & Sons.

Gardner L (2005). The use of stainless steel in structures. *Progress in Structural Engineering and Materials*; 7:45-55.

Gardner L (2008). The continuous strength method. *Proceedings of the Institution of Civil Engineers-Structures and Buildings* 2008; 161:127-33.

Gardner L and Ashraf M (2006). Structural design for non-linear metallic materials. *Engineering Structures*; 28:926-34.

Gardner L and Cruise RB (2009). Modelling of residual stresses in structural stainless steel sections. *Journal of Structural Engineering (ASCE)*; 135:42-53.

Gardner L and Nethercot DA (2004a). Experiments on stainless steel hollow sections, Part – 1: Material and cross-sectional behaviour. *Journal of Constructional Steel Research*; 60:1291-318.

Gardner L and Nethercot DA (2004b). Numerical modeling of stainless steel structural components - A consistent approach. *Journal of Structural Engineering*; 130:1586-601.

Gardner L and Theofanous M (2008). Discrete and continuous treatment of local buckling in stainless steel elements. *Journal of Constructional Steel Research*; 64:1207-16.

Gardner L, Talja A and Baddoo NR (2006). Structural design of high-strength austenitic stainless. *Thin-Walled Structures*; 44:517-28.

---

Gardner L, Saari N and Wang F (2010). Comparative experimental study of hot-rolled and cold-formed rectangular hollow sections. *Thin-Walled Structures*; 48:495-507.

Gardner L, Wang F and Liew A (2011). Influence of strain hardening on the behavior and design of steel structures. *International Journal of Structural Stability and Dynamics*; 11:855-75.

Gardner L, Cruise RB, Sok CP, Krishnan K and Ministro J (2007). Life cycle costing of metallic structures. *Proceedings of the Institution of Civil Engineers: Engineering Sustainability*; 160(ES4):167-77.

Gerges RR (1997). Web crippling of single web cold-formed steel members subjected to End One-Flange loading [MSc Project]. Canada: University of Waterloo.

Gonçalves R and Camotim D (2004). GBT local and global buckling analysis of aluminium and stainless steel columns. *Computers & Structures*; 82:1473-84.

Hetrakul N and Yu WW (1978). Structural behavior of beam webs subjected to web crippling and a combination of web crippling and bending. Final Report, Civil Engineering Study 78-4. Missouri, USA.

Hill HN (1944). Determination of stress–strain relations from offset yield strength values. Technical note No 927. Washington DC: National advisory committee for aeronautics.

Hofmeyer H (2000). Combined web crippling and bending moment failure of first-generation trapezoidal steel sheeting [dissertation]. The Netherlands: Eindhoven University of Technology.

Hofmeyer H (2005). Cross-section crushing behaviour of hat-sections (Part I: Numerical modelling). *Thin-Walled Structures*; 43:1143-54.

## REFERENCES

---

Hofmeyer H, Kerstens JGM, Snijder HH and Bakker MCM (2001). New prediction model for failure of steel sheeting subject to concentrated load (web crippling) and bending. *Thin-Walled Structures*;39:773-96.

Hradil P (2010). Work Package 2: Profiler-Abaqus lug-in. User's manual. Report to the RFCS Project - Structural applications of ferritic stainless steel (SAFSS). Contract no. RFSR-CT-2010-00026. Finland: VTT Technical Research Centre of Finland.

Hradil P, Talja A, Real E, Mirambell E and Bock M (2010). Work package 2: Review of available data. Report to the RFCS Project - Structural applications of ferritic stainless steel (SAFSS). Contract no. RFSR-CT-2010-00026. Finland: VTT Technical Research Centre of Finland.

Hradil P, Talja A, Real E, Mirambell E, Rossi B (2013). Generalised multistage mechanical model for nonlinear metallic materials. *Thin-Walled Structures*; 63:63-69.

Huang Y and Young B (2012). Material properties of cold-formed lean duplex stainless steel sections. *Thin-Walled Structures*; 54:72–81.

Investigation report S770 (1990). Compression tests of stainless steel tubular columns. Sydney: Centre for Advanced Structural Engineering, University of Sydney.

Jandera M, Gardner L and Machacek J (2008). Residual stresses in cold-rolled stainless steel hollow sections. *Journal of Constructional Steel Research*; 64:1255-63.

Johansson B and Lagerqvist O (1995). Resistance of plate edges to concentrated forces. *Journal of Constructional Steel Research*; 32:69-105.

Kaitila O (2004). Web crippling of cold-formed thin-walled steel cassettes [dissertation]. Finland: Helsinki University of Technology.

Kato B (1989). Rotation capacity of H-section members as determined by local buckling. *Journal of Constructional Steel Research*; 13:95-109.

- 
- Kato B (1990). Deformation Capacity of steel structures. *Journal of Constructional Steel Research*; 17:33-94.
- Korvink SA and van den Berg GJ (1994). Web crippling of stainless steel cold-formed beams. *Proceedings of the 12th International specialty conference on cold-formed steel structures*; 1994 Oct; Missouri, USA. p. 551-69.
- Korvink SA, van den Berg GJ and van der Merwe P (1995). Web crippling of stainless steel cold-formed beams. *Journal of Constructional Steel Research*; 34:225-48.
- Kuwamura H (2003). Local buckling of thin-walled stainless steel members. *Steel Structures*; 3:191-201.
- Lagerqvist O and Johansson B (1996). Resistance of I-girders to concentrated loads. *Journal of Constructional Steel Research*; 39:87-119.
- Langan JE, LaBoube RA and Yu WW (1994). Structural behavior of perforated web elements of cold-formed steel flexural members subjected to web crippling and a combination of web crippling and bending. *Final Report, Civil Engineering Study 94-3*. Missouri, USA.
- Macdonald M and Heiyantuduwa MA (2012). A design rule for web crippling of cold-formed steel lipped channel beams based on nonlinear FEA. *Thin-Walled Structures*; 53:123-30.
- Manninen T and Säynäjäkangas J (2012). Work package 1: Characterization of the stress-strain behavior. Report to the RFCS Project - Structural applications of ferritic stainless steel (SAFSS). Contract no. RFSR-CT-2010-00026. Finland: Outokumpu Stainless Oy, Tornio.
- Mirambell E and Real E (2000). On the calculation of deflections in structural stainless steel beams: an experimental and numerical investigation. *Journal of Construction Steel Research*; 54:109-33.

## REFERENCES

---

NASPEC-2001 (2001). North American specification for the design of cold-formed steel structural members. Washington, DC: American Iron and Steel Institute.

Natário P, Silvestre N and Camotim D (2014). Web crippling failure using quasi-static FE models. *Thin-Walled Structures*; 84:34-49.

Olsson A (2001). Stainless steel plasticity – material modelling and structural applications [dissertation]. Sweden: Luleå University of Technology.

Packer JA (1984). Web crippling of rectangular hollow sections. *Journal of Structural Engineering (ASCE)*; 110:2357-73.

Prabhakaran K (1993). Web crippling of cold-formed steel sections [Project Report]. Canada: University of Waterloo.

Quach WM, Teng JG, Chung KF (2008) Three-stage full-range stress-strain model for stainless steels. *Journal of Structural Engineering (ASCE)*; 134:1518-27.

Ramberg W and Osgood WR (1943). Description of stress–strain curves by three parameters. Technical note No 902, Washington DC: National advisory committee for aeronautics.

Rasmussen KJR (2003). Full-range stress-strain curves for stainless steel alloys. *Journal of Construction Steel Research*; 59:47-61.

Rasmussen KJR and Hancock GJ (1993a). Design of cold-formed stainless steel tubular members. I: Columns. *Journal of Structural Engineering (ASCE)*; 119:2349–2367.

Rasmussen KJR and Hancock GJ (1993b). Design of cold-formed stainless steel tubular members II: Beams. *Journal of Structural Engineering (ASCE)*; 119:2368-86.

Rasmussen KJR, Burns T, Bezkorovainy P, Bambach MR (2003). Numerical modelling of stainless steel plates in compression. *Journal of Constructional Steel Research*; 59:1345-62.

Real E (2001). Aportaciones al estudio del comportamiento a flexión de estructuras de acero inoxidable [dissertation]. Spain: Universitat Politècnica de Catalunya (UPC). Spanish.

Real E, Arrayago I, Mirambell E, Marimon F and Ferrer M (2013). Work package 3: Decking tests in the construction stage. Report to the RFCS Project - Structural applications of ferritic stainless steel (SAFSS). Contract no. RFSR-CT-2010-00026. Spain: Universitat Politècnica de Catalunya (UPC).

Ren WX, Fang SE and Young B (2006). Finite element simulation and design of cold-formed steel channels subjected to web crippling. *Journal of Structural Engineering (ASCE)*; 132:1697-1975.

Rhodes J and Nash D (1998). An investigation of web crushing behaviour in thin-walled beams. *Thin-Walled Structures*; 32:207-30.

Roberts TM and Rockey KC (1979). A mechanism solution for predicting the collapse loads of slender plate girders when subjected to in-plane patch loading. *Proceedings of the Institution of Civil Engineers*; 67:155-75.

Rossi B (2008). Mechanical properties, residual stresses and structural behavior of thin-walled stainless steel profiles [dissertation]. Belgium: University of Liège.

Rossi B (2010). Mechanical behavior of ferritic grade 3Cr12 stainless steel – Part 1: Experimental investigations. *Thin-Walled Structures*; 48:553-60.

Rossi B, Jaspart J and Rasmussen KJR (2010). Combined distortional and overall flexural-torsional buckling of cold-formed stainless steel sections: Design. *Journal of Structural Engineering (ASCE)*; 136:361-69.

Rossi B, Afshan S and Gardner L (2013). Strength enhancements in cold-formed structural sections – Part II: Predictive models. *Journal of Constructional Steel Research*; 83:189-96.

Saliba N and Gardner L (2013). Cross-section stability of lean duplex stainless steel welded I-sections. *Journal of Constructional Steel Research*; 80:1-14.

Santaputra C, Parks MB and Yu WW (1986). Web crippling strength of high strength steel beams. 8th International specialty conference on cold-formed steel structures; Missouri, USA.

Schafer BW (2008). Review: the direct strength method of cold-formed steel member design. *Journal of Constructional Steel Research*; 64:766-78.

Schafer BW and Peköz T (1998). Computational modeling of cold-formed steel: characterizing geometric imperfections and residual stresses. *Journal of Constructional Steel Research*; 47:193-210.

Schafer B and Ádány S (2006). Buckling analysis of cold-formed steel members using CUFSM: conventional and constrained finite strip methods. The 18th international specialty conference on cold-formed steel structures; p. 39-54.

Schardt R (1989). *Verallgemeinerte Technische Biegetheorie*. Berlin: Springer-Verlag. German

SCI (2013). Re-evaluation of EN 1993-1-4 partial resistance factors for stainless steel. The Steel Construction Institute; 2013.

Sedlacek G and Feldmann M (1995). The b/t-ratios controlling the applicability of analysis models in Eurocode 3, Part 1.1. Background Document 5.09 for chapter 5 of Eurocode 3, Part 1.1. Germany: Aachen.

SEI/ASCE 8-02 (2002). Specification for the design of cold-formed stainless steel structural members. Reston, VA: American Society of Civil Engineers.

Seif M and Schafer BW (2010). Local buckling of structural steel shapes. *Journal of Constructional Steel Research*; 66:1232-47.

Sélen E (2000). Work package 3: Web crippling. Report to the ECSC Project - Development of the use of stainless steel in construction. Contract no. 7210 SA/ 842. Sweden: Luleå Institute of Technology.

Seif M and Schafer BW (2010). Local buckling of structural steel shapes. *Journal of Constructional Steel Research*; 66:1232-47.

Sharp ML (1989). Behaviour of plates under partial edge loading. *Proceedings of the Structures congress*; 1989; San Francisco, USA: Steel Structures (ASCE).

Sharp ML (1990). Design parameters for web crippling of thin-walled members. Report No. 57-90-21. USA: Alcoa laboratories.

Sivakumaran K (1989). Analysis for web crippling behaviour of cold-formed steel members. *Computers & Structures*; 32:707-19

Stangenberg H (2000a). Work package 6: Ferritic stainless steel. Report to the ECSC Project - Development of the use of stainless steel in construction. Contract no. 7210 SA/ 842. Germany: Studiengesellschaft Stahlanwendung.

Stangenberg H (2000b). Work package 3: Classification of stainless steel welded I-sections and cold formed sheeting made of stainless steel. Report to the ECSC Project - Development of the use of stainless steel in construction. Contract no. 7210 SA/ 842. Germany: Studiengesellschaft Stahlanwendung.

Studnicka J (1990). Web crippling of wide deck sections. *Proceeding of the 10th International specialty conference on cold-formed steel structures*; 1990 Oct; Missouri, USA. p. 317-34.

Su M, Young B and Gardner L (2013). Continuous beam tests on aluminum alloy SHS and RHS with internal stiffeners. *Proceedings of the 5th international conference on structural engineering, mechanics and computation (SEMC 2013)*; 2013 Sep 2-4; Cape Town, South Africa: CRC Press; 2013. p. 1113-7.



Talja A (1997). Work package 3: Test report on sheetings. Report to the ECSC Project - Development of the use of stainless steel in construction. Contract no. 7210 SA/ 842. Finland: VTT Technical Research Centre of Finland.

Talja A (2004). Work packages 2 and 3: Test results of RHS, top hat and sheeting profiles. Report to the RFCS Project - Structural design of austenitic cold-worked stainless steel. Contract no. 7210 PR/ 318. Finland: VTT Technical Research Centre of Finland.

Talja A and Salmi P (1995). Design of stainless steel RHS beams, columns and beam-columns. VTT Research Notes 1619. Finland: VTT Technical Research Centre of Finland.

Talja A and Hradil P (2011). Work package 2: Model calibration tests - Test Report. Report to the RFCS Project - Structural applications of ferritic stainless steel (SAFSS). Contract no. RFSR-CT-2010-00026. Finland: VTT Technical Research Centre of Finland.

Theofanous M and Gardner L (2009). Testing and numerical modelling of lean duplex stainless steel hollow section columns. *Engineering Structures*; 31:3047-58.

Theofanous M and Gardner L (2010). Experimental and numerical studies of lean duplex stainless steel beams. *Journal of Constructional Steel Research*; 66:816-825.

Theofanous M and Gardner L (2011). Effect of element interaction and material nonlinearity on the ultimate capacity of stainless steel cross-sections. *Steel and Composite Structures*; 12:73-92.

Tsai YM (1987). Comportement sur appuis de tôles minces formées à froid. Thèse No. 689 [dissertation]. Switzerland: Ecole Polytechnique Fédérale de Lausanne. French.

---

Van den Berg GJ, Van der Merwe P (1992). Prediction of corner mechanical properties for stainless steels due to cold forming. Proceedings of the 11th international specialty conference on cold-formed steel structures; 1992 Oct; Missouri, USA. p. 571–86.

Wing BA (1981). Web crippling and the interaction of bending and web crippling of unreinforced multi-web cold-formed steel sections [MSc Project]. Canada: University of Waterloo.

Winter G (1952). 65th and 66th Progress reports on light gage steel beams of cold-formed steel. New York, USA (Unpublished).

Winter G and Pian RHJ (1946). Crushing strength of thin steel webs. Engineering experiment station, Bulletin no. 35, Part 1. New York, USA.

Wu S, Yu WW and LaBoube RA (1997). Strength of flexural members using structural grade 80 of A653 Steel (web crippling tests). 3rd Progress Report, Civil Engineering Study 97-3. Missouri, USA.

Xiao RY, Chin GPW and Chung KF. Testing and numerical analysis of cold-formed C-sections subjected to patch load. Proceedings of the 3rd international conference on advances in steel structures (ICASS 2002); 2002 Dec 9-11; Hong Kong: China. P.351-356

Young B and Hancock GJ (1998). Web crippling behavior of cold-formed unlipped channels. Proceedings of the 14th International specialty conference on cold-formed steel structures; 1998 Oct; Missouri, USA. p. 127-150.

Young B and Hancock GJ (2001). Design of cold-formed channels subjected to web crippling. Journal of Structural Engineering (ASCE); 127:1137-44.

Young B and Liu Y (2003). Experimental Investigation of cold-formed stainless steel columns. Journal of Structural Engineering (ASCE);129:169-176.

## REFERENCES

---

Young B and Lui WM (2005). Behavior of cold-formed high strength stainless steel sections. *Journal of Structural Engineering (ASCE)*; 131:1738-45.

Yu WW (1981). Web crippling and combined web crippling and bending of steel decks. *Structural Series, Civil Engineering Study 81-2*. Missouri, USA.

Yu WW and LaBoube RA (2010). *Cold-Formed Steel Design*. 4th ed. New York: John Wiley & Sons Inc.

Zhao XL and Hancock GJ (1992). Square and rectangular hollow sections subjected to combined actions. *Journal of Structural Engineering (ASCE)*; 118:648-68.

Zhao XL and Hancock GJ (1995). Square and rectangular hollow sections under transverse end-bearing force. *Journal of Structural Engineering (ASCE)*; 121:1323-9.

Zhou F and Young B (2006a). Cold-formed stainless steel sections subjected to web crippling. *Journal of Structural Engineering (ASCE)*; 132:134-44.

Zhou F and Young B (2006b). Yield line mechanism analysis on web crippling of cold-formed stainless steel tubular sections under two-flange loading. *Engineering Structures*;28:880-92.

Zhou F and Young B (2007a). Cold-formed high-strength stainless steel tubular sections subjected to web crippling. *Journal of Structural Engineering (ASCE)*; 133:368-77.

Zhou F and Young B (2007b). Experimental and numerical investigations of cold-formed stainless steel tubular sections subjected to concentrated bearing load. *Journal of Constructional Steel Research*; 63:1452-66.

Zhou F and Young B (2007c). Experimental investigation of cold-formed high-strength stainless steel tubular members subjected to combined bending and web crippling. *Journal of Structural Engineering (ASCE)*; 133:1027-34.

Zhou F and Young B (2008). Web crippling of cold-formed stainless steel tubular sections. *Advances in Structural Engineering*; 11:679-91.

Zhou F, Chen Y and Young B (2013). Cold-formed high strength stainless steel cross-sections in compression considering interaction effects of constituent plate elements. *Journal of Constructional Steel Research*; 80:32-41.

Zilli G (2004). Work package 3: Cold formed profiles and sheeting - Test results on unstiffened profiles. Report to the RFCS Project - Structural design of cold-worked austenitic stainless steel. Contract no. 7210 PR/ 318. Italy: Centro Sviluppo Materiali.